Stability Assessment of Aging Water-Retaining Earth Fill Dams

By

Irene Olivia Ubay

A Thesis submitted to the Faculty of Graduate Studies of

The University of Manitoba

In partial fulfilment of the requirements of the degree of

DOCTOR OF PHILISOPHY

Department of Civil Engineering

University of Manitoba

Winnipeg

ABSTRACT

Numerous earth fill water-retaining dams in power generating stations that were constructed in the 1950's are still in active service today. Stability of these dams is essential to maintain the serviceability of those stations as well the safety of surrounding areas. Despite satisfactory performance for over fifty years, an aging earth dam (referred to as CBBD2) began to show signs of instability by exhibiting sudden movement in its upstream side. Although remedial measures to increase stability has been put into place, it was imperative to understand what caused the sudden movement. There was a need to develop and calibrate a numerical model based on the observed conditions in CBBD2 using parameters determined from extensive laboratory tests conducted on collected soil samples. The calibrated model was then used to evaluate the long-term perform performance of six other aging earth fill dams to assess if they still meet current dam safety standards.

The calibrated model that represented the expected deformation and stability conditions of CBBD2 included time-dependent creep deformation analyses using clay strength values between the post peak and residual shear strengths. Both modified creep indices based on compression creep tests and based on shear creep tests produced the observed movements and delayed instability in CBBD2, suggesting that compression creep and shear creep tests are useful to describe creep deformations. Results indicated that the reduction of shear strength in fissured overconsolidated clays from a post peak value to the average between post peak and residual shear strengths with creep movement, predominantly occurring at the upstream slope, led to the delayed instability in CBBD2.

Stability assessment of the remaining earth dams (CBMD, WD, EF, MFRED, and MFLED), considering time-dependent creep deformation and using clay strength values between the post peak and residual shear strengths, indicated that these dams were still stable with factors of safety

greater than unity. Particular attention must be given to CBBD4 as the factor of safety was at unity which could be an indication of impending failure.

Based on the shear creep test results, a factor of safety higher than 1.3 would be needed in order to avoid long-term failure due to creep. Only two of the remaining seven earth fill dams (CBMD and WD) passed this criteria, implying that there is a need to closely monitor the other dams with regards to creep deformation to avoid creep rupture in the future. In addition, none of the dams had safety factors greater than 1.5 which meant that these dams are still subject to remedial measures to meet this safety requirement.

ACKNOWLEDGEMENTS

Sincere thanks to my adviser, Dr. Marolo Alfaro, for the guidance. I appreciate that he took a chance on someone that had a different research background. I take pride in being that girl who survived summer, fall, and winter seasons of fieldwork, as he trusted that I would be able to endure and learn from the experience. His support goes beyond words. Much appreciation to the members of my advisory committee: Dr. James Blatz and Dr. Stefan Cenkowski for their input on this research and kind words of encouragement.

Financial and technical support was provided by the owner and operator of the water-retaining earth fill dams considered in this research. Maple Leaf Drilling Ltd. provided their drilling services and expertise during site investigation and sampling. Special thanks to Moises Alfaro, Brian Wazney, Aron Piamsalee, Devon Adamson, and Dr. David Kurz for their assistance during fieldwork activities. I am also grateful for the immense help and knowledge that Kerry Lynch has given in terms of fieldwork preparations and laboratory works. Sincere gratitude to my colleagues from the Alfaro research group for the camaraderie that I have received during my stay in the University of Manitoba. The shared stories and memories created have helped me move forward.

Thank you to De La Salle University for granting me the opportunity to pursue my degree under the Mme. Maillefer Study Program. Also to the DLSU-Civil Engineering Department for their continuous encouragement throughout my studies, Animo!

My heart goes to my family and friends, whose support goes beyond distance and time zones. Drs. Lun and Zeny Mateo as well as Joash Adajar, who became my family in Winnipeg. Auntie Sylvia, my ticklish starfish in heaven, I hope I am making you proud. To my loving husband, Alitking, thank you for going on this journey with me. Mom and Dad, I love you beyond words.

Above all, thank you to the Almighty for always listening and giving me hope.

Table of Contents

ABSTRACT i

ACKNOWLEDGEMENTS iii

Table of Contents iv

List of Figures vii

List of Tables xiii

List of Notations and Symbols xiv

List of Appendices xvi

Chapter 1 INTRODUCTION 1

1.1 Brief Description of the Research Area 1

1.2 Research Hypotheses 3

1.3 Research Objectives 4

1.4 Significant Contribution 5

1.5 Organization of Thesis 6

Chapter 2 LITERATURE REVIEW 7

2.1 Previous Geotechnical Investigation Reports 7

2.2 Similar Water-Retaining Structures 10

2.3 Effects of Gypsum on the Behaviour of Clay 11

2.4 Effects of Fissures on the Behaviour of Clay 13

2.5 Time-dependent Creep Deformation 16

2.6 Numerical Modelling 21

2.6.1 Modified Cam-Clay Model 21

2.6.2 Soft Soil Creep Model 22
2.7 Summary of Reviewed Literature and Justification of Research 25
Chapter 3 SITE INVESTIGATION 35
3.1 Soil Sampling 35
3.1.1 On-shore soil sampling 35
3.1.2 Off-shore soil sampling 36
3.1.3 Test pit excavation 37
3.2 Instrumentation 38
3.3 Subsurface Characterization 39
3.3.1 CBBD2 39
3.3.2 CBBD4 40
3.3.3 CBMD 41
3.3.4 WD 41
3.3.5 EF 42
3.3.6 MFLED 43
3.3.7 MFRED 43
3.4 Summary 43
Chapter 4 LABORATORY TESTING 56
4.1 Index Properties 56
4.1.1 CBBD2 56
4.1.2 Other Earth Fill Dams 57

4.2 Particle Orientation and Mineralogy 58
4.3 Deformation Characteristics 59
4.4 Shear Strength Characteristics 60
4.4.1 Consolidated Drained Direct Shear Test 60
4.4.2 Consolidated Undrained Direct Simple Shear Test 61
4.4.3 Torsional Ring Shear Test 62
4.4.4 Isotropically Consolidated Undrained Triaxial Compression Test 62
4.5 Creep Characteristics 64
4.5.1 Creep in Compression 65
4.5.2 Creep in Shear 65
4.6 Summary 69
Chapter 5 NUMERICAL MODELLING 96
5.1 CBBD2 Numerical Model 96
5.2 CBBD2 Model Calibration Results 100
5.3 Assessment of remaining water-retaining earth fill dams 103
5.4 Summary 105
Chapter 6 CONCLUSION and RECOMMENDATIONS 126
6.1 Conclusion and Discussion 126
6.2 Recommendations 130
REFERENCES 132
APPENDICES 138

List of Figures

Figure 2.1 Deviatoric stress – strain behaviour of stable, unstable, and background clay samples from triaxial test results 30

Figure 2.2 Fully softened, mobilized, and residual stress ratios from field case histories.....31

Figure 2.3 Mean effective stress and volumetric strain during creep 31

Figure 2.4 Relationship between slope inclination, slope height, and time to failure for London clay in cut slopes.....32

Figure 2.5 Relationship between creep strain rates and time to failure based on case histories33

Figure 2.6 Yield surfaces of the SSC model in the p'-q plane.....34

Figure 3.1 Approximated location of boreholes, test pits and installed vibrating wire piezometers in CBBD2.....46

Figure 3.2 Approximated location of boreholes, test pits and installed vibrating wire piezometers in CBBD4.....47

Figure 3.3 Approximated location of boreholes, test pits and installed vibrating wire piezometers in CBMD 48

Figure 3.4 Approximated location of boreholes, test pits and installed vibrating wire piezometers in WD.....49

Figure 3.5 Approximated location of boreholes, test pits and installed vibrating wire piezometers in EF 50

Figure 3.6 Approximated location of boreholes, test pits and installed vibrating wire piezometers in MFLED.....51

Figure 3.7 Approximated location of boreholes, test pits and installed vibrating wire piezometers in MFRED 52

Figure 3.8 Collection of inclined samples in a CBBD2 test pit 53

Figure 3.9 Samples obtained in a CBBD2 test pit by means of a block sampler....53

Figure 3.10 Conventional soil block sampling in a CBBD2 test pit....53

Figure 3.11 Cross-section of CBBD2 Section B-B....54

Figure 3.12 Cross-section of CBBD2 Section A-A....54

Figure 3.13 Fissured clay in a CBBD2 test pit 54

Figure 3.14 Silt pockets observed within fissured clay in a CBBD2 test pit....55

Figure 4.1 CBBD2 clay core extruded Shelby tube sample 77

Figure 4.2 CBBD2 clay blanket extruded Shelby tube sample....77

Figure 4.3 CBBD2 clay foundation extruded Shelby tube sample 77

Figure 4.4 CBBD2 clay foundation sample at location further away from CBBD2....77

Figure 4.5 CBBD2 clay core sample 78

Figure 4.6 Polished surfaces observed in CBBD2 clay core sample 78

Figure 4.7 Fissures and polished surfaces observed in clay blanket samples 78

Figure 4.8 CBBD2 clay foundation samples....79

Figure 4.9 Plasticity chart....79

Figure 4.10 SEM image of a clay foundation sample from CBBD2 (with permission from Alfaro III, 2016) 80

Figure 4.11 SEM image of a clay core sample from CBBD2 80

Figure 4.12 SEM image of a clay blanket sample from CBBD2 81

Figure 4.13 XRD test results of CBBD2 clay samples 81

Figure 4.14 Consolidation curves from oedometer tests on CBBD2 samples 82

Figure 4.15 Stress-displacement behaviour of CBBD2 core samples from Direct Shear tests...82

Figure 4.16 Stress-displacement behaviour of CBBD2 foundation samples from Direct Shear tests 83

Figure 4.17 Stress-displacement behaviour of CBBD2 blanket samples from Direct Shear tests 83

Figure 4.18 Normalized stress-displacement behaviour of CBBD2 core samples from Direct Shear tests 84

Figure 4.19 Normalized stress-displacement behaviour of CBBD2 foundation samples from Direct Shear tests.....84

Figure 4.20 Normalized stress-displacement behaviour of CBBD2 blanket samples from Direct Shear tests.....85

Figure 4.21 Shear stress-vertical effective stress results from Direct Simple Shear tests on CBBD2 clay blanket samples 85

Figure 4.22 Stress-strain results from Direct Simple Shear tests on CBBD2 clay blanket samples 86

Figure 4.23 Pore water measurements from Direct Simple Shear tests on CBBD2 clay blanket samples 86

Figure 4.24 Stress-displacement behaviour of CBBD2 Section A-A specimens from Torsional Ring Shear tests 87

Figure 4.25 Stress-displacement behaviour of CBBD2 Section B-B specimens from Torsional Ring Shear tests 87

Figure 4.26 Stress paths in p'-q space of CBBD2 Section A-A CIU Triaxial test samples.....88

Figure 4.27 Stress-strain behaviour of CBBD2 Section A-A CIU Triaxial test samples.....88

Figure 4.28 Pore water measurements of CBBD2 Section A-A CIU Triaxial test samples.....89

Figure 4.29 Stress paths in p'-q space of CBBD2 Section B-B CIU Triaxial test samples.....89

Figure 4.30 Stress-strain behaviour of CBBD2 Section B-B CIU Triaxial test samples.....90

Figure 4.31 Pore water measurements of CBBD2 Section B-B CIU Triaxial test samples.....90

Figure 4.32 CBBD2 clay core post-CIU Triaxial test samples.....91

Figure 4.33 CBBD2 clay blanket post-CIU Triaxial Test test samples 91

Figure 4.34 CBBD2 clay foundation post-CIU Triaxial test samples 92

Figure 4.35 CBBD4 clay core post-CIU Triaxial test samples.....92

Figure 4.36 Experimental set-up used for Shear Creep tests 93

Figure 4.37 Vertical creep strain with respect to time from Creep in Shear tests 94

Figure 4.38 Volumetric creep strain with respect to time from Creep in Shear tests 94

Figure 4.39 Void ratio – log time curve for CBBD2 core sample from Creep in Compression test 95

Figure 4.40 Void ratio – log time curve for CBBD2 core sample from Creep in Shear test 95

Figure 5.1 CBBD2 Section A-A cross-section, generated mesh, and phreatic surface 112

Figure 5.2 CBBD2 Section B-B cross-section, generated mesh, and phreatic surface 112

Figure 5.3 Deformation development in CBBD2 Section A-A at different stages using Case 1: after (a) construction, (b) 1, (c) 10, (d) 30, and (e) 50 years after impounding 113

Figure 5.4 Deformation development in CBBD2 Section B-B at different stages using Case 1: after (a) construction, (b) 1, (c) 10, (d) 30, and (e) 50 years after impounding 114

Figure 5.5 Deformation development in CBBD2 Section A-A at different stages using Case 2: after (a) construction, (b) 1, (c) 10, (d) 30, and (e) 50 years after impounding 115

Figure 5.6 Deformation development in CBBD2 Section B-B at different stages using Case 2: after (a) construction, (b) 1, (c) 10, (d) 30, and (e) 50 years after impounding 116

Figure 5.7 Factor of safety values at time of failure at CBBD2 117

Figure 5.8 Mobilized shear stress and shear strength along slip surface at CBBD2 Section B-B using Case 1 118

Figure 5.9 Mobilized shear stress and shear strength along slip surface at CBBD2 Section B-B using Case 2 118

Figure 5.10 CBBD4 cross-section, generated mesh, and phreatic surface 119

Figure 5.11 CBMD cross-section, generated mesh, and phreatic surface 119

Figure 5.12 WD cross-section, generated mesh, and phreatic surface 120

Figure 5.13 EF cross-section, generated mesh, and phreatic surface 120

Figure 5.14 MFRED cross-section, generated mesh, and phreatic surface 121

Figure 5.15 MFLED cross-section, generated mesh, and phreatic surface 121

Figure 5.16 Factor of safety at CBBD4 122

Figure 5.17 Factor of safety at CBMD 122

Figure 5.18 Factor of safety at WD 122

Figure 5.19 Factor of safety at EF 123

Figure 5.20 Factor of safety at MFRED 123

Figure 5.21 Factor of safety at MFLED 123

Figure 5.22 Incremental displacement from safety calculations at CBBD4 124

Figure 5.23 Incremental displacement from safety calculations at CBMD 124

Figure 5.24 Incremental displacement from safety calculations at WD 124

Figure 5.25 Incremental displacement from safety calculations at EF 125

Figure 5.26 Incremental displacement from safety calculations at MFRED 125

Figure 5.27 Incremental displacement from safety calculations at MFLED 125

List of Tables

Table 2.1 Summary of index properties for clay foundation materials at CB Generating Station, Seven Sisters Dykes, and Red River Dyke (Hatch, 2010) 29

Table 3.1 Summary of installed piezometers, drilled boreholes, and excavated test pits per location 45

Table 4.1 Summary of index properties for CBBD2 72

Table 4.2 Summary of index properties for remaining earth dams.....72

Table 4.3 Summary of deformation characteristics.....73

Table 4.4 Summary of shear strengths from Direct Shear tests 74

Table 4.5 Summary of shear strengths from Direct Simple Shear tests.....74

Table 4.6 Summary of residual shear strengths from Torsional Ring Shear tests.....75

Table 4.7 Summary of shear strengths from CIU Triaxial tests.....76

Table 4.8 Summary of Creep in Compression test results.....76

Table 5.1 Model parameters for clay components of CBBD2 108

Table 5.2 Model parameters for non-clay components (provided by owner).....108

Table 5.3 Model parameters for clay components of CBBD4 and CBMD 109

Table 5.4 Model parameters for clay components of WD and EF.....109

Table 5.5 Model parameters for clay components of MFRED and MFLED.....110

Table 5.6 Factor of safety in remaining earth dams using Case 1 110

Table 5.7 Factor of safety and critical surface location in remaining earth dams using Case 2111

List of Notations and Symbols

q = deviatoric stress

p'_0 = initial mean effective stress

p' = mean effective stress

ε_v = volumetric strain

ε_v^e = elastic volumetric strain

ε_v^{cr} = creep volumetric strain

ε_{vc}^{cr} = creep volumetric strain during consolidation

ε_{vac}^{cr} = creep volumetric strain after consolidation

e = void ratio

e_0 = initial void ratio

λ = Cam-Clay isotropic compression index

κ = Cam-Clay isotropic swelling index

M = slope of critical state line

p'_p = preconsolidation stress

p_p^{eq} = equivalent preconsolidation stress

p^{eq} = actual stress state

c' = effective cohesion

φ' = effective angle of friction

p_{p0}^{eq} = initial equivalent preconsolidation stress

ε_v^c = plastic creep strain

λ^* = modified compression index

κ^* = modified swelling index

C_c = compression index

C_r = recompression index

σ'_{vc} = apparent preconsolidation pressure

Δu = change in pore water measurement

σ_v' = vertical effective stress

C_α = compression creep coefficient

q_{100} = deviator stress at a confining stress of 100 kPa

q_{200} = deviator stress at a confining stress of 200 kPa

$C_{\alpha\text{-}s}$ = shear creep coefficient

μ^* = modified creep index

γ = unit weight

List of Appendices

Appendix A: Borehole Logs

Appendix B: Images of Extruded Shelby Tube Samples

Appendix C: Laboratory Test Results

Appendix D: Numerical Modelling Results

Chapter 1 INTRODUCTION

In order to meet the increasing demand for power, numerous power-generating stations were constructed in the 1950's. Earth fill water-retaining dams are essential structures in hydroelectric generating stations and its stability is essential to maintain the serviceability of the stations as well as the safety of the surrounding areas. These aging earth fill dams are still being used today and despite its good performance for over 50 years, some began to show signs of instability. One earth dam in particular exhibited movement in the upstream side. Time-dependent deformations could have started to transpire causing some movement within the dam. Environmental loading which causes cyclic expansion and contraction of the soil due to wetting-drying and freeze-thawing could also have also altered the strength and deformation properties of the dam materials with respect to time. Although remedial measures to increase stability has been being put into operation, it is still imperative to understand what has caused the sudden movement. It is possible that such occurrence would not be an isolated case, especially if there are other aging earth dams with similar soil materials and structural geometry. Stability analysis on similar earth dams should be done in order to verify if they still meet current dam safety standards.

1.1 Brief Description of the Research Area

Earth fill dams that has been in operation for over 50 years were considered in this research. These dams have an impervious clay core and were mostly founded on glaciolacustrine clay. Seven earth fill water-retaining dams from four hydroelectric generating stations were investigated. The four generating stations, referred to as CB, WD, EF, and MF, are owned and operated by the same hydroelectric company. The generating stations, along with the earth dams investigated in this research, will be referred to with the use of acronyms as per the request of the dam operators and owners to not reveal the location of these dams.

WD has an earth fill dam with a central clay core founded on clay layer on silty sand or gravely sand overlying bedrock. EF has also a central clay core but is founded on sandy silt or clayey silt. There were two earth fill dams considered in MF and will be referred to as MFLED (left earth dam) and MFRED (right earth dam). Both earth fill dams have an impervious central clay core with an upstream compacted clay blanket. The foundation type is clay over silty sand and bedrock. The most number of earth fill dams investigated were from the CB generating station. The main dam (CBMD) has a central clay core and is founded on a shallow sand layer with fine gravel overlying bedrock. Block dam 2 (CBBD2) is an upstream inclined clay core earth fill dam whose foundation type is either bedrock, clay over sandy silt, sandy silt over sand and gravel, or sand and gravel depending on the location. Similar to the earth fill dams in MF, CBBD2 has an upstream clay blanket. Block dam 4 (CBBD4) has also an inclined clay core and an upstream compacted clay blanket, similar to CBBD2, at locations where the thickness of the clay foundation was deemed inadequate. The aforementioned earth fill dam is on clay overtopping silt and sandy silt foundation to depth.

Out of the seven considered aging earth fill dams, there was much interest in investigating CBBD2 due to the sudden irregular movement that occurred in its upstream slope despite its acceptable performance for over 50 years. A week after a routine site inspection, the upstream side of the dam slid about 1.5m towards the reservoir. The movement did not propagate the entire upstream slope of the dam, but was localized in the eastern section which will be referred to as Section B-B. The western section (Section A-A) remained stable.

The clay used to construct CBBD2 was often described in geotechnical investigation reports as high plastic lacustrine clay that was crumbly and fissured in nature. Natural clay was only present in Section A-A, and stretches from the upstream to the downstream side of the dam. Section B-B had a thick layer of permeable sandy silt and gravely sand as it used to be part of an old creek. With the absence of natural clay underlying the eastern section of the dam, a

compacted clay blanket was placed in the upstream side and was tied into the clay core to control seepage.

There is a need to understand the mechanisms behind the sudden movement in CBBD2 since it is not typical for such an occurrence to happen in the upstream side of a water-retaining earth fill dam. As this incident happened well into the long service-life of CBBD2, it is possible that other aging dams would behave similarly in the future. If so, any insight to the cause of the movement could be used to evaluate long-term performances of other aging earth dams so that the owner would be able to implement proactive measures should the performance not meet current dam safety standards.

1.2 Research Hypotheses

Several conditions could have led to the upstream movement in CBBD2 but it should be noted that such event happened well within the long and still active service life of the structure. Further compression and consolidation of soil could improve shear strength and stiffness but creep deformation could occur. High plasticity clays could display creep behaviour and inevitably cause enough movement that could lead to slumping over time. It is hypothesized that the placed clay blanket and the inclined clay core at Section B-B could have developed creeping.

The clay core, foundation and blanket could have also deteriorated with time due to environmental loading. Repeated freezing-thawing and wetting-drying could increase the intensity of fissuring which would alter strength and deformation characteristics of these materials. The change in the properties caused by intense fissuring is assumed to have led to the instability of the dam.

Another reason for the instability could be the leaching of naturally occurring cementation from the clay. If an ample amount of gypsum, a cementing agent in soil, is depleted due to water flow through the dam then soil brittleness would increase and could induce instability with time.

1.3 Research Objectives

In order to understand the cause of delayed instability of aging earth fill dams, there was a need to develop and calibrate a numerical model based on the observed conditions in CBBD2. The calibrated model was essential in evaluating the long-term performance of six other aging earth fill dams to assess if these dams meet modern dam safety standards. To meet these objectives, the study has been separated into three main phases: fieldwork and soil sampling, laboratory testing, and numerical modelling. Specifically, the research is aimed to:

- Conduct a geotechnical site investigation on seven earth fill water-retaining dams that would include undisturbed soil sampling of the clay core, foundation, and blanket, as well as test pit excavations of background clay;
- Determine soil properties, composition, strength, and deformation characteristics of collected soil samples by carrying out laboratory tests such as index tests, X-ray diffraction (XRD), scanning electron microscopy (SEM), direct shear tests, torsional ring shear tests, isotropically consolidated undrained triaxial tests, one-dimensional consolidation (oedometer) tests, creep in compression tests, and creep in shear tests;
- Calibrate a numerical model using a commercially available finite element computer software based on the observed conditions in CBBD2 and parameters determined from laboratory tested soil samples; and,
- Evaluate the long-term performance of six predetermined aging earth fill water-retaining dams (CBMD, CBBD4, WD, EF, MFLED, and MFRED) using the calibrated CBBD2 numerical model.

1.4 Significant Contribution

A better understanding on the cause of delayed instabilities of aging earth dams will be obtained from this research. At present, there are numerous water-retaining earth fill dams that will reach and have reached more than fifty years of its service life. The behaviour of the investigated earth dams in this research could provide important insight, allowing owners and operators of similar structures to be more vigilant so that irregular movements or instabilities as what happened in CBBD2 could be avoided.

Finite element method of analysis using a time-dependent soil creep model in water-retaining earth fill dams is not typically used by practicing engineers partly because of the limited commercially available software packages that have adopted soil creep models. However, the results of this research could initiate the need to consider this form of analysis on the design process of similar structures that are yet to be built. The predicted movement or instability from the long-term analysis could urge for the need for more frequent in-situ monitoring as well as plan for a remedial solution, if necessary.

Soil creep models integrated in commercially available geotechnical engineering software predict both volumetric and deviatoric creep behaviour with the use of parameters taken from one-dimensional consolidation tests. Comparing secondary compression values from one-dimensional consolidation tests and creep in shear tests could generate curiosity if the use of shear creep parameters could somehow affect numerical modelling results, especially with regards to investigations on slopes. If so, further understanding on creep in shear could be of future interest.

1.5 Organization of Thesis

Following this introductory chapter, Chapter 2 contains the review of related literature. Chapter 3 discusses the site investigation and characterization that was conducted. Chapter 4 is comprised of information regarding results on laboratory tests conducted on collected clay samples from fieldwork. Chapter 5 presents the results of numerical calibration and the assessment of the aging earth fill dams considered in this research. Lastly, Chapter 6 contains research conclusions and recommendations for future work. Appendices contain supplementary information for this research.

Chapter 2 LITERATURE REVIEW

Previous reports and studies that aided in the conception of the framework for this research were presented in this chapter. Past geotechnical investigation reports provided information on laboratory results and observations on the earth dams in CB Generating Station prior to the occurrence of the irregular movement in Block Dam 2 (CBBD2). Previous studies on the Seven Sisters and Red River dykes were presented as the foundation of these structures were thought to be similar to the CB clay. The effects of gypsum and fissures on the behaviour of clay along with the results of numerical modelling reflecting these effects were also briefly discussed in this chapter. Lastly, the importance of the investigation of time dependent creep deformation was explored and the Soft Soil Creep model of PLAXIS 2D was introduced.

2.1 Previous Geotechnical Investigation Reports

Annual dam safety reviews are typically completed in order to ensure that the operation and integrity of the structure is well-maintained. Previous assessment reports provided by the dam operator and owner were mostly on the earth dams of the CB Generating Station as this was the location of the reported irregular movement. Background information on the clay materials as well as some findings from previous investigations were reported. Determination of parameters used for the numerical modelling as well as the stability analyses were also presented.

Geotechnical investigation in CB was done separately by two independent consulting firms in 1999 and 2010. The investigation included extensive field exploration and sampling, laboratory testing, and stability assessment of the selected earth dams. In both reports, the foundation clay was classified as “fat clay” and was described as having nuggetty or blocky structure, highly fissured, and with laminations. The clay materials found in CB was compared to those in Seven

Sisters Generating Station and Red River Dykes because of its classification and description. However, the moisture content of the clay from the aforementioned dykes was higher and the corresponding dry unit weight lower. The comparison was mentioned in the 2010 investigation report and is shown in Table 2.1. It was further mentioned that this was an indication that although the classification and description was similar, the foundation clay from the dykes would have lower shear strength properties than the CB foundation clay.

Typical instrumentation installed in the different earth dams in CB were piezometers, survey pins, settlement points, chainage markers, and alignment posts. The 2010 investigation report, however, stated that there were some discrepancies with respect to the instrumentation found in-situ as compared to the documented instrumentation plans. The 1999 and 2010 inspections performed their own monitoring and recording of readings from the known instrumentations on site, independent from the records of the dam operator and owner.

The inspections performed in 1999 and 2010 reported notable observations on the history of settlements that occurred mostly on CBBD2 and CBBD4. Observed cracks on the crest above the upstream edge of the impervious core of CBBD2 were reported in 1960 but no evidence of said cracks were detected during the 1999 inspection. A hand level estimated that the crest elevation was lower than what was documented in construction drawings by 0.2 m. By 2001, surveying confirmed that the settlement was below design values by 0.25 m. The crest continued to settle based on 2006 monitoring results. The CBBD4 top core elevation was lower than the design elevation by 0.25 m but was topped as the crest elevation was satisfactory as reported in 1999. Apart from the documented settlement, no depressions, sinkholes, nor misalignments were detected in the earth dams.

Filter and transition zones were documented as satisfactory in all locations. Seepage through foundation soils were not detected making seepage and drainage conditions adequate. As inspections on seepage, drainage, and filter compatibility were considered satisfactory, both

1999 and 2010 reports indicated that piping and internal erosion was unlikely. In addition, the 1999 assessment mentioned that due to the adequate performance of all CB earth dams for over 40 years then it was likely that creep settlements would be very minimal and would not have any major time dependent structural design problems.

Laboratory tests were performed on collected samples from the two separate investigations. The results from the 1999 investigations were reviewed by the independent consulting firm, hired by the dam owner, who conducted the 2010 assessment after conducting their own comprehensive tests. The clay fill and foundation were regarded as similar materials based on resulting properties. An implication of this assessment was that similar shear strength parameters for both materials were used in the slope stability analyses. The shear strength parameters of the tested clay materials were similar to those at Seven Sisters Generating Station and Red River dykes as both were considered highly plastic fissured clay with blocky structures. With this precedent experience, the shear strength were also taken as the average between peak and residual strengths with no apparent cohesion values. Regression analysis on strength parameters with and without cohesion values rendered similar high coefficients of determination leading to use of zero cohesion.

Slope stability analysis was performed on all CB earth dams using limit equilibrium method. It was recommended that strength parameters from direct shear tests be applied at clay sections along the horizontal slip surface whereas strength parameters from triaxial tests applied to sections that would undergo cross-shearing. The reason for this procedure was to consider the anisotropic behaviour of clay in terms of shear strength. Factors of safety were determined from the performed slope stability analyses. A factor of safety of 1.5 was required against normal water level load cases whereas a value of 1.0 was required for a case considering normal water levels and seismic loading. Analysis was not done for rapid drawdown cases as normal reservoir fluctuations at the CB earth dams were considered to be relatively modest. Slope stability

analyses from both 1999 and 2010 investigations indicate that investigated dams were stable but did not meet the required criteria for all load cases. It was also recommended that remedial solutions were likely to be needed in the long term.

2.2 Similar Water-Retaining Structures

The CB Generating Station block dams have often been compared with the Red River and Seven Sisters dykes since these structures were founded on highly plastic clays that were often described as fissured. Though foundation conditions and dam configurations may be different for each location, the foundation clay properties were thought of as likely to be similar.

A study on water-retaining structures founded on high plasticity clays was done by Rivard and Lu (1978) which included the Red River and Seven Sisters dykes. The highly plastic clay foundation in these locations had structural discontinuities such as laminations, horizontal fissures, and a blocky or nugget structure.

Bjerrum (1969) explained that fissured clays would tend to soften when subjected to straining which would reduce cohesion values. It was suggested that for fissured clay at shallow depths, the assumption of using peak strengths with cohesion values close to zero would represent the reduction of strength of intact clays due to fissures. However, Rivard and Lu (1978) used post peak or critical state strengths with no cohesion as strength parameters for the analyses. Similarly, Mesri and Abdel-Ghaffar (1993) also applied no cohesion with post peak strengths to reanalyze 34 first-time slides on high plastic soft and stiff clays. Both studies indicated that the use of normally consolidated strength or fully softened strengths for highly plastic clays with structural discontinuities would obtain a reasonable factor of safety in slope stability analysis. Although these studies were insightful in terms of shear strength parameters which can be

applicable to the clay materials in CB, these studies were not able to explain the possible cause of irregular movements.

A major slide in the upstream slope of the San Luis Dam in San Francisco, California occurred owing to the cyclic loads caused by the repeated filling and emptying of the reservoir (Stark and Duncan, 1991). The cyclic stress changes caused cumulative deformations that were large enough to reduce strength to residual value leading to failure. Undrained cyclic loading in the form of seismic activity also caused the delayed upstream slope failure of the lower San Fernando Dam in California (Gu et al., 1993). Earthquake loading led to the generation of excess pore water pressures which reduced shear strength. The loss of strength also initiated stress redistribution and induced further yielding of the surrounding areas of the earth structure. Such occurrences provided additional insights on other causes of delayed failure in earth dams.

2.3 Effects of Gypsum on the Behaviour of Clay

Irregular slope instabilities occurred at the water retention dykes of the Seven Sisters Generating Station when the dykes were heightened in the late 1940s. The dyke had a clay core with riprap shell and the foundation was considered as soft high plastic clay. Instabilities were irregular as the location and the time delay (time between dyke heightening completion until instability occurrence) were different for each event that transpired. Most cases exhibited bulging at the toe with crest settlement at the dry side of the slope. Though all thirteen events were considered as instabilities, no uncontrolled loss of water happened as the dam operators and owners were proactive in addressing these events.

Investigations were performed on the stable and unstable sections of the dyke and was compared to a background location which has not experienced any loading. Results from several studies (Garinger et al., 2004; Man et al., 2011) linked the instabilities to the leaching of gypsum

from the foundation clay. Results indicated that the background samples were saturated with gypsum while unstable and stable sections were undersaturated with gypsum. Gypsum streaks were visible in the background samples that were examined during field investigation. Scanning Electron Microscope (SEM) images also revealed that there were more granular gypsum particles found in the background samples than the other locations (Man and Graham, 2010). Deviatoric stress-strain results of triaxial test samples show that both stable and unstable sections exhibit strain-softening indicating that the clay from these sections are brittle compared to the background clay (Figure 2.1). The softening from the unstable section was also more pronounced than in the stable section which was somehow correlated to the deceased amount of gypsum in this location.

It was believed that seepage from the forebay could have dissolved the gypsum contained within the clay foundation of the dyke as time progressed. Highly cemented gypsum-rich specimens strain softened after 13% axial strain (Man et al., 2011). Depletion of gypsum can then make clay more brittle as strain-softening would occur at a lower axial strain and could also possibly reduce soil shear strength. Gypsum-rich specimens have higher yield stresses than specimens that have been washed deionized water before consolidation. The rate at which gypsum dissolution occurred was thought to be influenced by the seepage rates from the forebay in addition to the continuity of silt-sand seams found within the foundation clay.

Parameters from laboratory tests results performed by Man et al. (2011) from tested samples taken from the stable and unstable dyke sections were used for the SIGMA/W stress deformation modelling. Results show that heightening the dyke produced shear straining over time that could produce significant strain softening in the clay foundation. This led to the justification of using post peak strengths and even residual strengths in the SLOPE/W slope stability modelling in order to evaluate the safety factors at the stable and unstable sections. Using post peak strengths, both stable and unstable sections had factors greater than unity rendering them both as safe. On the other hand, using residual shear strength values resulted in both

sections with factors of safety less than unity. Such results suggest that further analysis should still be done in order to determine the conditions that would induce instability only to the unstable section and would still render the stable section as safe.

Seepage and mass transport analyses using SEEP/W and CTRAN/W, respectively, was done by Man et al. (2011) in order to determine the possibility of flow paths to allow groundwater to pass beneath the dykes assuming that fractures, fissures, or permeable layers are interconnected. Such analysis was used to determine at which hydraulic parameters would induce seepage and mass transport of dissolved gypsum to penetrate the full width of the dyke. Further analyses was needed in order to determine the seepage and dissolution rate that would make the foundation clay undersaturated with gypsum, which would strengthen the claim that leaching of gypsum caused reduction in shear strength and strain softening in the unstable section of the dyke.

2.4 Effects of Fissures on the Behaviour of Clay

Previous reports indicate that the clay materials in the current research site where irregular movement occurred was often described as highly fissured, nuggetty, or crumbly in appearance. Cyclic freezing and thawing as well as wetting and drying cause repeated expansion and contraction in soils which leads to fissuring. Many stiff clays exists in its fissured state in core sections of zoned earth dams. It is possible that these fissures would develop during construction as embankment zones tend to form brittle layers between plastic layers that could develop localized cracks during deformation of the entire mass. The linking of pre-existing fissures and secondary cracks could potentially produce a failure surface (Vallejo, 1987; Vallejo and Shettima, 2019). Fissures tend to create planes with weaker strength and increased permeability which leads to degraded mechanical properties as compared to intact clays (Vitone et al., 2009). Though

easily detected in stiff clays in site investigations, fissures in soft clays tend to be only visible during soil sample extrusions or sample preparation prior to laboratory testing.

McGown and Radwan (1975) stated that fissures represent weak planes that have lower shear strength at which sliding would tend to initiate or occur. When subjected to further straining, fissured clay can also soften and could gradually have reduced cohesion. A study of the intensely fissured high plastic clays of Daunia, Italy by Cotecchia et al. (2007) revealed that intense fissuring caused an impoverishment of the mechanical properties (Cotecchia et al., 2007; Vitone et al., 2009; Vitone and Cotecchia, 2011). This implied that the use of peak shear strengths are not recommended in design for intensely fissured clays. Skempton and Hutchinson (1969) investigated the effects of fissures on the stability of natural slopes in overconsolidated London clay. The study determined that reduction in shear strength occurs as the degree and area of softening increases during shear straining. At fully softened conditions, highly consolidated fissured clays would be equivalent to normally consolidated clays.

Bishop (1965) summarized the typical characteristics of the shear strength behaviour overconsolidated fissured clays. Results from comprehensive tests done on London clay samples indicated that at low to medium stress levels, stress-strain curve results show brittle behaviour. Tested samples behaved in a ductile manner as the applied effective confining pressure was increased. Bjerrum (1969) reported that laboratory tests on small fissured clay samples would only measure their intact strength and not necessarily representing its field strength. Bjerrum suggested using a correction applied to the laboratory strength results by using the calculated friction angle but using a cohesion intercept value which is close to zero. Using a reduced cohesion value would represent the weakening of the intact clay samples due to fissures (Mesri and Adbel-Ghaffar, 1993; Gu et al., 1993). This was recommended for tested fissured clay samples at shallow depths that has experienced non-uniform straining due to repeated weathering and fluctuations in groundwater.

Stark and Eid (1997) analyzed field case histories of first-time slide in stiff fissured clays with a liquid limit range of 50% to 130%. For first-time slides, the mobilized shear strength may be as low as the average between the post peak or critical state and residual shear strengths (Figure 2.2). A possible explanation to this behaviour is that when the soil mass has reached the fully softened shear strength, progressive failure would tend to reduce the average shear along the failure surface to a value between the fully softened and residual shear strengths. Displacements preceding first-time slides can cause progressive failures which would reduce mobilized strength toward fully softened but not sufficient to reach residual conditions (Mesri and Shahien, 2003; Potts et al., 1997). Skempton (1985) found that for soils with high clay fraction of more than forty percent, the shear strength of clay could decrease from a fully softened value to about the average of fully softened and residual strengths in less than 15 mm of displacement. This somewhat explained why the mobilized shear strengths from the case history analysis of Stark and Eid (1997) were close to the average shear strength (of fully softened and residual) values.

Alfaro III (2016) was part of the current study and performed GeoStudio numerical models that focused on the effect of fissures in CBBD2. Using soil parameters attained from laboratory tests on collected soil samples, numerical models were completed to evaluate the stability of stable (Section A-A) and unstable (Section B-B) sections of the said earth dam. Stress-deformation distribution determined from finite element method analysis and seepage conditions from SIGMA/W and SEEP/W, respectively, were imported into SLOPE/W in order to determine the factor of safety of the chosen sections using limit equilibrium method of analysis.

Post peak shear strengths were considered in the slope stability analyses with the understanding that the clay materials have reached its fully softened state after a service period of more than 50 years. Results from stress-deformation analyses of CBBD2 show that the clay foundation dry side in stable section (Section A-A) yielded while the upper part of the clay blanket

on the wet side of unstable section (Section B-B) yielded. To consider that only part of the clay materials have yielded, the use of the average of fully softened strength and residual strength was accommodated in the analysis. This led to the formulation of three cases of slope stability analyses by Alfaro III in 2016 using: (a) fully softened strength for all clay materials; (b) the average of the fully softened and residual shear strength on only the clay blanket and clay foundation; and, (c) the average of the fully softened strength and the residual strength in all clay materials.

The safety factors generated from the SLOPE/W slope stability analyses from all three cases revealed similar results when performed in both stable and unstable sections. The calculated factor of safety using fully softened conditions of the clay materials had values of above unity for both sections. When yielding of the clay foundation and clay blanket were considered, both sections were at incipient failure with factors of safety of unity.

2.5 Time-dependent Creep Deformation

Time-dependent deformations are important in analyzing geotechnical structures in cases where long term behaviour is of interest. The time-dependence of soil properties is often ignored which could lead to excessive deformation leading to failure or collapse with time (Campanella and Vaid, 1974). Investigation of creep in soils is essential in order to have better means of predicting in-situ creep behaviour and possibly reduce, if not avoid, prolonged deformations that can result to instability or failure.

Time-dependent settlement in soils have two categories: primary consolidation and secondary compression. Primary consolidation results from the change in vertical effective stress due to the gradual dissipation of excess pore water pressures within the soil. Secondary compression, also known as creep, is a time-dependent deformation that occurs at constant

effective stress. There are two theories with regards to the occurrence of creep: first, a soil layer will not undergo secondary compression until it has completed primary consolidation; secondly, creep would occur simultaneously with primary consolidation.

Displacement investigation is important for geotechnical structures that expect large primary settlements such as in embankments founded on soft soils. However if creep would be a small percentage of the expected primary consolidation over the course of ten to thirty years, then it is imperative to include time-dependent settlement investigation in geotechnical structures as well. Large primary settlements of dams and embankments could be followed by significant creep movement in its later years of service. On the other hand, structures founded on initially overconsolidated soil could experience small primary settlements. However, a state of normal consolidation might be reached with respect to time and substantial creep might ensue. Such situation is seen as unsafe since creep was not preceded by a significant warning brought about by large primary settlements. Secondary compression also play a significant role in natural slopes as steep slopes could show continuous displacement and would have relatively lower factors of safety against stability. (Neher et al., 2001; Vermeer and Neher, 1999)

The time-dependent deformation behaviour of a soil could depend on several factors such as soil structure, stress history, drainage conditions, and changes in pressure and environment with time (Mitchell and Soga, 2005). Clayey soils under sustained constant pressure or self-weight usually exhibit creep behaviour in comparison with sandy materials. Soils with high clay content and high activity increases the effect of creep. In addition, creep tends to be of importance as the water content increases.

Normally consolidated soils tend to exhibit larger creep than overconsolidated soils. At low stress levels, creep may appear to cease or continue at an imperceptible rate after an extensive amount of elapsed time. At higher stress levels, the creep rate might start to accelerate after an elapsed time and lead to rupture. Normally consolidated clays on creep loading under fully or

partial drained conditions undergo a decrease in volume then a strength gain with time which would not experience creep failure. On the other hand, normally consolidated clays on creep loading under undrained conditions would have already ruptured at a lower constant stress (Campanella and Vaid, 1974). Heavily overconsolidated clays under drained conditions are also prone to creep failure due to softening connected with the increase in water by dilation and swelling (Mitchell and Soga, 2005).

Creep of clayey soil can be investigated by performing laboratory tests such as the conventional incremental loading oedometer test (creep in compression) and triaxial creep tests (creep in shear). Creep can be described based on the stress-strain-time behaviour of the tested samples. According to the strain-time curve, creep can divided into primary, secondary, and tertiary phases. After being subjected to a constant stress, the creep process is characterized by decreasing strain rate (primary phase) followed by constant strain rate (secondary phase) and finally increasing strain rate (tertiary phase) leading to failure (creep rupture).

Creep behaviour from oedometer (or one-dimensional consolidation) tests usually only consists of the primary and secondary creep phases as deformation tend to stabilize under a constant load with respect to time. Samples investigated using triaxial creep tests may or may not consist of all three phases and would depend on the applied stress or shear mobilization. The applied stress is typically taken as a percentage of the peak shear strength determined from standard triaxial compression tests. If the applied stress is low then only primary creep will take place. After crossing a certain level of shear mobilization, the primary phase will be followed by the secondary phase and could lead to the tertiary phase and creep failure (Havel, 2004). The shear mobilization level is taken as the percentage of the shear stress at which the soil has failed. A suggested initial shear mobilization value of 0.5 to 0.6 (corresponding to 50 to 60% of the shear stress at failure) could be used. The shear mobilization value in order to attain creep rupture tend to vary depending on the clay material and drainage conditions (Campanella and Vaid, 1974;

Havel, 2004; Shrestha, 2015; Tavenas et al., 1978; Ye et al., 2013). Creep failure happens when the accumulated creep strain reaches shear strain corresponding to the peak stress from typical triaxial test, regardless of the stress level (Singh and Mitchell, 1969; Hunter and Khalili, 2000; Bi et al., 2019).

The response of soil undergoing creep in compression can be seen in Figure 2.3. Consider a normally consolidated soil which is loaded from an initial p'_0 to p' for a certain time. As soil creeps under constant stress p' after an increment of time, deformation occurs. The total resulting volumetric strain is a combination of reversible elastic strain (ε_{vc}^{e}) and time-dependent creep (ε_{v}^{cr}) strains. The elastic volumetric strain is a function of the unload-reload line (URL). Volumetric creep strain comprises of creep strain during consolidation (ε_{vc}^{cr}) which is a function of the normal consolidation line (NCL) and creep strain after consolidation (ε_{vac}^{cr}) which is a function of secondary compression and time. This follows the theory that creep (or secondary compression) occurs simultaneously with consolidation. When soil creeps under constant load, void ratio decreases and the change of void ratio decreases over time. The overconsoldation ratio also changes during soil creep as the preconsolidation stress increases with respect to time. It can be inferred that creep rate decreases with respect to time (Den Haan, 1994) as the overconsolidation ratio increases. The creep rate is highest for normally consolidated soil. Such behaviour of volumetric creep can be seen in soils undergoing one-dimensional consolidation wherein lateral expansion is inhibited.

Deviatoric creep occurs when time-dependent shear deformation is caused by constant deviatoric stress. Deviatoric strains typically occur simultaneously with volumetric strains in triaxial creep tests (where lateral expansion is not restrained) and it could be complicated to analyze these plastic strains separately. Unlike volumetric creep, it is possible that deviatoric creep can lead to failure under certain conditions. The challenge in trying to study deviatoric creep is to ensure that an adequate shear mobilization value is applied in order for shear deformation to

occur at a constant state of stress. Failure can be expected under undrained conditions where the increase in volumetric creep strain with the increase in excess pore pressure would decrease the effective confining stress (Stolle et al., 1997). A continuous reduction in the effective confining stress will eventually lead to creep rupture.

Skempton (1977) compiled case histories of delayed failures of cut slopes in brown London clay. London clay is similar to CB clay as it is also stiff, fissured, and highly plastic. As the failures from the compiled case histories occurred in the same clay formation, it was assumed that the rate of pore pressure dissipation and the creep behaviour are identical. Leonards (1979) pointed out the relationship between slope inclination, slope heights, and time of failure which is seen in Figure 2.4. The figure provided a simple basis for the design of slopes in brown London clay wherein a 1.5/1 slope would be stable for 3 years at a height in excess of 10 m and a 4/1 slope would be stable for a very long time. Figure 2.5 shows the relation between the rate of creep deformation and creep rupture life of clay based on more case histories of delayed failure representing a wider variety of clays from stiff clays from England, Belgium, and South Africa; firm clays from Canada; very soft clay from the south of France; and slope failures in Japan. The broken lines in the figure indicate the limits from laboratory data. Both Figures Figure 2.4 and Figure 2.5 indicate that the observation of creep deformation in slopes can be considered as a means of assessing the time to slope failure.

Under creep, fissures within the clay could slowly propagate and induce delayed slope failure. Vallejo and Shettima (2017) revealed that fissures in stiff clay propagated during creep at 60% of monotonically increased uniaxial compressive failure stress. It is then reasonable to assume that fissures will propagate and lead to failure at a lower stress under creep. Observations of creep deformations could then be used as an indicator of incipient failure.

Bi et al. (2019) conducted unconsolidated undrained (UU) triaxial creep tests until creep failure. They also conducted a series of UU triaxial tests at constant strain rate following ASTM

standards. This allowed them to compare the soil behaviour of two different testing conditions, such that with and without creep. Bi et al. (2019) considered the inverse of the percentages of mobilized shear stress relative to maximum shear stress (such that percent of the maximum shear stress) as the factor of safety against failure. Through case histories of slope failures and creep modelling, they found longer time to creep failure at high factors of safety. Their results implied that a factor of safety higher than 1.3 would be needed in order to avoid long-term creep rupture; and a safety factor of 2.0 would imply low creep movements with low risk of rupture due to creep. Their findings gave an insight on how to interpret factor of safety values in terms of long-term creep deformations.

2.6 Numerical Modelling

The advancement in technology and increase in knowledge along with the motivation of researchers and developers led to the generation of various computer programs that can perform complicated analysis of geotechnical problems. There are several commercially available computer programs that incorporate creep. PLAXIS 2D (PLAXIS, 2018) is one of them.

2.6.1 Modified Cam-Clay Model

The Modified Cam-Clay (MCC) model if often described in numerous literature on critical state soil mechanics such as Muir Wood (1990). In MCC, there is an assumed logarithmic relation between the void ratio, *e*, and the mean effective stress, *p'*, in virgin isotropic compression, which is formulated as

$$e - e^0 = -\lambda ln\left(\frac{p'}{p'^0}\right) \qquad (Equation\ 2.1)$$

where: λ is the Cam-Clay isotropic compression index that determines the soil compressibility in primary loading, and e^0 and p'^0 are the initial void ratio and initial mean effective stress, respectively. And during unloading and reloading, it is formulated as

$$e - e^0 = -\kappa ln\left(\frac{p'}{p'^0}\right) \qquad (Equation\ 2.2)$$

where the parameter κ is the Cam-Clay isotropic swelling index that determines the compressibility of the soil under unloading and reloading.

The yield surface of the MCC model forms an elliptical curve in the mean effective stress – deviatoric stress (p' – q) plane and the yield function is defined as

$$f = \frac{q^2}{M^2} + p'(p' - p'_p) \qquad (Equation\ 2.3)$$

where M is the slope of the critical state line (CSL) and p'_p is the preconsolidation stress. The CSL gives the relation between q and p' in a state of failure. The yield surface (f = 0) is the boundary of elastic stress states and stress paths within this boundary would give elastic strain increments. Stress paths crossing this boundary would give both elastic and plastic strain increments.

Some soil models in PLAXIS 2D, such as the Soft Soil Creep model, has adopted the MCC yield surface and yield function. The aforementioned soil model will be discussed further in the next section.

2.6.2 Soft Soil Creep Model

The Soft Soil Creep (SSC) model implemented in PLAXIS 2D is an extension of the pre-existing Soft Soil (SS) model. It was developed by transforming the logarithmic creep law for secondary consolidation into a differential form and extending it towards general three-dimensional states of stress and strain by incorporating concepts of Modified Cam-Clay and viscoplasticity, with a Mohr-Coulomb failure criteria. A more detailed information on the

formulation of the model is discussed in the paper written Vermeer and Neher (1999). The yield surface adapted from the MCC model, as shown in Figure 2.6, shows a fixed Mohr-Coulomb failure line but the cap may increase in compression. The stress paths inside the boundary will produce elastic strains whereas stress paths that would cross the boundary would generally produce both elastic and plastic strains including creep. The equivalent preconsolidation stress (p_p^{eq}) is a function of plastic creep strain (ε_v^c) while p^{eq} is related to an actual stress state. The SSC model in PLAXIS 2D uses the following formulae:

$$p^{eq} = p' + \frac{q^2}{M^2(p' + c' \cot \varphi')} \qquad (Equation\ 2.4)$$

$$M = \frac{6 \sin \varphi'}{3 - \sin \varphi'} \qquad (Equation\ 2.5)$$

$$p_p^{eq} = p_{p0}^{eq} exp\left(\frac{\varepsilon_v^c}{\lambda^* - \kappa^*}\right) \qquad (Equation\ 2.6)$$

$$\lambda^* = \frac{C_c}{2.3(1+e)} \quad , \quad \kappa^* = \frac{2C_r}{2.3(1+e)} \qquad (Equation\ 2.7)$$

where: *c'* and *φ'* are the cohesion and friction angle of the soil used to define its shear strength with a Mohr-Coulomb criterion, *λ** is the modified compression index related to the compression index (C_c), *κ** is the modified swelling index related to the recompression index (C_r), and *e* is the void ratio. The subscript "$_0$" indicates the initial condition when time and creep volumetric strain are zero. A "threshold ellipse" with a minimum p^{eq} value of $c' cot \varphi'$ ensures that the cap will remain in the compression zone. If cohesion is zero, then the minimum p^{eq} value of a stress unit is used.

PLAXIS indicated that the required parameters for the SSC model can be determined from either a standard oedometer test or triaxial compression creep test provided that the duration of the applied constant stress is sufficient for secondary compression to occur. PLAXIS also allowed

Rocscience to include the SSC model as an extension option in its software bundle (Rocscience, 2019), allowing more engineers and researches to have access to this time-dependent analysis.

The SSC model was used to simulate the undrained triaxial creep behaviour of Haney clay and the results were compared with the findings of Vaid and Campanella (1977). Material parameters used were from Matsui and Abe (1988). Samples were consolidated under the same confining stress then undrained samples were loaded with different deviatoric stresses. Simulations indicate that the SSC model compared well with the experimental data. Other studies (Van Baars, 2003; Havel, 2004) have also simulated triaxial creep tests (under drained or undrained condition) as well as one-dimensional oedometer consolidation tests and found that the simulations were in good agreement with the laboratory test results.

Analyzed data from the Soft Soil Creep model was also verified with field measurements of instrumented geotechnical structures. A case study of a test embankment near an interstate highway founded on Boston blue clay was performed by Fatahi et al. (2013). The test embankment had installed instrumentations such as piezometers, settlement rods, and inclinometers and was frequently monitored. The recorded data was compared with the performed SSC analyses. It was observed that the SSC model can predict the ground settlement more precisely below the embankment crest and that the location of the maximum lateral displacement was predicted reasonably well.

Neher et al. (2001) also compared field measurements taken from another test embankment founded on Boston blue clay with SSC model results. An elapsed time of about 2000 days (about five and a half years) was used. Findings indicate that the SSC model slightly overestimated the displacements and pore water pressures. Neher et al. (2001) performed another simulation in a test embankment 25 km west of Stockhom that was founded on soft clay on top of till or rock. The fill was instrumented with piezometers and settlement markers with recorded data for 20 years. Results indicated that SSC model and the measured data agree fairly

well and that simulations using the Soft Soil (SS) model demonstrated that the settlements, horizontal displacements, and pore pressures were strongly underestimated. It was also observed that in overconsolidated soil layers, both SSC and SS model results behaved similarly with the field data but the SSC model faired better as the SS model underestimates deformations and pore pressures in normally consolidated soil layers.

The Terlicko Dam in the Czech Republic was investigated for creep behaviour as a continuous uplift of the right-hand slope hillside together with the dam has been observed for about twelve years. The study of the in-situ behaviour of the dam was performed by Havel (2004) using the PLAXIS SSC soil model. The result of this study validated that the inclusion of the time-dependent behaviour with the use of PLAXIS SSC soil model greatly aided in determining the plausible cause of the observed movement of the dam. With the aid of the simulations from PLAXIS, Havel and his research team was able to provide significant information to the local authorities and suggested reasonable solutions to the observed problem.

2.7 Summary of Reviewed Literature and Justification of Research

Previous geotechnical reports provided by the dam operator and owner were on CB Generating Station since it was the primary focus of the investigation as the instability occurred in one of the earth dams (CBBD2) in this location. Information on the expected soil properties were given for each earth dam to be studied in this area. The clay soil was characterized as Fat Clay and was often described as highly plastic, fissured, and with blocky structure. A notable observation from the field investigations done in the CB earth dams is that CBBD2 had crest and core elevations that were below the design values. As the last recorded measurements from instrumentation was reported in 2010, there was insufficient information with regards to whether this settlement has continued or ceased.

The reviewed investigation reports were performed prior to the occurrence of the instability. Due to this, there is a need to conduct a more current field investigation that would include soil sampling, instrumentation, and laboratory testing. This would provide an update about current conditions the earth fill water-retaining dams as well as provide updated information that could be used to further examination as to the cause of instability in CBBD2.

The clay materials in CB was often compared to the foundation clay of the Seven Sisters and Red River dykes. The investigation in 2010 stated that although the dam configurations and condition of the clay foundation may be different in CB, Red River, and Seven Sisters, the clay material properties are likely similar. With this, the previous studies done in the Seven Sisters and Red River dykes can be utilized as a guideline in the initial analysis of the CB earth dams.

The water retention dykes of the Seven Sisters Generating Station has experienced irregular instabilities at the dry side of the dykes since it was heightened. Investigations indicated that leaching of gypsum from the foundation clay possibly due to seepage from the forebay caused the reduction in shear strength and strain softening in the unstable section of the dyke. Visible gypsum nodules were found at the background clay samples and SEM analysis also indicated that gypsum particles were more pronounced in the background clay samples as compared to the stable and unstable clay foundation samples. Because of the similarities in soil properties with Seven Sisters dyke clay foundations, it is plausible that clay materials in CB could also have gypsum streaks or nodules. Visual inspections for gypsum must be done on a background source by means of excavated test pits or undisturbed soil sampling. Results should be compared with the dam foundation clay. SEM analysis can also be performed on extruded soil samples for the same purpose.

The previous study done by Alfaro III (2016), as part of the current investigation, focused on the effect of fissures on CBBD2. Post peak shear strengths were used in the limit equilibrium method of stability analyses with the understanding that the clay materials have reached its fully

softened state after 50 years. The resulting factor of safety using post peak strengths show values greater than unity for both stable and unstable sections. If the average of post peak and residual shear strengths of all clay soils were used, both sections generated factor of safety values of less than unity. These results suggest that further analysis should still be done to determine the conditions that would induce instability only to the unstable section.

Previous numerical modelling results of CB earth dams using limit equilibrium method (LEM) were reported to be stable but was not able to meet the criteria for the required load cases during the 1999 and 2010 geotechnical investigations. These dams would be re-evaluated using finite element method (FEM) analysis in PLAXIS 2D. The deformation analysis of the structure with respect to time will also be taken into account. Input parameters would be taken from updated laboratory test data performed on undisturbed clay samples.

Studies on time-dependent creep behaviour has increased over the years as a number of geotechnical problems involve application of sustained loads. Yet despite the importance of analyzing time-dependent deformation, most practicing engineers tend to focus on stability and forego long-term deformation development assessments. One reason could be that most commercially available geotechnical engineering software have yet to implement a soil constitutive model that considers creep to evaluate long-term performance. Another reason is the notion that advanced soil model would pose a challenge in finding the information needed for the model parameters. PLAXIS software adopted the Soft Soil Creep (SSC) model that incorporates the time-dependent settlement process in the analysis of geotechnical engineering problems. The model uses parameters that can be determined typically from long-term incremental loading oedometer tests. Creep parameters from triaxial creep tests will also be compared to parameters from oedometer tests for any significant difference and possible effect in the deformation development of the numerical model using SSC. In addition, further information would be attained from shear creep tests in terms of long-term failure due to creep rupture.

Despite the claim of previous investigation reports that creep settlement would not be an issue due to the satisfactory performance of the earth dams for over fifty years, the observed displacement beyond forty years of service and occurrence of the sudden movement in CBBD2 indicated otherwise. The SSC model can be used in the numerical modelling of both Sections A-A and B-B to determine whether time-dependent behaviour is related to the irregular movement in CBBD2.

As most of the recently gathered information are related to CBBD2, the findings from this earth dam will be applied in the analysis of the remaining earth dams in CB, WD, EF, and MF. Any insight to the cause of the irregular movement will be used to evaluate long-term performances of other aging earth filled water-retaining dams so that proactive measures could be planned and implemented should the performance not meet current dam safety standards.

Table 2.1 Summary of index properties for clay foundation materials at CB Generating Station, Seven Sisters Dykes, and Red River Dyke (Hatch, 2010)

Foundation Clay		Water Content	Liquid Limit	Plastic Limit	Wet Unit Weight
		(%)	(%)	(%)	(kN/m^3)
CB Generating Station	Range	24.2 to 46.3	79 to 99	30 to 35	17.3 to 18.2
	Average	37.3	91	33	17.9
Seven Sisters Dykes	Range	30 to 61	65 to 120	22 to 40	15.7 to 18.4
	Average	48	97	30	16.5
Red River Dyke	Range	19 to 61	62 to 102	22 to 27	15.9 to 18.9
	Average	47	87	24	16.5

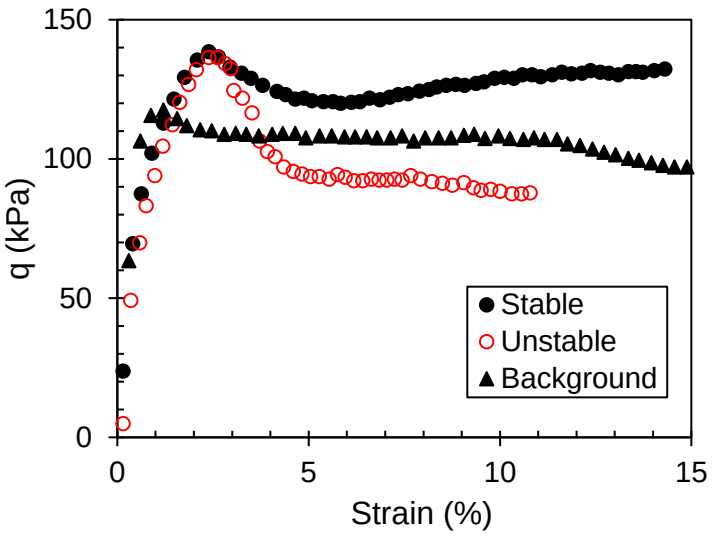

Figure 2.1 Deviatoric stress – strain behaviour of stable, unstable, and background clay samples from triaxial test results (Republished with permission of Canadian Science Publishing, from Instability of dykes at Seven Sisters Generating Station, Garinger, et al., 41, 5, 2004; permission conveyed through Copyright Clearance Center, Inc.)

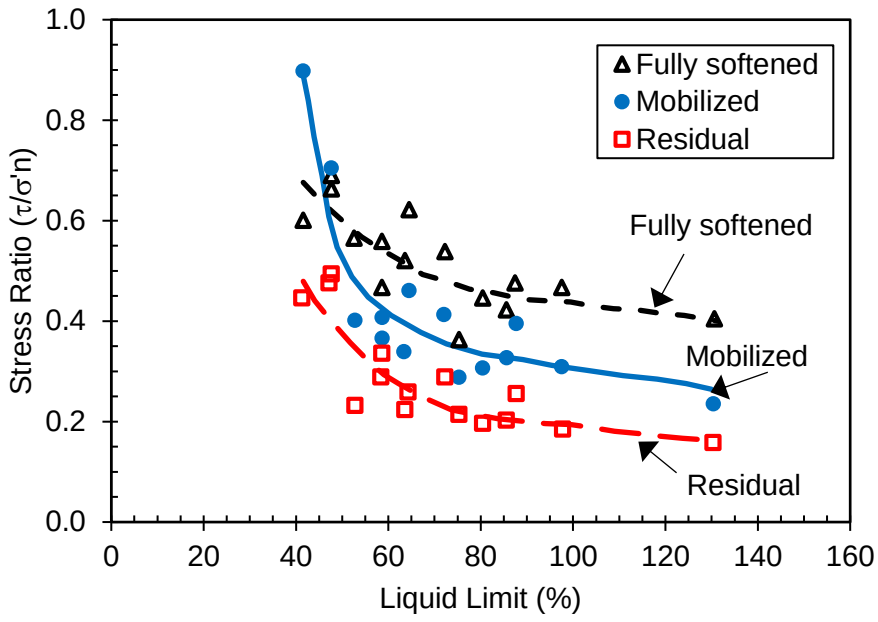

Figure 2.2 Fully softened, mobilized, and residual stress ratios from field case histories (Stark and Eid, 1997; With permission from ASCE)

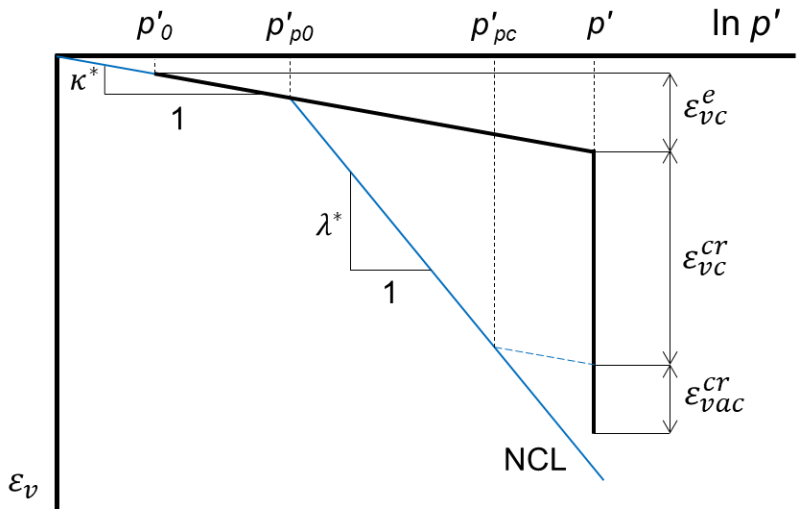

Figure 2.3 Mean effective stress and volumetric strain during creep (Neher et al., 2001; Reproduced with permission of Informa UK LImited through PLSclear)

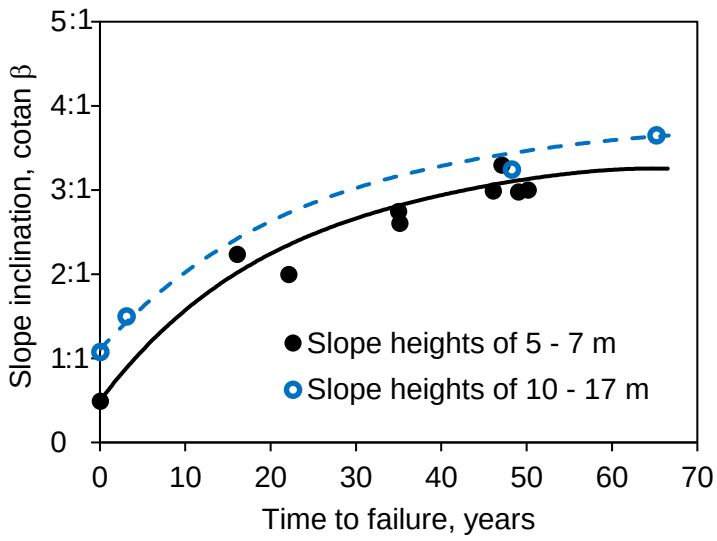

Figure 2.4 Relationship between slope inclination, slope height, and time to failure for London clay in cut slopes (Republished with permission of Canadian Science Publishing, from Creep and failure of slopes in clays, Tavenas and Leroueil, 18, 1, 1981; permission conveyed through Copyright Clearance Center, Inc.)

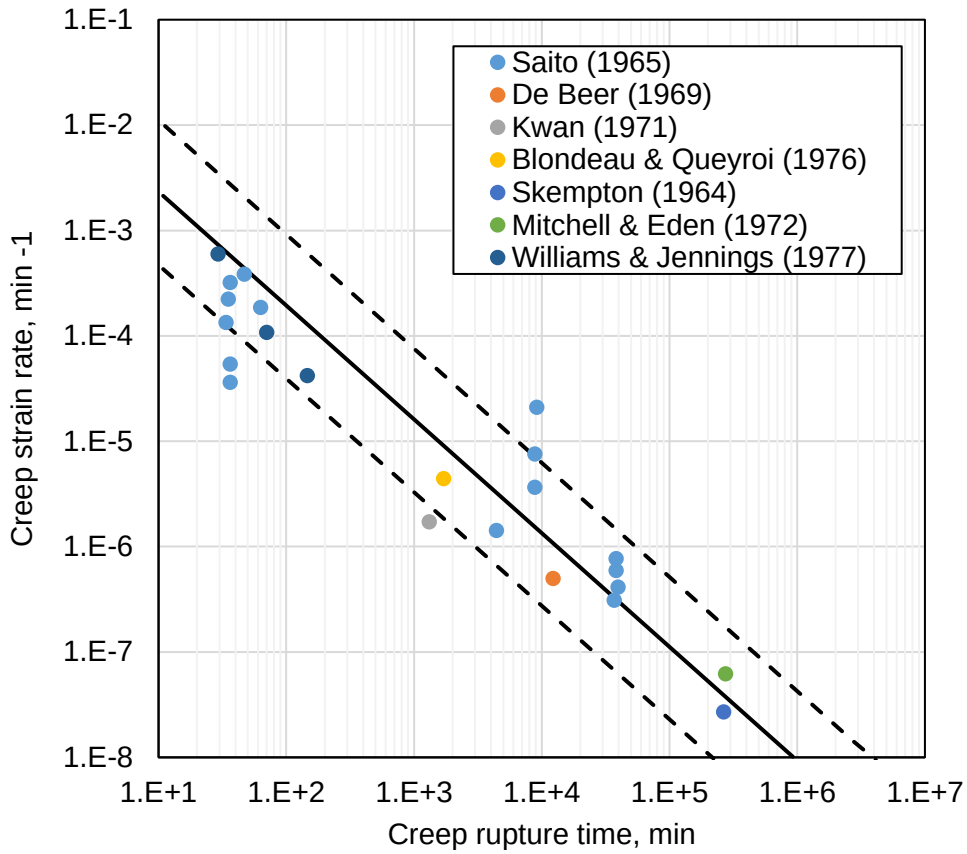

Figure 2.5 Relationship between creep strain rates and time to failure based on case histories (Republished with permission of Canadian Science Publishing, from Creep and failure of slopes in clays, Tavenas and Leroueil, 18, 1, 1981; permission conveyed through Copyright Clearance Center, Inc.)

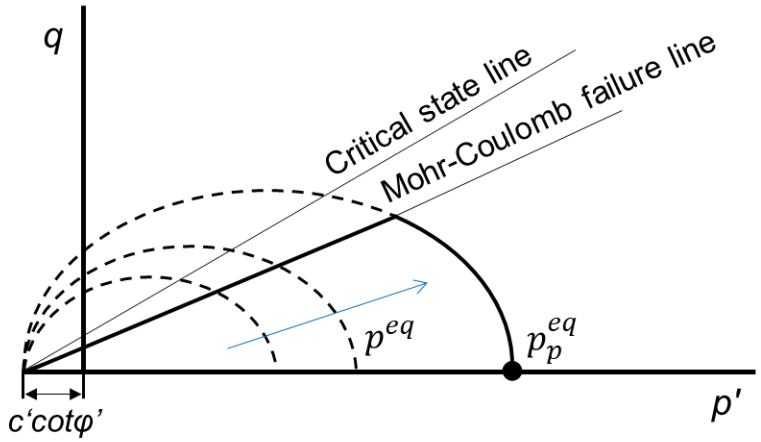

Figure 2.6 Yield surfaces of the SSC model in the p'-q plane

Chapter 3 SITE INVESTIGATION

Field investigation was conducted to gather site characterization information. Soil sampling programmes were developed based on previous investigations done on CB, WD, EF, and MF generating station earth fill dams. Instrumentation such as vibrating wire piezometers were installed to monitor the pore water pressure within the dams and downstream foundation. Site investigation, soil sampling, and instrumentation installation were conducted in accordance with the American Society for Testing and Materials (ASTM) standards.

3.1 Soil Sampling

Three separate drilling and soil sampling programs were carried out in order to complete all seven earth fill dam sites. Soil samples from the clay core, foundation clay, and clay blanket (where available) were obtained from predetermined borehole and test pit locations. The soil sampling programs were conducted with the guidance and expertise of the personnel from Maple Leaf Drilling Ltd. Collected field samples were sealed with paraffin wax in order to prevent moisture loss and properly transport them without further disturbance. Samples were stored in the temperature-controlled storage chamber of the Geotechnical Engineering Laboratory of University of Manitoba.

3.1.1 On-shore soil sampling

On-shore undisturbed soil sampling was done during the fall season of 2015 (for CB generating station earth dams) and summer of 2016 (for WD, EF, and MF generating station earth dams) when the ground was still unfrozen. Continuous soil sampling of the clay core and clay foundation were retrieved in 102 mm (4 in) Shelby tubes with the use of a track-mounted Hollow Stem Auger (HSA). The use of a larger diameter Shelby tube,

than the typical 76.2 mm (3 in) tube, was implemented in order to obtain a better representation of fissures in the collected soil samples (Vallejo, 1989). To collect undisturbed clay core samples, coring through riprap and rockfill was necessary. Sampling was only done until a certain depth within the clay core (not reaching refusal) so as not to potentially create preferential flow paths for water through the clay core of the aging dam. As for samples taken from the clay foundation at the downstream section of the dam, boreholes were advanced until refusal. All boreholes were sealed with cement-bentonite grout covered with bentonite chips until the ground surface.

Out of a total of thirty five on-shore boreholes, eight boreholes were drilled in CBBD2: From the five drilled at the dam crest, two were located at Section A-A and the rest at Section B-B. Two boreholes were drilled at the downstream toe of Section A-A as this was the only section with clay foundation (to be further discussed in Section 3.3.1). One borehole was located at the toe of Section B-B where a vibrating wire piezometer to monitor pore water pressure was installed and was not sampled. The estimated locations of these boreholes can be seen in Figure 3.1. A summary of the on-shore boreholes for the other dams can be seen in Table 3.1 with its estimated locations in Figures 3.2 to 3.7.

3.1.2 Off-shore soil sampling

Off-shore undisturbed soil sampling could only be done during the winter season of 2016 when the reservoir was adequately frozen in order to safely collect clay blanket samples in CBBD2 and CBBD4. Drilling and sampling could only proceed safely if the reservoir was frozen with about 40 to 46 cm (16 to 18 inches) of blue ice thickness or its equivalent in white ice. A track mounted drill rig with a 76.2 mm (3 in) piston tube sampler retrieved clay blanket samples underneath the frozen reservoir. A smaller diameter Shelby tube, as compared to the ones used for on-shore soil sampling, was used as the clay blanket was believed to be less fissured. A smaller drill rig in CBBD4 as the thickness of

ice was thinner at this location (at least 35 cm or 14 inches of blue ice or its equivalent white ice thickness) and would not be able to safely support the rig that was used in CBBD2. Professional divers were hired in order to ensure that the drilling locations underwater were free from debris in order to not further disturb the clay blanket, whether it was natural clay or placed. Once drilling was completed, the divers also aided in guaranteeing that the boreholes were properly and completely backfilled with bentonite grout or bentonite pellets topped with bentonite chips and sand to seal the holes.

Twenty-seven off-shore boreholes were drilled in total. Twenty-one boreholes were located at CBBD2: sixteen at Section B-B and five at Section A-A. Majority of the off-shore boreholes in CBBD2 Section B-B were close to the location of the scarp as seen in Figure 3.1. The remaining six from the total drilled off-shore boreholes were located at CBBD4 (Figure 3.2). A summary of the off-shore boreholes can be also be seen in Table 3.1.

3.1.3 Test pit excavation

Test pits were excavated at locations where possible using a Caterpillar wheel excavator operated by Maple Leaf Drilling Ltd. Observations can be made from these test pits with regards to fissures as well as notable gypsum inclusions in the soil layers, if any. The excavator bucket was used to push the 102 mm (4 in) Shelby tubes vertically into the test pit floor in order to obtain soil samples. This was done at different depths. Once sampling was done, test pits were backfilled with spoils, relevelled, and compacted.

At CBBD2, inclined soil samples were also collected (in addition to the vertical samples) by pushing the Shelby tubes into the test pit wall at a 53° with respect to the horizontal (Figure 3.8). The vertical and inclined soil samples determined the cross shear and horizontal shear strength of the clay foundation, respectively, and results were presented by Alfaro III (2016) in his study. Block soil samples were only obtained in

CBBD2 by pushing a block sampler (23 cm by 23 cm wide and 25 cm deep) at different depths as seen in Figure 3.9. Conventional block samples were also obtained from the said dam. Conventional block sampling (Figure 3.10) was done without the use of a mold or a block sampler. This soil block is manually excavated and waxed on site. Once sampling was done, test pits were backfilled with spoils, relevelled, and compacted. The aforementioned sampling methods were only carried out in two test pit locations in CBBD2 Section A-A. Another test pit was excavated in a location further downstream from CBBD2 (not indicated in Figure 3.1). This location was chosen as it has not experienced any dam loading and could provide additional information with regards to the foundation soil. Vertical Shelby tubes samples were only taken from this location.

Four other test pits were excavated near the downstream toe of CBBD4, WD, and EF with one excavated on the crest in CBBD4. Only vertical Shelby tube samples were taken from these locations. The estimated locations for the excavated test pits from the seven earth dams can be seen in Figures 3.1 to 3.7

3.2 Instrumentation

Vibrating wire (VW) piezometers were installed in the crest and toe of the selected earth dams in order to monitor pore water pressure. Installations were done in accordance to the manual provided by RST Instruments Ltd. Every VW piezometers installed were fully-grouted throughout the entire installation length. Nested piezometers were installed in some locations in order to verify the groundwater flow and gradient. These were mostly placed between the clay core and downstream filter, should there be any differential piezometric level. Information from the piezometers were collected via single channel data loggers although some in CBBD2 were connected to an automatic data collection system. Data acquisition is currently managed by the dam operators.

Thirty four VW piezometers were installed in total and were completed alongside on-shore borehole drilling and sampling activities. Twenty one were installed in the clay core from the crest, and thirteen were installed in the downstream side of the dam. A summary of the installed piezometers can be seen in Table 3.1. The estimated locations of the instrumentations per earth dam can be seen in Figures 3.1 to 3.7.

3.3 Subsurface Characterization

The stratigraphic boundaries inferred from the soil sampled during drilling were intended to signify a transition from one geological unit to another. These descriptions were not necessarily an exact plane of geological change. The actual stratigraphic sequence of the soil material between the drilled boreholes may differ from those deduced from the information obtained from drilling. Soil characterization of the clay samples were mostly done after the samples were extruded in the laboratory and during sample preparation for strength testing as on-site soil stratigraphy identification was not possible based on the drilling method used. Borehole logs can be seen in Appendix A.

3.3.1 CBBD2

The embankment core material used for CBBD2 generally consists of silty clay fill with matted texture, contains trace random silt lenses and silt pockets. The samples of the silty clay fill material recovered during drilling were moist, mottled mix of brown and grey in color, medium to stiff, and exhibited high plasticity. No traces of visible gypsum were seen at the bottom of Shelby tube samples as well as from inspected trimmings taken from the drilling auger.

The clay blanket material used for CBBD2 Section B-B generally consisted of silty clay with matted texture. The samples of the silty clay blanket material recovered during drilling were moist, the upper 0.6 m were brown in color and was soft to medium in

consistency; at depths 0.6 m and below, the clay blanket were mottled mix of brown and grey in color and was stiff to very stiff in consistency. The clay blanket material exhibited high plasticity. Similar to the clay core samples, gypsum crystals were not observed in auger trimmings. Underlying the clay blanket is a bedrock knob at location near the mid-length of the dam and a very dense silty fine sand in the rest of the area (see Figure 3.11).

Natural clay exists at Section A-A of CBBD2 which extends from the upstream to the downstream side of the dam overlying a very dense fine sand (Figure 3.12). Soil stratigraphy identification was performed based on the test pit excavated at the downstream side of the dam. The top soil is moist, brown to black in color, medium to stiff in consistency, has medium to high plasticity, and is weathered with some organics and fine gravel. Underlying the top soil is a layer of silty clay layer, moist, weathered in nature, medium to stiff consistency, with trace of organics, random silt pockets, crumbly, and intensely fissured in nature (Figure 3.13). Underlying the natural clay is a very fine sand layer, contains trace organics, light grey in color, moist to wet. Standard Penetration Test (SPT) confirmed that this layer is dense in consistency. Ground water was observed to be seeping through from this layer and was detected to be at El. 311.78. At test pit locations, there were no traces of gypsum nodules were observed in any of the excavations. Further inspection in terms of Shelby tube sample extrusions and laboratory tests would be needed to determine if there were gypsum inclusions in CBBD2 clay. The presence of silt was more pronounced in clay foundation as compared to the other sampled locations in CBBD2 and was also prominent in the test pit that was further downstream from CBBD2 (Figure 3.14).

3.3.2 CBBD4

The clay core material generally consists of silty clay fill with matted texture and contained some random silt lenses and silt inclusions. The samples of the silty clay fill

material recovered during drilling were moist, mottled mix of brown and grey in color, medium to stiff, and exhibited high plasticity. It also had random traces of organics and small pebbles.

The foundation material generally consists of silty clay with matted texture and contained random silt inclusions. The samples of the silty clay material recovered during drilling were wet to moist, mottled mix of brown and grey in color, and was medium to stiff. Underlying silty clay is a layer of fine silty sand, light grey in color that became brown with depth, with traces of organics, and was moist to wet.

Collected clay blanket samples were not extruded nor tested as most of the samples were mostly disturbed during collection. The samples recovered during drilling were moist, mottled mix of brown and grey in color, moist, and stiff. Underlying the clay blanket is a layer of fine sand. It was brown in color, wet to moist with respect to depth and was dense at the bottom.

3.3.3 CBMD

Similar to CBBD4, the core generally consists of silty clay fill with matted texture and contained some random silt pockets and silt inclusions. The samples of the silty clay fill material recovered during drilling were moist, mottled mix of brown and grey in color, medium to stiff and exhibited high plasticity.

The silty clay foundation material recovered during drilling were moist, mottled mix of brown and grey in color. Underlying the silty clay is a layer of fine silty sand, light grey in color, with traces of organics, and is moist to dry at the bottom of the borehole.

3.3.4 WD

The clay core material consists generally of silty clay fill with matted texture and contained some random silt pockets and inclusions. The samples recovered during drilling

were moist, mottled mix of brown and grey in color, stiff to very stiff with depth and exhibited high plasticity.

The clay foundation generally consists of silty clay with matted texture and contained some random silt lenses. The samples were moist, mottled mix of dark brown and grey in color, and was medium to stiff. The clay exhibited high plasticity but appeared nuggetty towards the bottom of the borehole.

3.3.5 EF

The embankment fill material generally consists of silty clay fill with matted texture and contained some random traces of some organics. The recovered samples during drilling were moist, mottled mix of dark grey with some brown patches in color, soft to medium, plastic but becomes brittle with depth. Underlying the fill layer was moist grey silt and at some depth from the crest, sensitive fines were encountered. At the layer of sensitive fines, no value was recorded from the Standard Penetration Test as the split spoon moved through the layer under its own weight.

The foundation generally consists of silty clay with matted texture and contained some random traces of organics. The samples of the foundation material recovered during drilling were wet to moist, mottled mix of dark grey with brown patches in color, soft to medium, plastic but becomes brittle with depth. Underlying the thin foundation layer was moist grey silt. As the foundation samples were soft to medium, there was a tendency of the soil to slide out of the Shelby tube during sampling. Attempts to obtain downstream foundation samples using a Piston sampler only led to disturbed samples. As samples were attempted to be recovered via a Piston sampler, the soil tends to flow out of the tube.

Cracks (which were sealed) and undulations were observed along the crest at EF and were reported to dam owner. Site engineers indicated that these cracks and undulations were from rutting created by vehicles that frequent the earth dam. According

to them, these cracks were surficial and did not go beyond the blacktop depth along the dam crest.

3.3.6 MFLED

The core material generally consists of silty clay fill with matted texture that contained some random silt inclusions and traces of organic material. Recovered samples were moist, mottled mix of dark grey with dark brown in color, medium to stiff, and exhibited high plasticity.

The foundation soil was mostly silty sand. It was described as moist to wet having brown color at the top then grey with depth. It was described as wet and grey in color. Water was seen at around 0.6 m from the top in some of the downstream boreholes.

3.3.7 MFRED

The embankment core generally consists of silty clay fill with matted texture, contained some random silt inclusions, and some traces of small pebbles. Samples recovered during drilling were moist, mottled mix of dark grey with brown patches in color, medium to stiff, and exhibited high plasticity.

The foundation soil was mostly silty sand similar to MFLED. Water was seen at around 1.5 m from the top in some of the downstream boreholes.

3.4 Summary

Three separate drilling and soil sampling programmes were completed and covered all seven earth fill dams from four different generating stations. A total of thirty five on-shore boreholes, twenty seven off-shore borehole, and seven test pits were accomplished. Out of the thirty five on shore boreholes, nineteen were drilled at the dam crest and sixteen were drilled at

the downstream toe. The drilling and sampling operation were performed under the guidance and continuous supervision of Maple Leaf Drilling Ltd.

A total of thirty four RST vibrating wire (VW) piezometers were installed in the earth fill dam locations to monitor the pore water pressure. Twenty one were installed in the clay core from the crest, and thirteen were installed in the downstream side of the dam. Data acquisition was managed by the dam operators.

The clay found in CBBD2 was observed to have silt inclusions, highly plastic, and fissured. Visual inspection at test pits noted that silt was seen to be more pronounced in the foundation than the core or blanket locations. Test pit excavations also indicated that gypsum nodules or streaks were not observed in any of the examined locations. Further inspection in terms of Shelby tube sample extrusions and laboratory tests would be needed determine if there were gypsum inclusions in CBBD2 clay.

Similar to CBBD2, silty clay was also observed in the remaining earth dam sites. There were no visual indications of depressions, sinkholes, or misalignments in any of the sites. The earth dam at the EF generating station was a bit different from the other studied earth dams as the clay observed during drilling and sampling seem to have more silt content. In addition, cracks (which were sealed) and undulations were observed along the crest at EF and were reported to dam owner. Site engineers indicated that these cracks and undulations were from rutting created by vehicles that frequent the earth dam. Engineers stated that these cracks were surficial and did not go beyond the blacktop depth along the dam crest.

Table 3.1 Summary of installed piezometers, drilled boreholes, and excavated test pits per location

Location	Piezometers		Boreholes			Test Pits
	Crest	Toe	Core	Foundation	Blanket	
CBMD	2	2	3	3	--	--
CBBD2	6	4	5	3	21	3
CBBD4	3	1	3	2	6	2
WD	4	2	2	3	--	1
EF	2	2	2	2	--	1
MFLED	2	1	2	2	--	--
MFRED	2	1	2	1	--	--

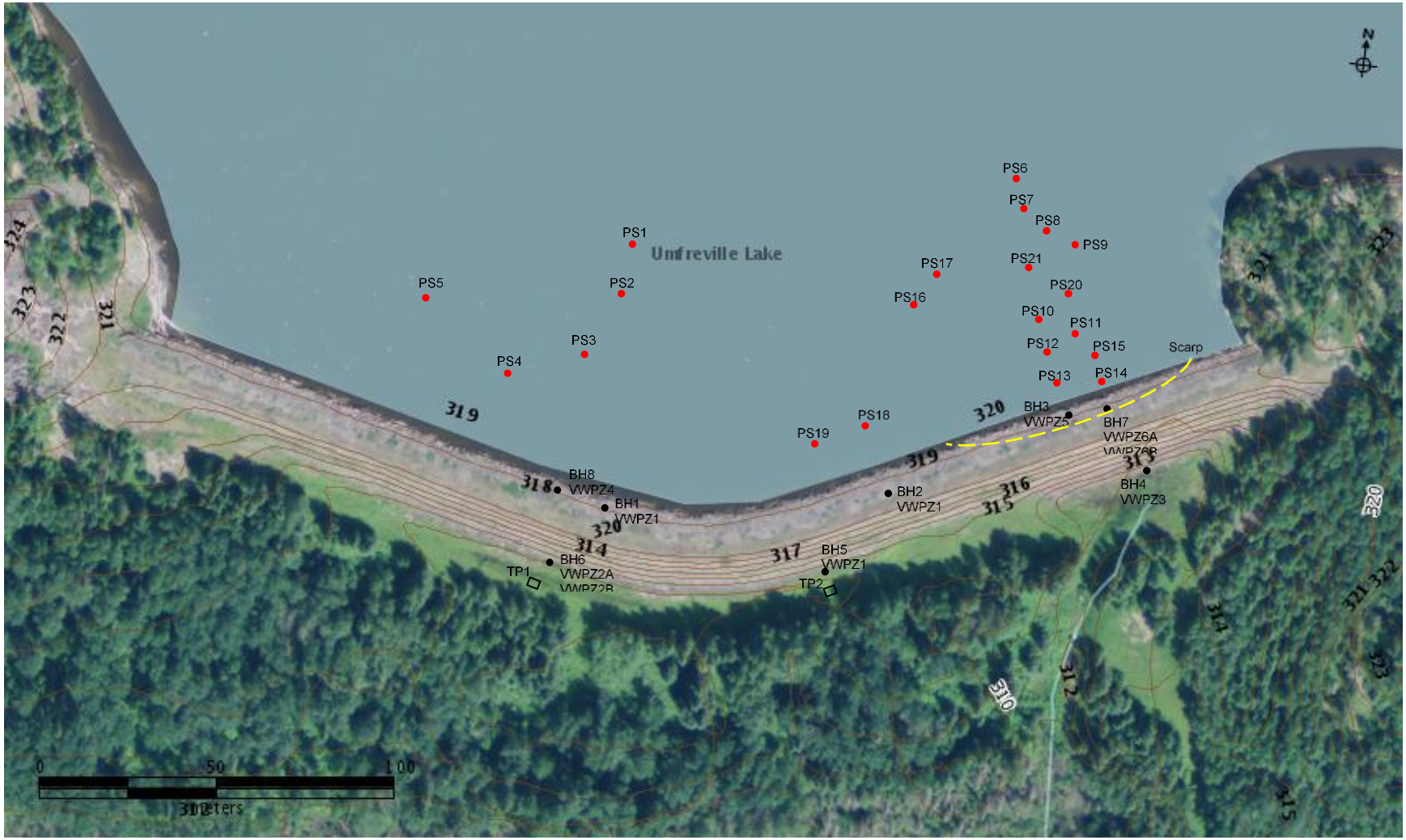

Figure 3.1 Approximated location of boreholes, test pits and installed vibrating wire piezometers in CBBD2

Figure 3.2 Approximated location of boreholes, test pits and installed vibrating wire piezometers in CBBD4

Figure 3.3 Approximated location of boreholes, test pits and installed vibrating wire piezometers in CBMD

Figure 3.4 Approximated location of boreholes, test pits and installed vibrating wire piezometers in WD

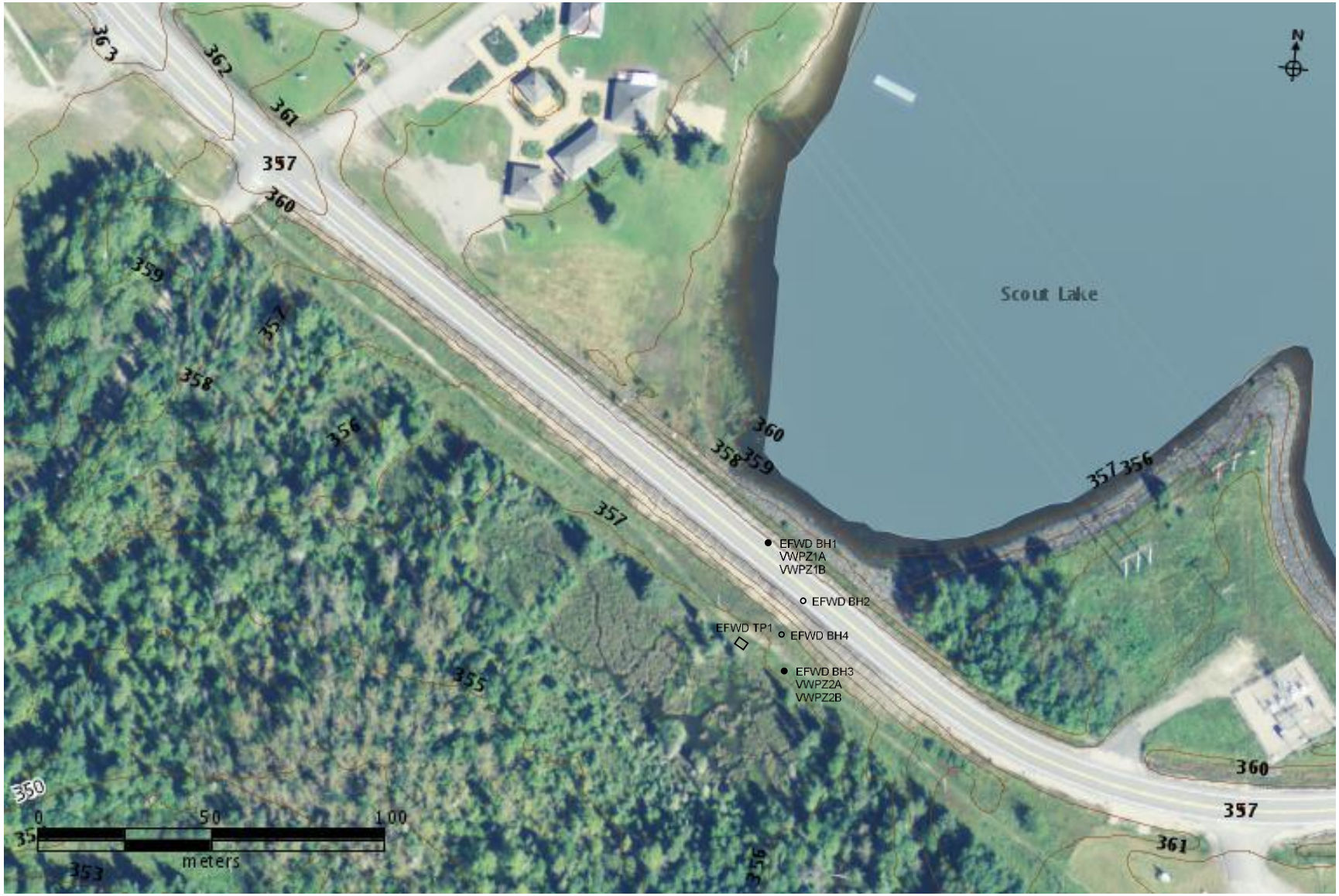

Figure 3.5 Approximated location of boreholes, test pits and installed vibrating wire piezometers in EF

Figure 3.6 Approximated location of boreholes, test pits and installed vibrating wire piezometers in MFLED

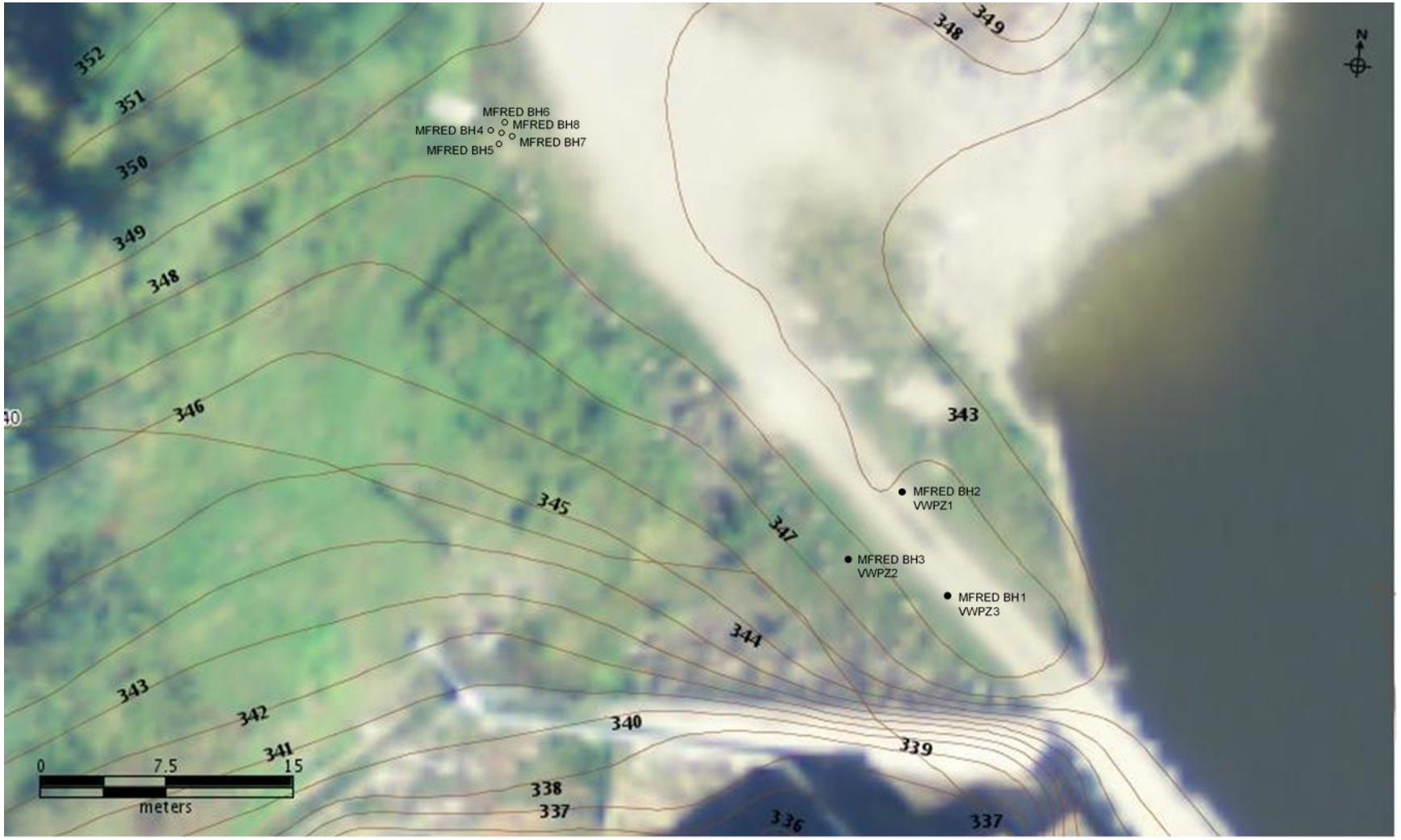

Figure 3.7 Approximated location of boreholes, test pits and installed vibrating wire piezometers in MFRED

Figure 3.8 Collection of inclined samples in a CBBD2 test pit

Figure 3.9 Samples obtained in a CBBD2 test pit by means of a block sampler

Figure 3.10 Conventional soil block sampling in a CBBD2 test pit

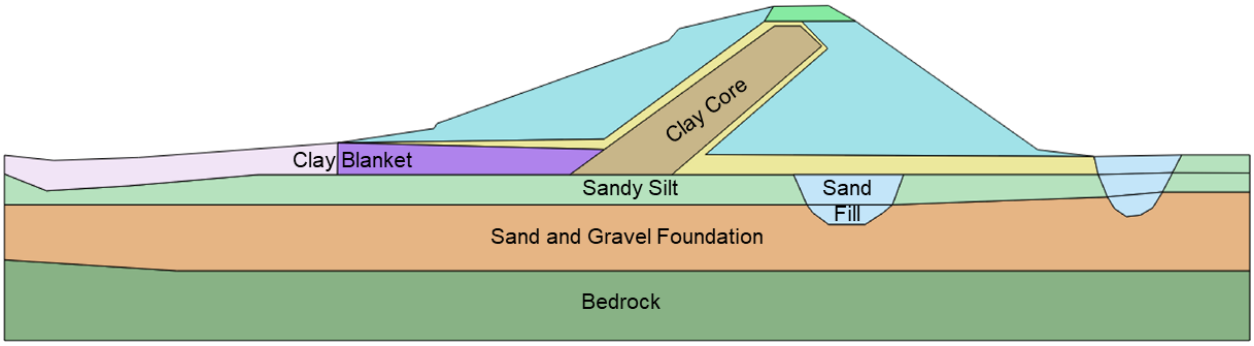

Figure 3.11 Cross-section of CBBD2 Section B-B

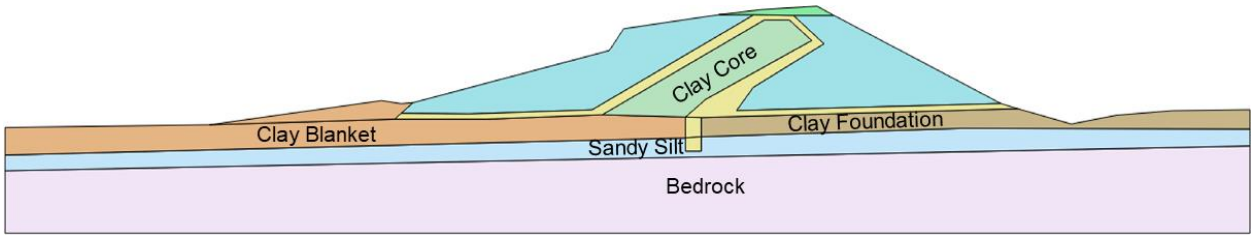

Figure 3.12 Cross-section of CBBD2 Section A-A

Figure 3.13 Fissured clay in a CBBD2 test pit

Figure 3.14 Silt pockets observed within fissured clay in a CBBD2 test pit

Chapter 4 LABORATORY TESTING

Laboratory tests were performed on the samples obtained from boreholes and test pits to represent the clay core, foundation, and clay blanket (at some locations) of the aging earth dams. The index properties, deformation, and strength characteristics were determined from these tests in accordance with ASTM standards. Creep behaviour of undisturbed soil samples were determined by conducting creep in compression and creep in shear tests. Parameters needed for the numerical modelling would also be inferred from the laboratory test results to evaluate the deformation development and stability of the selected earth fill dams. Laboratory testing were done in accordance with the following ASTM standards: D421, D422, D854, D2217, D2435, D3080, D4318, D4767, D6528, and D6467.

4.1 Index Properties

Index property tests would facilitate in determining the soil classification in which the clay core, foundation, and clay blanket are grouped with. This would provide an idea of the expected behaviour of the soil. Since there was very limited information on the borrow source for the materials used in the dams, the USCS classification would somehow indicate if the materials from a particular earth embankment dam came from the same source. Tests performed were moisture content, specific gravity, Atterberg Limits, and particle-size analysis of soils.

4.1.1 CBBD2

Collected samples were examined once extruded from Shelby tubes. Further observations were also made during sample preparations for laboratory tests. Clay core, blanket, and foundation samples were observed to be a mottled mix of brown and grey (Figures 4.1 to 4.4). Cross sections of clay samples show a blocky and fissured texture as

seen in Figure 4.5. Medium to stiff consistency, high plasticity, and silt inclusions were observed during sample trimming. Polished surfaces (Figure 4.6) with varying sizes and random orientation were also noticed. Clay blanket extruded samples were similar to the clay core though the upper layer (until 0.6 m) was soft and brown in appearance. Samples were a mottled mix of brown and grey (beyond 0.6 m) with medium consistency and high plasticity. Fissures and polished surfaces were also observed (Figure 4.7) and pieces of clay can easily broken off along fissure planes. Extruded samples taken from the foundation were more blocky and fissured as seen in Figure 4.8. It can also be seen that silt was more prominent in the foundation samples as compared to the other locations. Gypsum nodules were not observed in any of the samples when extruded and trimmed which reinforced the findings during site investigations.

The average moisture content of CBBD2 clay ranges from 25% to 59%. Atterberg limit results indicate that the liquid limit ranges from 71% to 100% with plasticity indices ranging from 44% to 69%. Hydrometer analysis results revealed that the clay fraction ranged from 68% to 79%. CBBD2 clay, regardless of the location, were classified as “fat clay” of high plasticity (CH) according to the Unified Soil Classification System (USCS) which can be seen in Figure 4.9. This is indicative that the source for the clay fill could be the same material as the foundation. The summary of the index properties for CBBD2 clay per location can be seen in Table 4.1.

4.1.2 Other Earth Fill Dams

The plasticity chart shown in Figure 4.9 indicated that most of the clay samples from the remaining earth dams were classified as “fat clay” of high plasticity (CH), with the exemption of EF which was classified as “lean clay” of low plasticity (CL). Results from CBBD4, CBMD, and WD were clustered closer to CBBD2 data points, compared to EF results, which could imply that the silty clay used in these earth dams are similar to each

other. The CB and WD earth dams are also in close proximity with each other in terms of location. This is also an indication that CB earth dams (CBBD2, CBBD4, and CBMD) had the same source for its clay fill. Extruded clay samples in CBBD4, CBMD, WD, MFLED, and MFRED were observed to be mottled mix of brown and grey and was similar to was what observed in CBBD2 samples.

Table 4.2 summarizes the index property test results on the remaining CB, WD, EF, and MF earth dam clay samples. As seen in Table 4.2, EF samples had lesser clay fraction as compared to the other locations which affected soil plasticity. This supports observations made during site investigations that silt was indeed prevalent in EF. Images of extruded Shelby tube samples can be seen in Appendix B.

4.2 Particle Orientation and Mineralogy

Specimens from CBBD2 were examined using Scanning Electron Microscope (SEM) with back-scattered electron and Energy Dispersive X-ray (EDX) system to determine the clay particle shape, orientation, and possible presence of gypsum particles. Specimens were also inspected by X-ray Diffraction (XRD) to detect the mineralogical composition of the clay and non-clay constituents, as it is a more definitive test compared to EDX analysis. The XRD results would also distinguish the existence of gypsum in the soil, or absence thereof. The SEM and XRD tests were not readily available at the Geotechnical Engineering Laboratory of University of Manitoba. These tests were outsourced in order to obtain the relevant information needed.

The SEM results show that clay particles from the foundation exhibit predominantly edge-to-edge contacts with random non-clay particles (Figure 4.10) without any preferred alignment or orientation with some micro-fissures between flocs. The observed non-clay particles were identified as quartz (*Q*) and dolomite (*D*) by means of EDX, and were marked accordingly in the figure. Clay core specimens, seen in Figure 4.11, show a more flocculated structure with slight

particle alignment wherein micro fissures were also observed. Clay blanket specimens show most particles forming broad overlapping sheets (Figure 4.12).

The XRD results from clay core, blanket, and foundation specimens show the same mineralogical composition as seen in Figure 4.13. Clay minerals present were mostly interlayered smectite and illite with some kaolinite and mica and traces of attapulgite. The dominant clay mineral was smectite which suggested that CBBD2 clay was expansive. Results also indicated that the mineralogy of the clay specimens also did not indicate the presence of gypsum. Instead, the non-clay minerals observed were composed of quartz, feldspar, and dolomite which are typically found in silt. These findings were consistent with the observed presence of silt and the absence of gypsum during site investigations and sample extrusions. The absence of gypsum in clay samples at all locations signified that leaching was unlikely to have caused the delayed instability in CBBD2.

Alfaro III (2016), who also worked on CBBD2 samples as part of this research project, discussed the results of SEM and XRD tests performed on CBBD2 clay samples in more detail in his study.

4.3 Deformation Characteristics

One-dimensional consolidation (oedometer) tests were performed in order to identify the deformation characteristics of the tested samples. Specimens were loaded from 50 kPa with an increment ratio of 2 and a loading cycle of at least twenty-four hours. Test specimens were incrementally loaded until 800 kPa, unloaded back to 50 kPa, then reloaded until the maximum load of 1600 kPa. Apparent preconsolidation pressures (σ'_{vc}) were determined using Casagrande method. Compression (C_c) and recompression (C_r) indices were obtained from the slopes of the void ratio (e) – vertical effective stress (σ_v') graphs.

Table 4.3 shows the deformation parameters from the performed oedometer tests on CBBD2 and the remaining six earth dams. Specimens were overconsolidated with overconsolidation ratio (OCR) values ranging from 2 to 6 for clay core, 5 to 9 for clay foundation, and 11 to 14 for clay blanket. The compression index values indicate that the samples from CB, WD, and MF earth dams were categorized as stiff clay with slight compressibility whereas EF clay samples were classified as firm clay with low compressibility following the category described by Ameratunga et al. (2016) and Widodo and Ibrahim (2012). Consolidation curves based on the results of the oedometer tests performed on CBBD2 specimens can be seen in Figure 4.14. Consolidation curves for the remaining earth dams can be seen in Appendix C.

4.4 Shear Strength Characteristics

Direct shear, torsional ring shear, and triaxial tests were carried out to establish the peak, critical state (post peak), and residual strength of the clay from different sites. These parameters were necessary in the numerical modelling analysis of the different earth dams.

4.4.1 Consolidated Drained Direct Shear Test

Consolidated drained direct shear tests (ASTM D3080) determined the shear strength of the samples along the horizontal plane using a very slow shear rate. The normal stress range applied for the clay core and foundation samples was from 100 kPa to 500 kPa. A lower normal stress range of 50 kPa to 200 kPa was used for clay blanket specimens as clay was squeezed out of the shear box under higher normal loads during the consolidation and shearing stages of the test. Specimens were sheared multiple times (by multi-reversal method) along the horizontal plane in order to achieve residual strength. A specimen would typically take 7 to 8 days to complete the test, from consolidation to end of multiple shearing.

Peak and residual shear strengths determined from completed direct shear tests were summarized in Table 4.4. Figures 4.15 to 4.17 show the stress-displacement graphs generated from direct shear tests on CBBD2 core, foundation, and blanket samples, respectively. Results indicate that tested specimens displayed strain softening behaviour. Shear strength was observed to decrease after reaching peak strength as samples were continuously strained. Investigating normalized stress (shear stress divided by the applied vertical stress) versus displacement indicated that the degree of softening decreased as the applied vertical stress increased (Figures 4.18 to 4.20). This behaviour was considered typical for fissured overconsolidated clays as discussed by Bishop et al. (1965). The stress-strain curve gradually changes from a brittle to ductile behaviour as the confining stress increases. Strain softening was also more prominent in the clay foundation and blanket compared to the clay core. This could be due to the foundation and blanket to be more fissured (Yoshida et al., 1991). Strain softening was also observed in direct shear test results performed on samples from the remaining earth dams. Stress-displacement graphs from these tests can be seen in Appendix C.

4.4.2 Consolidated Undrained Direct Simple Shear Test

Consolidated undrained direct simple shear tests (ASTM D6528) were performed only on CBBD2 clay blanket samples. Compared to direct shear tests wherein shearing occurs along a predetermined shear plane, direct simple shear tests distorts the entire specimen without the formation of a shearing surface. Tests were conducted at the University of British Columbia since the testing apparatus was not available at the University of Manitoba.

Results can be seen in Figures 4.21 to 4.23. The peak shear strength and undrained shear strength at large strains (USALS), also known as post peak shear

strength, are summarized in Table 4.5. Peak shear strength values were comparable to clay blanket direct shear results.

4.4.3 Torsional Ring Shear Test

Torsional ring shear tests (ASTM D6467) complemented direct shear test results as it also provides information on residual shear strength. In this test, prepared specimens were sheared by a continuous rotational shearing action at a very slow shear rate until residual strength was attained. Reconstituted specimens were prepared such that its moisture content was at least be at liquid limit, prior to testing. The normal stress ranges used for the consolidation and shearing phases were the same as what was applied in the direct shear tests.

Figures 4.24 to 4.25 present the stress-displacement graphs of specimens tested from CBBD2. Results from remaining earth dams can be seen in Appendix C. It was observed that the residual strength values from Torsional Ring Shear tests, summarized in Table 4.6, were higher in all tested specimens compared to what was obtained from Direct Shear tests. This could be attributed to the inherent tendency of the ring shear apparatus to squeeze out clay from the cell due to the non-uniform distribution of stresses along its circular shape. Higher stresses tend to accumulate at the outer edges of the ring shear cell while the inner edge was understressed. In contrast, the direct shear box has both sides equally stressed which allows a more uniform distribution of stresses and strains to register lower friction angles (Osano, 2009).

4.4.4 Isotropically Consolidated Undrained Triaxial Compression Test

Isotropically consolidated undrained triaxial compression (CIU) tests (ASTM D4767) determined the cross-shear strengths. Test specimens were prepared so that it adhered to the standard 2:1 height to diameter ratio and were trimmed to a recommended diameter of 71.12 mm (2.80 in) in order to take the effect of fissures in soil strength into

consideration. Specimens were consolidated at an effective stress of 400 kPa prior to the shearing phase. Shearing was done at an effective stress range from 100 kPa to 400 kPa for clay core, foundation, and clay blanket samples. The specimens were re-consolidated (for shearing effective stresses lower than 400 kPa) and had to have a B-test value of at least 0.98 before shearing was initiated.

Peak and post peak shear strength parameters were interpreted using Critical State Soil Mechanics approach. Post peak shear strengths were determined using end-of-test values which occurred at around axial strain values of 14% to 16%. Table 4.7 shows the summarized strength values obtained from the completed tests. Figures 4.26 to 4.31 show results from CIU triaxial tests performed on CBBD2 specimens. Figures Figure 4.27 and Figure 4.30 show the stress-strain curves. Strain softening was generally observed. Similar behaviour was also seen in specimens from the remaining earth dams whose results can be seen in Appendix C.

Post-test inspections of CBBD2 clay core (Figure 4.32) and blanket specimens (Figure 4.33) show polished surfaces in various sizes, orientation, and location. Fissures were also seen once post-test specimens were taken apart. It was noticed that specimens were easily broken into pieces along fissured planes, further revealing these polished surfaces. Examination of post-test clay foundation specimens (Figure 4.34) from CBBD2 also uncovered fissured surfaces and silt inclusions or pockets. Polished surfaces were also observed in CBBD4 clay core post-triaxial test specimens (Figure 4.35) but were not seen in any other locations. This is further indication that CB earth dams had the same borrow source for clay fill. It is possible that the borrowed clay was already intensely fissured and compaction during construction could have led to localized slickensides along these fissures, creating these polished surfaces. However, these polished surfaces were not interconnected thereby not able to generate failure surfaces. Another possibility is that

water has been trapped within these micro fissures prior to its use as clay fill and has smoothened the contact surface with respect to time. Further compaction of the borrowed clay and creep movement could have somehow increased the intensity of polishing of the locally unconnected slickensides as time progressed. Such insights show that the fissures in the clay core and clay blanket were pre-existent from the borrow source and less likely brought about by environmental loading (of repeated wetting-drying and freezing-thawing).

4.5 Creep Characteristics

Long-term deformation caused by creep movements could accumulate over time. The cumulative deformation could lead to stability issues, as in the case of slopes. Creep failure in slopes can be defined as a delayed or long-term failure under a constant effective stress, initiated by a sudden acceleration of creep rate movement (Bi et al., 2019).

In order to have a better understanding of the creep behaviour of clayey soils in CBBD2, creep tests were performed in two cases: creep in compression and creep in shear. Compression creep tests allowed secondary compression to occur with lateral restrictions applied to the prepared specimens. Creep parameters from compression tests were used successfully to predict deformations and failure of foundations. Shear creep tests, on the other hand, permitted creep without lateral restrictions which could lead to failure under high shear stresses. Creep tests in shear simulate closely the creep movements in slopes such as landslides. In earth dams, not all sections would tend to behave similar to a specimen under compression creep as the clay core would behave similarly to a creep specimen under shear loading. Interest in comparing these tests arose as creep parameters required in soil models recommended creep compression tests to be performed. Comparisons on creep coefficients (C_α) determined from compression creep and

shear creep tests performed on CBBD2 clay core samples were done and discussed in the following sections.

4.5.1 Creep in Compression

The behaviour of the soil under creep in compression was investigated using the incrementally loaded oedometer test. Following the procedure of the standard one-dimensional consolidation test (ASTM D2435), the duration of the applied load must be at least twenty-four hours to be sufficient. To ensure the development of secondary compression (creep), the heaviest load from the aforementioned test was applied for two weeks and displacement readings were taken daily within this observation period. During secondary compression, the changes of void ratio with logarithmic time is approximately linear and the slope is defined as the coefficient of secondary compression or creep (C_α).

Creep in compression results are summarized in Table 4.8 for all tested specimens. CBBD2 test results were presented a range of values as there were more specimens tested from this site, whereas the remaining investigated earth fill dams only had one specimen tested per location. The range of C_α values were from 0.002 to 0.005 which corresponds to clays with low to medium secondary compressibility. The ratio of C_α/C_c fall within the range of 0.012 to 0.030 which was considered to be similar to the field condition of overconsolidated clays tested by Ameratunga et al. (2016).

4.5.2 Creep in Shear

Triaxial creep tests, or creep in shear tests, were performed on CBBD2 clay core samples taken from the same location as creep in compression tests. A triaxial creep test equipment was not readily available in the Geotechnical Engineering Laboratory. Modifications had to be done to a conventional triaxial test setup such that a constant axial load could be applied with the use of mass hangers. Specimen dimensions and set up was the same as in conventional triaxial tests. Clay specimens were consolidated at an

effective stress of 400 kPa when saturation has reached a *B* value of at least 0.98. The pressure was then decreased to an effective stress of either 100 kPa or 200 kPa and the specimens were allowed to reconsolidate prior to commencing the creep in shear process under drained condition. This stage of unloading simulated the overconsolidation behaviour of the clay. A constant load was applied by the multi-stage loading method (Vaid and Campanella, 1977; Mesri et al., 1981; Lai et al., 2014) wherein a specimen was loaded to different deviator stress levels. Constant load levels were 0.50, 0.65, and 0.80 of the peak axial load from the performed triaxial tests. Creep deformation was measured per applied deviator stress level. When the axial deformation rate was lower than 0.005 mm per day, the specimen had reached stabilization at the current stress level. At stabilization, the required load for the next stress level was added onto the mass hanger. Volume changes were monitored by taking readings from the top and bottom burettes. The test was stopped once creep rupture or failure was reached. The shear creep test set-up used is shown in Figure 4.36.

The constant load levels of 0.50, 0.65, and 0.80 of the peak axial load from completed triaxial tests corresponded to 0.58, 0.76, and 0.93 of the peak deviator stress at a confining stress of 100 kPa (q_{100}); and 0.53, 0.68, and 0.84 of the peak deviator stress at a confining stress of 200 kPa (q_{200}). Specimen stabilization under the constant load took about 2 to 4 weeks, depending on the degree of shear mobilization. The degree of shear mobilization is the ratio between the applied shear stress over the shear stress at failure which could also be further simplified as the ratio of the applied deviator stress with respect to the deviator stress at failure.

Rupture was attained at $0.93q_{100}$ and $0.84q_{200}$. These failures could be due to the specimens behaving similarly to an undrained failure condition rather than creep rupture as the failure occurred only within 4 minutes and 3 days respectively, for $0.93q_{100}$ and $0.84q_{200}$. Failure happened too abruptly for the specimen to drain under the constant load.

The rupture time was also too short for creep to occur. Consequently, only four cases were analyzed: $0.58q_{100}$, $0.76q_{100}$, $0.53q_{200}$, and $0.68q_{200}$.

The vertical creep strain and volumetric creep strain were plotted against time as shown in Figures 4.37 to 4.38. The slope of the vertical creep strain with time was observed to have increased as the shear mobilization level was increased (Figure 4.37). As the degree of shear mobilization was increased, heavier loads were applied which led to the increase in the vertical displacement. On the other hand, the slope of the volumetric creep strain decreased as the degree of shear mobilization was increased (Figure 4.38). As the specimen was being vertically compressed under heavier loads, it was also expanding (swelling) in the radial direction. The specimen swelling could have led to water being retained, if not increased, within the sample instead of being drained (Mitchell and Soga, 2005). This led to little or no change in the burette readings (representing the change in volume) under heavier loads. It is important to note that Figure 4.38 indicated a distinct difference in creep behaviour with respect to the confining stress. Results show that at low confining stresses, volumetric shear creep would be significant. This information is important to be considered especially for clay cores at shallow depths within earth dams.

In order to compare creep shear with compression creep outcomes, results were plotted in terms of void ratio with respect to log of time. Figure 4.39 shows the results from creep in compression while Figure 4.40 presents the results from creep in shear. Results indicated that the coefficient of creep from performed shear creep tests ($C_{\alpha\text{-}s}$) were 0.001 and 0.002 for tested specimens with confining stress of 100 kPa and 200 kPa, respectively, regardless of the degree of shear mobilization. These values were lower than C_α from compression creep tests on CBBD2 clay core which ranged from 0.003 to 0.005. This could be due to the higher stress applied onto the soil specimen in compression creep (1600 kPa) compared to shear creep (100 to 200 kPa), which resulted in the higher rate

of void ratio reduction with respect to time. As $C_{\alpha\text{-}s}$ generated lower values, the use of C_{α} for clay would be more conservative.

To further look into the shear creep tests results and how they can be applied to stability analysis of earth dams, the discussion and interpretation of creep test results made by Bi et al. (2019) were closely followed. As indicated earlier the constant levels in creep tests in the current study are 0.50, 0.65, and 0.80 of the peak axial load from completed standard CIU triaxial tests corresponded to 0.58, 0.76, and 0.93 of the maximum (peak) deviatoric stress at a confining stress of 100 kPa (q_{100}); and 0.53, 0.68, and 0.84 of the maximum deviatoric stress at a confining stress of 200 kPa (q_{200}). This normalization helps to define the standard strength from the beginning of the creep test curve and assist in inferring the percentage of strength the sample failed during creep stage. It should be noted that the normalization is based on the peak shear strength of the clay, not on the shear strength at critical state.

Bi et al. (2019) considered the inverse of the percentages of mobilized shear stress relative to maximum shear stress (such that percent of the maximum shear stress) as the factor of safety against failure. Their findings gave an insight on how to interpret factor of safety values in terms of long-term creep deformations. Based on the results of the current study, it was that if less than 65% of the load is applied with respect to the peak axial load (corresponding to 76% of q_{100} and 68% of q_{200}), creep movement would be minimal and shear creep rupture would be unlikely to occur. This suggests that a factor of safety lower than 1.3 would indicate that creep would be significant and could lead to delayed instability.

Figure 4.38 indicate that for a range of factor of safety values from 1.5 to 1.9, creep is insignificant at high confining stresses; whereas values from 1.3 to 1.7 would display significant creep at low confining stresses. This suggests that the current dam safety factor of safety requirement of 1.5 for long-term stability (Canadian Dam Association, 2013)

would be sufficient at high confining stresses. However, this safety criteria might not be enough when confining stresses are lower than 100 kPa as significant creep would transpire. Part of the clay core within the earth dam that has confining stress lower than 100 kPa would display significant creep movement, even with a factor of safety of 1.5. These findings strengthens the need to include creep in long-term stability analyses.

4.6 Summary

Index property tests performed in CB clay indicated that the samples were high plasticity clay (CH) or “fat clay” in accordance with the Unified Soil Classification System. Deformation characteristics revealed that the collected clay were stiff and had slight compressibility. This is an indication that CB earth dams (CBBD2, CBBD4, and CBMD) had the same source for its clay fill.

Tests on CBBD2 clay core, blanket, and foundation particle orientation and mineralogy (via SEM and XRD tests, respectively) showed no trace of gypsum. These results coincided with site observations. The absence of gypsum within the clay samples signified that leaching of this naturally occurring cementing agent could not have caused the delayed instability in CBBD2.

Post-test investigations also revealed that specimens were easy to break along fissures, which are found in all CBBD2 location (clay core, blanket, or foundation). Silt lenses or pockets and fissures were also observed to be more prominent in clay foundation locations. Polished surfaces were also seen in various sizes and orientation in CBBD2 post-test specimens. They were also observed in CBBD4 clay core specimens. This is further indication that CB earth dams has the same borrow source for clay fill. It is possible that the borrowed clay was already intensely fissured and compaction could have led to localized slickensides along these fissures. However, these polished surfaces were not interconnected thereby not able to generate failure surfaces.

Clay samples from WD and MF generating stations were also classified as highly plastic clay. This clay was described as stiff with high compressibility, similar to CB clay. On the other hand, EF clay was designated as “lean clay” or low plasticity clay (CL) and was stiff with low compressibility. Investigations of post-test specimens from WD, EF, and MF earth dams did not reveal polished surfaces when broken into pieces. EF strength parameters were larger compared to the values generated from the other dams owing to the lean clay found in this location.

Deformation and shear strength characteristics revealed that all tested clays were overconsolidated. This was further verified as Direct Shear test results indicated strain-softening behaviour which is prevalent in overconsolidated clays. Residual shear strengths from Torsional Ring Shear tests indicated higher values compared to those generated from Direct Shear tests attributed to the non--uniform distribution of stresses accumulated at the outer and inner edges of the ring shear cell.

Creep tests were performed on CBBD2 clay core specimens. Shear creep tests indicated that as the degree of mobilization was increased, the slope of the vertical creep strain with time increased but the slope of the volumetric creep strain decreased with time. Creep coefficients determined from shear creep ($C_{\alpha\text{-}s}$) were lower than the compression creep (C_{α}) values, regardless of the level of shear mobilization.

Creep shear tests indicated that if less than 65% of the load is applied with respect to the peak axial load (corresponding to $0.76q_{100}$ and $0.68q_{200}$, where q_{100} and q_{200} are the maximum deviatoric or shear stress), creep movement would be minimal and shear creep rupture would be unlikely to occur. Considering the inverse of the percentage of the mobilized shear stress relative to maximum shear stress as the factor of safety against failure, the current study indicate that for a range of factor of safety values from 1.5 to 1.9, creep is insignificant at high confining stresses; whereas values from 1.3 to 1.7 would display significant creep at low confining stresses. This suggests that the current dam safety factor of safety requirement of 1.5 for long-term stability

would be sufficient at high confining stresses. However, the current safety criteria might not be enough when confining stresses are lower than 100 kPa as significant creep would transpire. This suggests that part of the clay core within the earth dam would already display creep movement, even with a factor of safety of 1.5. As creep movement would be expected, this demonstrates the need to include creep in the analysis for long-term stability. This type of analysis would be useful for earth fill structures that are expected to maintain safety and serviceability throughout the service life of the structure.

Table 4.1 Summary of index properties for CBBD2

Index Properties	CBBD2			
	Foundation	Core A-A	Core B-B	Blanket B-B
Moisture Content (%)	25 to 58	26 to 59	33 to 43	35 to 51
Liquid Limit (%)	80 to 100	79 to 89	80 to 92	71 to 93
Plasticity Index (%)	50 to 69	51 to 66	57 to 65	44 to 66
Specific Gravity	2.67 to 2.75	2.70 to 2.77	2.67 to 2.75	2.63 to 2.73
Minus #200, <0.075mm (%)	100	100	100	100
Clay Fraction, <0.002mm (%)	72 to 75	74	73 to 79	68 to 73

Table 4.2 Summary of index properties for remaining earth dams

Index Properties	CBBD4		CBMD	WD		EF		MFRED	MFLED
	Foundation	Core	Core	Foundation	Core	Foundation	Core	Core	Core
Moisture Content (%)	18 to 47	28 to 44	23 to 41	35 to 41	29 to 50	23 to 34	24 to 33	30 to 37	29 to 36
Liquid Limit (%)	101 to 104	90 to 92	84	87 to 97	82 to 88	40 to 51	37 to 51	67 to 72	69 to 73
Plasticity Index (%)	62 to 73	61 to 64	53	56 to 63	48 to 54	20 to 28	17 to 28	40 to 46	40 to 45
Specific Gravity	2.72	2.68 to 2.71	2.70 to 2.78	2.60 to 2.67	2.68 to 2.73	2.67 to 2.72	2.65 to 2.73	2.70 to 2.73	2.67 to 2.75
Minus #200, <0.075mm (%)	100	100	100	100	100	100	100	100	100
Clay Fraction, <0.002mm (%)	82	70	63	68	71	56	58	70	72

Table 4.3 Summary of deformation characteristics

Location	σ'_{vc} (kPa)	C_c	C_r
CBBD2 Foundation	150 to 180	0.109 to 0.151	0.032 to 0.035
CBBD2 Core A-A	150 to 190	0.109 to 0.110	0.037 to 0.038
CBBD2 Core B-B	120 to 150	0.106 to 0.113	0.031
CBBD2 Blanket	120 to 170	0.121 to 0.125	0.037 to 0.041
CBBD4 Foundation	180	0.119	0.041
CBBD4 Core	200	0.121	0.028
CBMD Core	175	0.118	0.034
WD Foundation	200	0.108	0.037
WD Core	190	0.149	0.043
EF Foundation	180	0.065	0.012
EF Core	175	0.076	0.014
MFLED Core	200	0.119	0.020
MFRED Core	185	0.090	0.021

Table 4.4 Summary of shear strengths from Direct Shear tests

Location	Stress Range (kPa)	Peak		Post Peak		Residual	
		c' (kPa)	φ' (deg)	c' (kPa)	φ' (deg)	c' (kPa)	φ' (deg)
CBBD2 Foundation	50 to 300	44	16	0	16	0	8
CBBD2 Core*	100 to 500	30	13	0	11	0	8
CBBD2 Blanket	50 to 200	20	17	0	13	0	9
CBBD4 Foundation	100 to 400	22	13	0	10	0	5
CBBD4 Core	50 to 300	37	13	0	18	0	7
CBMD Core	100 to 300	23	21	0	18	0	10
WD Foundation	100 to 300	41	17	0	14	0	9
WD Core	100 to 300	51	10	0	13	0	8
EF Foundation	100 to 300	30	30	0	23	0	21
EF Core	100 to 300	40	24	0	22	0	14
MFRED Core	100 to 300	39	16	0	13	0	8
MFLED Core	100 to 300	24	22	0	15	0	8

*Performed by M. Alfaro III

Table 4.5 Summary of shear strengths from Direct Simple Shear tests

Location	Description	Stress Range (kPa)	Peak		Post Peak	
			c' (kPa)	φ' (deg)	c' (kPa)	φ' (deg)
CBBD2 Blanket	Under the rockfill	50 to 200	10	11	0	21
CBBD2 Blanket	Outside the rockfill	50 to 200	6	17	0	20

Table 4.6 Summary of residual shear strengths from Torsional Ring Shear tests

Location	Stress Range (kPa)	Residual	
		c' (kPa)	φ' (deg)
CBBD2 Foundation	50 to 200	0	10
CBBD2 Core	50 to 200	0	12
CBBD2 Blanket	50 to 200	0	11
CBBD4 Foundation	100 to 400	0	10
CBBD4 Core	100 to 300	0	11
CBMD Core	100 to 300	0	14
WD Foundation	100 to 300	0	12
WD Core	100 to 300	0	13
EF Foundation	100 to 300	0	27
EF Core	100 to 300	0	24
MFRED Core	100 to 300	0	14
MFLED Core	100 to 300	0	15

Table 4.7 Summary of shear strengths from CIU Triaxial tests

Location	Stress Range (kPa)	Peak		Post Peak	
		c' (kPa)	φ' (deg)	c' (kPa)	φ' (deg)
CBBD2 Foundation	100 to 400	26	22	0	19
CBBD2 B-B Core	100 to 400	34	24	0	18
CBBD2 A-A Core	100 to 400	18	21	0	19
CBBD2 Blanket	50 to 200	18	21	0	21
CBBD4 Foundation	100 to 400	54	23	0	18
CBBD4 Core	100 to 200	48	25	0	18
CBMD Core	100 to 400	38	25	0	18
WD Foundation	100 to 400	25	21	0	18
WD Core	100 to 400	2	24	0	19
EF Foundation	100 to 400	14	32	0	28
EF Core	100 to 400	45	30	0	27
MFRED Core	100 to 400	26	27	0	20
MFLED Core	100 to 400	57	26	0	21

Table 4.8 Summary of Creep in Compression test results

Location	C_α	C_α / C_c
CBBD2 Foundation	0.004 to 0.005	0.026 to 0.046
CBBD2 Core A-A	0.004 to 0.005	0.036 to 0.046
CBBD2 Core B-B	0.003 to 0.004	0.023 to 0.038
CBBD2 Blanket	0.004 to 0.005	0.032 to 0.041
CBBD4 Foundation	0.003	0.025
CBBD4 Core	0.004	0.033
CBMD Core	0.003	0.025
WD Foundation	0.004	0.037
WD Core	0.005	0.034
EF Foundation	0.003	0.046
EF Core	0.002	0.026
MFLED Core	0.004	0.034
MFRED Core	0.004	0.044

Figure 4.1 CBBD2 clay core extruded Shelby tube sample

Figure 4.2 CBBD2 clay blanket extruded Shelby tube sample

Figure 4.3 CBBD2 clay foundation extruded Shelby tube sample

Figure 4.4 CBBD2 clay foundation sample at location further away from CBBD2

Figure 4.5 CBBD2 clay core sample

Figure 4.6 Polished surfaces observed in CBBD2 clay core sample

Figure 4.7 Fissures and polished surfaces observed in clay blanket samples

Figure 4.8 CBBD2 clay foundation samples

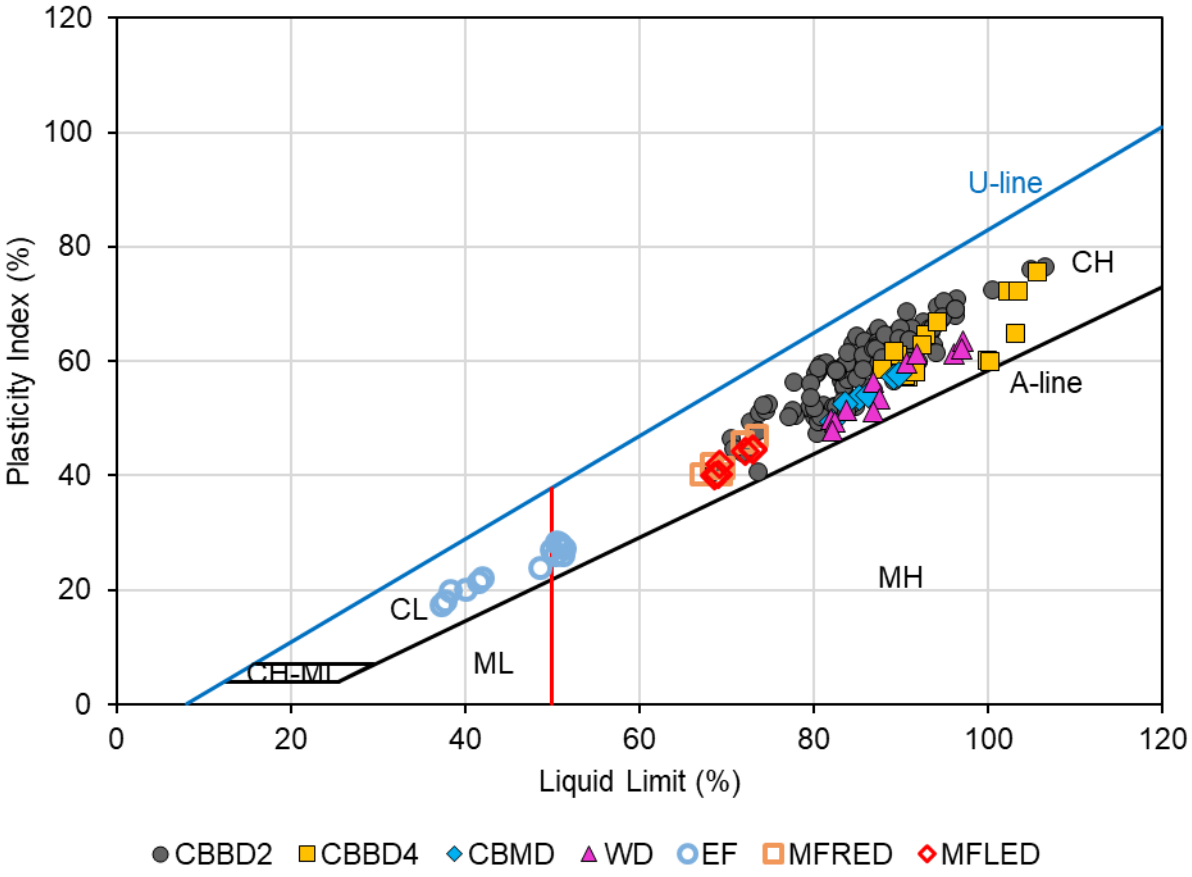

Figure 4.9 Plasticity chart

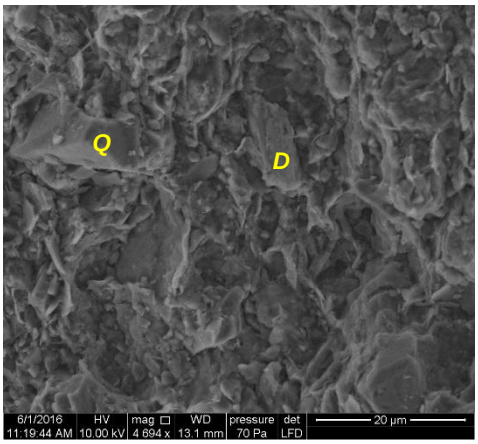

Figure 4.10 SEM image of a clay foundation sample from CBBD2 (with permission from Alfaro III, 2016)

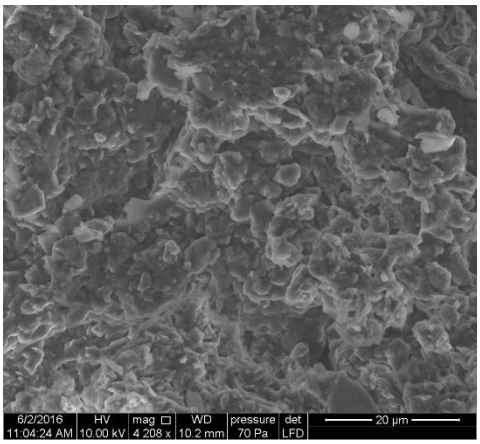

Figure 4.11 SEM image of a clay core sample from CBBD2 (with permission from Alfaro III, 2016)

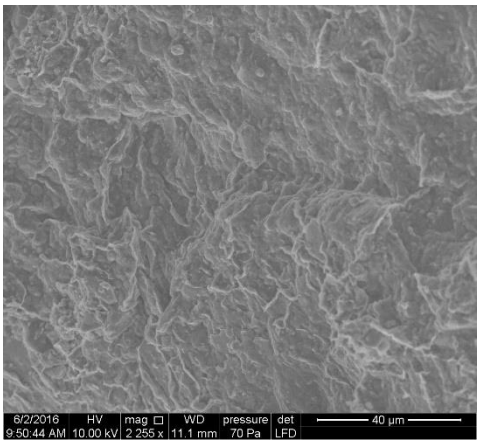

Figure 4.12 SEM image of a clay blanket sample from CBBD2 (with permission from Alfaro III, 2016)

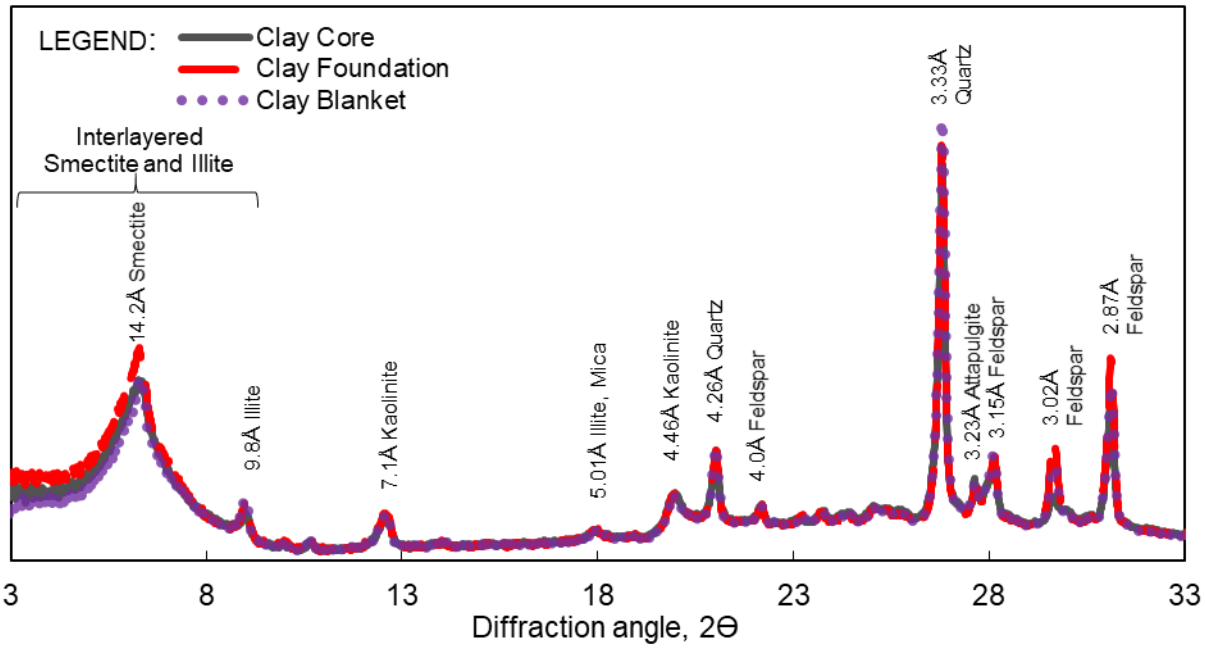

Figure 4.13 XRD test results of CBBD2 clay samples (with permission from Alfaro III, 2016)

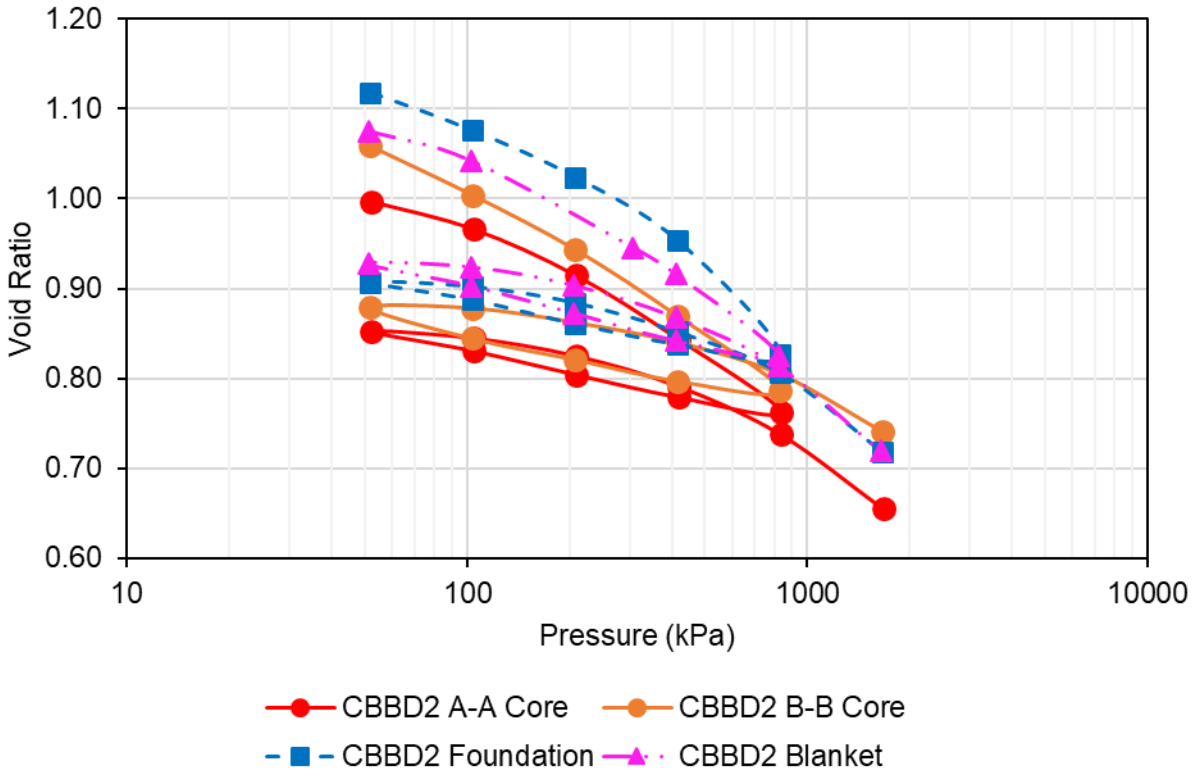

Figure 4.14 Consolidation curves from oedometer tests on CBBD2 samples

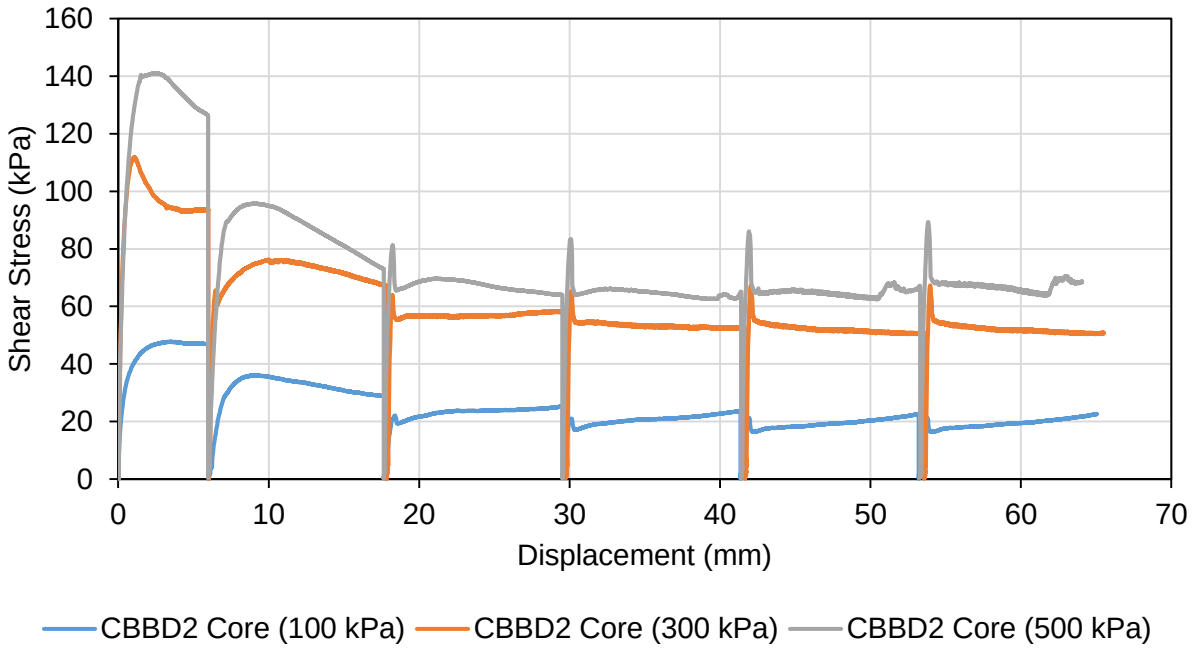

Figure 4.15 Stress-displacement behaviour of CBBD2 core samples from Direct Shear tests

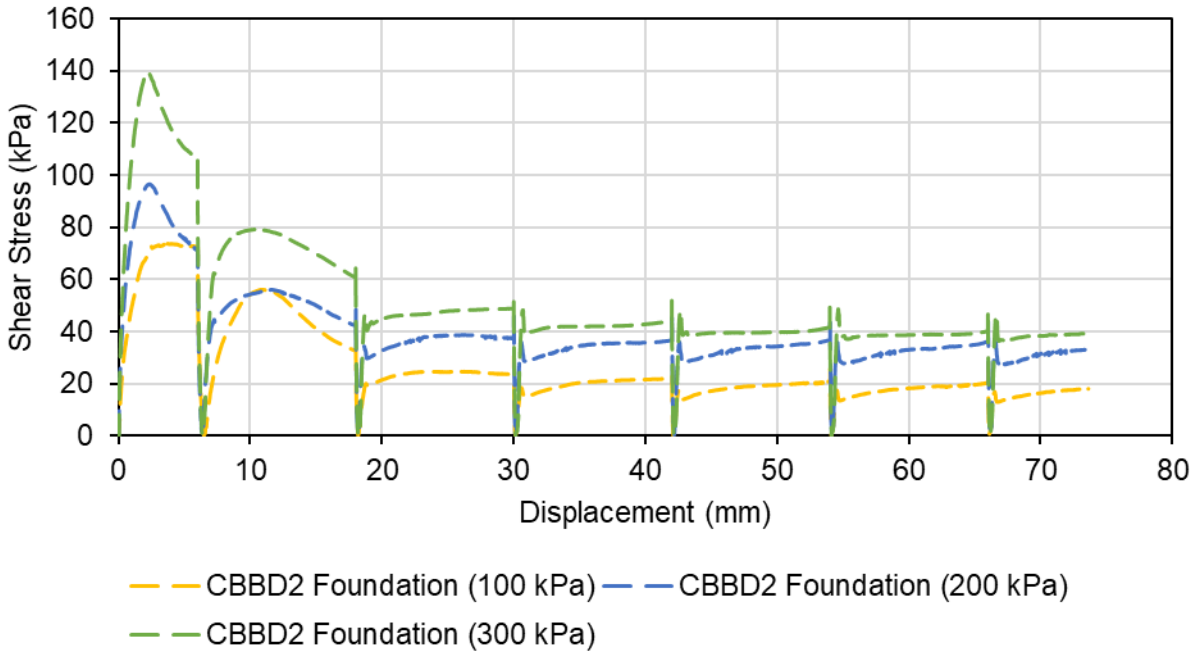

Figure 4.16 Stress-displacement behaviour of CBBD2 foundation samples from Direct Shear tests

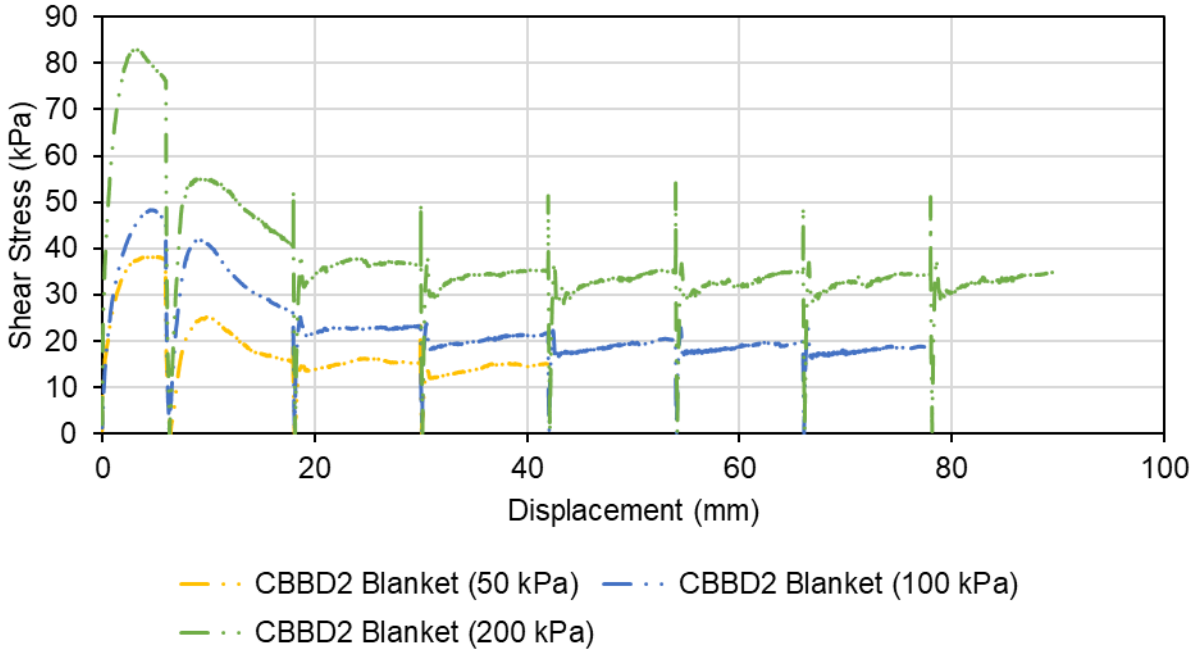

Figure 4.17 Stress-displacement behaviour of CBBD2 blanket samples from Direct Shear tests

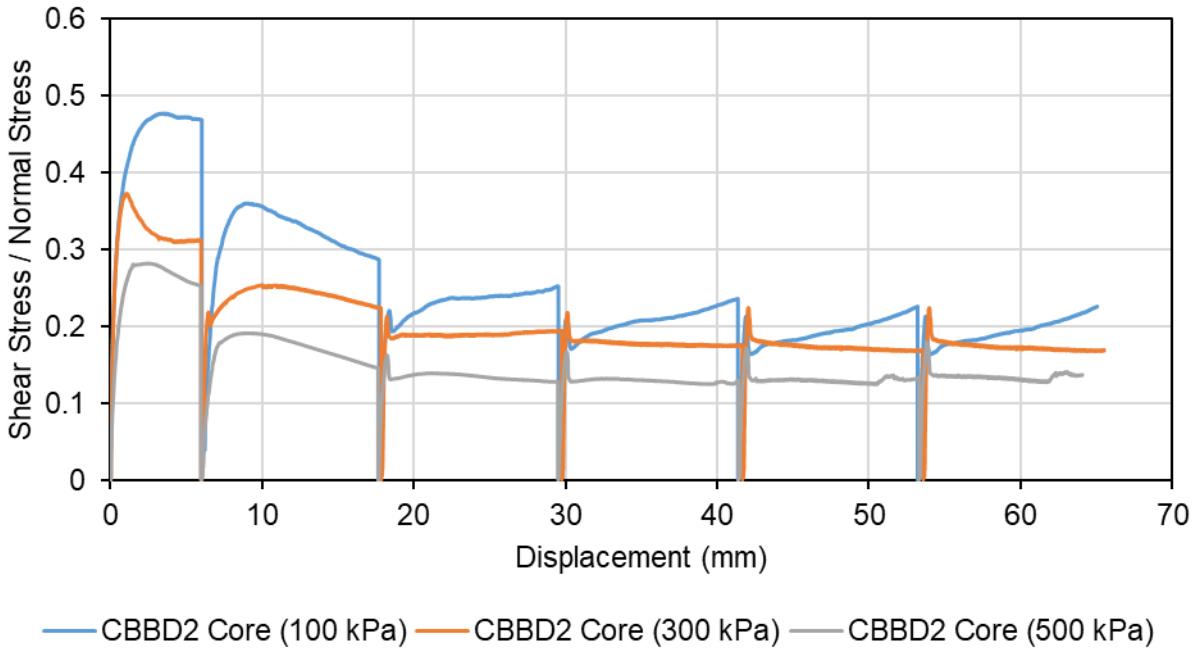

Figure 4.18 Normalized stress-displacement behaviour of CBBD2 core samples from Direct Shear tests

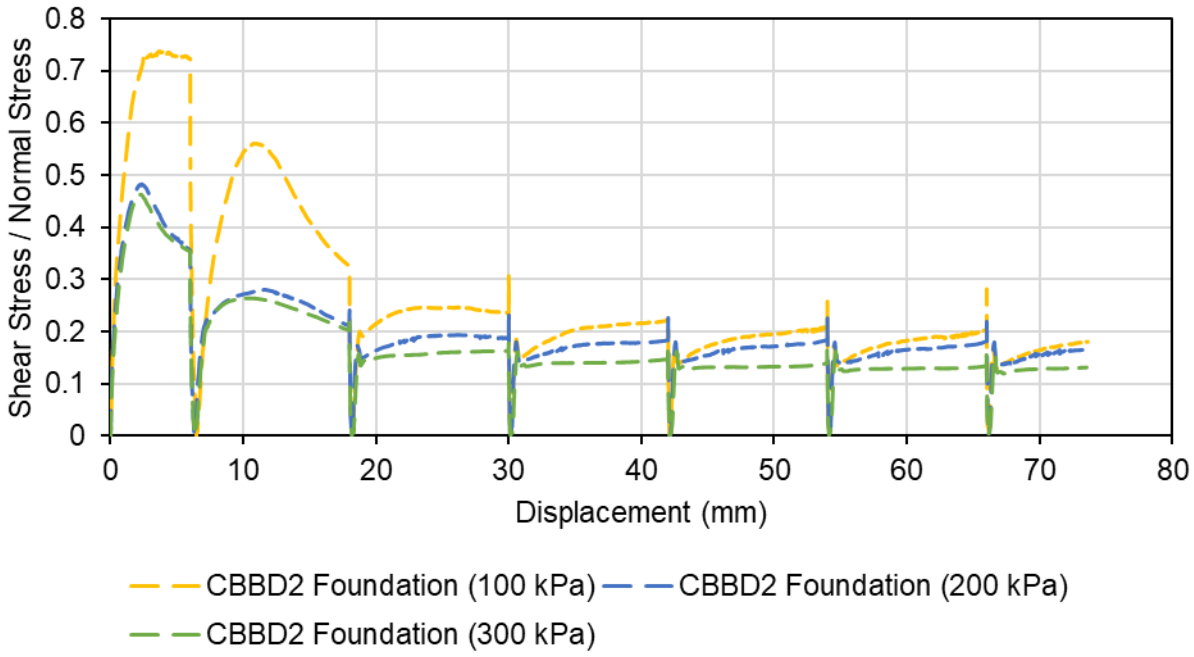

Figure 4.19 Normalized stress-displacement behaviour of CBBD2 foundation samples from Direct Shear tests

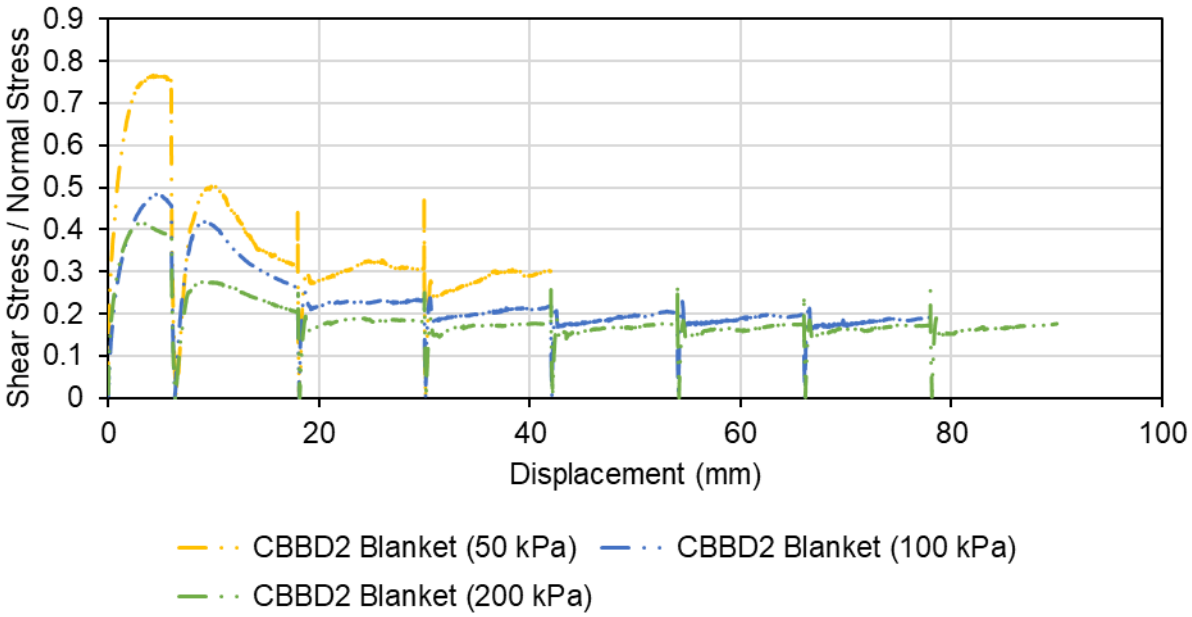

Figure 4.20 Normalized stress-displacement behaviour of CBBD2 blanket samples from Direct Shear tests

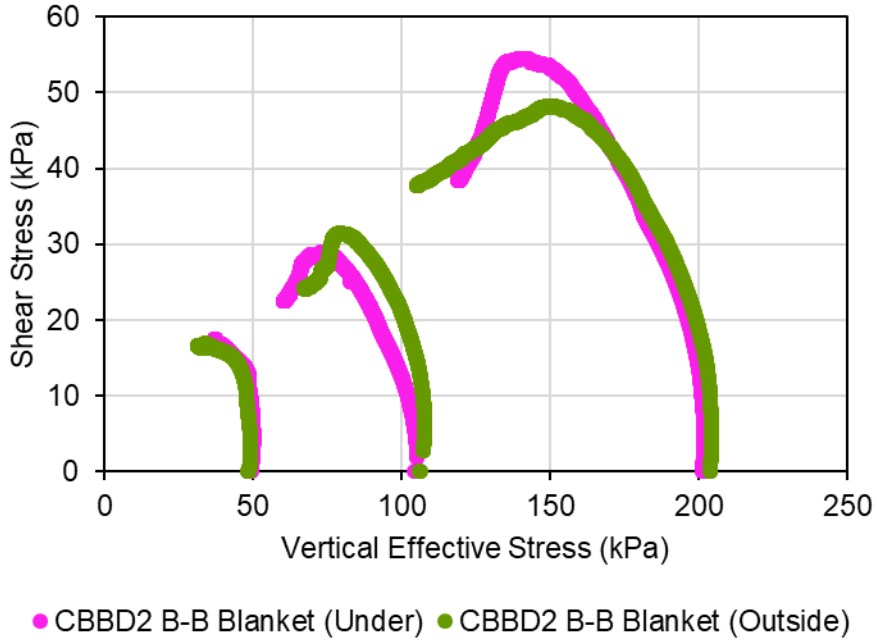

Figure 4.21 Shear stress-vertical effective stress results from Direct Simple Shear tests on CBBD2 clay blanket samples

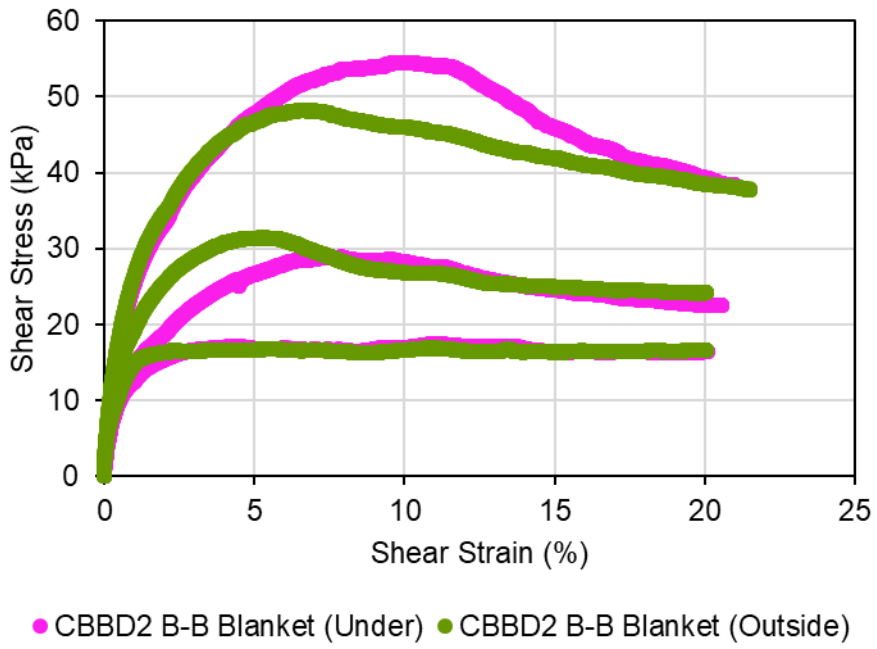

Figure 4.22 Stress-strain results from Direct Simple Shear tests on CBBD2 clay blanket samples

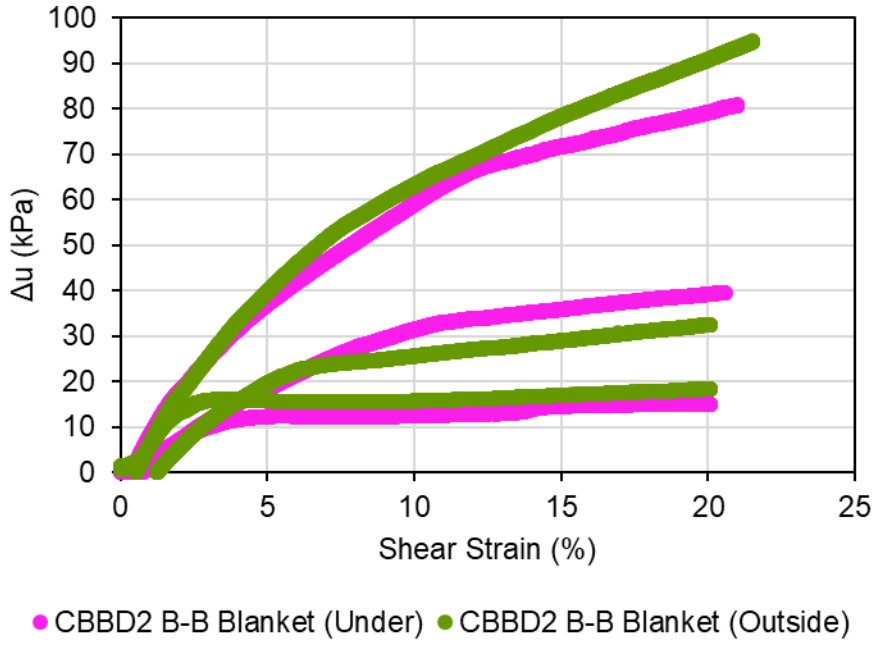

Figure 4.23 Pore water measurements from Direct Simple Shear tests on CBBD2 clay blanket samples

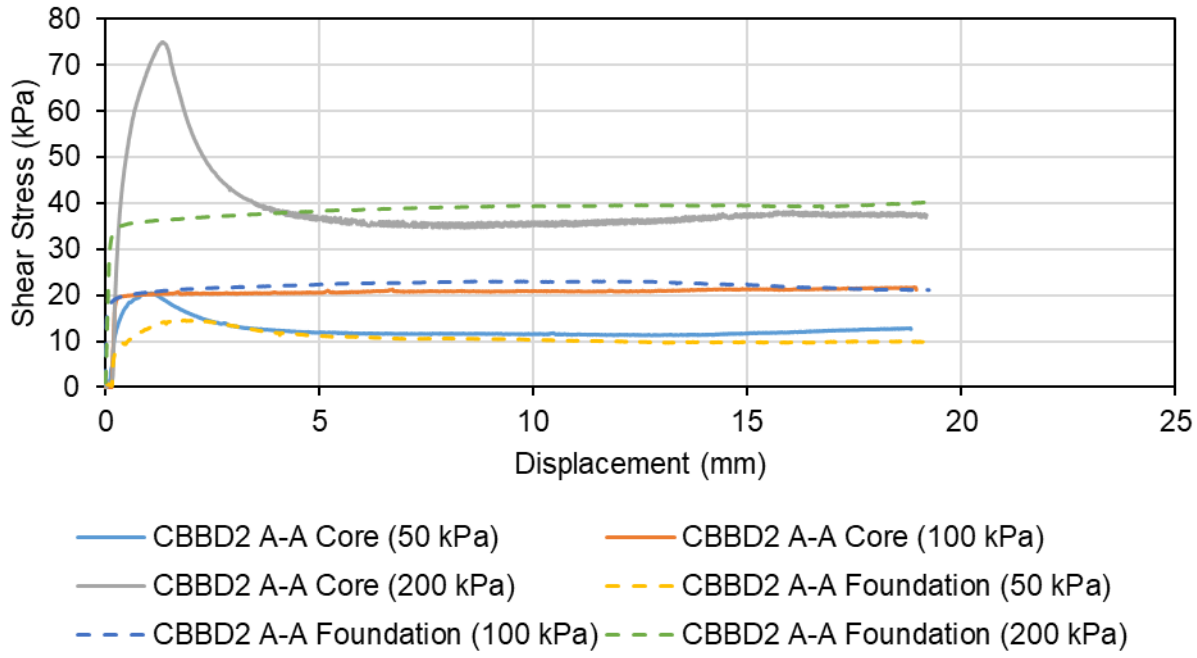

Figure 4.24 Stress-displacement behaviour of CBBD2 Section A-A specimens from Torsional Ring Shear tests

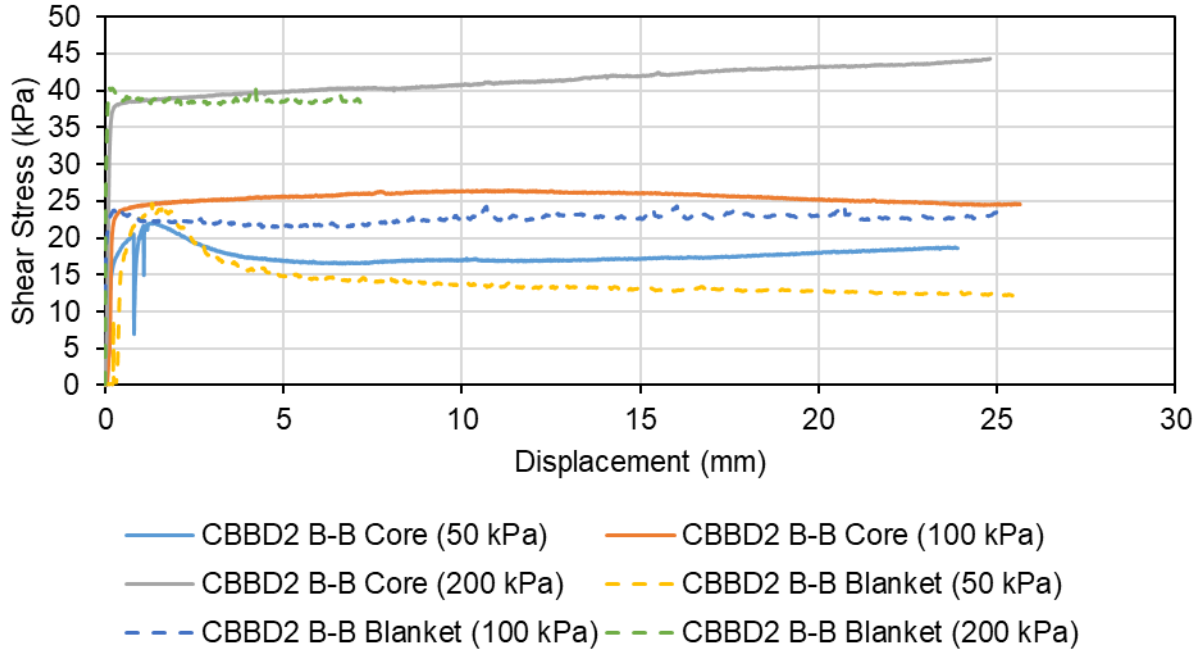

Figure 4.25 Stress-displacement behaviour of CBBD2 Section B-B specimens from Torsional Ring Shear tests

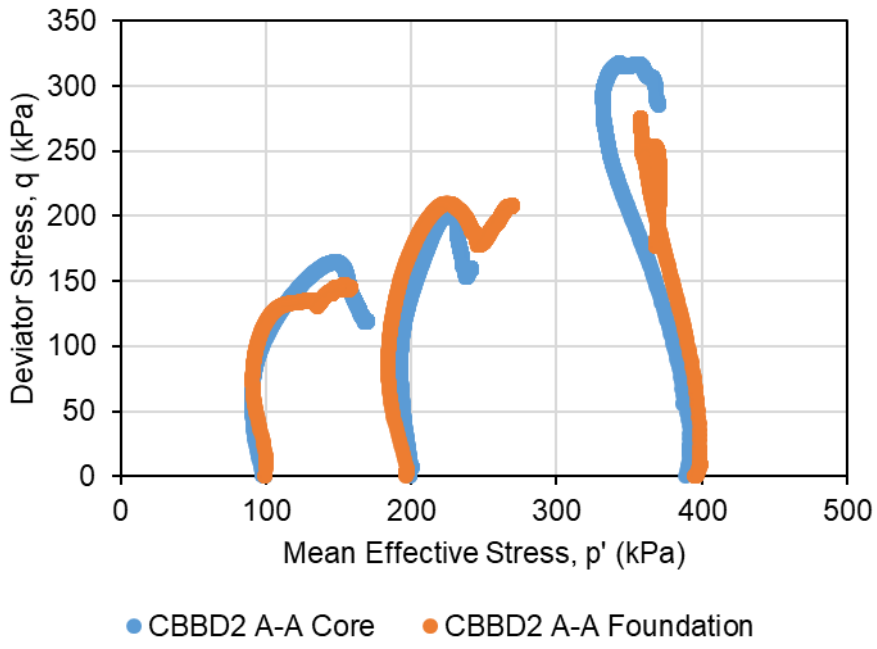

Figure 4.26 Stress paths in p'-q space of CBBD2 Section A-A CIU Triaxial test samples

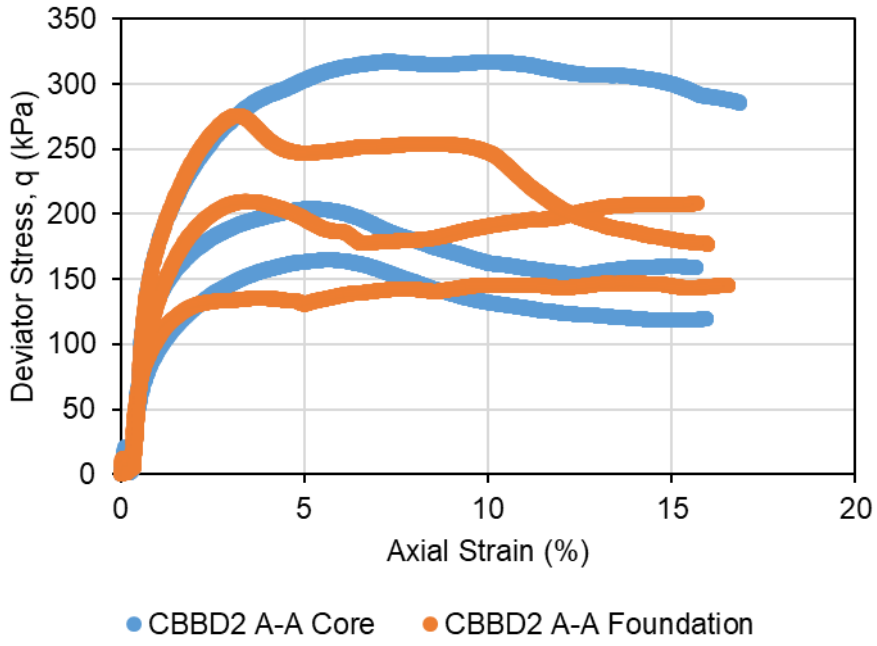

Figure 4.27 Stress-strain behaviour of CBBD2 Section A-A CIU Triaxial test samples

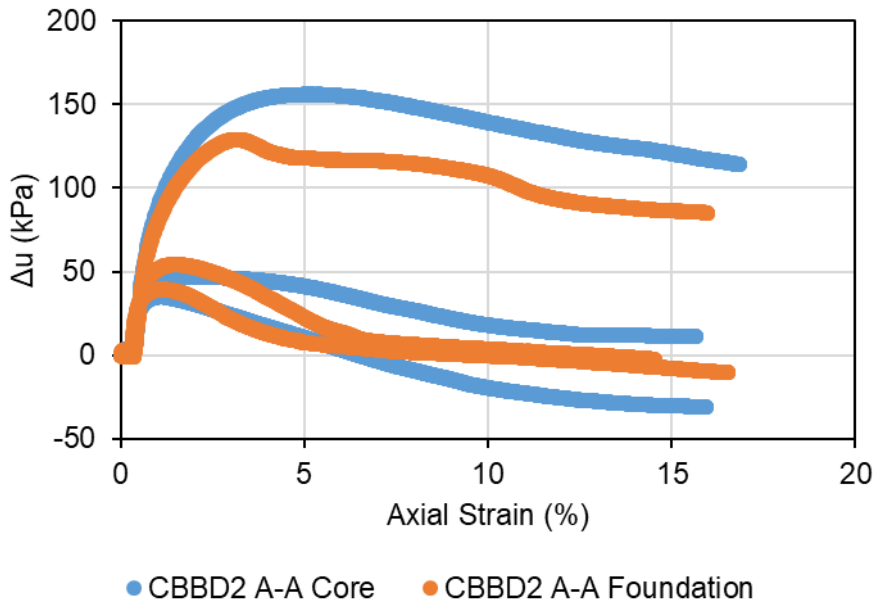

Figure 4.28 Pore water measurements of CBBD2 Section A-A CIU Triaxial test samples

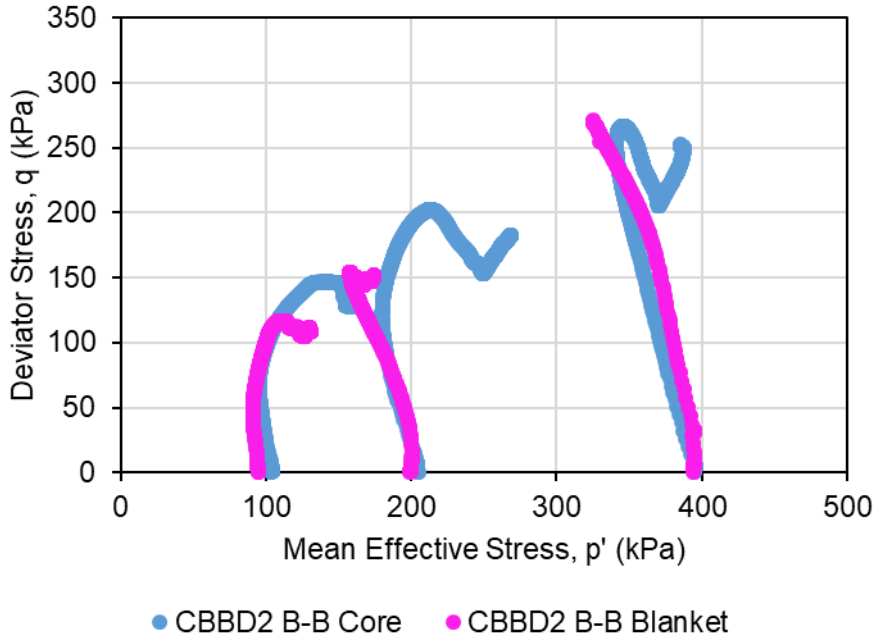

Figure 4.29 Stress paths in p'-q space of CBBD2 Section B-B CIU Triaxial test samples

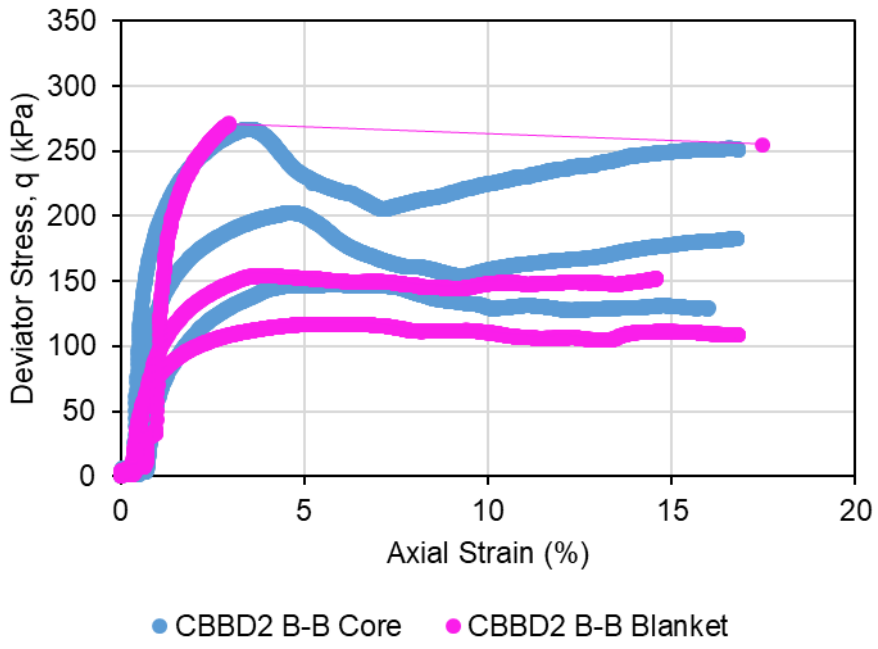

Figure 4.30 Stress-strain behaviour of CBBD2 Section B-B CIU Triaxial test samples

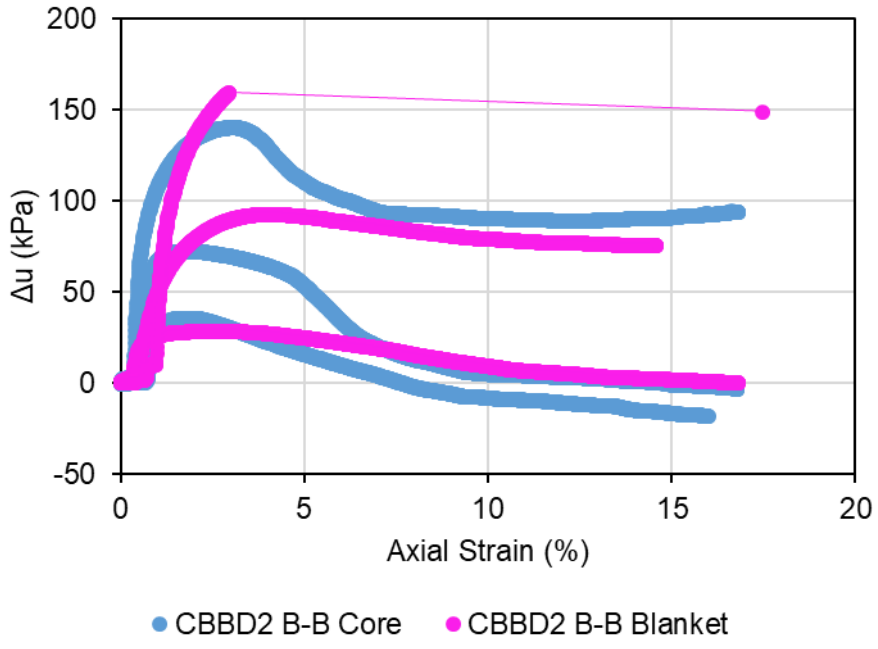

Figure 4.31 Pore water measurements of CBBD2 Section B-B CIU Triaxial test samples

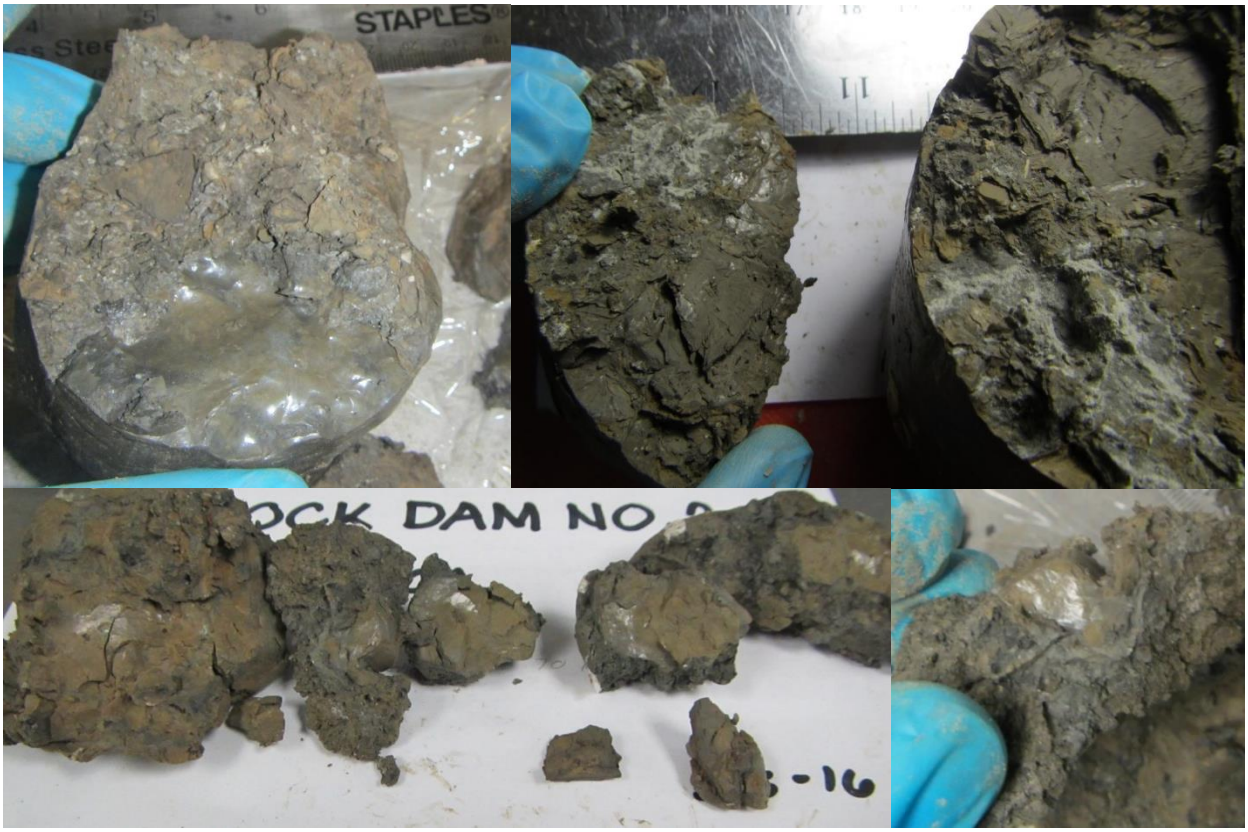

Figure 4.32 CBBD2 clay core post-CIU Triaxial test samples

Figure 4.33 CBBD2 clay blanket post-CIU Triaxial Test test samples

Figure 4.34 CBBD2 clay foundation post-CIU Triaxial test samples

Figure 4.35 CBBD4 clay core post-CIU Triaxial test samples

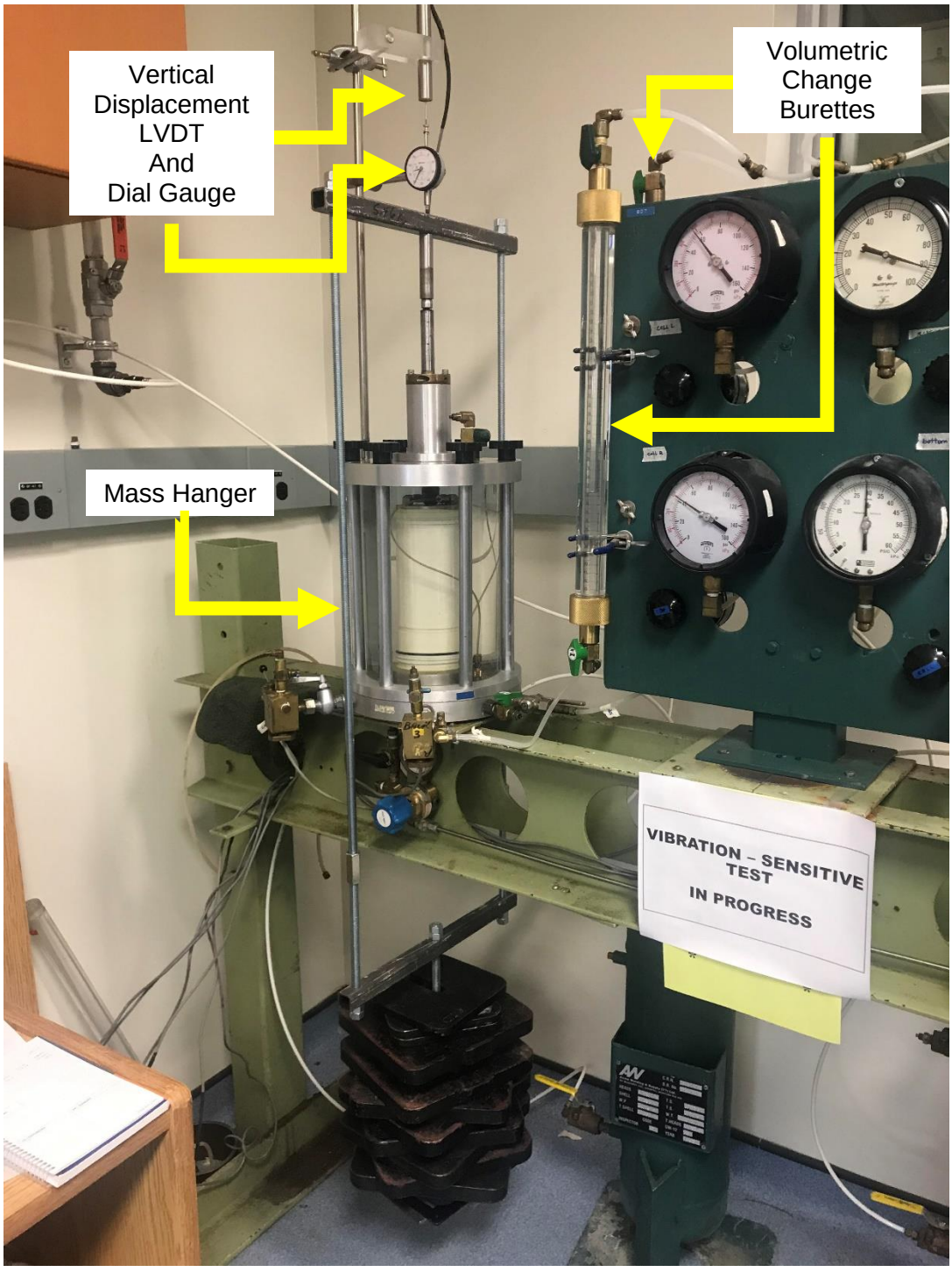

Figure 4.36 Experimental set-up used for Shear Creep tests

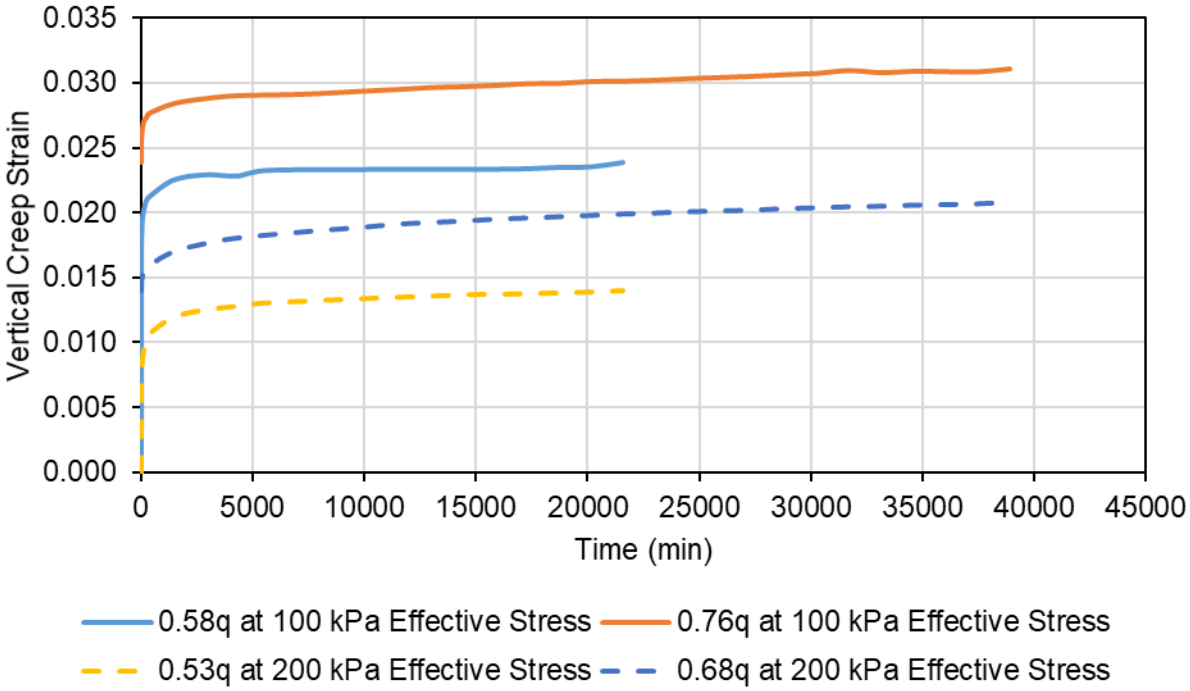

Figure 4.37 Vertical creep strain with respect to time from Creep in Shear tests

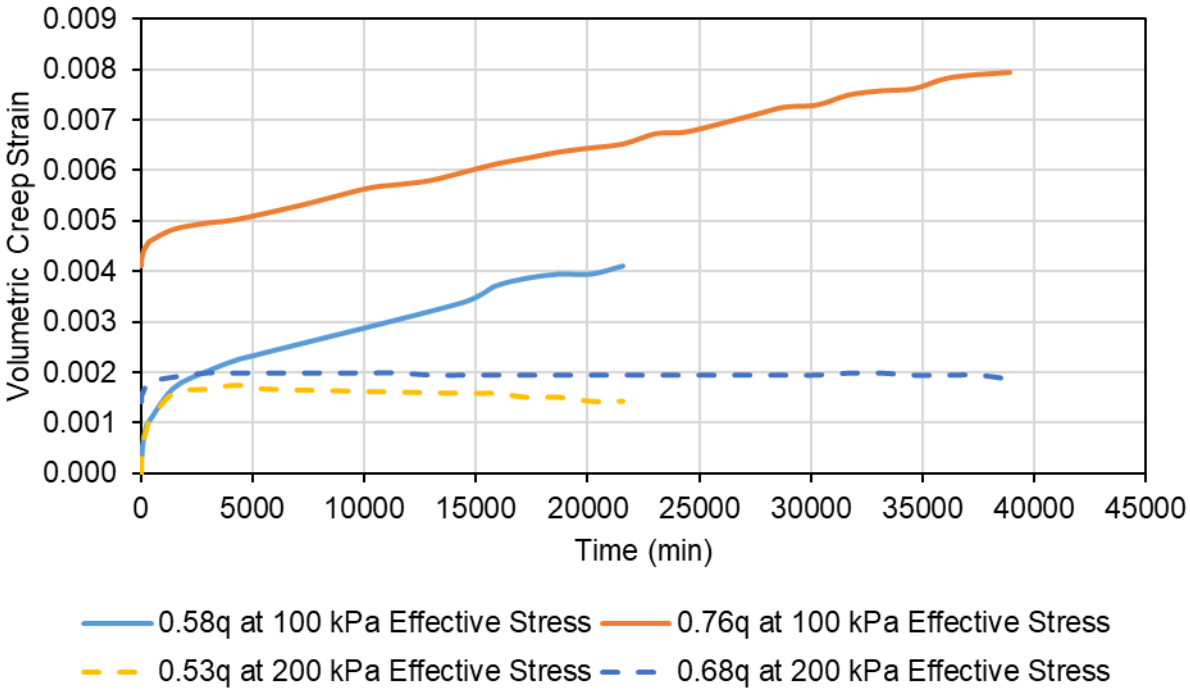

Figure 4.38 Volumetric creep strain with respect to time from Creep in Shear tests

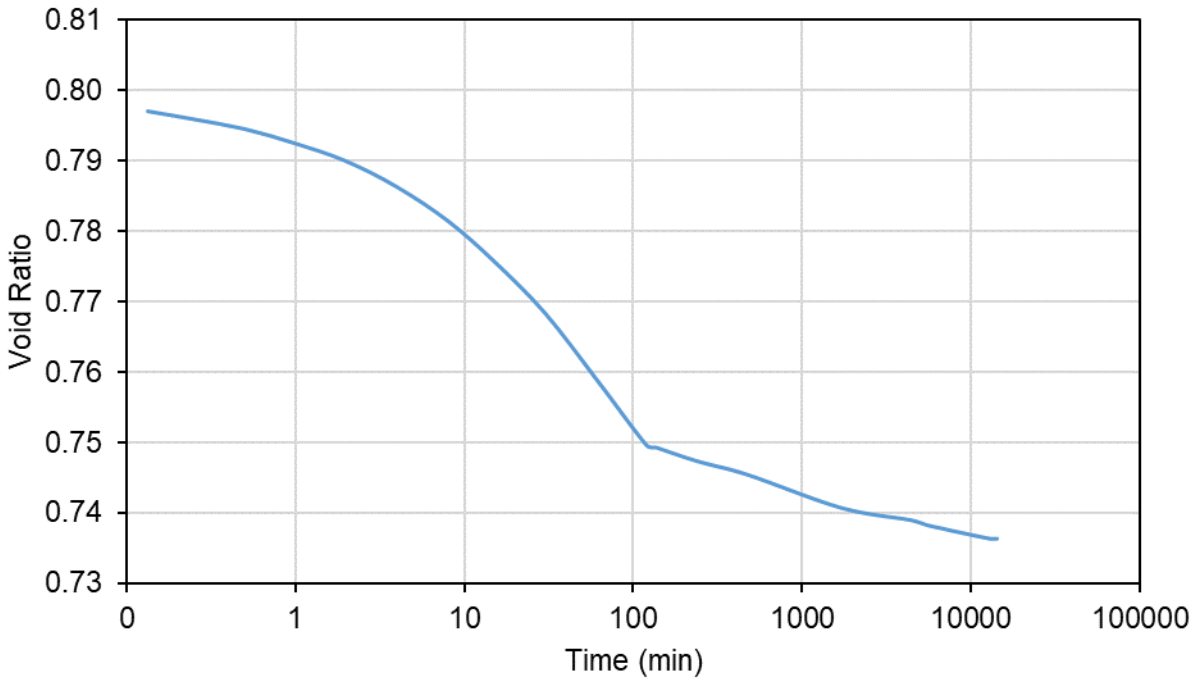

Figure 4.39 Void ratio – log time curve for CBBD2 core sample from Creep in Compression test

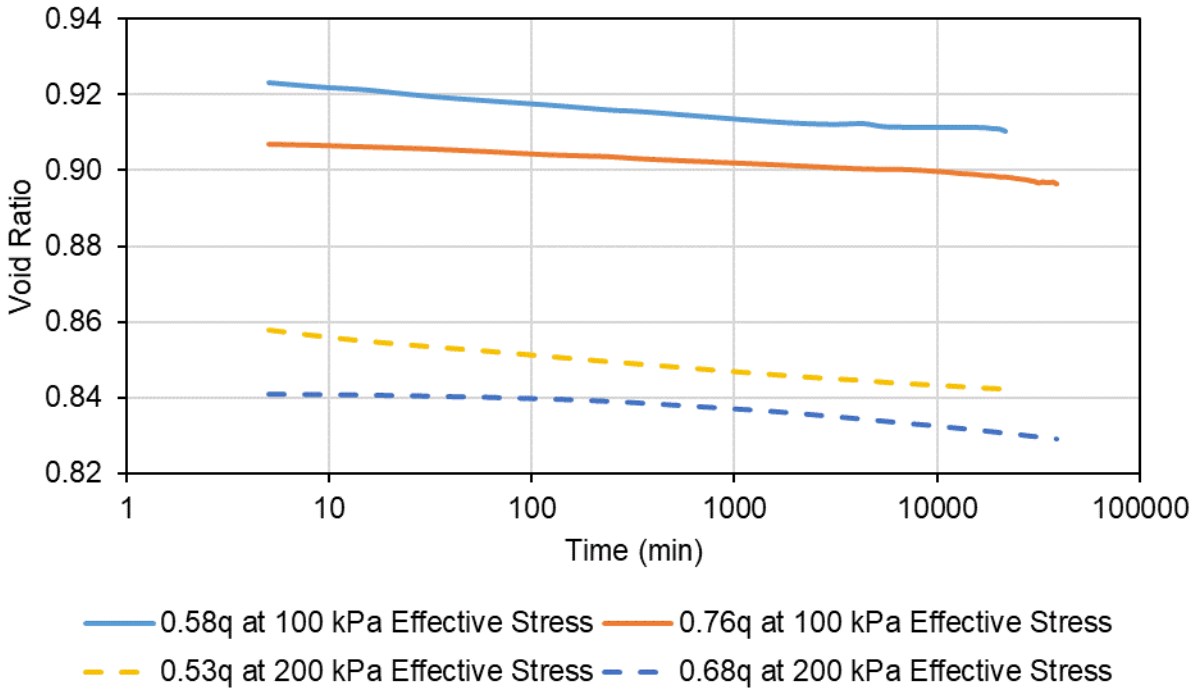

Figure 4.40 Void ratio – log time curve for CBBD2 core sample from Creep in Shear test

Chapter 5 NUMERICAL MODELLING

A numerical model was developed and calibrated using the observed conditions in CBBD2 and results from the laboratory investigation of collected samples. The calibrated model was used to evaluate the stability of the remaining earth dams in CB, WD, EF, and MF generating stations to check if these structures meet current dam safety standards.

5.1 CBBD2 Numerical Model

Numerical modelling was implemented using PLAXIS 2D, a finite element geotechnical engineering software that can perform deformation and stability analyses. PLAXIS 2D was chosen as the modelling platform because it has the capability to incorporate time-dependent creep behavior into the deformation analysis with the use of its Soft Soil Creep model. The highly plastic clay in the core and blanket allowed creep to occur under constant stress during its service years as there were little or no changes in the dam geometry of CBBD2 since its completion in the 1950s. Very slow creep movement could have occurred for many years before the accelerated movement (Tavenas and Leroueil, 1981) at the upstream section of the dam. Due to this, incorporating time-dependent creep deformation analysis in the model was needed.

The Soft Soil Creep (SSC) model was developed by transforming the logarithmic creep law of secondary consolidation into a differential form. It was then extended towards general three-dimensional states of stress and strain by incorporating Modified Cam-Clay and viscoplasticity, with a Mohr-Coulomb failure criteria (Vermeer and Neher, 1999). SSC is an extension of the pre-existing Soft Soil (SS) model, with the addition of the modified creep index (μ^*) parameter to the modified compression (λ^*) and modified swelling (κ^*) indices. The modified

compression and swelling indices were determined using Equation 2.7. The modified creep index was calculated using the following formula:

$$\mu^* = \frac{C_\alpha}{2.3(1+e)} \qquad (Equation\ 3.1)$$

Values for C_α were taken from oedometer test results. The variable *e* corresponded to the initial void ratio from the same test. Soil model parameters used for CBBD2 clay can be seen in Table 5.1. Numerical model parameters for non-clay components (provided by the dam operator and owner) are shown in Table 5.2.

Two cases were considered in terms of shear strength parameters as indicated in Table 5.1. Case 1 used post peak or critical state strengths as the placed compacted clay blanket was assumed to have reached its fully softened state after being underwater for over fifty years. Moreover, the clay core was thought to have strain softened due to the presence of silt lenses and its fissured structure. Strain softening until the residual shear strength was also evident in the consolidated drained direct shear test results. Case 2 used the average between the post peak and residual shear strengths, considering that only a portion of the clay core and clay blanket had yielded. This represents the case wherein certain elements in the model reached residual strength along the slip surface during displacement consistent to that what was reported by Stark and Eid (1997). The reduction of strength from a post peak value to the average between post peak and residual strengths would occur with relatively large movement or straining. For this reason, creep was integrated in Case 2 by means of the SSC model. Case 1 used the SS model.

Post peak shear strength values were available from CIU Triaxial compression tests and Direct Simple Shear (DSS) tests. Based on the postulated slip surface shape, clay core shear strength values were taken from CIU Triaxial compression test results, with post peak strength values at the end of test typically at 15% strain. Clay blanket and foundation strengths were taken from Direct Simple Shear and Direct Shear tests, respectively. The use of shear strengths from

different types of tests is associated with the different stress paths in different parts of the dam. The post peak strength values determined from DSS tests were taken at the end of test strain of 20%. As DSS tests were only performed on CBBD2 clay blanket samples, post peak strengths were determined at 20% strain from Direct Shear tests when needed. Residual shear strength values were preferred to be based on Direct Shear test results. Although Torsional Ring Shear tests were also performed, the Direct Shear test gave slightly lower values of residual shear strength.

As CBBD2 was constructed over fifty years ago, information was limited in terms of the design geometry and construction sequence of these dams. The geometry used in the numerical modelling were based on construction drawings and other documentation provided by the dam operator and owner. Model parameters for other dam elements were inferred from documentation provided from various sources. Details of the construction timeline were not provided by the dam operator and owner. An article by Haines (1959) on earth dams built in the late 1950's in nearby locations, including CBBD2, was used as a guide for the construction details. The article stated that the CBBD2 was constructed within five months. Ten months after construction, the dam reservoir was impounded and was in service. Due to the lack of detailed information, the dam was assumed to have been constructed in stages until completion. Hence, the model dam geometry was divided in lifts of 1 to 2 meters. After fully defining the dam geometry, the finite element mesh was generated. PLAXIS 2D generates 15-node triangular elements based on a robust triangulation procedure. The mesh was then further refined as needed for model convergence. In terms of boundary conditions, vertical and horizontal movement was restricted at the base of the model. The boundary condition along the horizontal ends of the model are fixed in the x-direction and free in the y-direction. Groundwater flow was restricted at the bottom boundary of the model. Hydraulic conditions applied on the upstream side of the earth dam were based on the operational head pond level. Seepage conditions were established by performing a steady-state analysis in

order to determine the phreatic surface within the dam. Hydraulic conductivity values used were 7.47 x 10^{-6} m/day for clay core and clay blanket, and 4.99 x 10^{-6} m/day for the clay foundation, based on permeability test results provided by the dam owner. The location of the phreatic surface was comparable based on back-calculations from installed vibrating wire piezometer readings from Alfaro III (2016). The cross-section, generated mesh, and phreatic surface for CBBD2 Section A-A and B-B can be seen in Figures 5.1 to 5.2, respectively.

Construction stages were defined in the staged construction mode in PLAXIS 2D. After initial stress generation, consolidation calculation was conducted per construction phase. The consolidation option considered pore water dissipation for a predefined period of time and included the effect of changes to the active geometry of the dam. Construction duration per construction stage or lift was assumed, provided that the total construction time was five months as indicated by Haines (1959). Consolidation time of 10 months was used prior to impounding. Additional consolidation calculation phases were needed in order to observe the deformation behaviour of CBBD2 at time intervals after the start of the full service of CBBD2. Both sections were investigated at 1, 10, 30, 40, and 50 years after the reservoir was filled.

A safety calculation would determine the factor of safety against stability. The calculations for the factors of safety were carried out in sequence (sequential modelling). A finite element method of analyses was done to establish the stresses, deformations and pore water pressures. They are then used in stability analysis using the strength reduction approach to calculate the factor of safety of the dam. PLAXIS 2D adopted the phi-cohesion (φ'-c') reduction technique, also known as strength reduction method, in calculating the factor of safety. The shear strength parameters were successively reduced until the final step has resulted in a fully developed failure mechanism. The incremental displacements generated during the safety calculation phase could be used to verify the probable failure surface supplementary to displacement results (PLAXIS, 2018). The factor of safety values were compared against the required criteria that were adopted

by previous investigations and current dam safety practice (Canadian Dam Association, 2013): a factor of safety of 1.5 against normal water level load cases, and a value of 1.0 considering normal water levels and seismic loading.

The numerical model must represent the observed conditions of the dam throughout its service life. Settlement was still observed even after forty years of being in service until the sudden movement in the upstream section occurred after over fifty years based on previous reports provided by the dam operator (also discussed in Section 2.1). Although the movement did not cause complete collapse of the dam, it was still seen as a sign of instability. These conditions must be shown in the calibrated model of CBBD2.

5.2 CBBD2 Model Calibration Results

The development of deformation in CBBD2 using Case 1 can be seen in Figures 5.3 to 5.4 for Section A-A and B-B, respectively. Results indicated that displacements slightly increased as the shaded areas slightly changed and became constant thirty years after impounding was completed. As previous investigations (mentioned in Section 2.1) noted movement in the dam even after 40 service years, this meant that Case 1 was not able to show observed dam conditions.

Using Case 2, deformation development results revealed that displacements continued to occur way into the service life of CBBD2. Figure 5.5 displayed that Section A-A was deforming in a more uniform manner when compared to Section B-B (Figure 5.6). The presence of clay from the upstream to the downstream side of Section A-A permitted settlement to be somewhat uniform with respect to time. On the other hand, the absence of clay at the downstream side of Section B-B led to the concentrated creeping movement on the upstream side. It was also observed that Case 2 was able to approximately match the reported settlement (at forty years) of 0.25 m from

the crest from previous investigations. Both sections had a recorded settlement of about 0.27 m along the centreline of the model at 40 years into the service life of CBBD2.

Factor of safety calculation results can be seen in Figure 5.7. Using Case 1 at the end of the analyses revealed that Section A-A had a factor of safety of 1.35 while Section B-B had 1.36. Considering creep with post peak strengths, the factor of safety was reduced to 1.28 and 1.20 for Sections A-A and B-B, respectively. As displayed in Figure 5.7, the increase in displacement when creep was included in the analyses even with post peak strengths allowed for sufficient shear mobilization led to the decrease in factor of safety. Knowing that CBBD2 already showed signs of instability, a factor of safety less than unity for Section B-B was expected. Further reduction in the factor of safety values was observed when Case 2 was used in the analyses. Section A-A remained stable with a factor of safety of 1.15 while a factor of safety value of 0.99 was obtained for Section B-B. As previously mentioned, the average of the fully softened and residual shear strengths would only be reached when sufficient shear displacement is reached. Such sufficient shear displacement was attained with creep.

Figures 5.8 to 5.9 illustrates the shear strength and mobilized shear stress along the approximated slip surface from safety calculations in CBBD2 Section B-B using Case 1 and Case 2, respectively. The x-coordinates corresponded to the coordinates from the toe towards the crest along the upstream slope of Section B-B. Figure 5.8 show that in using Case 1, the mobilized shear stress curve was below the available shear strength at most points. It can also be observed that yielding has started at the crest and along the clay core as the curves overlapped at these points. On the other hand, it was clear from Figure 5.9 that failure was imminent using Case 2 as the mobilized shear stress and shear strength curves coincided with each other brought about by sufficient shear displacement over time due to creep. It should be noted that creep deformation did not only affect the shear strength but also the mobilized shear stress.

Another simulation using Case 2 on Section B-B was performed using a modified creep index clay core value based on shear creep results. Safety calculation on this simulation returned a factor of safety value of 1.03 indicating instability, which also matches actual conditions in Section B-B. This meant that the use of both modified creep index based on compression creep tests and based on shear creep tests could produce the observed movements and delayed instability in CBBD2. Both compression creep and shear creep tests are useful to describe creep deformations. Shear creep test has an added benefit of providing information on creep rupture or failure (refer to Section 4.5.2).

Case 2 was able to represent both the expected deformation and stability conditions for both Section A-A and Section B-B. This implied that the calibrated numerical model based on the observed conditions of the dam should include time-dependent creep deformation analysis using clay strength values between the post peak and residual shear strengths. Furthermore, findings from numerical model calibration have shown that the mobilized shear strength for first-time slides in fissured clay (which CBBD2 had) was as low as the average between the post peak and residual shear strengths. This was similar to results from studies by Skempton (1985) as well as Stark and Eid (1997).

Model calibration results gave insights as to the cause of the delayed instability in CBBD2. CBBD2 has been under constant load as there were no changes in the dam (such as dam heightening) for over fifty years since it has been constructed. High clay content and plasticity in the clay core, blanket, and foundation allowed creep movement to occur under the constant load of the dam. Creeping in Section A-A was occurring both in the upstream and downstream side owing to the presence clay underneath the dam. On the other hand, settlement was transpiring over time over the upstream section due the placed compacted blanket that was tied into the inclined clay core in Section B-B. The absence of the naturally occurring clay in the downstream side led to the predominant upstream movement within this section. Over the service years of

CBBD2, sufficient movement or straining developed due to creep. This warrants the use of a reduced clay shear strength value in the stiff fissured clay from a post peak value to an average value between post peak and residual shear strengths. This reduction occurred at the later service years as initial creep movement in overconsolidated clays tend to be small and would increase with respect to time. The predominant creep movement at the upstream slope and the reduction of shear strength of the fissured overconsolidated clays with respect to time led to the instability in CBBD2 Section B-B.

5.3 Assessment of remaining water-retaining earth fill dams

Numerical model generation for the remaining earth dams was completed following the construction stages and duration used for CBBD2. Model dam geometry were based on provided construction drawings. Hydraulic conductivity values were assumed to be the same as CBBD2 due to lack of information. Shear strength parameters for clay core elements were taken from CIU Triaxial compression test results while clay blanket and foundation strengths were taken from Direct Shear tests. Stability analysis was performed sixty years after the reservoir was filled. The cross-section, generated mesh, and phreatic surface for the remaining dams can be seen in Figures 5.10 to 5.15. Soil model parameters used can be seen in Tables 5.2 to 5.5.

Stability analyses were initially performed on the remaining earth dams using Case 1. The results summarized in Table 5.6 indicate that all dams were stable with factors of safety greater than unity with only CBMD and WD satisfying the current dam safety requirement. However based on findings from shear creep tests discussed from the previous chapter, satisfying a factor of safety of 1.5 might no longer be sufficient as part of the clay core would already exhibit creeping behavior. This reinforces the need to include creep in the long-term stability analysis using strength parameters taken as the average of fully softened and residual shear strengths. Comparing safety calculations results with the required current dam safety factor of 1.5 should at

least incorporate time-dependent displacements that could possibly affect the long-term stability and serviceability of dams.

The stability analyses using Case 2 are presented in Figures 5.16 to 5.21 and summarized in Table 5.7. Particular attention must also be given to CBBD4 that had a factor of safety of unity which could mean that the earth dam is at a condition of impending instability. As for the remaining earth dams (CBMD, WD, EF, MFRED, and MFLED), they are considered stable with factor of safety values greater than unity though they do not conform to the long-term stability required factor of safety value of at least 1.5 when creep is considered in the analysis. Based on shear creep test results, a factor of safety higher than 1.3 would be needed in order to avoid delayed instability due to creep rupture. Only two of the remaining seven earth fill dams (CBMD and WD) passed this criteria, implying that there is a need to monitor the other dams with regards to possible delayed instability caused by creep. The results of analyses using Case 2 has shown that the investigated dams are in need of remedial measures to improve its stability.

Since these dams were showing movement in the upstream and downstream side, verification was needed to determine the probable failure surface location by looking into incremental displacements generated from safety calculations, as recommended by PLAXIS 2D. The incremental displacement contours indicate the localization of deformations within the soil at failure for the current calculation step (PLAXIS, 2018). Findings can be seen in Figures 5.22 to 5.27. Darker shades of red indicated where the highest incremental movement could occur. The location of the probable failure surface could provide information in terms of where to strengthen these earth dams in order to improve dam stability. Moreover, locations of instrumentation can be planned accordingly in order to effectively monitor these dams against instability. Probable failure surface location are summarized in Table 5.7. Displacement development of these dams using Case 2 can be seen in Appendix D.

The outcome of the assessment of the aging earth dams has shown the significance of considering long term analysis of structures considering creep. Structures such as water-retaining dams are expected to have long-service lives and instability of these structures would have detrimental consequences. The use of a finite element method of analysis with a time-dependent soil creep model would be able to provide predicted movement or instability with respect to time from the long-term analysis. In so doing, findings from this type of analysis would urge for the need for more frequent long term in-situ monitoring as well as a proper remedial plan should it be necessary.

The limitation of the numerical modelling used in this study is associated with sequential modelling to calculate the factor of safety. This is an inherent limitation with PLAXIS 2D where degradation or reduction of shear strength due to creep deformation is only evoked prior to the calculation of the factor of safety. A more rigorous fully-coupled modelling is desirable, which coupled time dependent deformation and its associated degradation of shear strength.

5.4 Summary

A numerical model was calibrated based on the actual conditions of CBBD2. Two cases were considered in terms of the model parameters for clay. Case 1 used post peak shear strengths without creep, while Case 2 used the average value between post peak and residual strengths considering creep.

The calibrated model that represented the expected deformation and stability conditions of CBBD2 included time-dependent creep deformation analysis using clay strength values between the post-peak and residual shear strengths. Results revealed that displacements continued to occur way into the service life of CBBD2 and was able to approximately match the reported settlements at Section B-B, when Case 2 was used. Displacement development at Section A-A

indicated that movement was occurring both along its upstream and downstream side with respect to time. On the other hand, Section B-B only experienced movement along its upstream side over time. Factor of safety calculations using Case 2 agreed with actual stability conditions wherein Section A-A remained stable (FS = 1.15) while Section B-B was unstable (FS = 0.99). Another simulation using Case 2 on Section B-B was performed using a modified creep index clay core value based on shear creep results which produced a factor of safety of 1.03, also indicating failure. This suggests that the use of both modified creep index based on compression creep tests and based on shear creep tests could produce the observed movements and delayed instability in CBBD2. Model calibration results indicated that the predominant creep movement at the upstream slope and the reduction of shear strength of the fissured overconsolidated clays with respect to time led to the delayed instability in CBBD2 Section B-B.

As discussed in the previous chapter, satisfying a factor of safety of 1.5 might no longer be sufficient as part of the clay core would already exhibit creeping behavior. This strengthens the need to include creep long-term stability analysis using strength parameters taken as the average of fully softened and residual shear strengths. Time-dependent displacements that could possibly affect the long-term stability and serviceability of dams should be included in the stability analyses prior to comparing the results with the required current dam safety factor of 1.5. Using Case 2, calculated factors of safety indicated that CBMD, WD, EF, MFRED, and MFLED were still stable (FS > 1.0). However, these values did not pass the factor of safety criteria of 1.5 against normal water level load cases which calls for proper remediation in order for these dams to satisfy current safety standards. Particular attention must also be given to CBBD4 that had a factor of safety is at unity which could mean that the earth dam is at a condition of impending instability. A factor of safety higher than 1.3 would be needed in order to avoid long-term failure due to creep based on shear creep test results. Only two of the remaining seven earth fill dams (CBMD and WD) passed

this criteria, implying that there is a need to monitor the other dams with regards to possible delayed instability due to creep rupture.

Table 5.1 Model parameters for clay components of CBBD2

Parameters	**Section A-A**		**Section B-B**	
	Core	Foundation	Core	Blanket
Soil Model	Soft Soil/Soft Soil Creep			
Unit weight, γ (kN/m^3)	17			
Modified compression index, λ^*	0.0245	0.0282	0.0230	0.0254
Modified swelling index, κ^*	0.0169	0.0139	0.0126	0.0164
Modified creep index, μ^*	0.0023	0.0021	0.0018	0.0020
Overconsolidation ratio	1.6	8.5	3.1	12.7
Post peak φ' (°)	19	14	18	21
Average[1] φ' (°)	15	11	13	15

[1] average of post peak and residual angles of friction

Table 5.2 Model parameters for non-clay components (provided by owner)

Parameters	Rockfill	Topping	Filter	Sandy Silt	Sand Fill	Sand and Gravel	Bedrock
Soil Model	Mohr-Coulomb						Non-porous Linear Elastic
Unit weight, γ (kN/m^3)	20.4	18.9	18.1	18.1	18	17.7	23
Young's modulus, E (kN/m^2)	4.0E+05	1.5E+05	1.0E+05	4.0E+04	1.0E+05	1.0E+05	5.0E+06
Poisson's ratio, v'	0.35	0.3	0.334	0.334	0.334	0.334	0.15
Post peak φ' (°)	45	35	34	30	33	36	--

Table 5.3 Model parameters for clay components of CBBD4 and CBMD

Parameters	CBBD4			CBMD	
	Core	Foundation	Blanket	Core	Foundation
Soil Model	Soft Soil/Soft Soil Creep				
Unit weight, γ (kN/m^3)	17				
Modified compression index, λ^*	0.0263	0.0260	0.0254	0.0263	0.0263
Modified swelling index, κ^*	0.0122	0.0179	0.0164	0.0152	0.0152
Modified creep index, μ^*	0.0021	0.0018	0.0020	0.0017	0.0021
Overconsolidation ratio	3.0	5.4	13.9	5.6	8.5
Post peak φ' (°)	18	10	17	18	16
Average[1] φ' (°)	13	5	12	11	11

[1] average of post peak and residual angles of friction

Table 5.4 Model parameters for clay components of WD and EF

Parameters	WD		EF	
	Core	Foundation	Core	Foundation
Soil Model	Soft Soil/Soft Soil Creep			
Unit weight, γ (kN/m^3)	17			
Modified compression index, λ^*	0.0297	0.0237	0.0182	0.0163
Modified swelling index, κ^*	0.0171	0.0162	0.0067	0.0060
Modified creep index, μ^*	0.0021	0.0020	0.0013	0.0016
Overconsolidation ratio	3.6	5.1	2.0	6.7
Post peak φ' (°)	22	14	26	23
Average[1] φ' (°)	16	12	20	22

[1] average of post peak and residual angles of friction

Table 5.5 Model parameters for clay components of MFRED and MFLED

Parameters	MFRED	MFLED
	Core	Core
Soil Model	Soft Soil/Soft Soil Creep	
Unit weight, γ (kN/m^3)	17	
Modified compression index, λ^*	0.0263	0.0205
Modified swelling index, κ^*	0.0088	0.0096
Modified creep index, μ^*	0.0022	0.0019
Overconsolidation ratio	4.0	3.8
Post peak φ' (°)	16	12
Average[1] φ' (°)	12	10

[1] average of post peak and residual angles of friction

Table 5.6 Factor of safety in remaining earth dams using Case 1

Location	Factor of Safety (FS)	FS > 1.0	FS ≥ 1.5
CBBD4 (with blanket)	1.1	Yes	No
CBBD4 (without blanket)	1.1	Yes	No
CBMD	1.5	Yes	Yes
WD	1.5	Yes	Yes
EF	1.4	Yes	No
MFRED	1.4	Yes	No
MFLED	1.3	Yes	No

Table 5.7 Factor of safety and critical surface location in remaining earth dams using Case 2

Location	Factor of Safety (FS)	FS > 1.0	FS ≥ 1.3	FS ≥ 1.5	Critical Surface
CBBD4 (with blanket)	1.0	No	No	No	Downstream
CBBD4 (without blanket)	1.0	No	No	No	Downstream
CBMD	1.4	Yes	Yes	No	Upstream
WD	1.3	Yes	Yes	No	Downstream
EF	1.2	Yes	No	No	Downstream
MFRED	1.1	Yes	No	No	Upstream
MFLED	1.1	Yes	No	No	Upstream

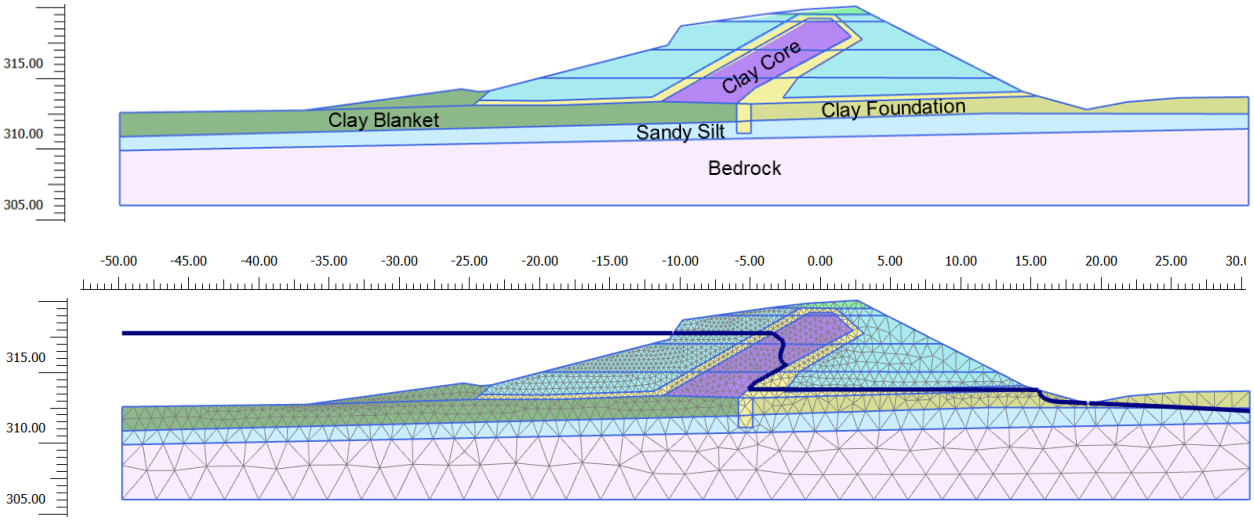

Figure 5.1 CBBD2 Section A-A cross-section, generated mesh, and phreatic surface

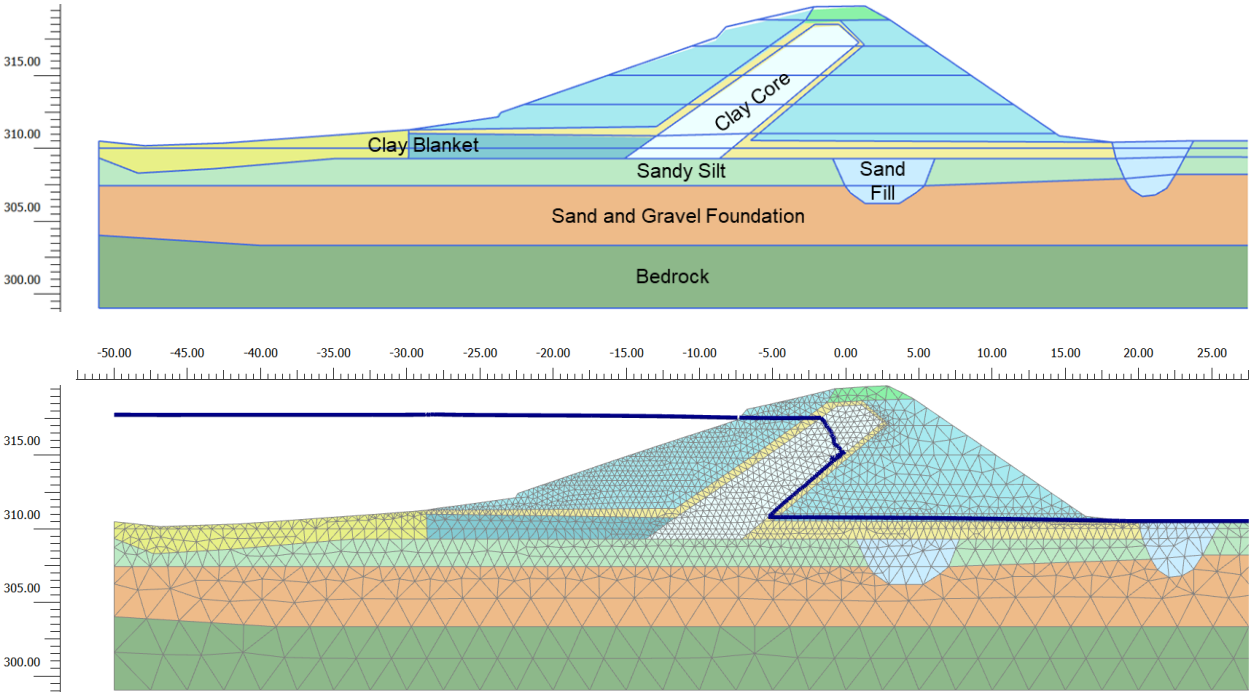

Figure 5.2 CBBD2 Section B-B cross-section, generated mesh, and phreatic surface

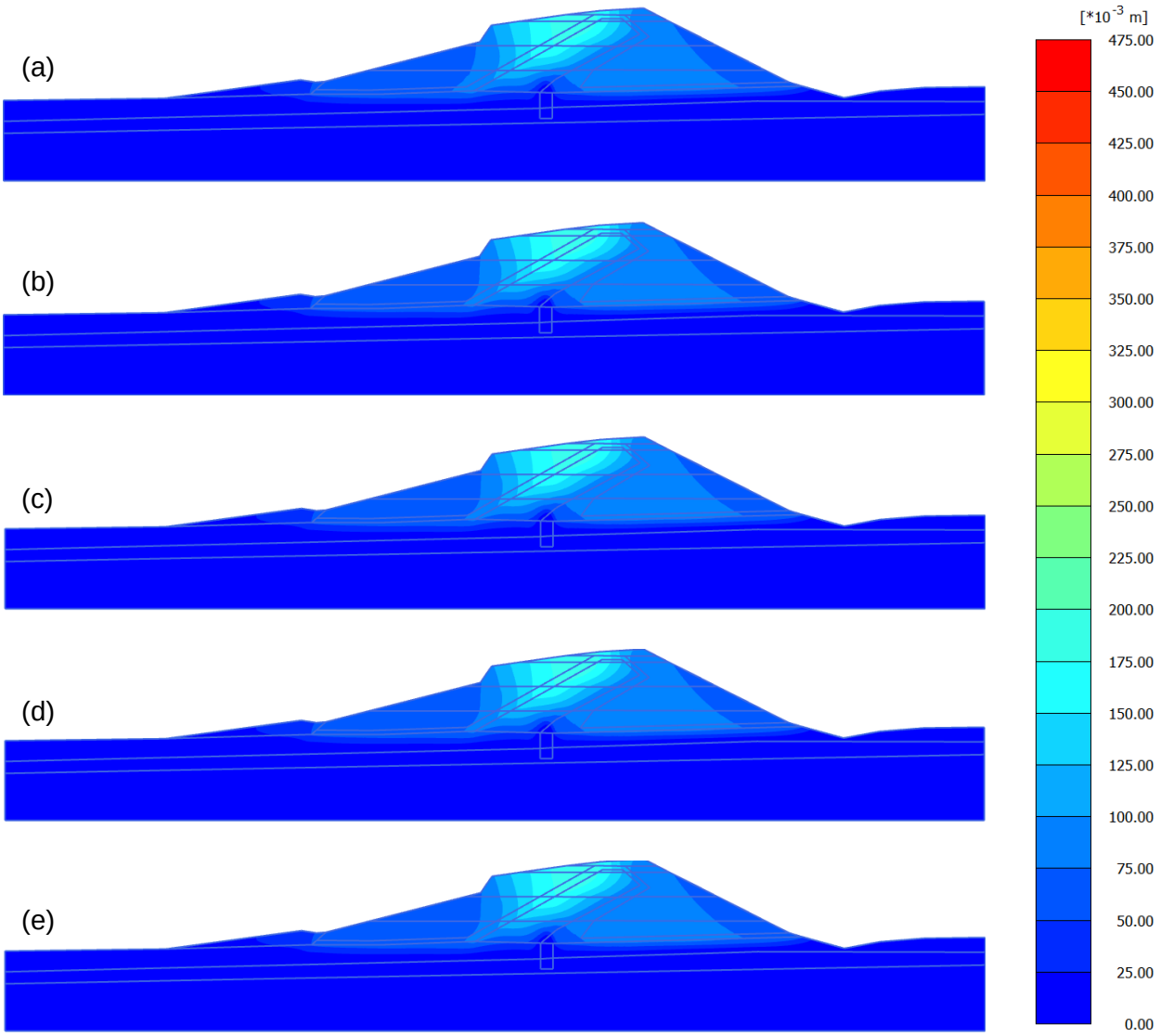

Figure 5.3 Deformation development in CBBD2 Section A-A at different stages using Case 1: after (a) construction, (b) 1, (c) 10, (d) 30, and (e) 50 years after impounding

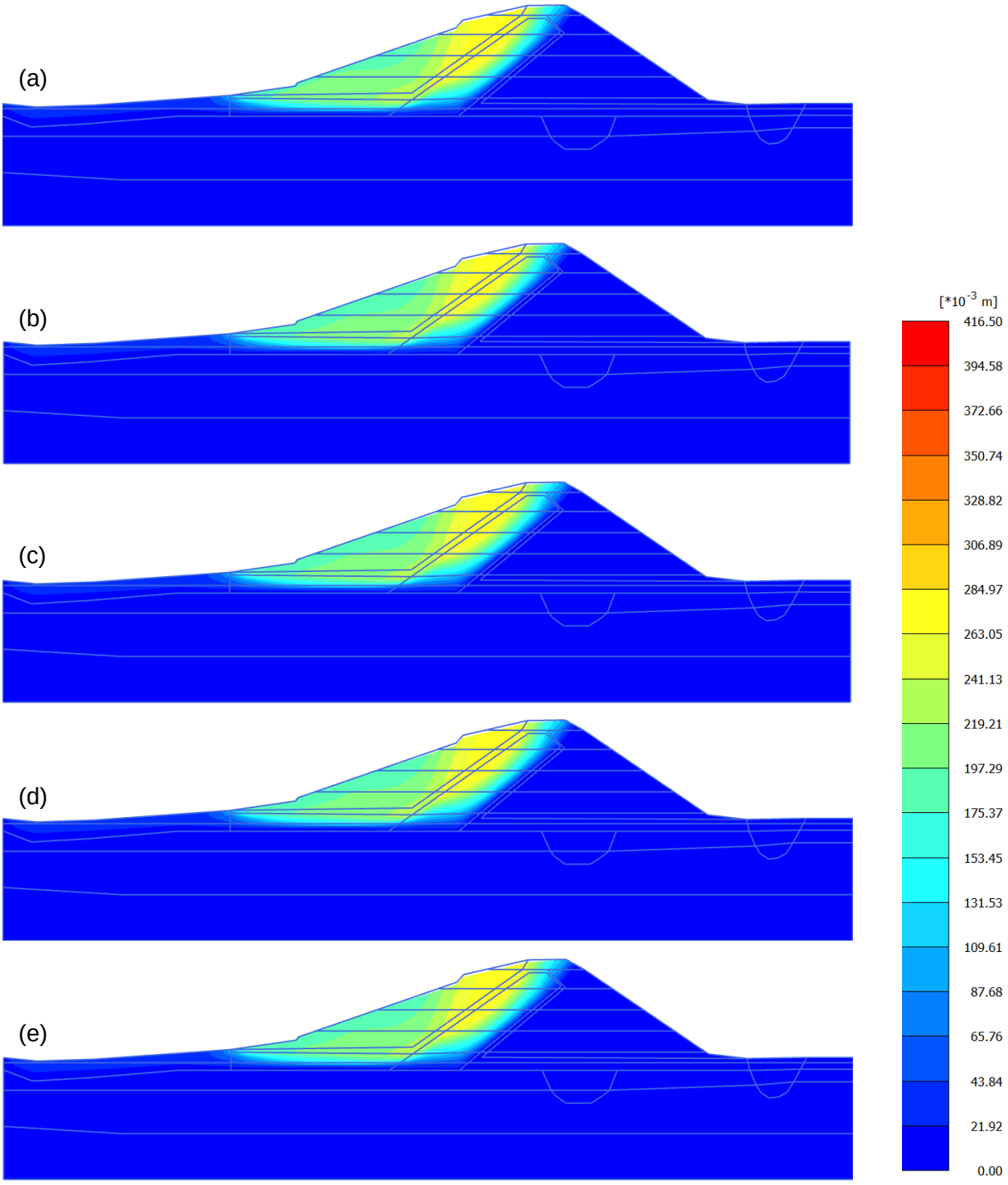

Figure 5.4 Deformation development in CBBD2 Section B-B at different stages using Case 1: after (a) construction, (b) 1, (c) 10, (d) 30, and (e) 50 years after impounding

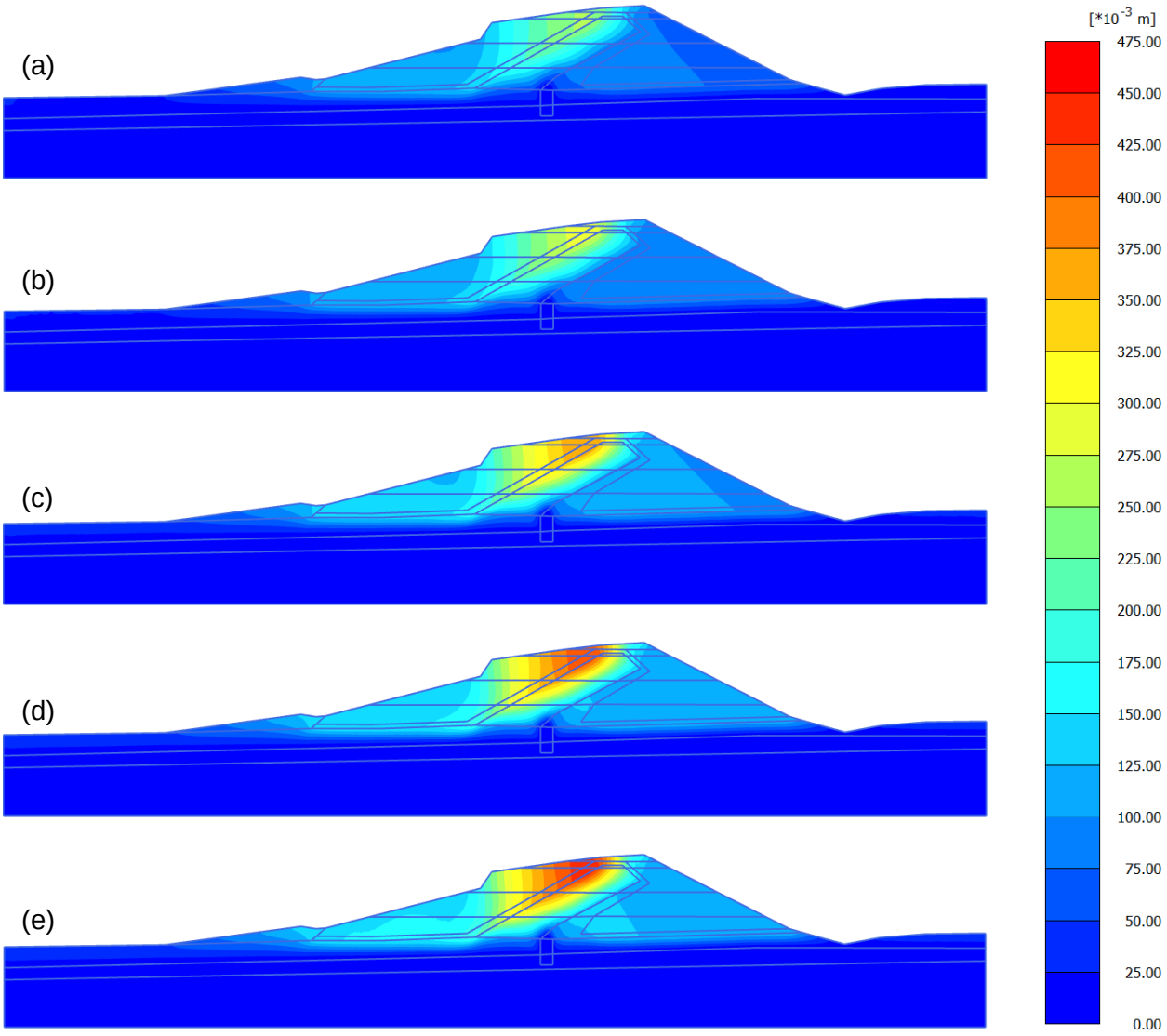

Figure 5.5 Deformation development in CBBD2 Section A-A at different stages using Case 2: after (a) construction, (b) 1, (c) 10, (d) 30, and (e) 50 years after impounding

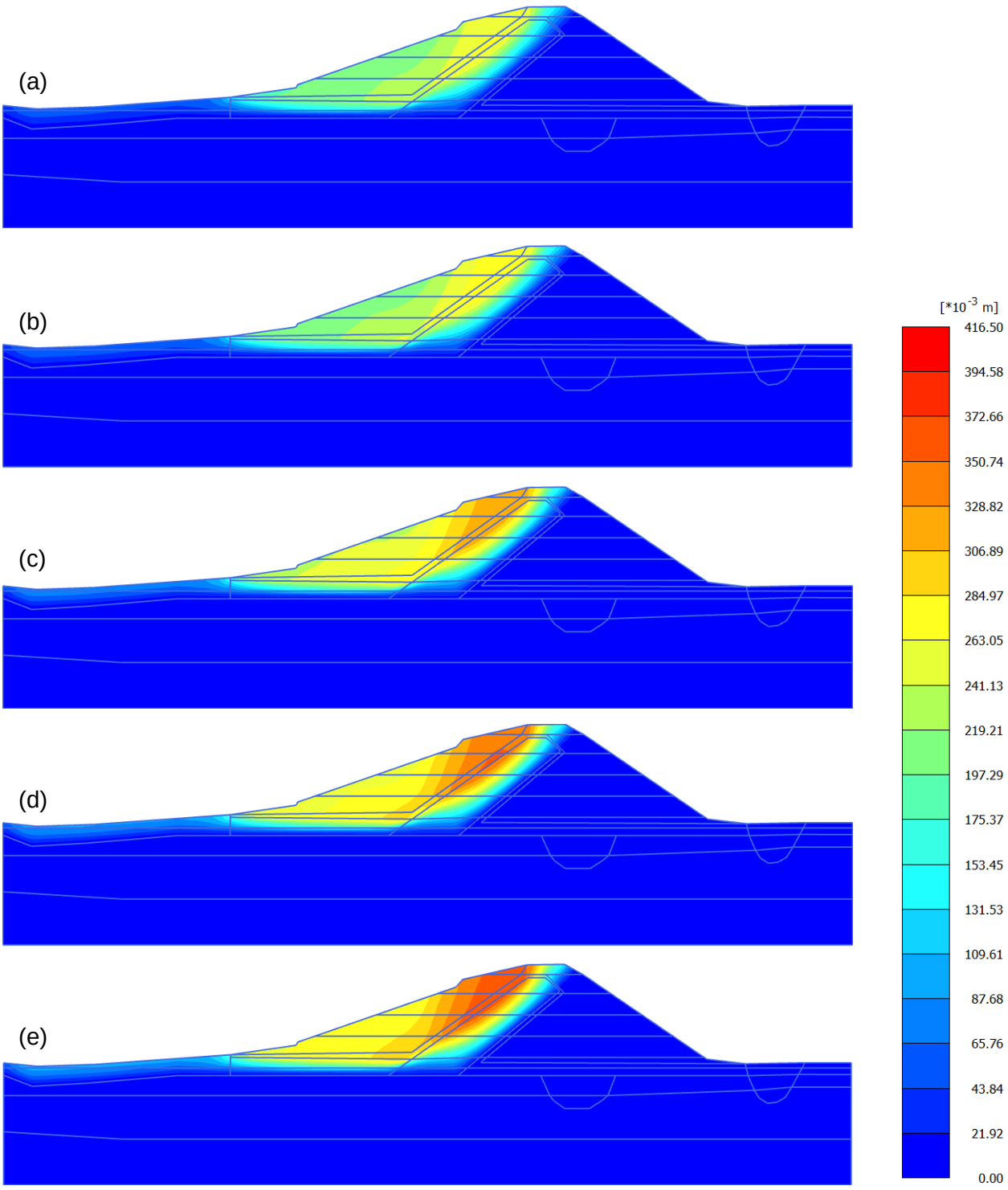

Figure 5.6 Deformation development in CBBD2 Section B-B at different stages using Case 2: after (a) construction, (b) 1, (c) 10, (d) 30, and (e) 50 years after impounding

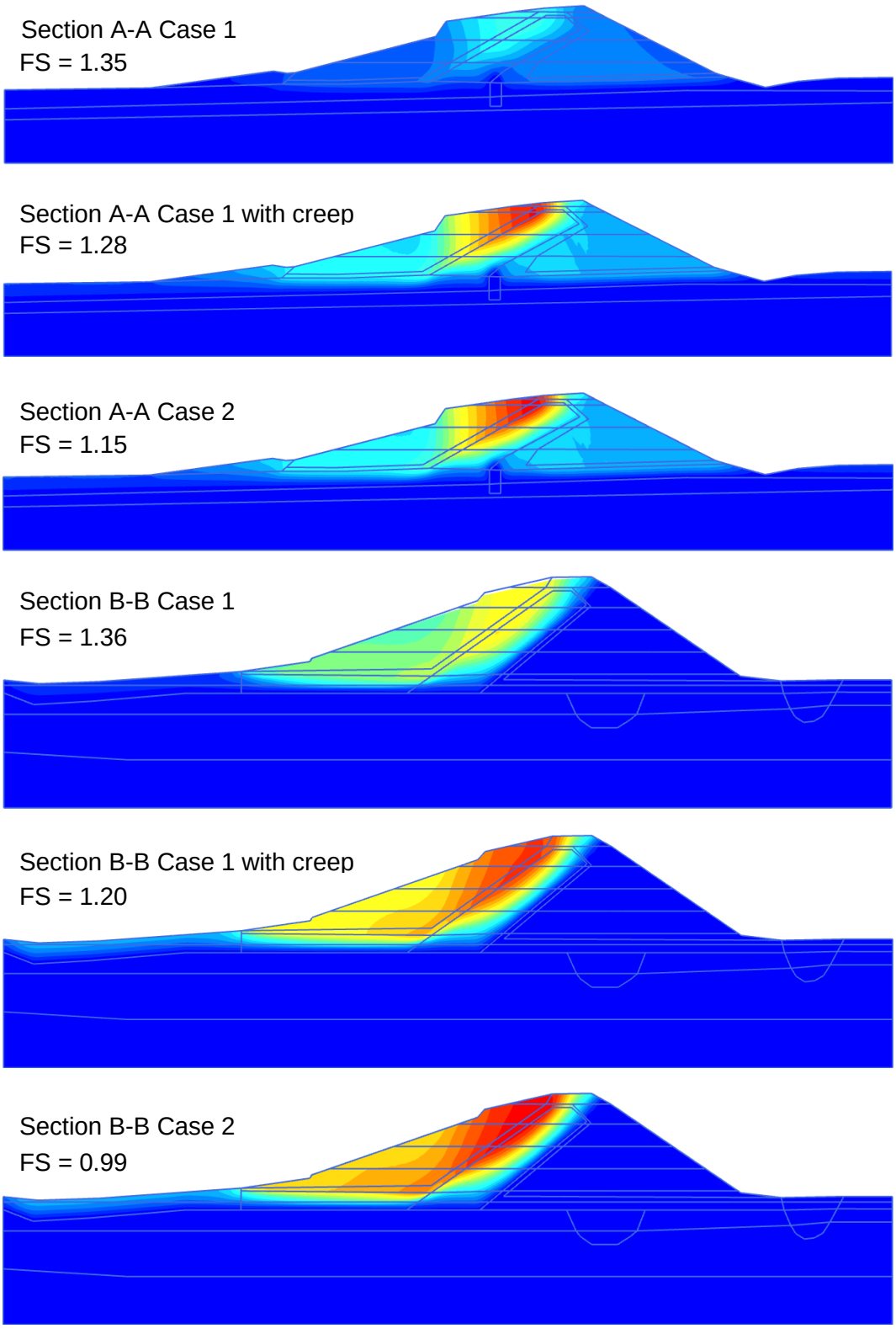

Figure 5.7 Factor of safety values at time of failure at CBBD2

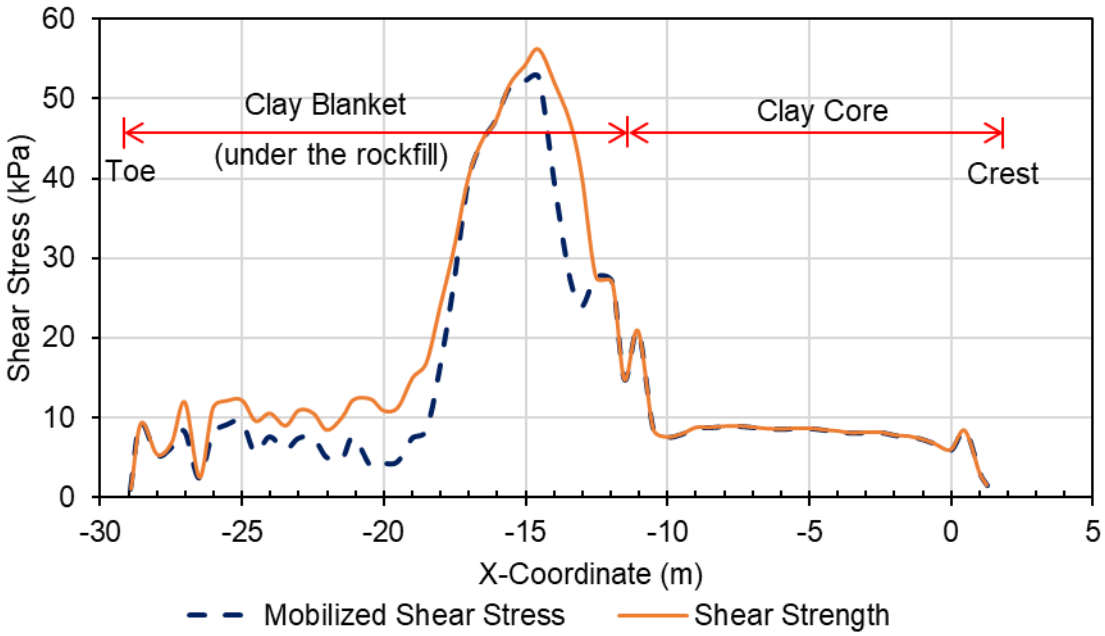

Figure 5.8 Mobilized shear stress and shear strength along slip surface at CBBD2 Section B-B using Case 1

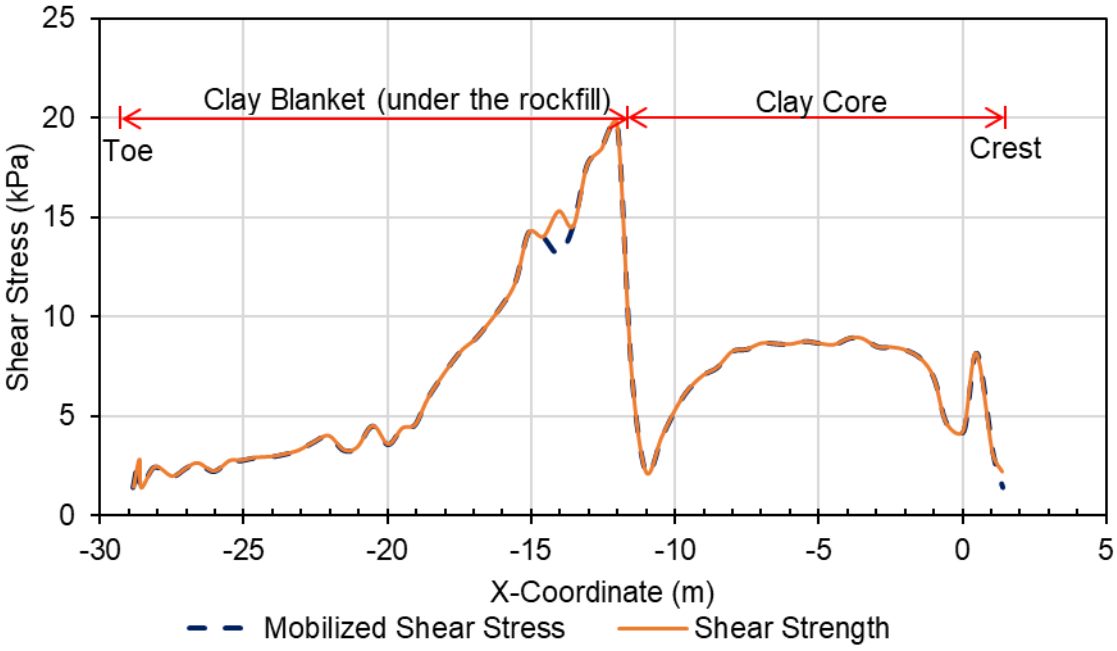

Figure 5.9 Mobilized shear stress and shear strength along slip surface at CBBD2 Section B-B using Case 2

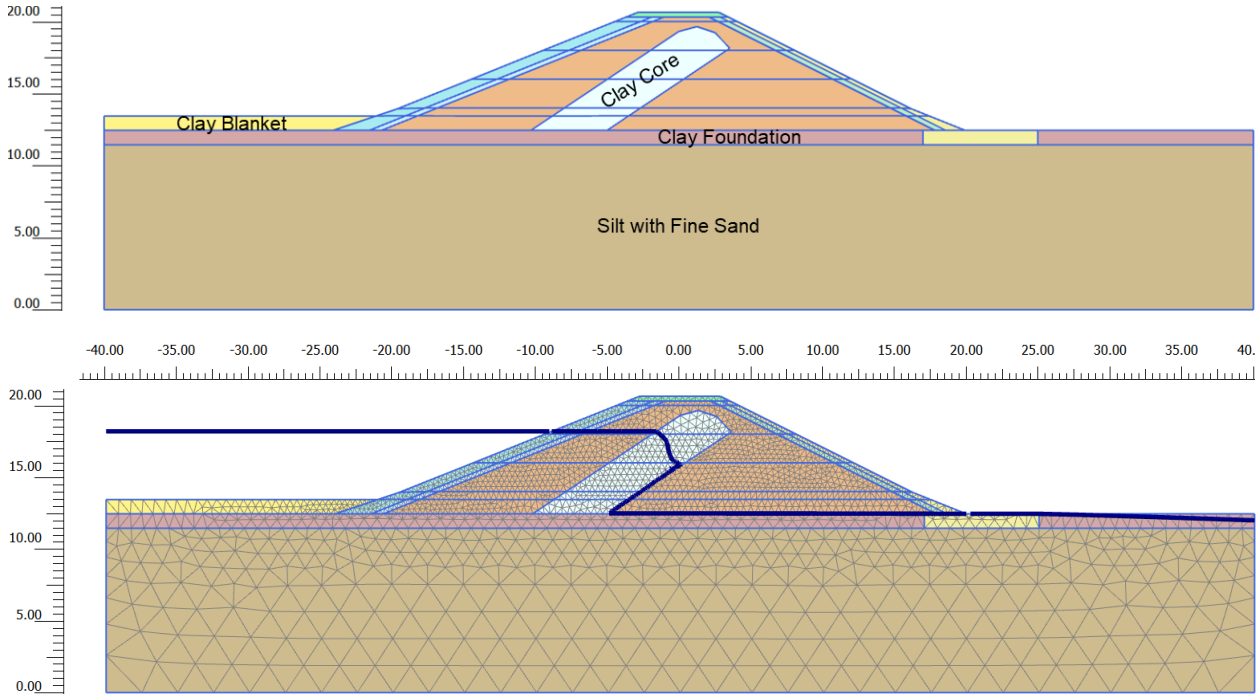

Figure 5.10 CBBD4 cross-section, generated mesh, and phreatic surface

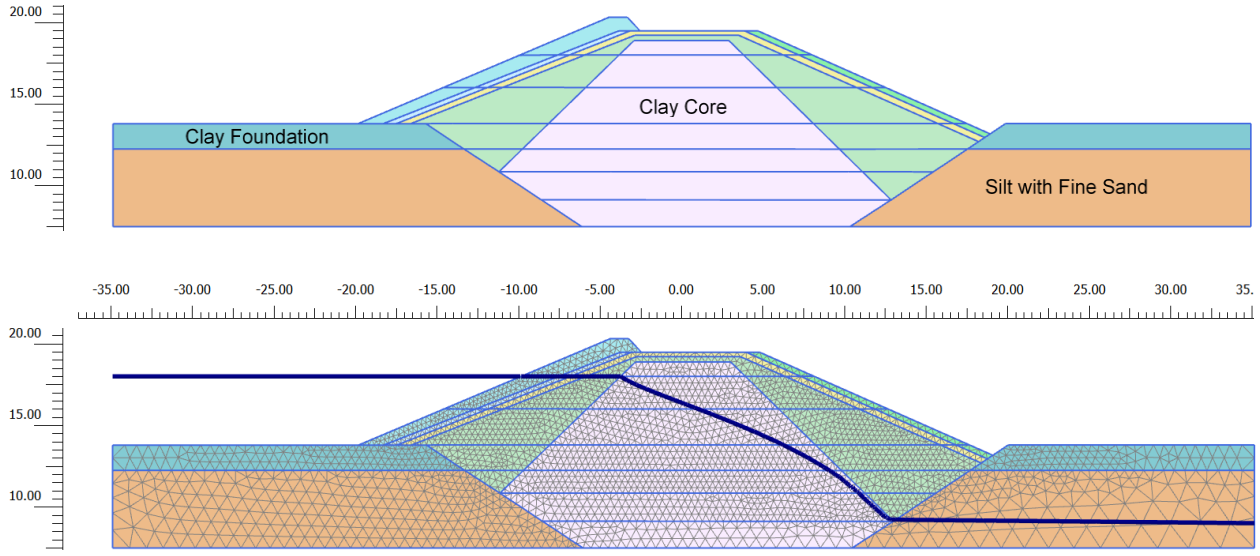

Figure 5.11 CBMD cross-section, generated mesh, and phreatic surface

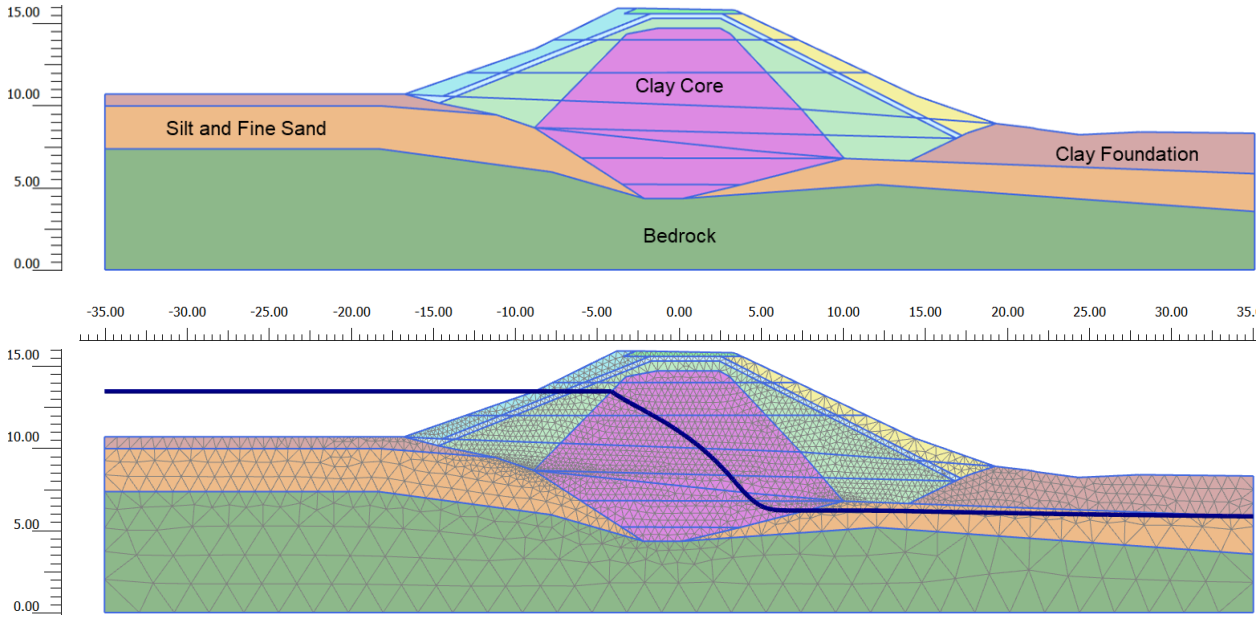

Figure 5.12 WD cross-section, generated mesh, and phreatic surface

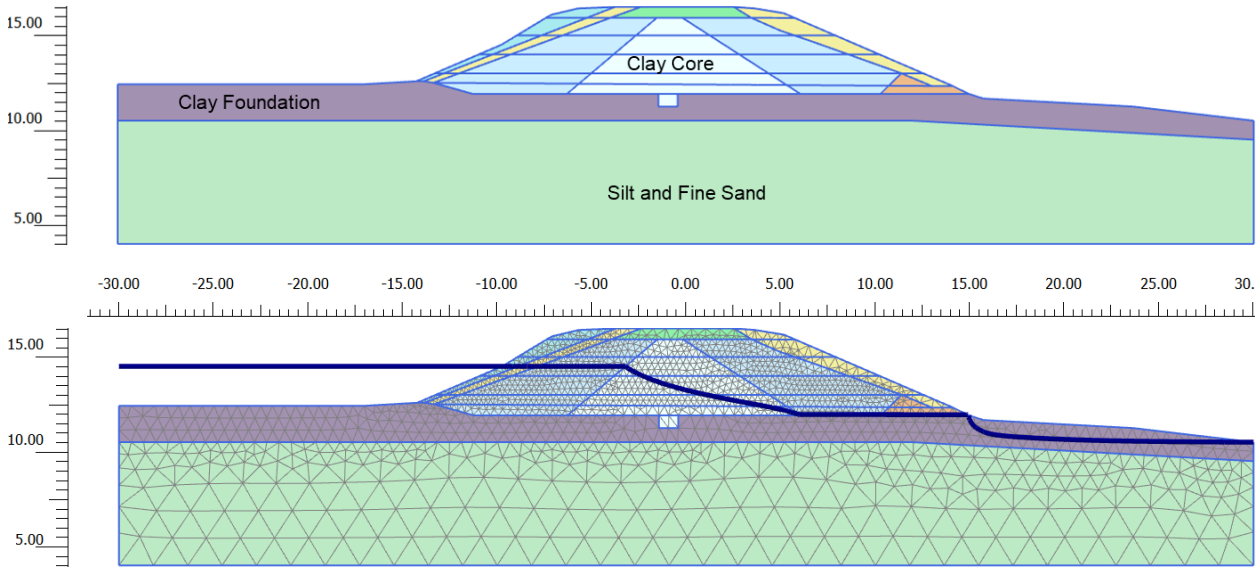

Figure 5.13 EF cross-section, generated mesh, and phreatic surface

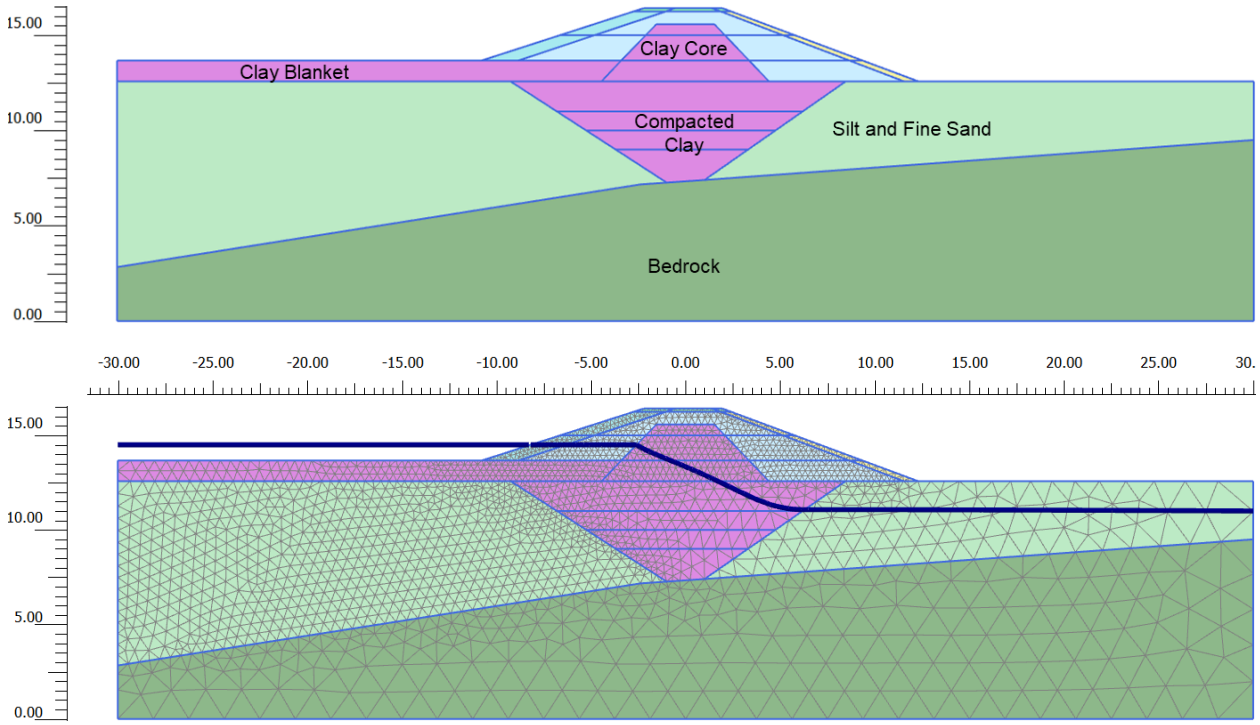

Figure 5.14 MFRED cross-section, generated mesh, and phreatic surface

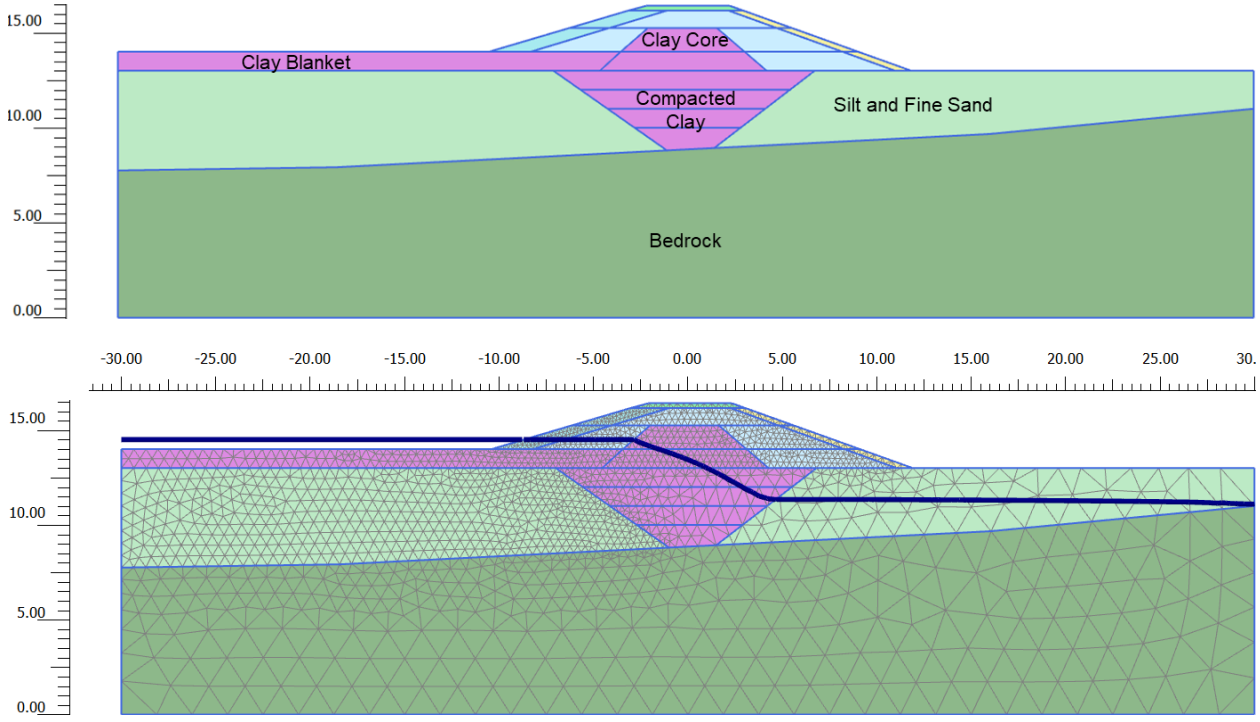

Figure 5.15 MFLED cross-section, generated mesh, and phreatic surface

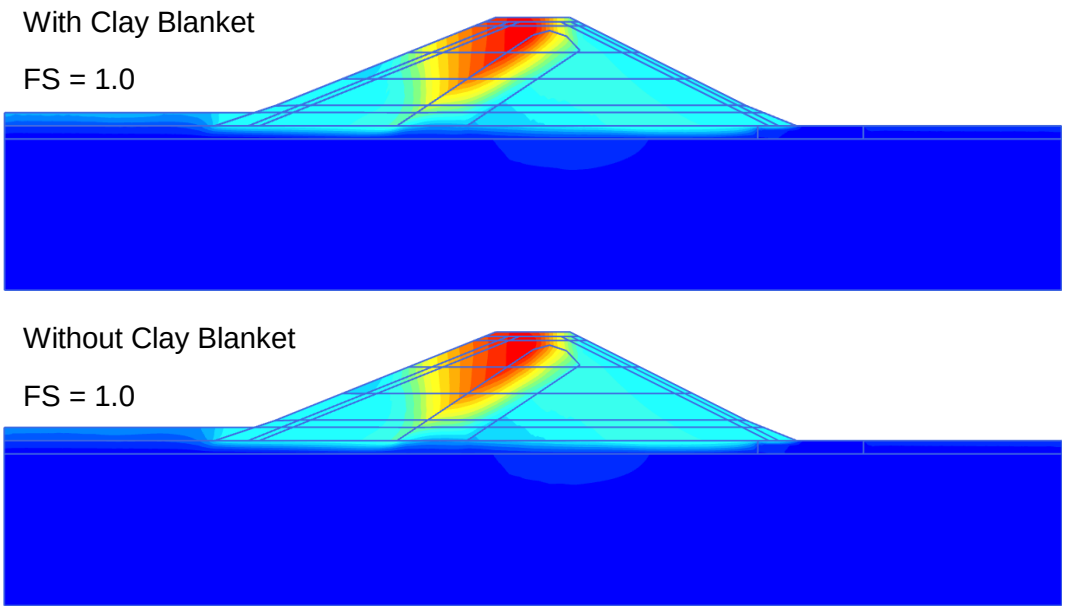

Figure 5.16 Factor of safety at CBBD4

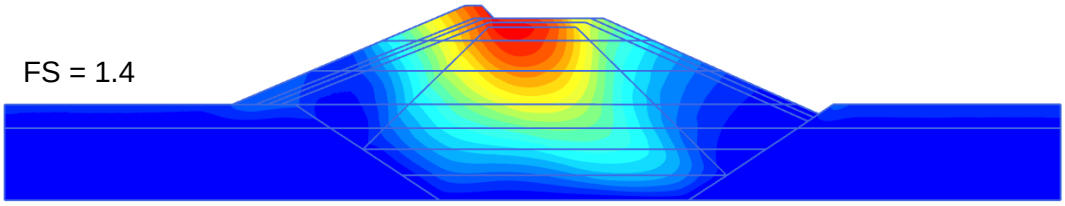

Figure 5.17 Factor of safety at CBMD

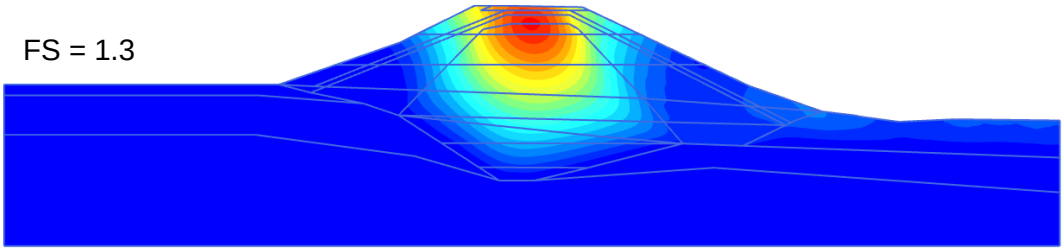

Figure 5.18 Factor of safety at WD

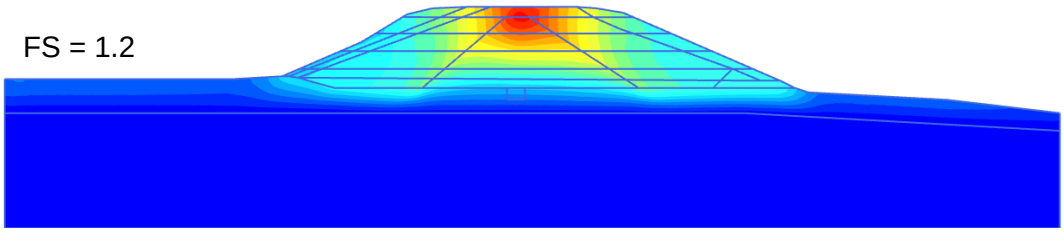

Figure 5.19 Factor of safety at EF

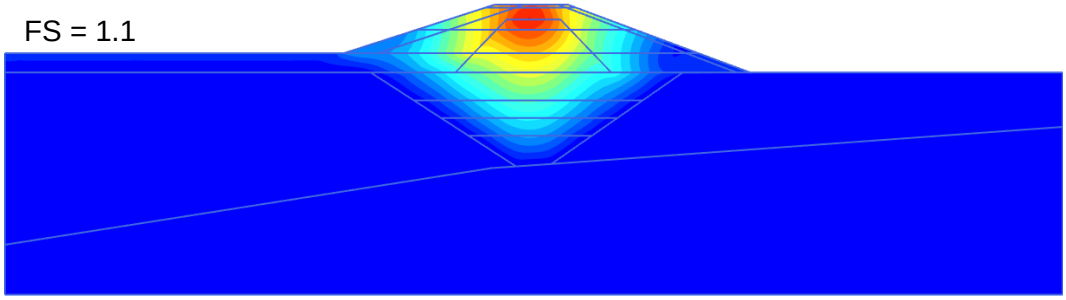

Figure 5.20 Factor of safety at MFRED

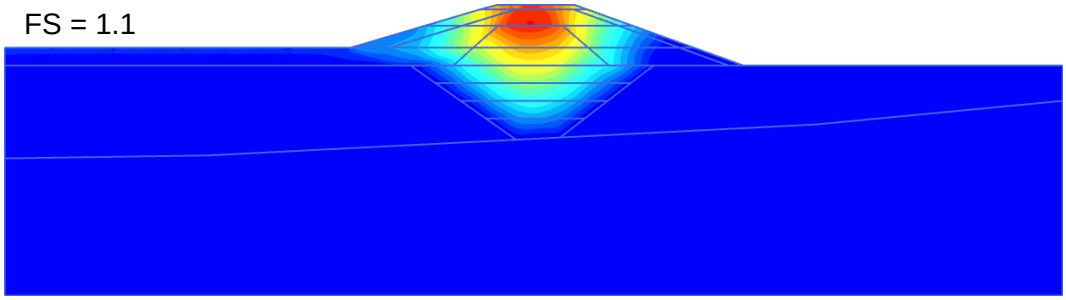

Figure 5.21 Factor of safety at MFLED

With Clay Blanket

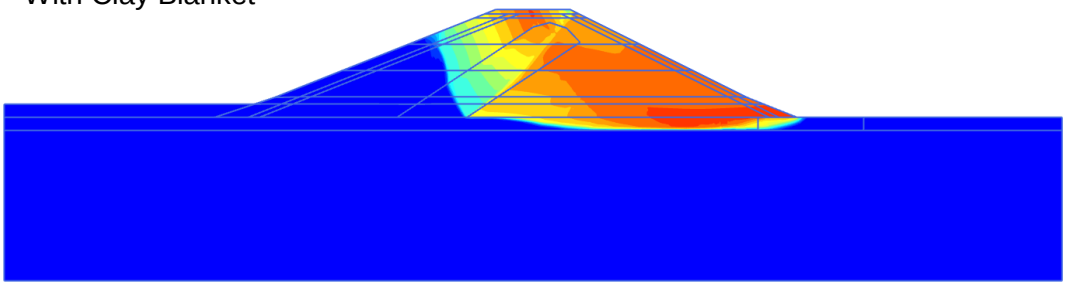

Without Clay Blanket

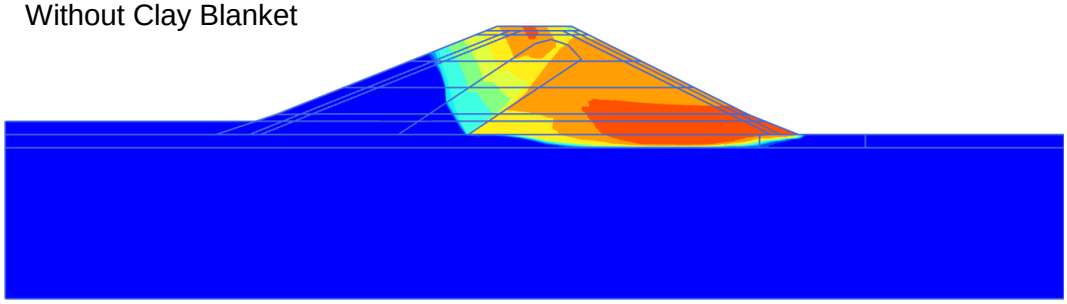

Figure 5.22 Incremental displacement from safety calculations at CBBD4

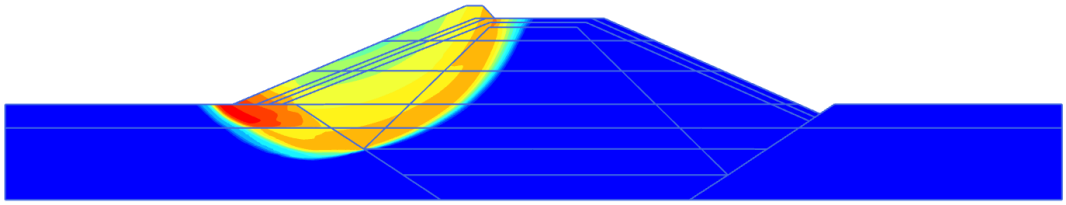

Figure 5.23 Incremental displacement from safety calculations at CBMD

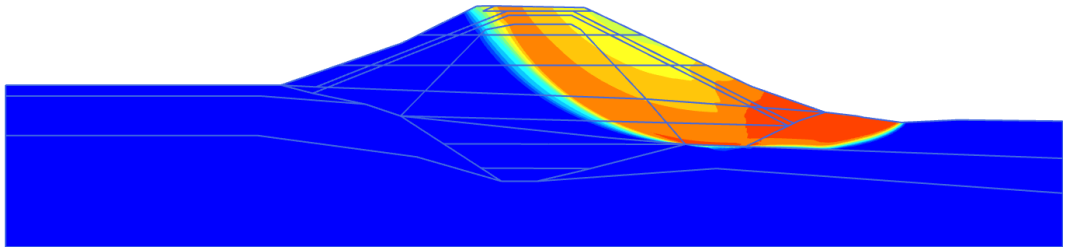

Figure 5.24 Incremental displacement from safety calculations at WD

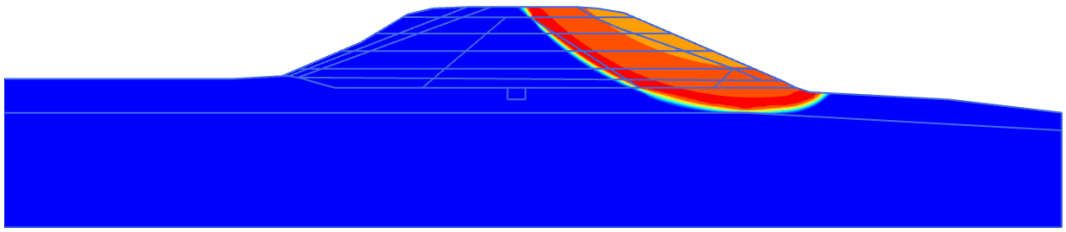

Figure 5.25 Incremental displacement from safety calculations at EF

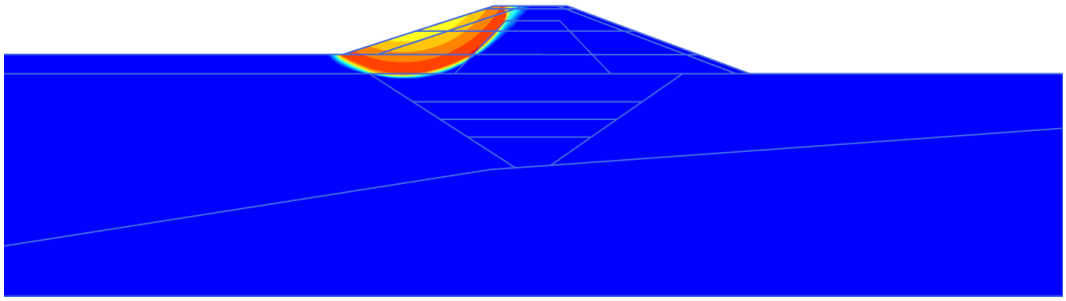

Figure 5.26 Incremental displacement from safety calculations at MFRED

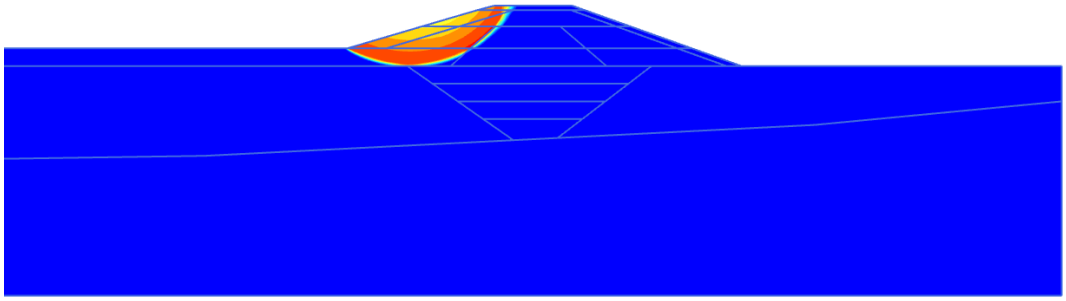

Figure 5.27 Incremental displacement from safety calculations at MFLED

Chapter 6 CONCLUSION and RECOMMENDATIONS

A numerical model was calibrated based on the observed conditions in CBBD2 as it exhibited sudden movement in its upstream side despite its satisfactory performance for over fifty years. Parameters used for numerical modelling were determined from laboratory tests performed on collected samples from site investigations. The completed calibrated model was then used to assess the long-term performance of six other aging earth dams (CBBD4, CBMD, WD, EF, MFRED, and MFLED) which, similar to CBBD2, have been in operation for over fifty years. These earth fill dams were assessed if they still meet current dam safety standards.

6.1 Conclusion and Discussion

Upon completion of the soil sampling, laboratory testing, and numerical modelling, the following findings were obtained:

1. CB clay samples were classified as “fat clay” or high plasticity clay in accordance with the Unified Soil Classification System and were described as stiff with slight compressibility based on index properties and deformation characteristics. This indicated that CB earth dams (CBBD2, CBBD4, and CBMD) had the same source for its clay fill. CB clay was also observed to be fissured with silt lenses or pockets. Silt was observed to be more prominent in clay foundation than in the clay core and blanket.
2. There were no traces of gypsum in CBBD2 clays based on observations from site and sample extrusions. This was further verified by particle orientation and mineralogy from SEM and XRD tests. The absence of gypsum within the clay samples signified

that leaching of this naturally occurring cementing agent could not have caused the delayed instability in CBBD2.

3. Polished surfaces were seen in various sizes and orientation in CBBD2 post-test specimens and CBBD4 clay core specimens. It is possible that the borrowed clay was already intensely fissured and further compaction of the clay fill could have led to localized slickensides along these fissures.
4. Fissures found in the clay core and blanket in CBBD2 was not due to environmental loading but were already pre-existent from the borrow source.
5. Clay samples from WD and MF generating stations were classified as highly plastic clay and was described as stiff with slight compressibility, similar to CB clay. On the other hand, EF clay was designated as “lean clay” or low plasticity clay (CL) and was stiff with low compressibility.
6. Creep tests performed on CBBD2 clay core specimens indicated that secondary compression coefficients determined from shear creep ($C_{\alpha\text{-}s}$) were slightly lower than the compression creep (C_{α}) values, regardless of the degree of shear mobilization ($0.58q_{100}$, $0.76q_{100}$, $0.53q_{200}$, and $0.68q_{200}$).
7. Shear creep tests on CBBD2 clay core specimens indicated that the slope of the vertical creep strain with time was observed to have increased as the shear mobilization level was increased as heavier loads resulted in the increase in the vertical displacement as the stress was increased. On the other hand, the slope of the volumetric creep strain decreased as the deviator stress level was increased. As the specimen was being compressed under heavier loads, it was also dilating and swelling in the radial direction. The swelling could have led to water being retained, if not increased, within the sample instead of being drained which led to little or no change in volume.

8. Shear creep test results suggested that a factor of safety (FS) higher than 1.3 is needed in order to avoid long-term failure or delayed instability due to creep rupture.
9. Satisfying a factor of safety of 1.5 for long-term stability might no longer be sufficient when confining stresses are lower than 100 kPa as this condition would indicate that part of the clay core would already exhibit creeping behavior. This reinforces the need to include creep in the long-term stability analysis using strength parameters taken as the average of fully softened and residual shear strengths. Comparing generated safety factors using this recommended type of analysis against the required current dam safety factor of 1.5 would at least incorporate time-dependent displacements that could possibly affect the long-term stability and serviceability of dams.
10. The calibrated model that represented the operating deformation and stability conditions of CBBD2 involved time-dependent creep deformation analysis using clay strength values between the post peak and residual shear strengths.
11. Both modified creep index based on compression creep tests and based on shear creep tests could produce the observed delayed instability in CBBD2. This suggests that compression creep and shear creep tests are useful to describe creep deformations. Shear creep tests provides information with regards to creep rupture.
12. When creep is considered, simulated displacements at Section A-A indicated that movements occurred both along its upstream and downstream side. On the other hand, Section B-B only experienced movement along its upstream side over time.
13. Stability assessment considering time-dependent creep deformation and using clay strength values between the post peak and residual shear strengths indicated that the remaining earth dams (CBMD, WD, EF, MFRED, and MFLED) were still stable (FS > 1.0). Particular attention must be given to CBBD4 as the factor of safety was at unity which could be an indication of impending failure. Only two of the remaining seven earth fill dams (CBMD and WD) had a FS ≥ 1.3 which implied that the remaining dams

need to be properly monitored or remediated against possible delayed instability due to creep. In addition, none of the dams had factors of safety greater than 1.5 which means that these dams are still subject to remedial and monitoring measures to meet this safety requirement.

Calibrated models gave insights as to the cause of the delayed instability in CBBD2. CBBD2 has been under constant load as there were no changes in the dam (such as dam heightening) for over fifty years since it has been constructed. High clay content and plasticity in the clay core, blanket, and foundation allowed creep movement to occur under the constant load of the dam. Creep movement in Section A-A was occurring both in the upstream and downstream side owing to the presence clay underneath the dam. On the other hand, displacement was transpiring over time at the upstream section due the placed compacted blanket that was tied into the inclined clay core in Section B-B. The absence of the naturally occurring clay in the downstream side led to the predominant upstream movement within this section. Over the service years of CBBD2, sufficient movement or straining developed that led to the reduction in the clay shear strength in the stiff fissured clay from a post peak value to an average value between post peak and residual shear strengths. This reduction occurred at the later service years as initial creep movement in overconsolidated clays tend to be small and would increase with respect to time. The reduction of shear strength in fissured overconsolidated clays with creep movement, predominantly occurring at the upstream slope, led to the delayed instability in CBBD2.

Structures such as water-retaining dams are expected to have long-service lives and instability of these structures would have detrimental consequences. The outcome of the assessment of the aging earth dams has shown the significance of considering long term analysis of structures considering creep. As parameters from creep analysis can be obtained from oedometer tests, one of the routine tests performed on field samples, time-dependent creep can be conveniently integrated in the design process. Shear creep test results would provide

additional criteria for safety against the possibility of long-term failure or delayed instability due to creep. The use of a finite element method of analysis with a time-dependent soil creep model would provide predicted movements or instabilities with respect to time from the long-term analysis. Instrumentation can be planned accordingly in order to effectively monitor these dams against instability. This would also urge for the need for more frequent long term in-situ monitoring as well as a proper remedial plan should it be necessary.

6.2 Recommendations

The completed research will be used by the dam owner and operator as an initial assessment of the studied aging earth dams. Laboratory tests initially performed were also used to aid in the on-going remedial measures in CBBD2. Verification of the dam geometry must also be done as information used in this research was only based on construction drawings. Actual construction details could also improve the accuracy of the numerical model as construction stages used were just assumed due to lack of information.

Proactive remedial measures are recommended for CBBD4, CBMD, WD, EF, MFRED and MFLED earth dams, especially for CBBD4 since results indicated an impending instability condition. Probable failure surface results provides information as to where these dams could be strengthened in order to improve its stability. Results from safety calculation could also be used as a guide for possible locations of additional instrumentation to be installed, if needed. Validation of the stability assessment of these dams could be done with instrumentation data. This would mean that frequent and long-term monitoring of installed instrumentations must be done.

Although visual inspections and mineralogy results indicated that there was no gypsum in CBBD2 clay, pore fluid investigations could still be conducted. Pore fluid chemistry tests could be

performed in order to check for any other possible cementing agent, in addition to dissolved gypsum, that could have leached from the clay.

Time constraints allowed for only a few shear creep tests to be performed for this research as modifications and adjustments had to be made to the shear creep apparatus used. Supplementary shear creep tests must be performed on the remaining samples in order to further verify the behaviour of vertical and volumetric strain with respect to time and degree of shear mobilization. Tests should include normally consolidated conditions as overconsolidated samples were only considered in this study. Further understanding on the mechanism of shear creep may lead to possible improvements or modifications of existing soil creep models.

The stability assessment of the earth dams in this research were performed with the use of a commercially available software with the needed soil model that engineers of the dam owners would have access to. In which case, dam engineers would be able to make necessary adjustments should additional data or information would be available. However, the current Soft Soil Creep (SSC) model in PLAXIS does not have a strain softening function. Future research could look into using or developing a soil model that incorporates strain softening with time-dependent creep movement. Such soil model would allow soil strength to change over time with respect to straining brought about by creep. This type of analysis could provide information with regards to progressive yielding of clay elements over time and perhaps be able to provide an estimated time to failure. An example of a rigorous solution was used by Kalos and Kavvadas (2018) with a fully coupled shear strength degradation with deformation due to creep. The use of more advanced models would improve the sequential modelling that was employed in this study.

REFERENCES

Alfaro III, M. (2016). *Slope Stability Evaluation of an Old Earth Fill Dam Founded on Glaciolacustrine Clays* (Master's thesis). University of Manitoba.

Ameratunga, J., Sivakugan, N., & Das, B. M. (2016). *Correlations of Soil and Rock Properties in Geotechnical Engineering*. New Delhi, India: Springer India.

American Society for Testing and Materials Annual. (2010). *Annual Book of ASTM Standards*. Philadelphia, PA, USA.

Baracos, A. (1977). *Compositional and structural anisotropy of Winnipeg soils - a study based on scanning electron microscopy and X-ray diffraction analyses*. Canadian Geotechnical Journal, 14, 125–137.

Bi, G., Briaud, J. L., Sanchez, M., & Kharanaghi, M. M. (2019). *Power Law Model to Predict Creep Movement and Creep Failure*. Journal of Geotechnical and Geoenvironmental Engineering, 145(9), 1–10.

Bishop, A.W., Webb, D.L., & Lewin, P.I. (1965). *Undisturbed Samples of London Clay from Ashford Common Shaft: Strength-Effective Stress Relationships*. Géotechnique, 15(1), 1–31.

Bjerrum, L. (1969) Discussion of main session 5, Stability of natural slopes and embakment foundations. In *Seventh International Conference on Soil Mechanics and Foundation Engineering*. Mexico City, Mexico.

Campanella, R. G., & Vaid, Y. P. (1974). *Triaxial and Plane Strain Creep Rupture of an Undisturbed Clay*. Canadian Geotechnical Journal, 11(1), 1–10.

Canadian Dam Association. (2013). *Dam Safety Guidelines 2007* (Revised 2013) (Vol. 2007).

Cotecchia, F., Vitone, C., Cafaro, F., & Santaloia, F. (2007). The mechanical behaviour of intensely fissured high plasticity clays from Daunia. *Proceedings of the Second International Workshop on Characterisation and Engineering Properties of Natural Soils*, 1975–2001.

Den Haan, E. J. (1994). Stress-Independent Parameters for Primary and Secondary Compression. In *International Conference on Soil Mechanics and Foundation Engineering*. 65–70.

Fatahi, B., Minh Le, T., Quang Le, M., & Khabbaz, H. (2013). Soil creep effects on ground lateral deformation and pore water pressure under embankments. *Geomechanics and Geoengineering Geomechanics and Geoengineering: An International Journal*, 8(2), 107–124.

Garinger, B., Alfaro, M., Graham, J., Dubois, D., & Man, A. (2004). Instability of dykes at Seven Sisters Generating Station. *Canadian Geotechnical Journal*, 41(5), 959–971.

Graham, J., & Houlsby, G. T. (1983). Anisotrophic elasticity of a natural clay. *Géotechnique*, 33(2), 165–180.

Gu, W. H., Morgenstern, N. R., & Robertson, P. K. (1993). Progressive Failure of Lower San Fernando Dam. *Journal of Geotechnical Engineering*, 119(2), 333–349.

Haines, N.S., Whitedog Falls and Caribou Falls Generating Stations Hydroelectric Development on the Winnipeg and English Rivers. *The Engineering Journal*, October 1959, 73-84.

Hatch Ltd., Geotechnical investigation reports. Unpublished report, 2010.

Havel, F. (2004). *Creep in soft soils* (Doctorate dissertation). Norwegian University of Science and Technology.

Kalos, A., & Kavvadas, M. (2018). Slope instabilities triggered by creep induced strength degradation. *Numerical Methods in Geotechnical Engineering IX,* 2(October 2019), 1097–1104.

Lai, X. L., Wang, S. M., Ye, W. M., & Cui, Y. J. (2014). Experimental investigation on the creep behavior of an unsaturated clay. *Canadian Geotechnical Journal*, 51, 621–628.

Leonards, G. A., 1979, Stability of slopes in soft clays. Special lecture, *6th Pan American Conference on Soil Mechanics and Foundation Engineering*, Lima.

Man, A., & Graham, J. (2010). Pore fluid chemistry, stress-strain behaviour, and yielding in reconstituted highly plastic clay. *Engineering Geology*, 116, 296–310.

Man, A., Graham, J., & Blatz, J. (2011). Seepage, leaching, and embankment instability. *Canadian Geotechnical Journal*, 48(3), 473–492.

Matsui, T. & N. Abe, 1988, Verification of elasto-viscoplastic model of normally consolidated clays in undrained creep, *Proceedings of 6th International Conference Numerical Methods in Geomechanics*, Innsbruck: 453-459.

McGown, A., & Radwan, A. M. (1975). The Presence and Influence of Fissures in the Boulder Clays of West Central Scotland. *Canadian Geotechnical Journal*, 12, 84–97.

Mesri, G., & Abdel-Ghaffar, M. E. M. (1993). Cohesion Intercept in Effective Stress-Stability Analysis. *Journal of Geotechnical Engineering*, 119(8), 1229–1249.

Mesri, G., Castro, A., Febres-Cordero, E., & Shields, D. R. (1981). Shear stress-strain-time behaviour of clays. *Géotechnique*, 31(4), 537–552.

Mitchell, J., & Soga, K. (2005). *Fundamentals of Soil Behaviour (3rd Ed.)*. John Wiley & Sons, Inc.

Muir Wood, D. (1990). *Soil Behaviour and Critical State Soil Mechanics*. Cambridge University Press.

Neher, H. P., M.Wehnert, & Bonnier, P. G. (2001). An evaluation of soft soil models based on trial embankments. Computer Methods and Advances in Geomechanics, *Proceedings of the 10th International Conference on Computer Methods and Advances in Geomechanics, Tucson/Arizona 2001*, Rotterdam: Balkema, 373–378.

Osano, S. N. (2009). Direct Shear Box and Ring Shear Test Comparison: Why Does Internal Angle of Friction Vary. *ICASTOR Journal of Engineering*, 5(2), 77–93.

PLAXIS. (2018). *PLAXIS 2D Material Model 2018 (2018 ed.)*. PLAXIS bv, The Netherlands.

Potts, D. M., Kovacevic, N., & Vaughan, P. R. (1997). Delayed collapse of cut slopes in stiff clay. *Géotechnique*, 47(5), 953–982.

Rocscience. (2019). *Soft Soil Creep Model*. In Rocscience RS2 2019 Material Model Manual.

Rivard, P. J., & Lu, Y. (1978). Shear strength of soft fissured clays. *Canadian Geotechnical Journal*, 15(3), 382–390.

Shrestha, S. (2015). *Shear Creep in Sensitive Clays* (Master's thesis). Norwegian University of Science and Technology.

Skempton, A. W. (1977). Slope Stability of Cuttings in Brown London Clay. In *9th International Conference in Soil Mechanics* (pp. 261–270). Tokyo, Japan.

Skempton, A. W. (1985). Residual strength of clays in landslides, folded strata and the laboratory. *Géotechnique*, 35(1), 3–18.

Skempton, A. W., & Hutchinson, J. (1969). Stability of Natural Slopes and Embankment Foundations. In *Seventh International Conference on Soil Mechanics and Foundation Engineering* (pp. 291–340). Mexico City, Mexico.

Stark, T., & Eid, H. (1997). Slope Stability Analyses in Stiff Fissured Clays. *Journal of Geotechnical and Geoenvironmental Engineering*, 123(4), 335–343.

Stolle, D. F. E., Bonnier, P. G., & Vermeer, P. A. (1997). A soft soil model and experiences with two integration schemes. *Proceedings of 6th International Symposium on Numerical Models in Geomechanics* (pp. 123–127). Montreal, Canada.

Stolle, D. F. E., Vermeer, P. A., & Bonnier, P. G. (1999). A consolidation model for a creeping clay. *Canadian Geotechnical Journal*, 36(4), 754–759.

Tavenas, F., & Leroueil, S. (1981). Creep and failure of slopes in clays. *Canadian Geotechnical Journal*, 18(1974), 106–120.

Tavenas, F., Leroueil, S., La Rochelle, P., & Roy, M. (1978). Creep behaviour of an undisturbed lightly overconsolidated clay. Canadian Geotechnical Journal, 15, 402–423.

Vaid, Y. P., & Campanella, R. G. (1977). Time-dependent behaviour of undisturbed clay. *Journal of Geotechnical Engineering*, 103(7), 693–709.

Vallejo, L. E. (1987). The influence of fissures in a stiff clay subjected to direct shear. *Géotechnique*, 37(1), 69–82.

Vallejo, L. E. (1989). Fissure Parameters in Stiff Clays under Compression. *Journal of Geotechnical Engineering*, 115(9), 1303–1317.

Vallejo, L. E., & Shettima, M. (2017). An explanation for the delayed failures of natural slopes and earth dams. *Geotechnical Frontiers 2017* (pp. 372–381). Orlando, Florida.

Vallejo, L. E., & Shettima, M. (2019). Fatigue Crack Propagation in Stiff Clays Forming Part of Earth Dams and Natural Slopes. *Eighth International Conference on Case Histories in Geotechnical Engineering* (pp. 610–617). Philadelphia, Pennsylvania.

Van Baars, S. (2003). Soft Soil Creep Modelling of Large Settlements. *In 2nd International Conference on Advances in Soft Soil Engineering and Technology*. Putrajaya, Malaysia.

Vermeer, P. A., & Neher, H. P. (1999). A soft soil model that accounts for creep. *In Beyond 2000 in Computational Geotechnics* (pp. 249–261). Amsterdam, The Netherlands.

Vitone, C., & Cotecchia, F. (2011). The influence of intense fissuring on the mechanical behaviour of clays. *Géotechnique*, 61(12), 1003–1018.

Vitone, C., Cotecchia, F., Desrues, J., & Viggiani, G. (2009). An approach to the interpretation of the mechanical behaviour of intensely fissured clays. *Soils and Foundations*, 49(3), 355–368.

Widodo, S., & Ibrahim, A. (2012). Estimation of primary compression index (Cc) using physical properties of Pontianak soft clay. *International Journal of Engineering Research and Applications*, 2(5), 2232–2236.

Ye, Y., Zhang, Q., Cai, D., Chen, F., Yao, J., & Wang, L. (2013). Study on New Method of Accelerated Clay Creep Characteristics Test. *18th International Conference on Soil Mechanics and Geotechnical Engineering* (pp. 461–464). Paris, France.

Yoshida, N., Morgenstern, R., & Chan, D. H. (1991). Finite-element analysis of softening effects in fissured, overconsolidated clays and mudstones. *Canadian Geotechnical Journal*, 28(1), 51–61.

APPENDICES

APPENDIX A

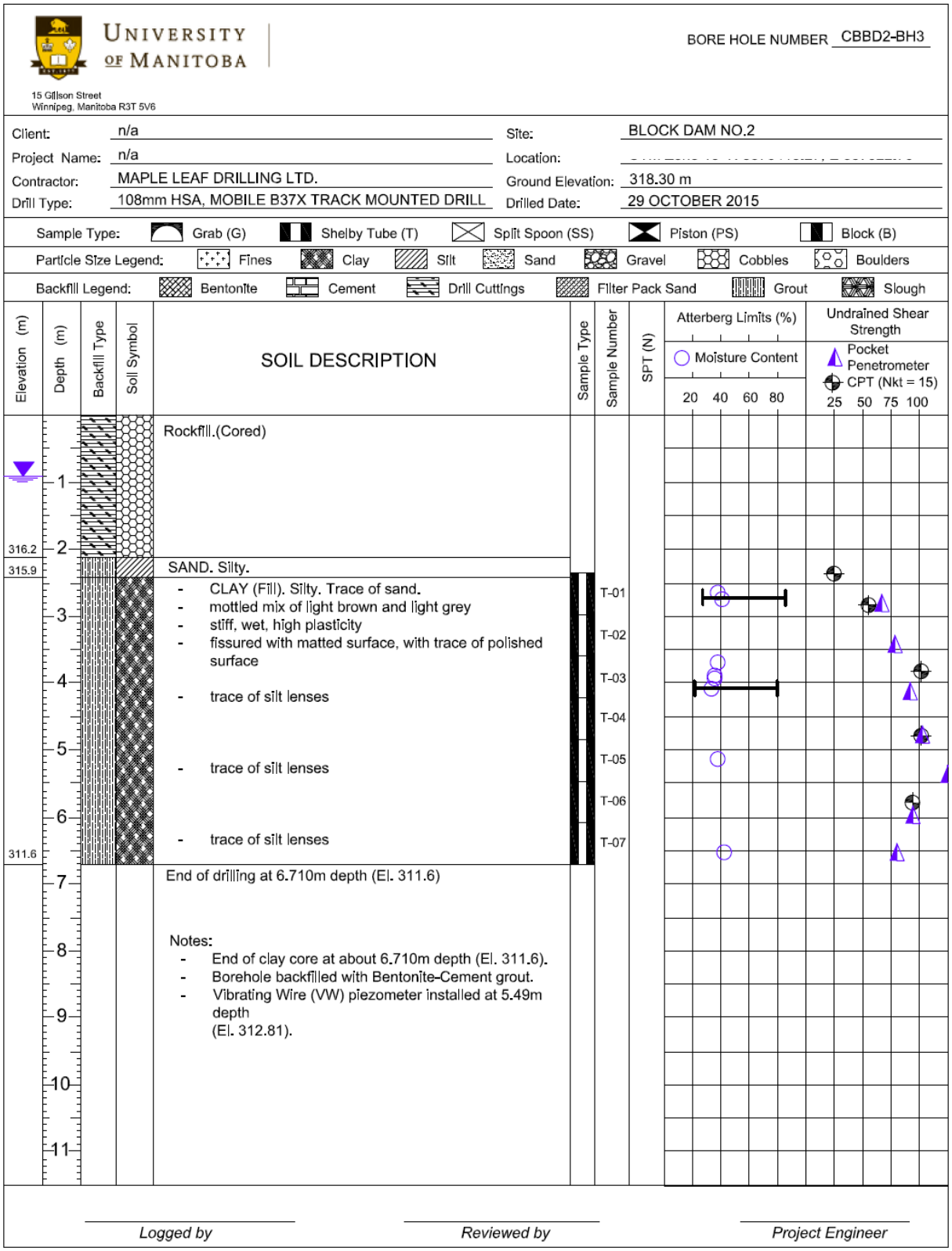

Figure A-A.1 Borehole log from CBBD2 Core at Section A-A (Alfaro III, 2016)

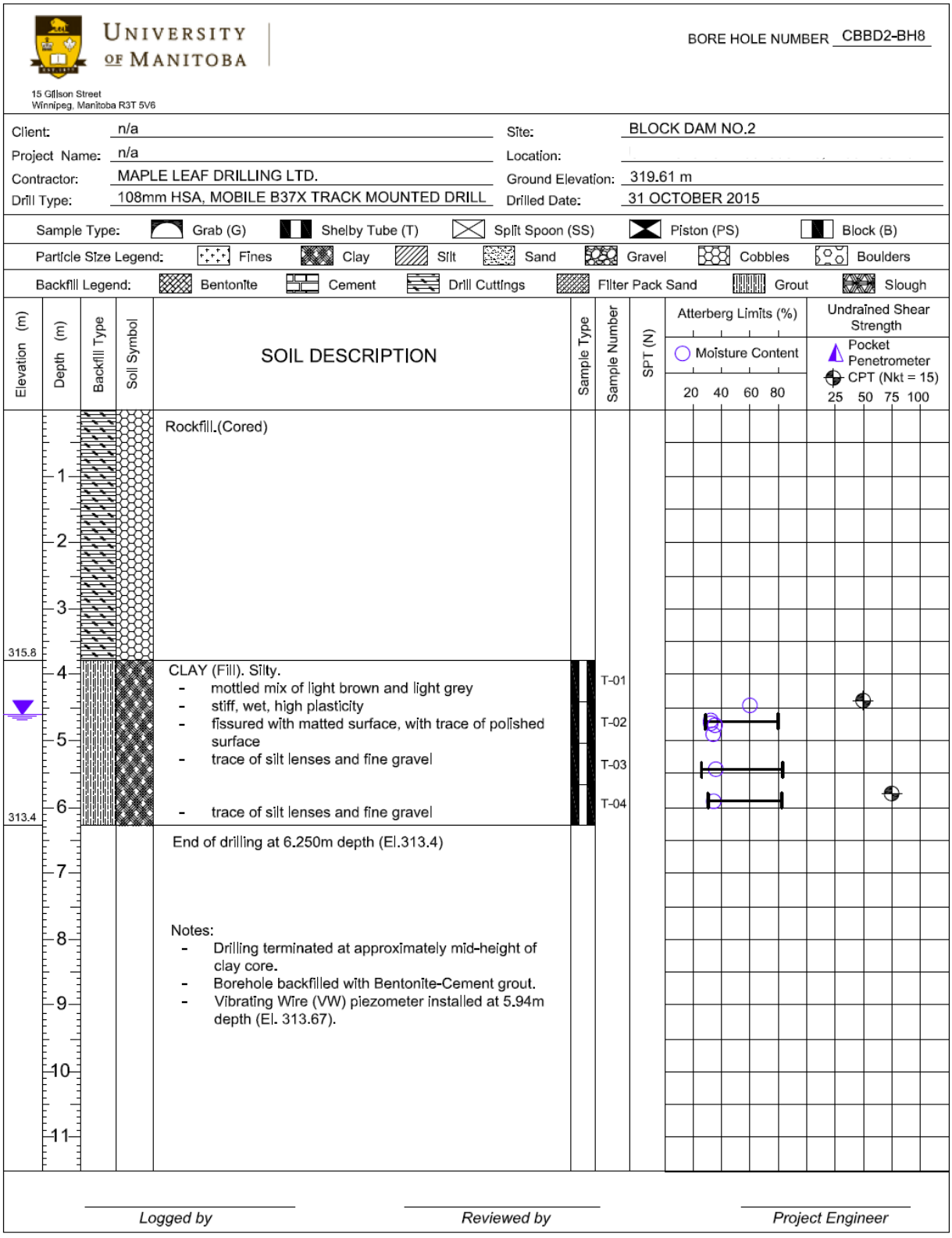

Figure A-A.2 Borehole log from CBBD2 Core at Section B-B (Alfaro III, 2016)

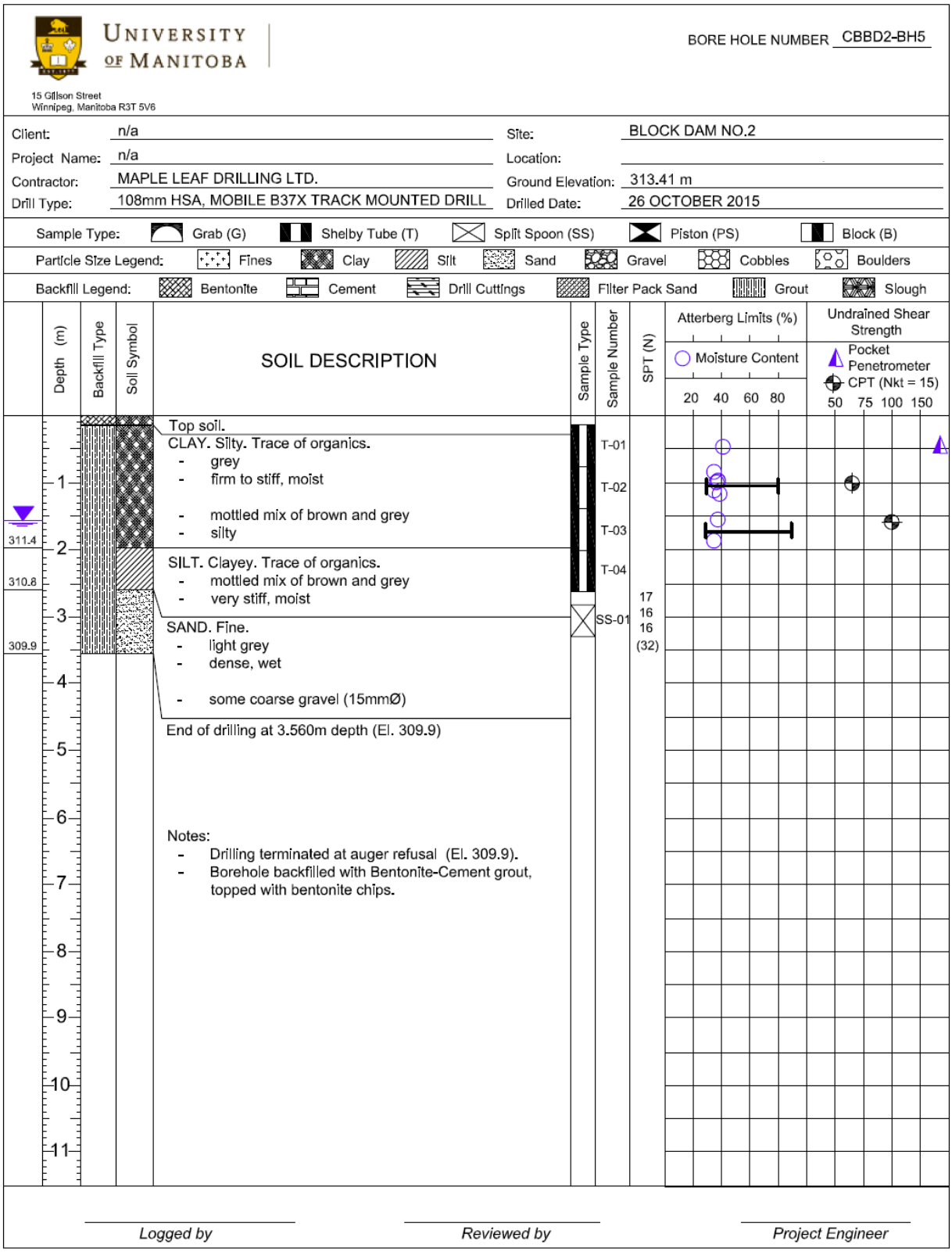

Figure A-A.3 Borehole log from CBBD2 Foundation (Alfaro III, 2016)

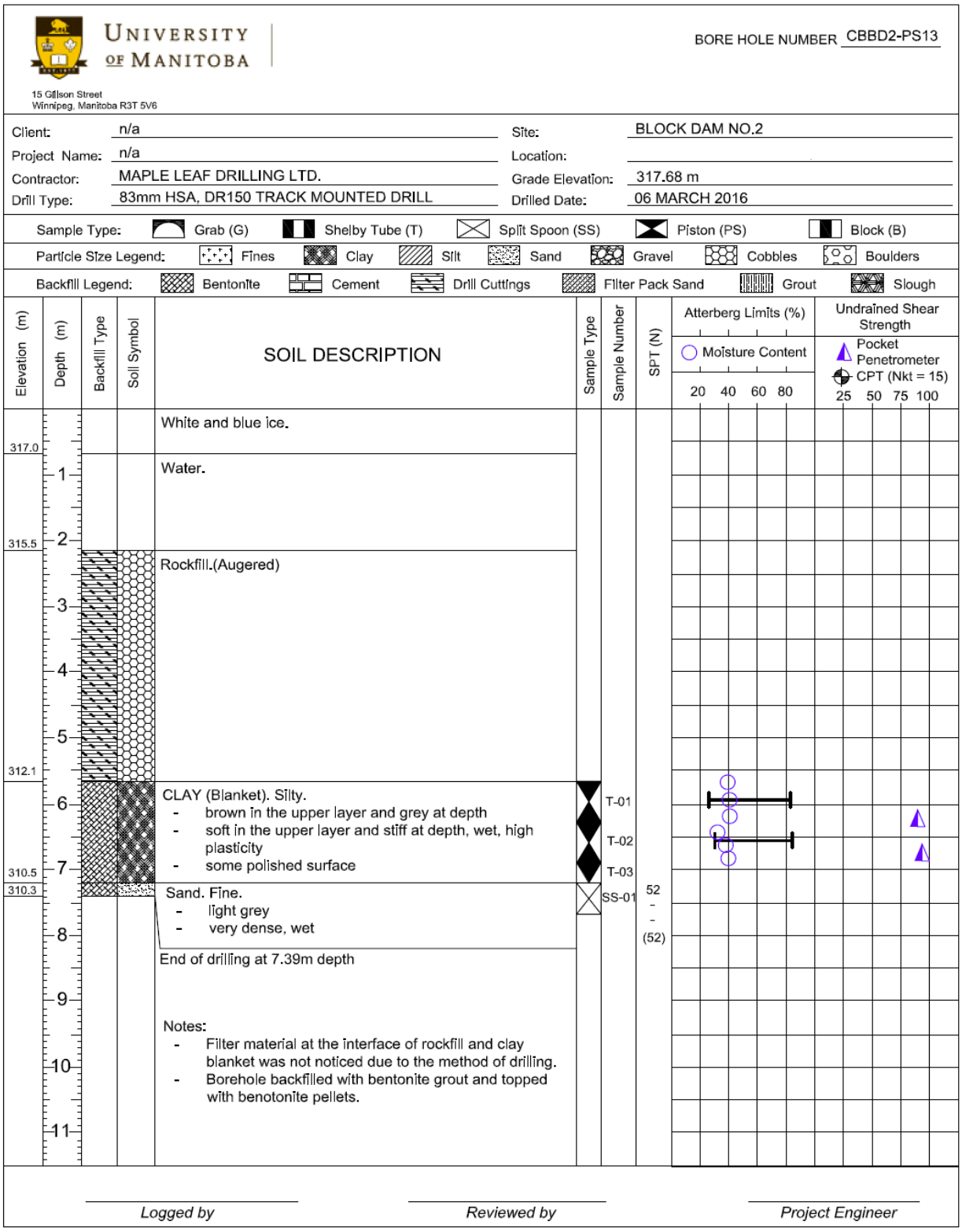

Figure A-A.4 Borehole log from CBBD2 Blanket (Alfaro III, 2016)

UNIVERSITY OF MANITOBA

Sub-Surface Log

Borehole CBBD4-BH2
1 of 1

Client: Ontario Power Generation
Project Name: Caribou Falls Block Dam No. 4 Geotechnical Investigation
Contractor:
Method:
Project Number:
Location:
Ground Elevation:
Date Drilled: 2015 November 4 - 2015 November 4

Sample Type: Grab (G) | Shelby Tube (T) | Split Spoon (SS) | Split Barrel (SB) | Core (C)

Particle Size Legend: Fines | Clay | Silt | Sand | Gravel | Cobbles | Boulders

Depth (m)	Soil Symbol	MATERIAL DESCRIPTION	Sample Type	Sample Number	SPT (N)	Bulk Unit Wt (kN/m³) 16 17 18 19 20 21 / Particle Size (%) 0 20 40 60 80 100 / PL MC LL	Penetration Tests (blows/300mm) Dynamic Cone / Becker / SPT N VALUE 0 20 40 60 80 100
0		ROCKFILL - augered through rockfill					
0.5		SAND - gravelly sand					
1.0							
1.5							
2.0							
2.5							
3.0							
3.5		- sand on top of tube; brown; moist; clay; light grey to light brown; with iron stain; moist; stiff		T01			
4.0		CLAY - clay; light grey to light brown; with iron stain; moist; stiff; cracks at end of sample		T02			
4.5		- clay; light grey to more brown; with iron stains and silt spots; moist; stiff; traces of roots		T03			
5.0		- clay; light grey to brown with silt spots; moist; stiff		T04			
5.5		- clay; dark grey; moist; very stiff		T05			
6.0		END OF BOREHOLE AT 6.25 m					

Notes:
1. Stopped at 6.25 m
2. Installed PZ3A at 6.04m
3. Grouted to ground surface topped with bentonite chips

Logged By: **Reviewed By:** **Project Engineer:**

SUB-SURFACE LOG BLOCK DAM NO 4.GPJ TREK GEOTECHNICAL.GDT 18-12-7

Figure A-A.5 Borehole log from CBBD4 Core

UNIVERSITY OF MANITOBA

Sub-Surface Log

Borehole CBBD4-BH4
1 of 1

Client: Ontario Power Generation
Project Name: Caribou Falls Block Dam No. 4 Geotechnical Investigation
Contractor:
Method:
Project Number:
Location:
Ground Elevation:
Date Drilled: 2015 November 6 - 2015 November 6

Sample Type: Grab (G) | Shelby Tube (T) | Split Spoon (SS) | Split Barrel (SB) | Core (C)

Particle Size Legend: Fines | Clay | Silt | Sand | Gravel | Cobbles | Boulders

Depth (m)	Soil Symbol	MATERIAL DESCRIPTION	Sample Type	Sample Number	SPT (N)	Bulk Unit Wt (kN/m³) 16 17 18 19 20 21 / Particle Size (%) 0 20 40 60 80 100 / PL MC LL	Penetration Tests (blows/300mm) Dynamic Cone / Becker / SPT N VALUE 0 20 40 60 80 100
		AUGERED					
0.5		CLAY - gravelly sand on top; silty; grey; traces of roots; wet		T01		101	
1.0		- clayey silty sand; grey; wet		T02			
1.5							
2.0							

END OF BOREHOLE AT 2.44 m
Notes:
1. Advanced until 2.44 m
2. Installed PZ2A at 2.13 m
3. Grouted to ground surface topped with bentonite chips

Logged By: **Reviewed By:** **Project Engineer:**

SUB-SURFACE LOG BLOCK DAM NO.4.GPJ TREK GEOTECHNICAL.GDT 18-12-7

Figure A-A.6 Borehole log from CBBD4 Foundation

UNIVERSITY OF MANITOBA

Sub-Surface Log

Borehole CBMD-BH1

Client:	Ontario Power Generation	**Project Number:**	
Project Name:	Caribou Falls Main Dam Geotechnical Investigation	**Location:**	
Contractor:		**Ground Elevation:**	
Method:		**Date Drilled:**	2015 November 2

Sample Type: Grab (G) | Shelby Tube (T) | Split Spoon (SS) | Split Barrel (SB) | Core (C)

Particle Size Legend: Fines | Clay | Silt | Sand | Gravel | Cobbles | Boulders

Depth (m)	Soil Symbol	MATERIAL DESCRIPTION	Sample Type	Sample Number	SPT (N)
0		SAND - sand, gravelly			
0.5		CLAY			
		- clay; light grey to light brown; wtih iron stains; moist; stiff		T01	
1.0					
1.5				T02	
2.0				T03	
2.5				T04	
3.0		- clay; light grey to light brown with iron stains; silt pockets; moist; stiff		T05	
3.5					
		- clay; light grey to light brown; with iron stains; moist; stiff		T06	
4.0				T07	
4.5					
5.0		- clay; light grey to light brown; with iron stains; silt pockets; moist; stiff		T08	
5.5				T09	
6.0				T10	
6.5				T11	
7.0				T12	
7.5				T13	
8.0				T14	
8.5					

Bulk Unit Wt (kN/m³): 16 17 18 19 20 21

Particle Size (%): 0 20 40 60 80 100

PL MC LL: 0 20 40 60 80 100

Penetration Tests (blows/300mm): ☐ Dynamic Cone ☐ ⌖ Becker ⌖ ◆ SPT N VALUE ◆ 0 20 40 60 80 100

Logged By: _____ **Reviewed By:** _____ **Project Engineer:** _____

SUB-SURFACE LOG CARIBOU FALLS - MAIN DAM V2.GPJ TREK GEOTECHNICAL.GDT 19-4-29

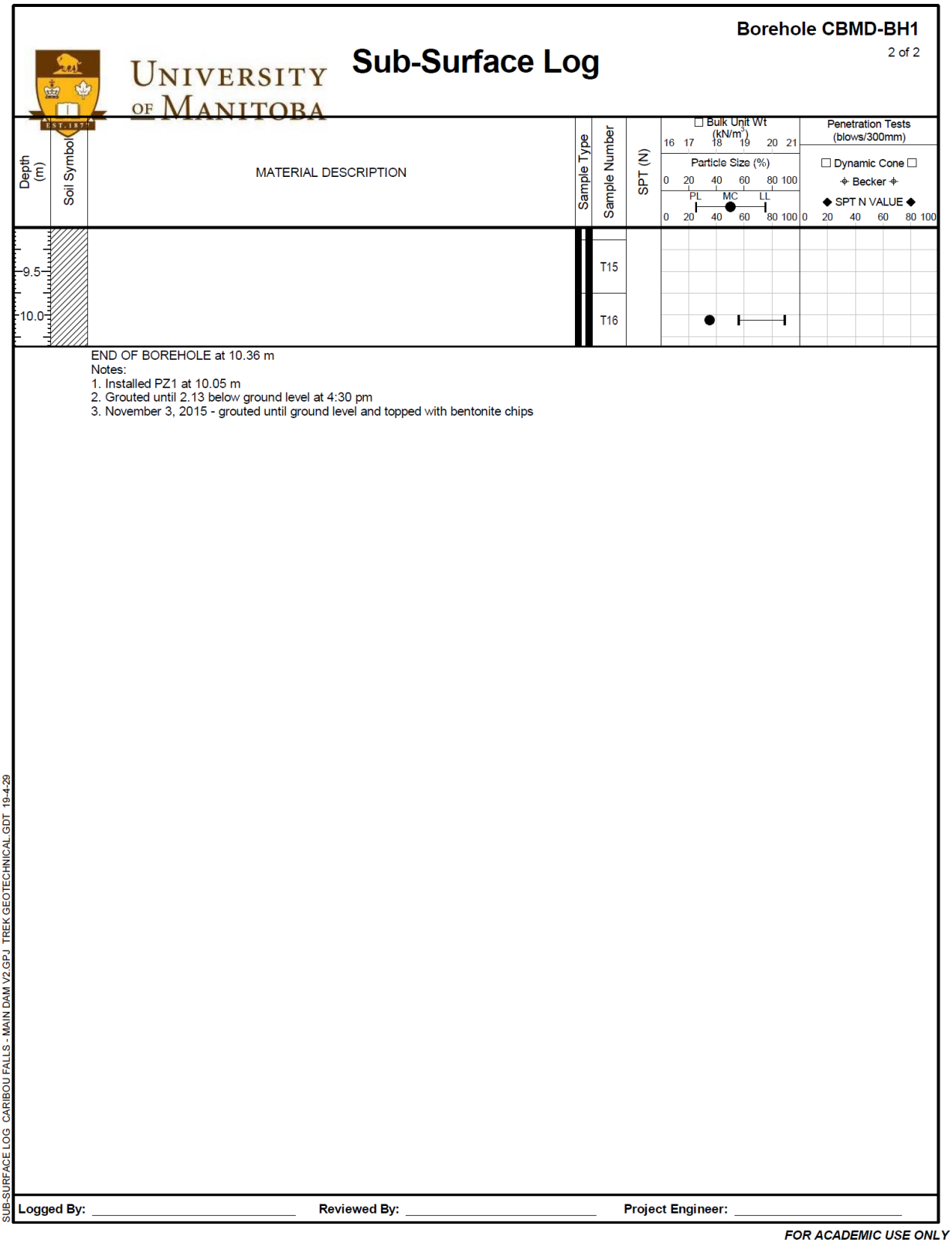

Figure A-A.7 Borehole log from CBMD Core

UNIVERSITY OF MANITOBA

Sub-Surface Log

Borehole WD-BH1
1 of 2

Client:	Ontario Power Generation	**Project Number:**	
Project Name:	Whitedog Falls - North Wing Dam Geotechnical Investigation	**Location:**	
Contractor:		**Ground Elevation:**	
Method:	Acker Renegade	**Date Drilled:**	2016 August 3

Sample Type: Grab (G) | Shelby Tube (T) | Split Spoon (SS) | Split Barrel (SB) | Core (C)

Particle Size Legend: Fines | Clay | Silt | Sand | Gravel | Cobbles | Boulders

Depth (m)	Soil Symbol	MATERIAL DESCRIPTION	Sample Type	Sample Number	SPT (N)	Bulk Unit Wt (kN/m³) 16 17 18 19 20 21 / Particle Size (%) 0 20 40 60 80 100 / PL MC LL	Penetration Tests (blows/300mm) Dynamic Cone / Becker / SPT N VALUE 0 20 40 60 80 100
0.5		SAND - sandy gravel; blacktop approximately 2.54 cm					
		- fine sand on top					
1.0		- clay started around 0.91 m					
1.5		CLAY - moist; dark brown; looked fissured		T01			
2.0				T02			
2.5				T03			
3.0				T04			
3.5		- light brown; clay with silt pockets		T05			
4.0				T06			
4.5		- brown; clay; silt pockets					
5.0		- auger advanced					
5.5		- clay; dark grey; moist		T07			
6.0		- shelby tube slipped off		T08			
6.5		- auger advanced to 7.16 m to recover T08					
7.0		- brown clay; silt pockets; nuggety		T09			
7.5		- brown clay with light brown specs; silty		T10			
8.0		- brown clay; silt pockets		T11			
8.5							

Logged By: _____ **Reviewed By:** _____ **Project Engineer:** _____

SUB-SURFACE LOG WHITEDOG FALLS - NORTH WING DAM.GPJ TREK GEOTECHNICAL.GDT 18-12-7

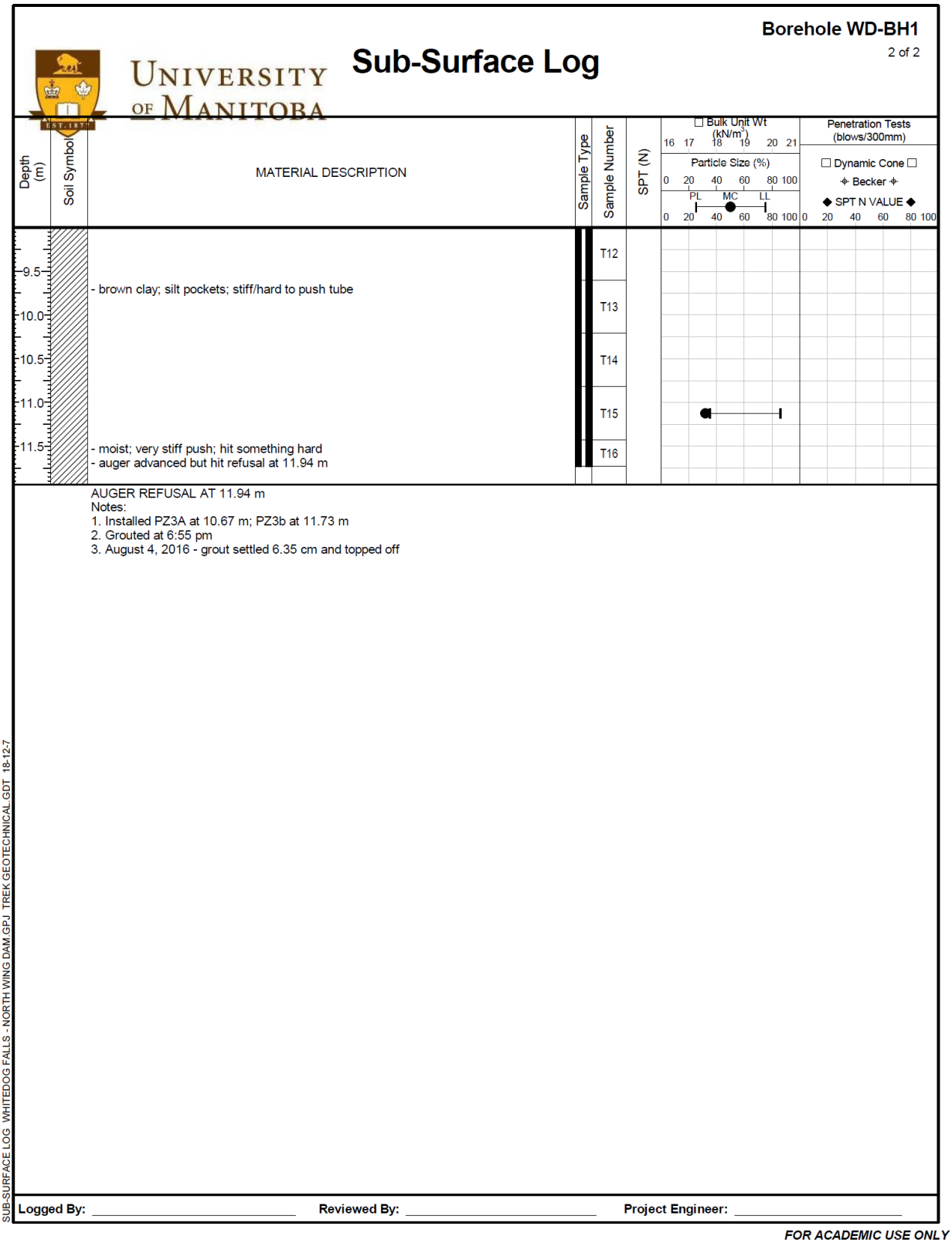

Figure A-A.8 Borehole log from WD Core

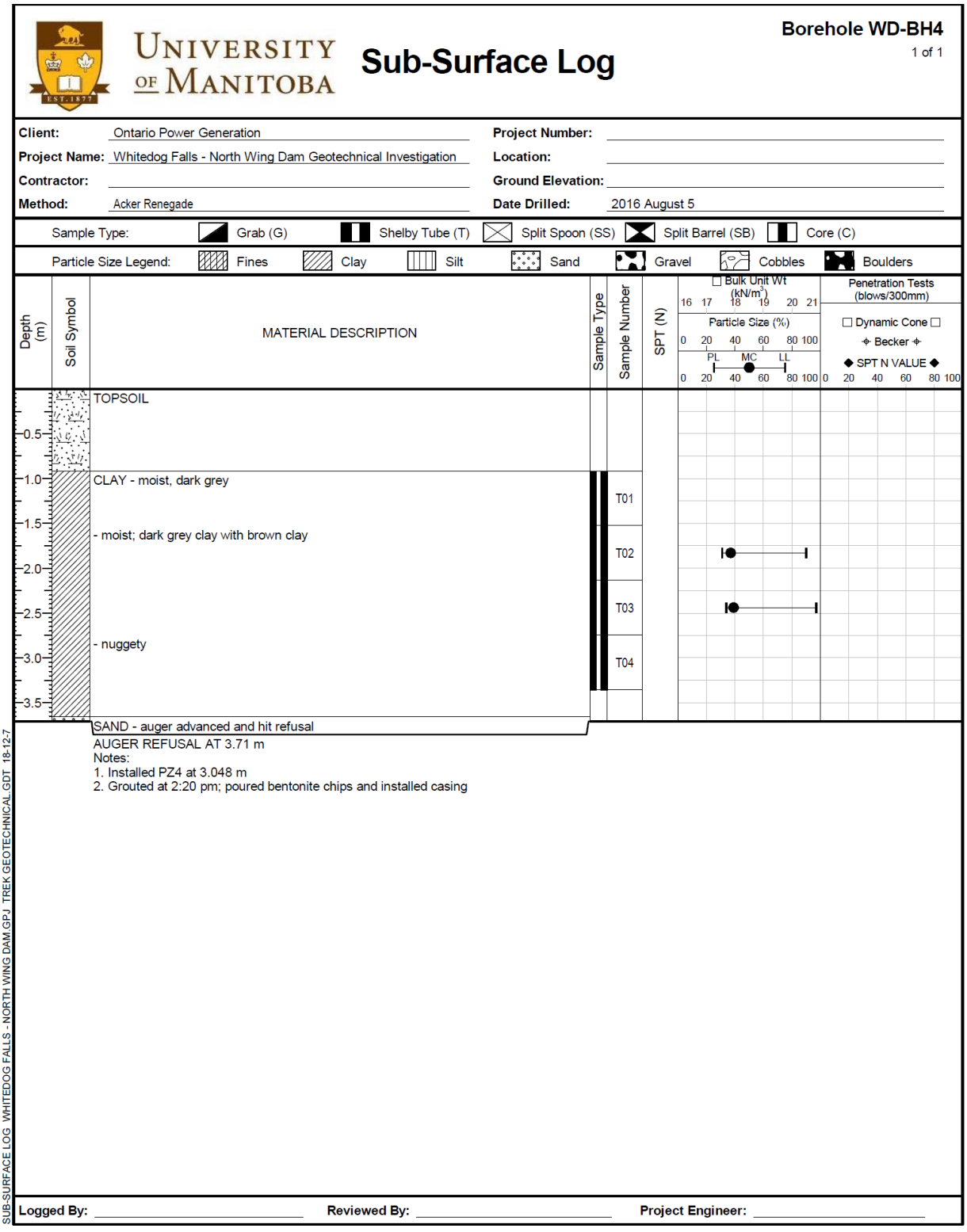

Figure A-A.9 Borehole log from WD Foundation

Sub-Surface Log

Borehole EF-BH1

UNIVERSITY OF MANITOBA

Client:	Ontario Power Generation	**Project Number:**	
Project Name:	Ear Falls Generating Station Dam Geotechnical Investigation	**Location:**	
Contractor:		**Ground Elevation:**	
Method:	Acker Renegade	**Date Drilled:**	2016 August 9

Sample Type: Grab (G) | Shelby Tube (T) | Split Spoon (SS) | Split Barrel (SB) | Core (C)

Particle Size Legend: Fines | Clay | Silt | Sand | Gravel | Cobbles | Boulders

Depth (m)	Soil Symbol	MATERIAL DESCRIPTION	Sample Type	Sample Number	SPT (N)
0		BLACKTOP PAVEMENT			
		SAND - sand gravel on top yellowish grey moist clay		SS01 (11/3/5)	8
1.5		CLAY - cannot push tube; changed to split spoon; silty clay; grey; moist		SS02 (7/3/5)	8
		- auger advanced to 3.05 m			
3.0		- moist; grey clay; with organics		T01	
				T02	
4.5				T03	
		- moist; grey clay		T04	
5.5				T05	
6.0		SILT - shelby tube recovered no clay; grey silt saturated with water collected		SS03 (2/3/4)	7 / 152mm
6.5		- saturated silt; grey		SS04 (3/5/5)	10 / 152mm
		- extremely soft; split spoon started dropping on its own weight		SS05 (1/1/1)	2
7.5				SS06 (2/3/5)	8
8.0				SS07 (2/1/1)	2
8.5		- split spoon just sunk down without blows		SS08	

Bulk Unit Wt (kN/m^3): 16 17 18 19 20 21

Particle Size (%): 0 20 40 60 80 100

PL MC LL: 0 20 40 60 80 100

Penetration Tests (blows/300mm): ☐ Dynamic Cone ☐ ◆ Becker ◆ ◆ SPT N VALUE ◆ 0 20 40 60 80 100

7 / 152mm

10 / 152mm

Logged By: _____ **Reviewed By:** _____ **Project Engineer:** _____

SUB-SURFACE LOG EAR FALLS GENERATION STATION DAM.GPJ TREK GEOTECHNICAL.GDT 19-4-29

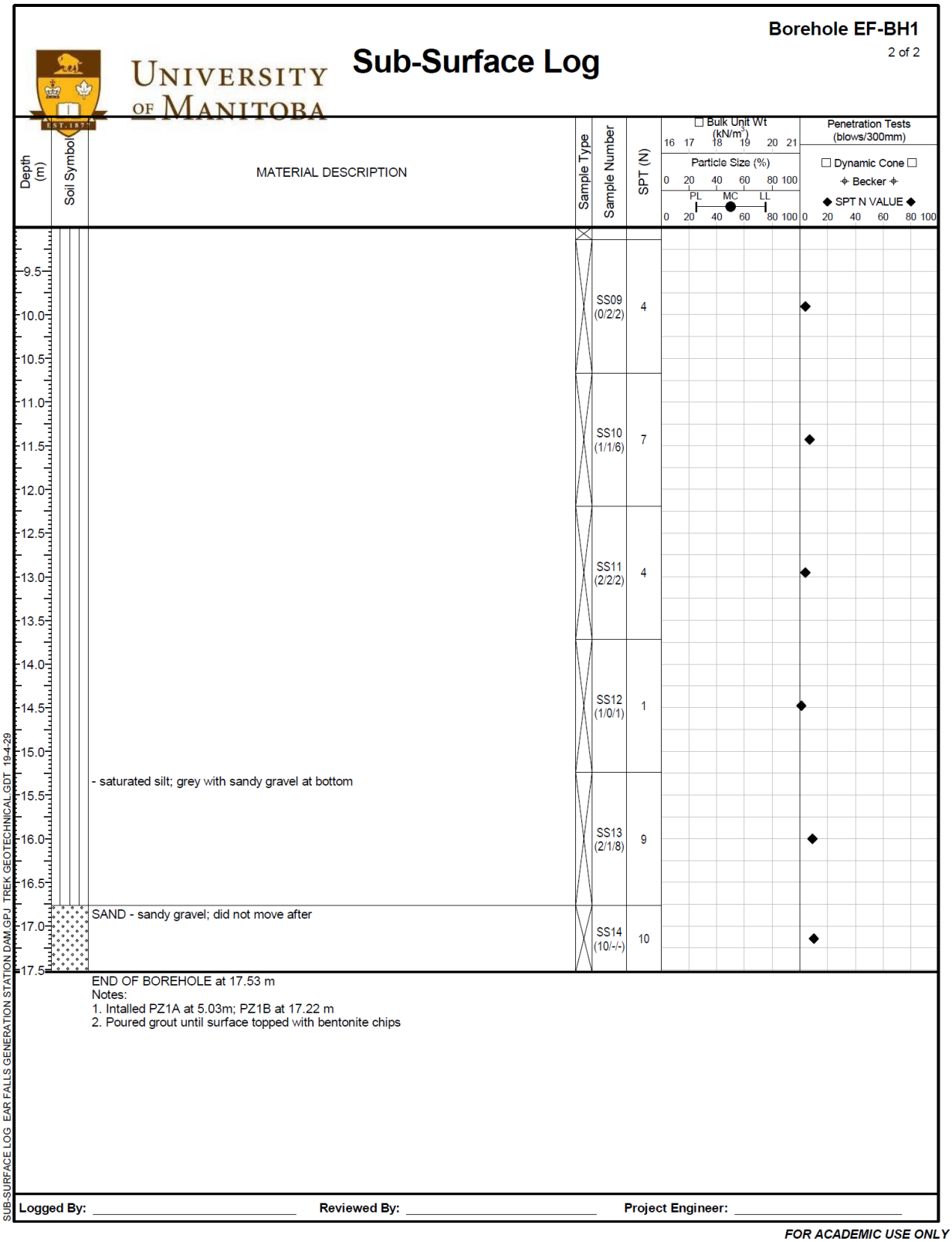

Figure A-A.10 Borehole log from EF Core

UNIVERSITY OF MANITOBA

Sub-Surface Log

Borehole EF-BH3

Client:	Ontario Power Generation	**Project Number:**	
Project Name:	Ear Falls Generating Station Dam Geotechnical Investigation	**Location:**	
Contractor:		**Ground Elevation:**	
Method:	Acker Renegade	**Date Drilled:**	2016 August 11

Sample Type: Grab (G) | Shelby Tube (T) | Split Spoon (SS) | Split Barrel (SB) | Core (C)

Particle Size Legend: Fines | Clay | Silt | Sand | Gravel | Cobbles | Boulders

Depth (m)	Soil Symbol	MATERIAL DESCRIPTION	Sample Type	Sample Number	SPT (N)
0.5		TOPSOIL			
1.0		SILTY CLAY - moist; grey with brown-red spots	T	T01	
1.5			T	T02	
2.0					
2.5		- grey with brown spots; saturated	SS	SS01 (1/1/5)	6
3.0		SILT - saturated; grey with brown spots	SS	SS02 (2/3/4)	7
3.5			SS	SS03 (1/3/3)	6
4.0		SILTY FINE SAND - saturated; grey with brown spots	SS	SS04 (2/3/4)	7
4.5		- grey			
5.0		- dark grey	SS	SS05 (2/1/0)	1
5.5		SILT - saturated; dark grey - split spoon dropped under its own weight	SS	SS06	
6.0		- split spoon dropped under its own weight	SS	SS07	
6.5			SS	SS08 (0/1/1)	2
7.0			SS	SS09 (0/1/1)	2
7.5					
8.0		SILTY SAND - saturated; grey	SS	SS10 (0/1/1)	2
8.5					

Bulk Unit Wt (kN/m³): 16 17 18 19 20 21

Particle Size (%): 0 20 40 60 80 100

PL MC LL: 0 20 40 60 80 100

Penetration Tests (blows/300mm): Dynamic Cone | Becker | SPT N VALUE: 0 20 40 60 80 100

Logged By: _____ **Reviewed By:** _____ **Project Engineer:** _____

SUB-SURFACE LOG EAR FALLS GENERATION STATION DAM.GPJ TREK GEOTECHNICAL.GDT 19-4-29

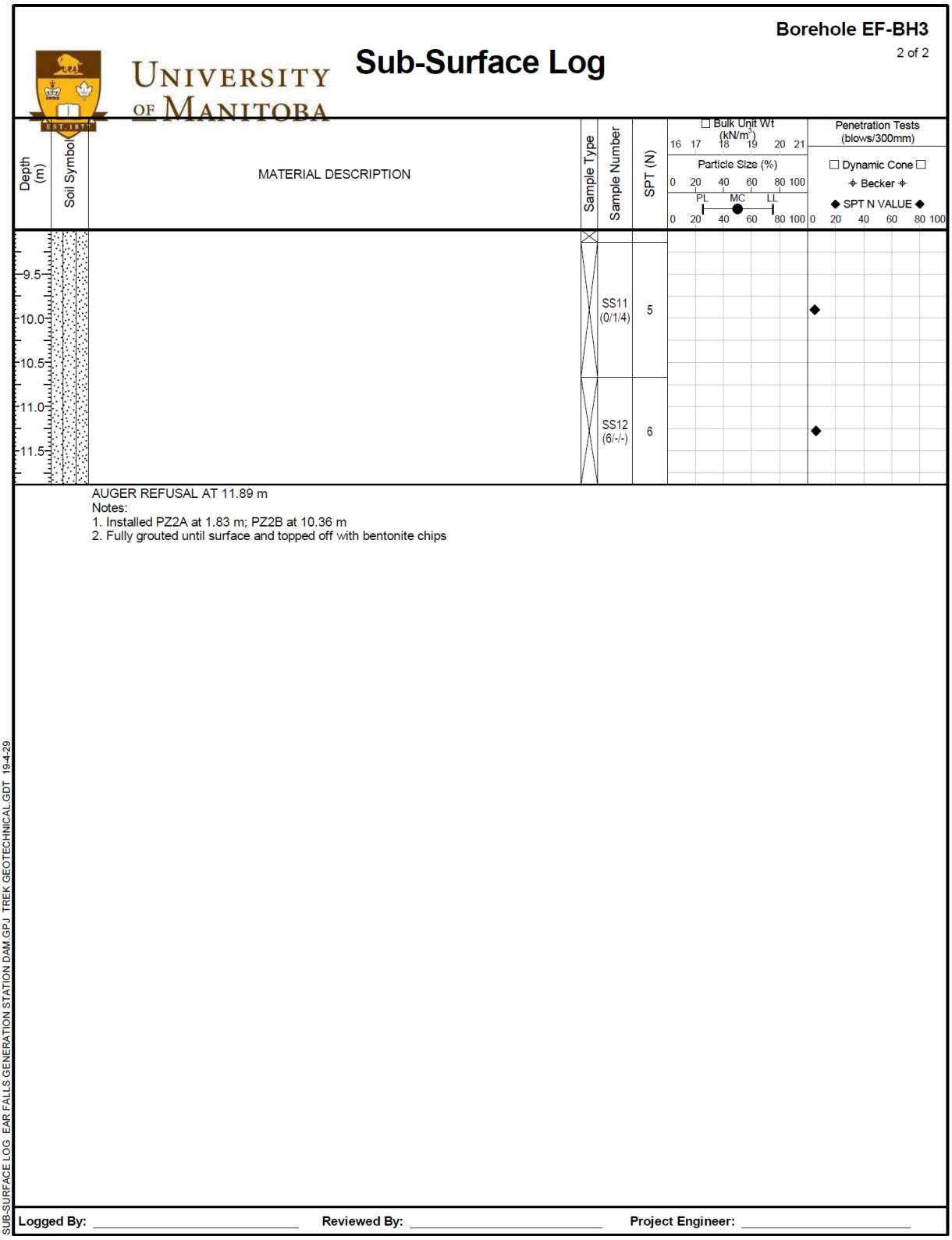

Figure A-A.11 Borehole log from EF Foundation

UNIVERSITY OF MANITOBA

Sub-Surface Log

Borehole MFRED-BH2
1 of 1

Client:	Ontario Power Generation	**Project Number:**	
Project Name:	Manitou Falls Right Earthfill Dam Geotechnical Investigation	**Location:**	
Contractor:		**Ground Elevation:**	
Method:	Acker Renegade	**Date Drilled:**	2016 August 12

Sample Type: Grab (G) | Shelby Tube (T) | Split Spoon (SS) | Split Barrel (SB) | Core (C)

Particle Size Legend: Fines | Clay | Silt | Sand | Gravel | Cobbles | Boulders

Depth (m)	Soil Symbol	MATERIAL DESCRIPTION	Sample Type	Sample Number	SPT (N)	Bulk Unit Wt (kN/m³) 16 17 18 19 20 21 / Particle Size (%) 0 20 40 60 80 100 / PL MC LL	Penetration Tests (blows/300mm) Dynamic Cone / Becker / SPT N VALUE 0 20 40 60 80 100
0.5		SAND - Auger advanced through gravelly sand					
1.0							
1.5							
2.0							
2.5		CLAY - very moist; dark grey with brown spots		T01			
3.0		- dark grey		T02			
3.5		- auger advanced					
4.0							
4.5				T03			
5.0							
5.5							
6.0		- dark grey with brown spots		T04			
6.5		- SPT check but hammer only bounced and did not move					
7.0							

END OF BOREHOLE AT 7.32 m

Notes:
1. Installed PZ3 at 7.01 m
2. Poured grout until surface topped with bentonite chips

Logged By: _____ **Reviewed By:** _____ **Project Engineer:** _____

SUB-SURFACE LOG MANITOU FALLS RIGHT EARTHFILL DAM.GPJ TREK GEOTECHNICAL.GDT 18-12-7

Figure A-A.12 Borehole log from MFRED Core

UNIVERSITY OF MANITOBA

Sub-Surface Log

Borehole MFLED-BH2

1 of 1

Client:	Ontario Power Generation	**Project Number:**	
Project Name:	Manitou Falls Left Earthfill Dam Geotechnical Investigation	**Location:**	
Contractor:		**Ground Elevation:**	
Method:	Acker Renegade	**Date Drilled:**	2016 August 16

Sample Type: Grab (G) | Shelby Tube (T) | Split Spoon (SS) | Split Barrel (SB) | Core (C)

Particle Size Legend: Fines | Clay | Silt | Sand | Gravel | Cobbles | Boulders

Depth (m)	Soil Symbol	MATERIAL DESCRIPTION	Sample Type	Sample Number	SPT (N)	Bulk Unit Wt (kN/m³) 16 17 18 19 20 21 / Particle Size (%) 0 20 40 60 80 100 / PL MC LL	Penetration Tests (blows/300mm) Dynamic Cone / Becker / SPT N VALUE 0 20 40 60 80 100
0.5		SAND - auger advanced through gravelly sand					
1.0							
1.5		- moist; sand on top; grey clay at bottom		SS01 (2/3/4)	7		◆
2.0		CLAY - moist; grey with brown spots					
2.5		- 10 cm of sand on top		T01		● —	
3.0		- moist; dark grey with brown spots		T02			
3.5				T03			
4.0				T04		● —	
4.5				T05			
5.0				T06			
5.5				T07			
6.0				T08			
6.5		- very wet; grey with brown spots; bottom of tube is dented; water at end of tube					
7.0		AUGER REFUSAL AT 7.01 m					

Notes:
1. Split spoon check but 7/--/--
2. Installed PZ2 at 6.7 m
3. Poured grout until surface topped with bentonite chips

Logged By: _____ **Reviewed By:** _____ **Project Engineer:** _____

SUB-SURFACE LOG MANITOU FALLS LEFT EARTHFILL DAM.GPJ TREK GEOTECHNICAL.GDT 18-12-7

FOR ACADEMIC USE ONLY

Figure A-A.13 Borehole log from MFRED Core

APPENDIX B

Figure A-B.1 CBBD4 clay core extruded Shelby tube sample

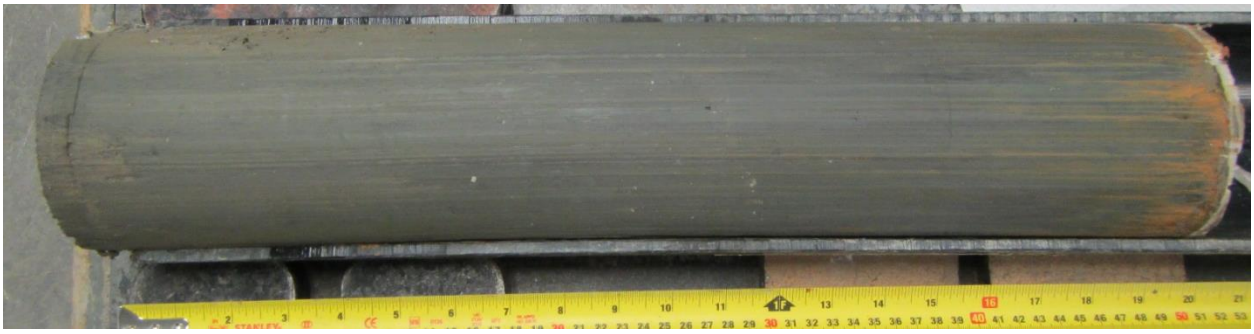

Figure A-B.2 CBBD4 clay foundation extruded Shelby tube sample

Figure A-B.3 CBMD clay core extruded Shelby tube sample

Figure A-B.4 WD clay core extruded Shelby tube sample

Figure A-B.5 WD clay foundation extruded Shelby tube sample

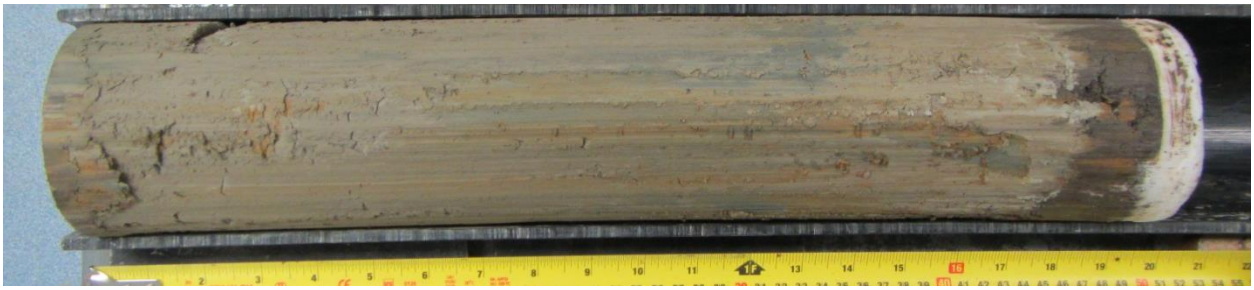

Figure A-B.6 EF clay core extruded Shelby tube sample

Figure A-B.7 EF clay foundation extruded Shelby tube sample

Figure A-B.8 MFRED clay core extruded Shelby tube sample

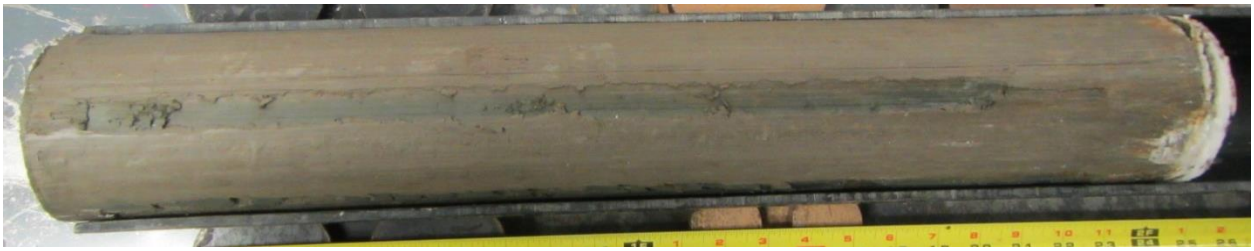

Figure A-B.9 MFLED clay core extruded Shelby tube sample

Figure A-B.10 CBBD4 clay foundation trimmed sample

Figure A-B.11 WD clay core trimmed sample

Figure A-B.12 WD clay foundation trimmed sample

Figure A-B.13 EF clay core trimmed sample

Figure A-B.14 EF clay foundation trimmed sample

Figure A-B.15 MFRED clay core trimmed sample

Figure A-B.16 MFLED clay core trimmed sample

APPENDIX C

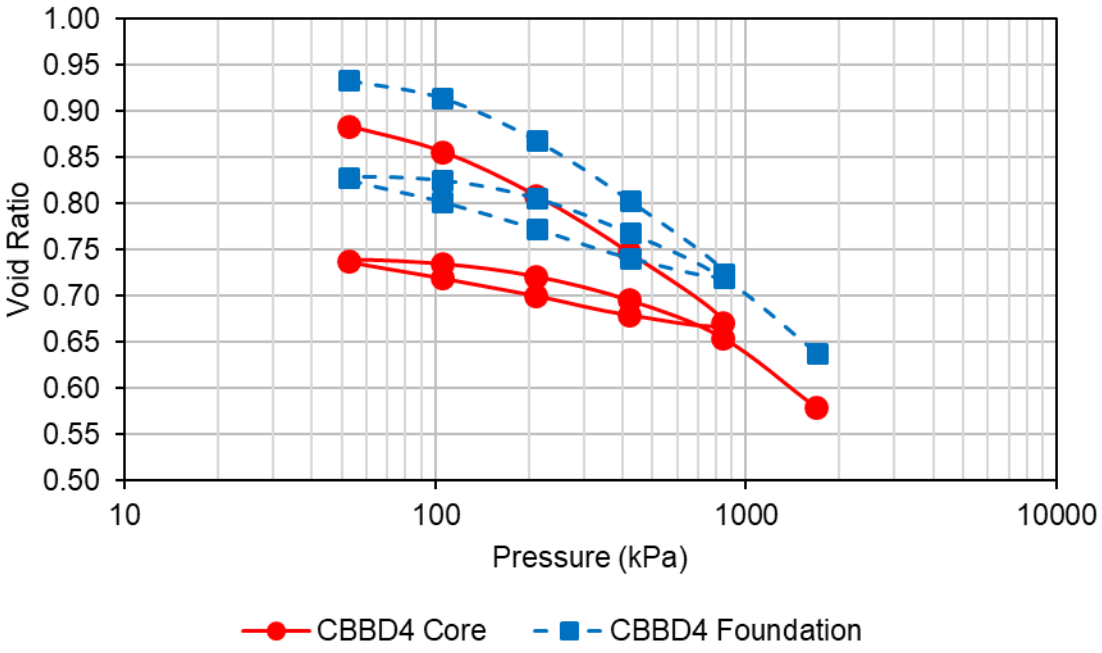

Figure A-C.1 Consolidation curves from oedometer tests on CBBD4 samples

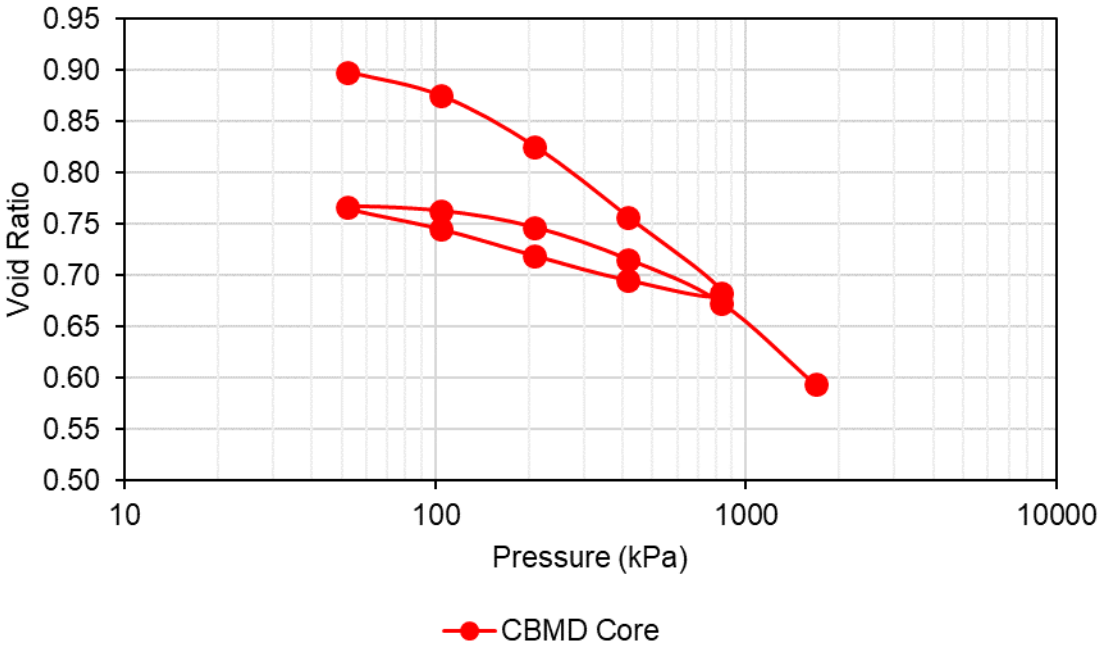

Figure A-C.2 Consolidation curve from oedometer tests on CBMD samples

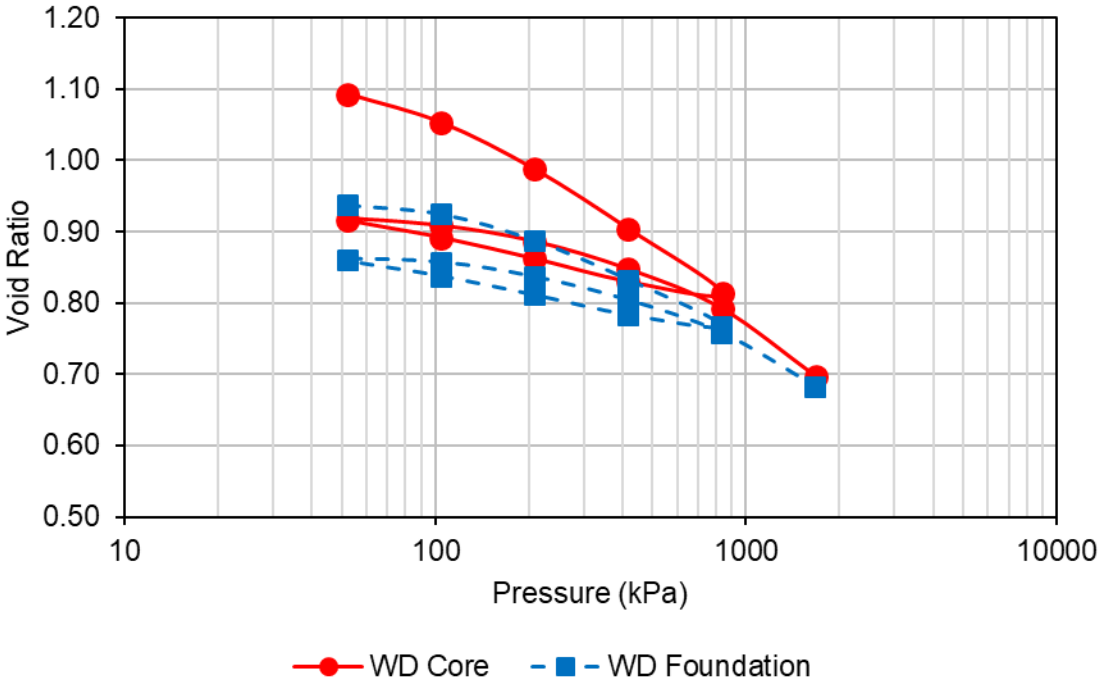

Figure A-C.3 Consolidation curves from oedometer tests on WD samples

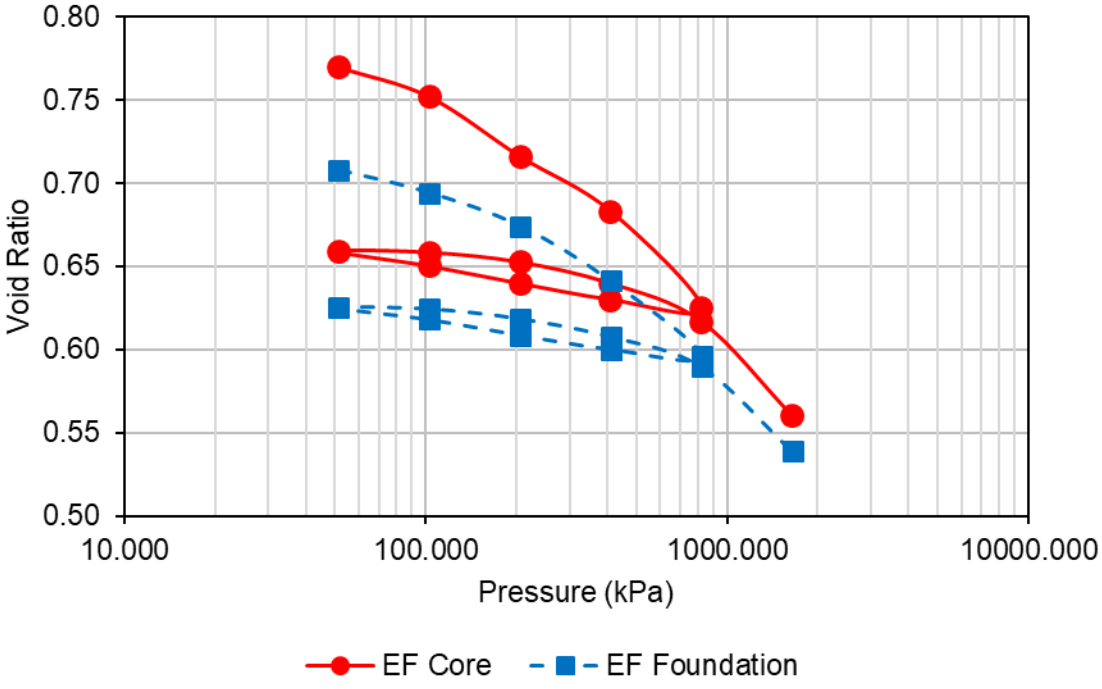

Figure A-C.4 Consolidation curves from oedometer tests on EF samples

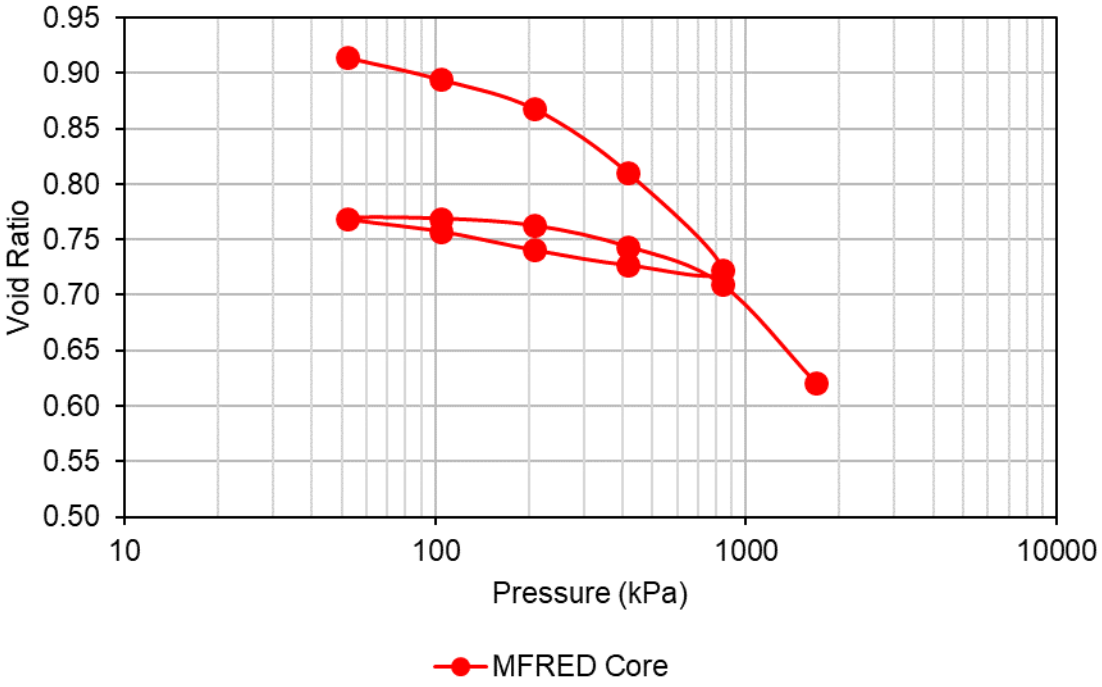

Figure A-C.5 Consolidation curve from oedometer tests on MFRED samples

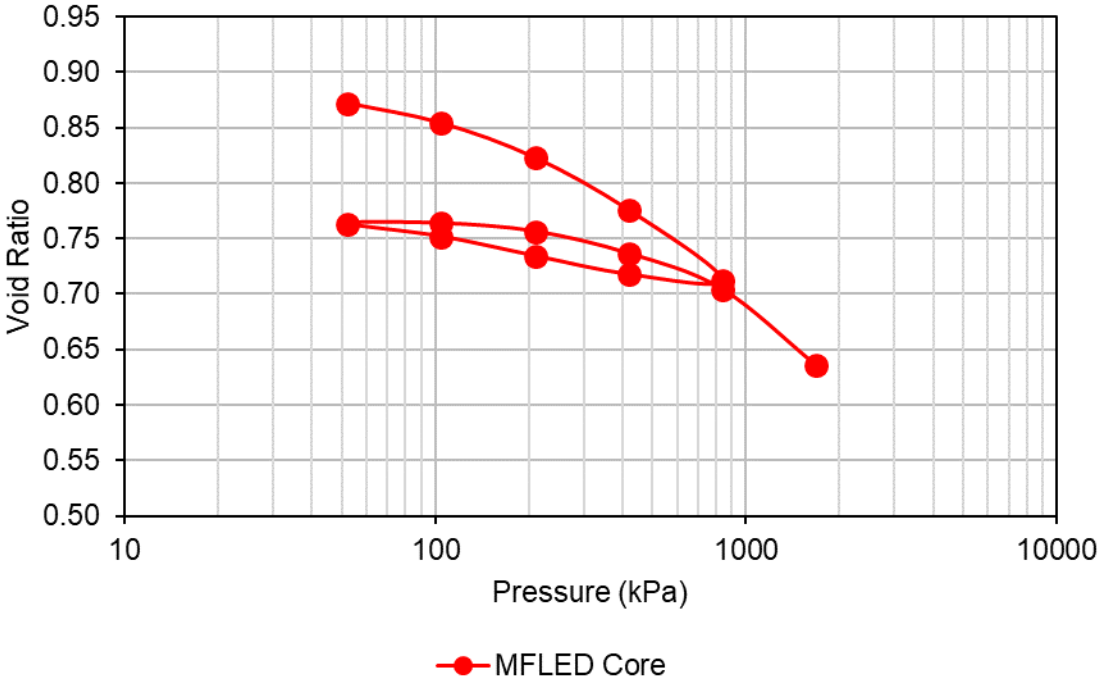

Figure A-C.6 Consolidation curve from oedometer tests on MFLED samples

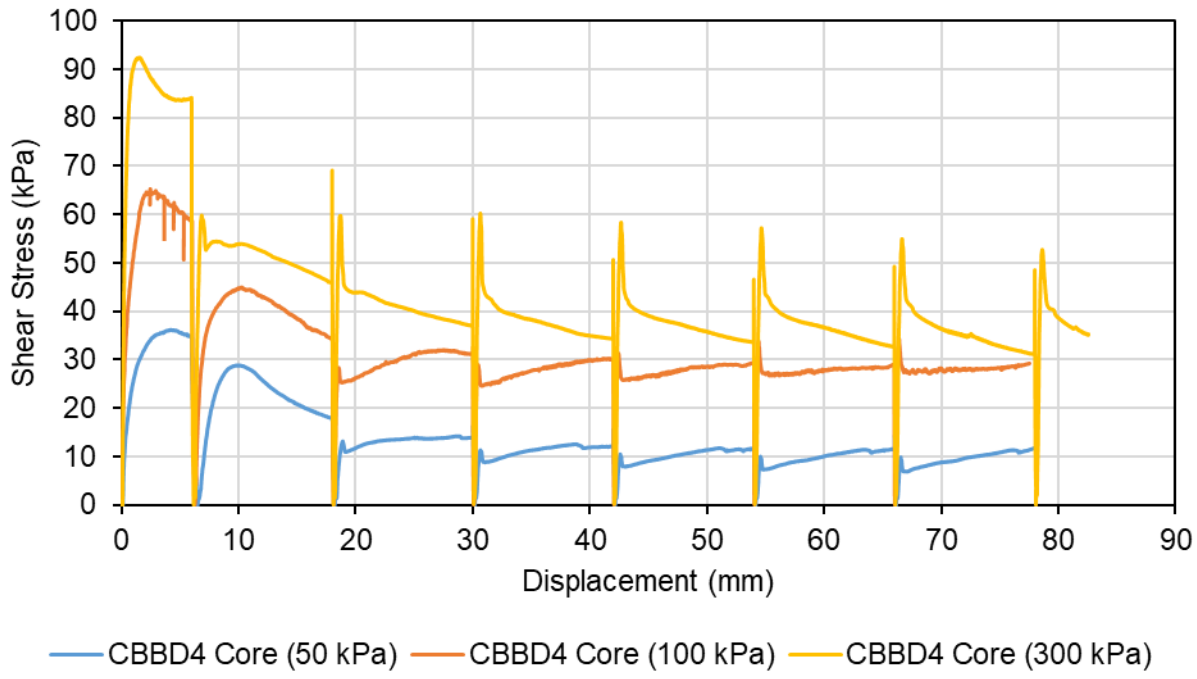

Figure A-C.7 Stress-displacement behaviour of CBBD4 core samples from Direct Shear Tests

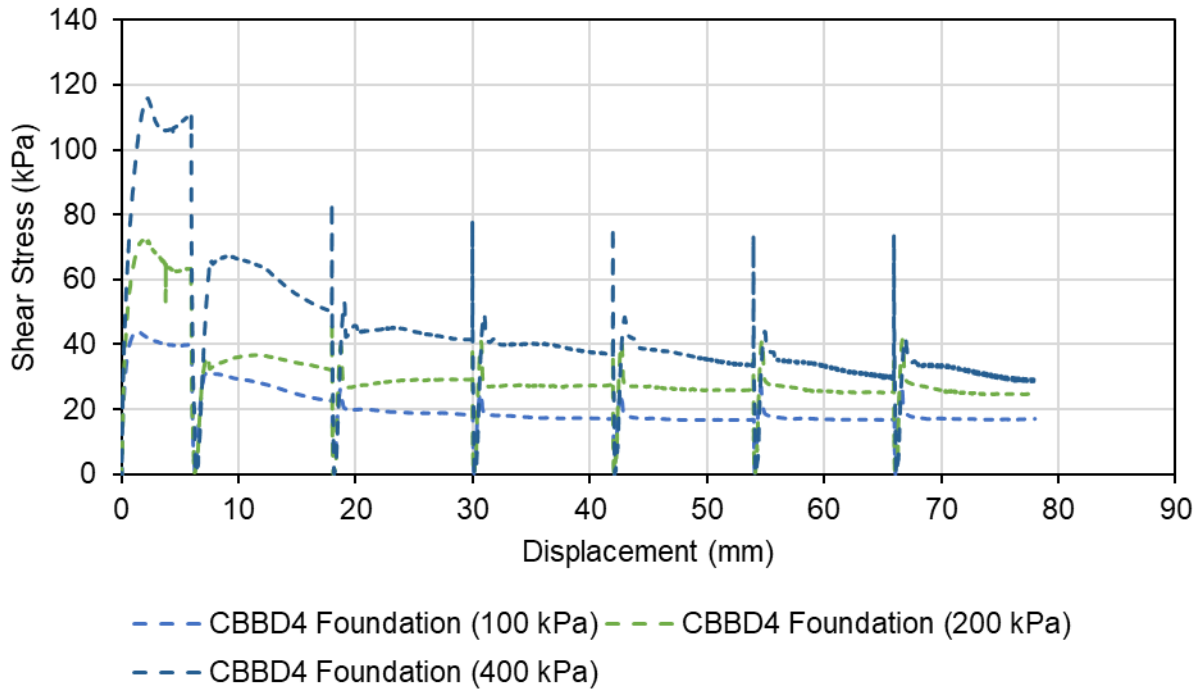

Figure A-C.8 Stress-displacement behaviour of CBBD4 foundation samples from Direct Shear Tests

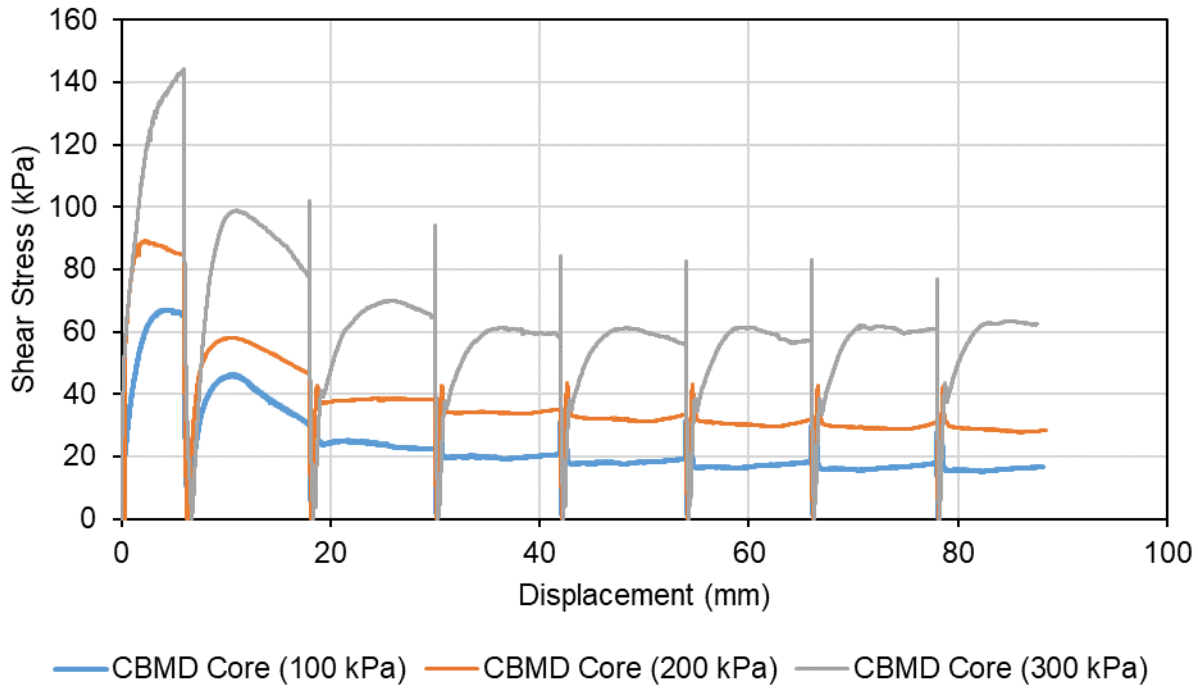

Figure A-C.9 Stress-displacement behaviour of CBMD core samples from Direct Shear Tests

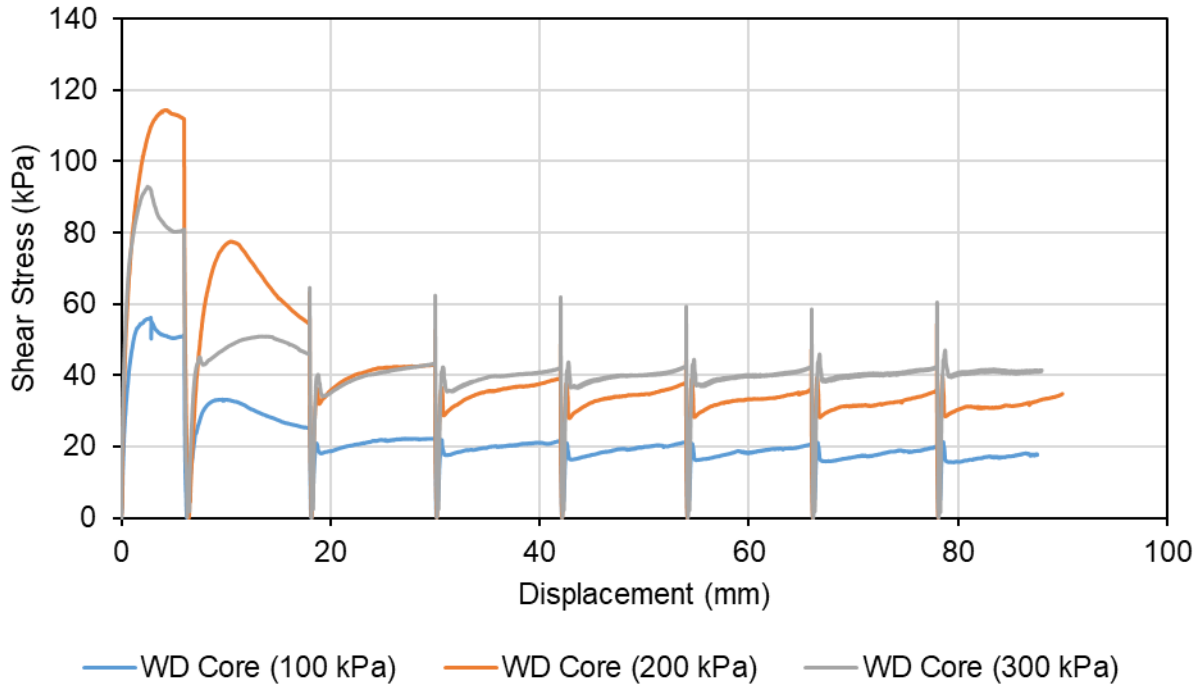

Figure A-C.10 Stress-displacement behaviour of WD core samples from Direct Shear Tests

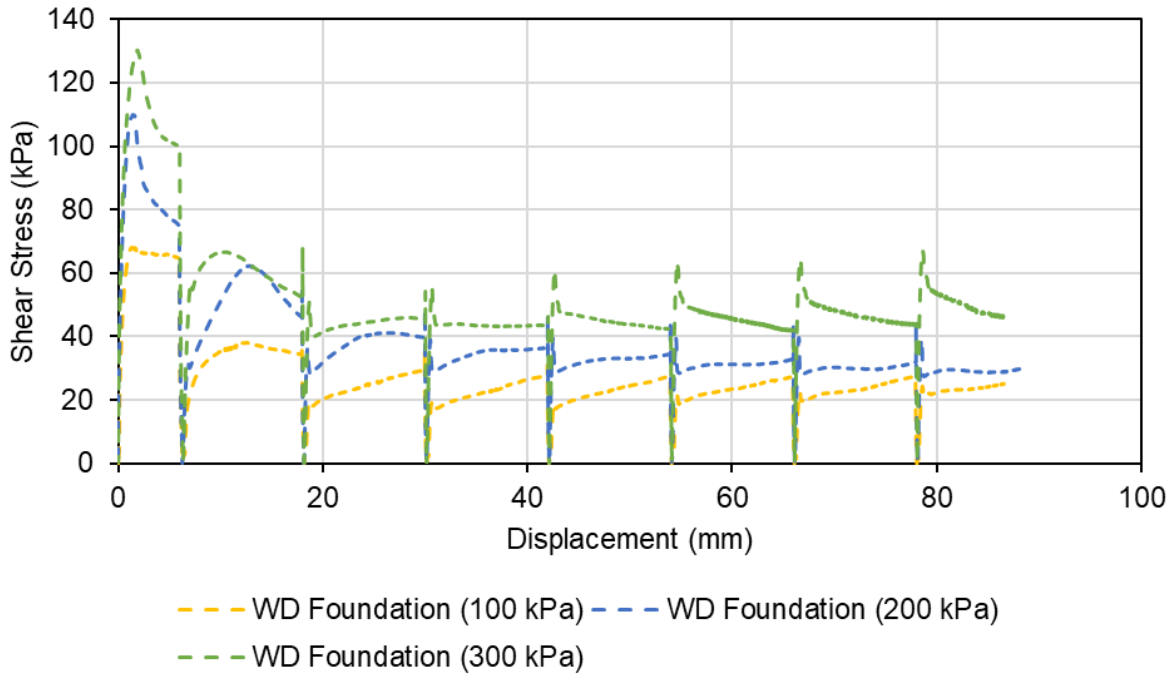

Figure A-C.11 Stress-displacement behaviour of WD foundation samples from Direct Shear Tests

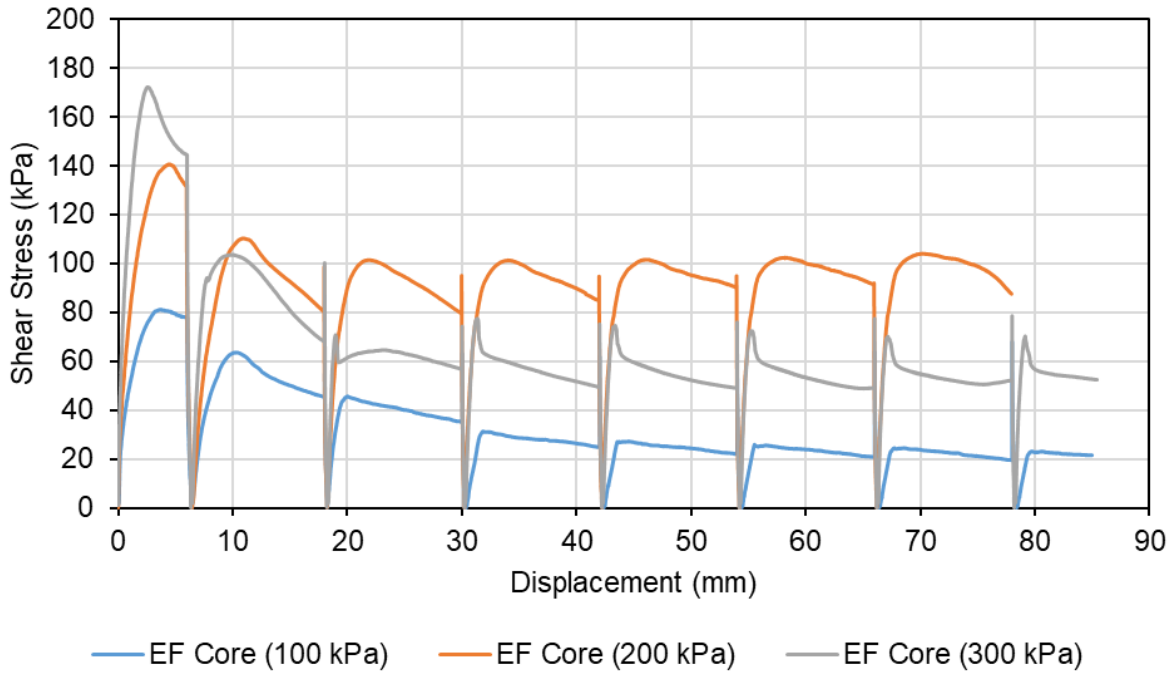

Figure A-C.12 Stress-displacement behaviour of EF core samples from Direct Shear Tests

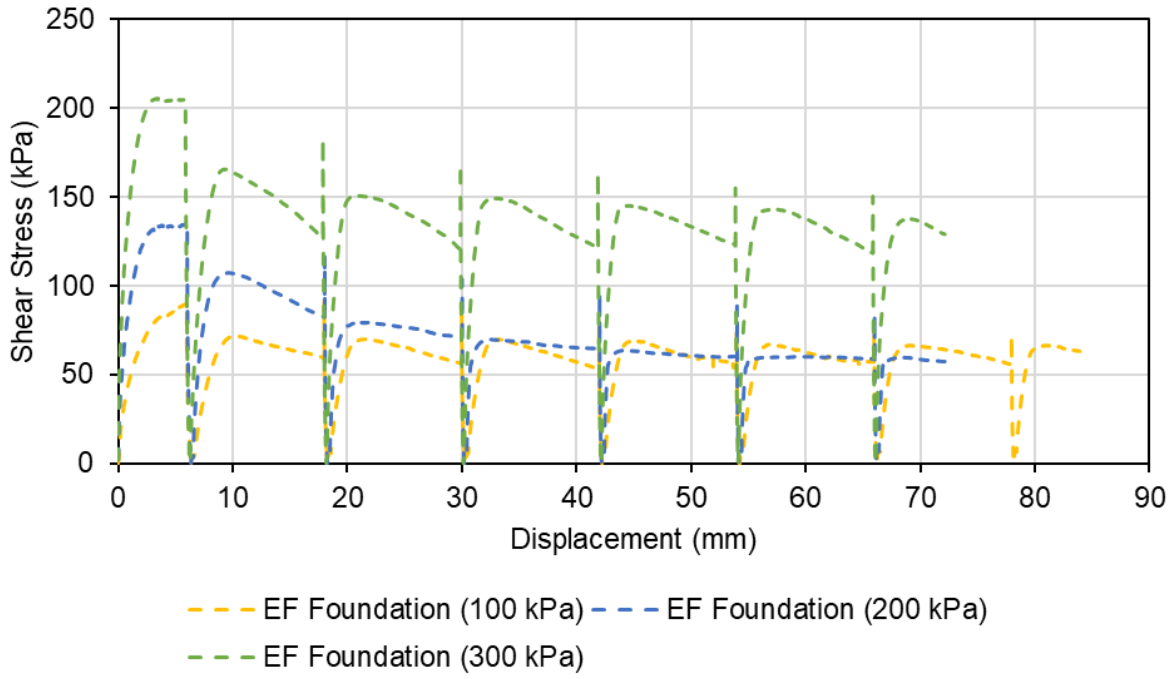

Figure A-C.13 Stress-displacement behaviour of EF foundation samples from Direct Shear Tests

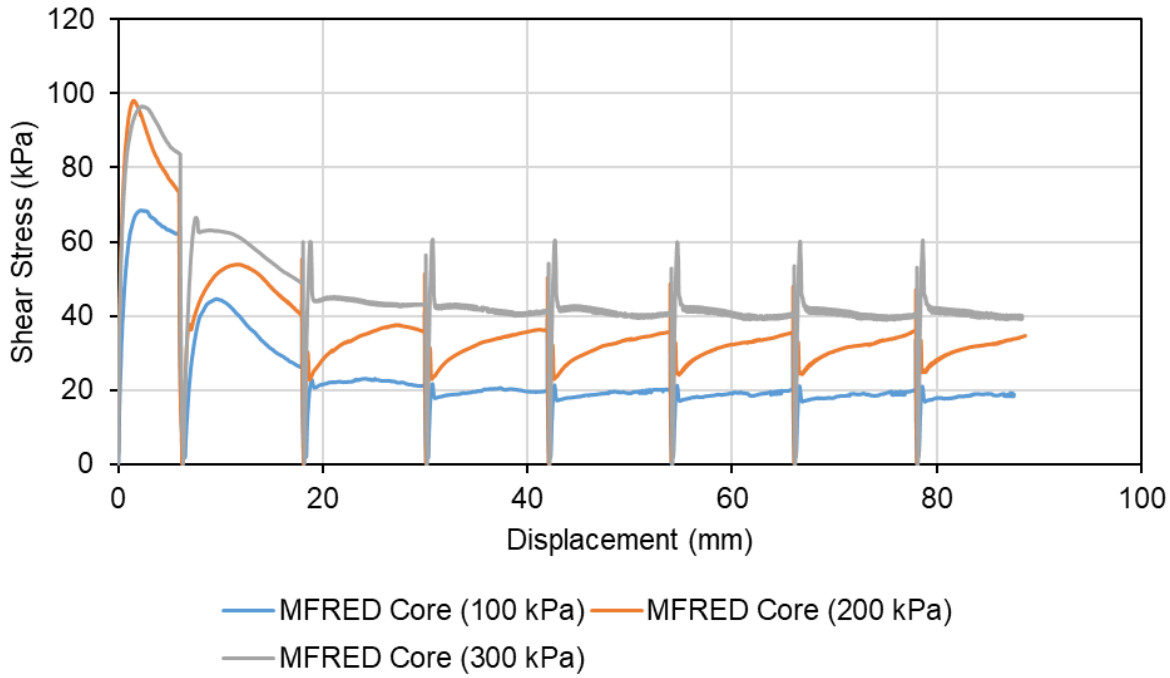

Figure A-C.14 Stress-displacement behaviour of MFRED core samples from Direct Shear Tests

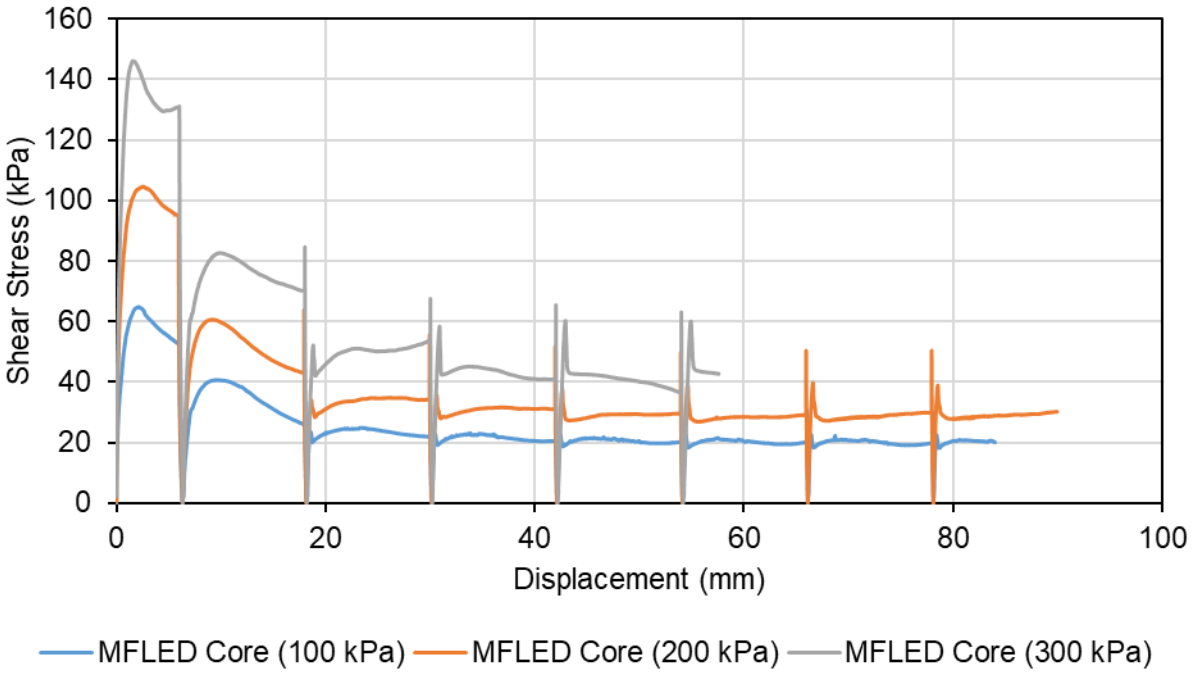

Figure A-C.15 Stress-displacement behaviour of MFLED core samples from Direct Shear Tests

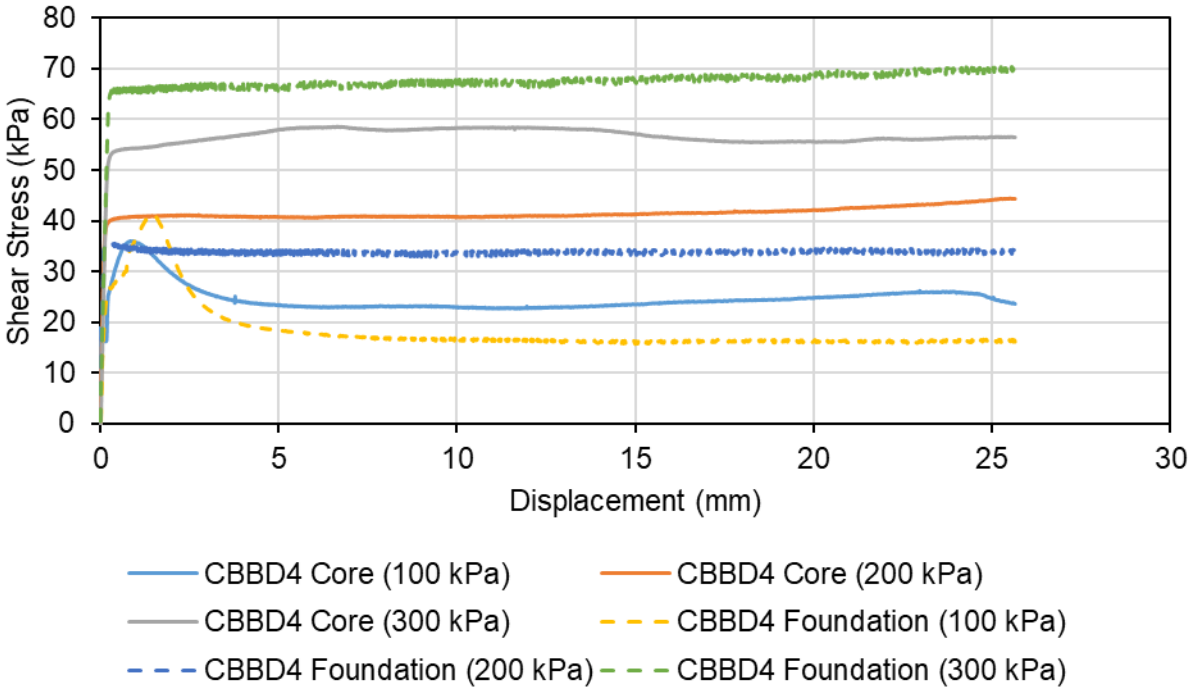

Figure A-C.16 Stress-displacement behaviour of CBBD4 samples from Torsional Ring Shear Tests

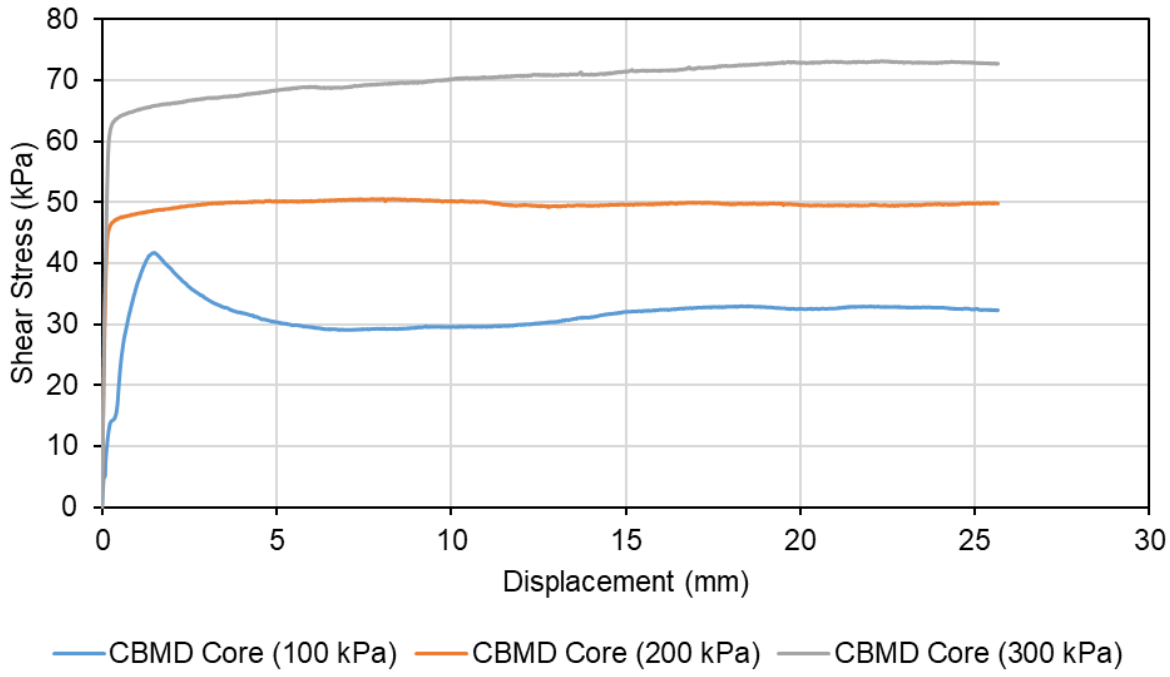

Figure A-C.17 Stress-displacement behaviour of CBMD samples from Torsional Ring Shear Tests

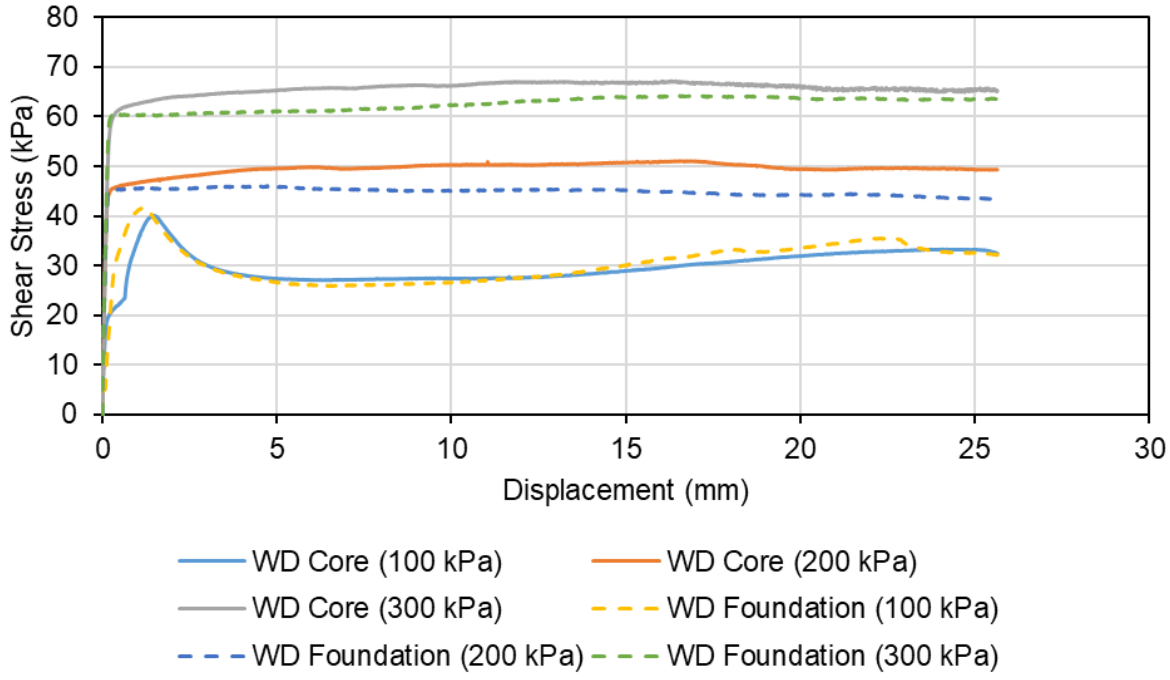

Figure A-C.18 Stress-displacement behaviour of WD samples from Torsional Ring Shear Tests

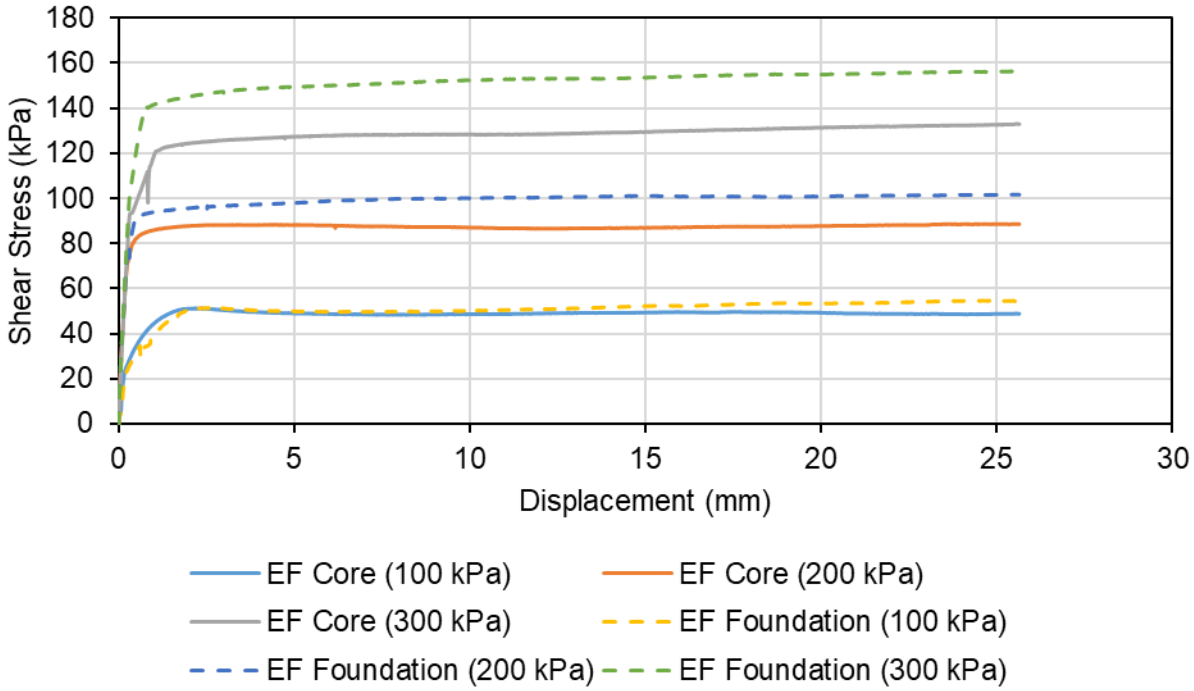

Figure A-C.19 Stress-displacement behaviour of EF samples from Torsional Ring Shear Tests

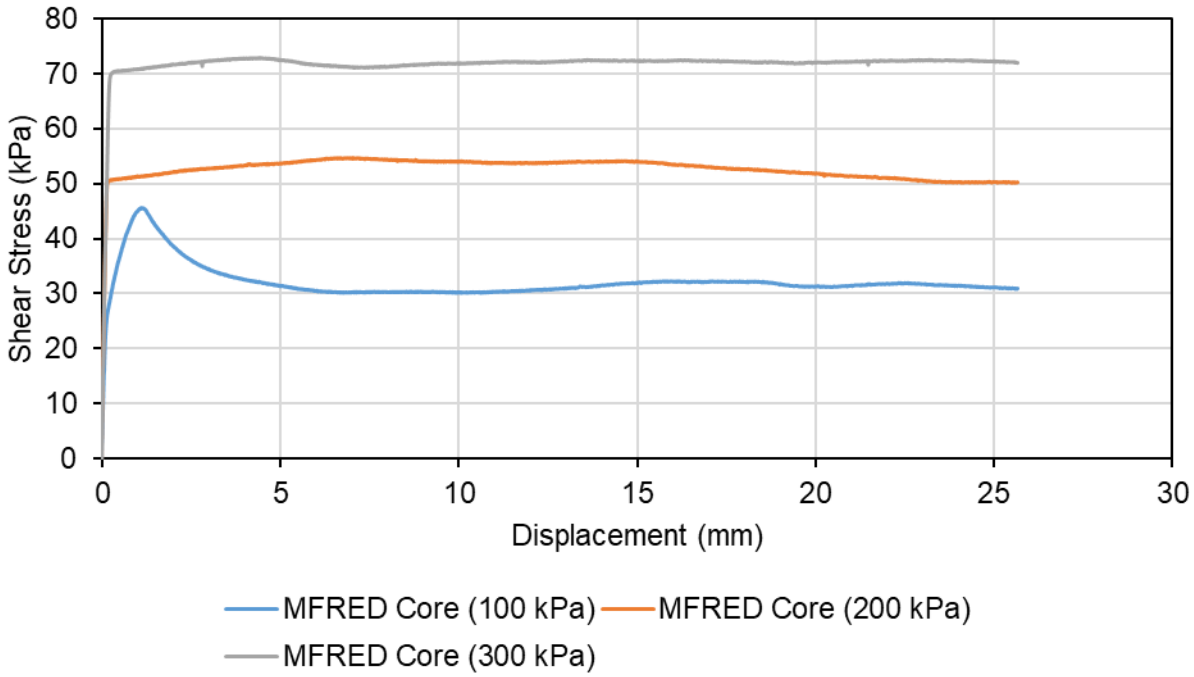

Figure A-C.20 Stress-displacement behaviour of MFRED samples from Torsional Ring Shear Tests

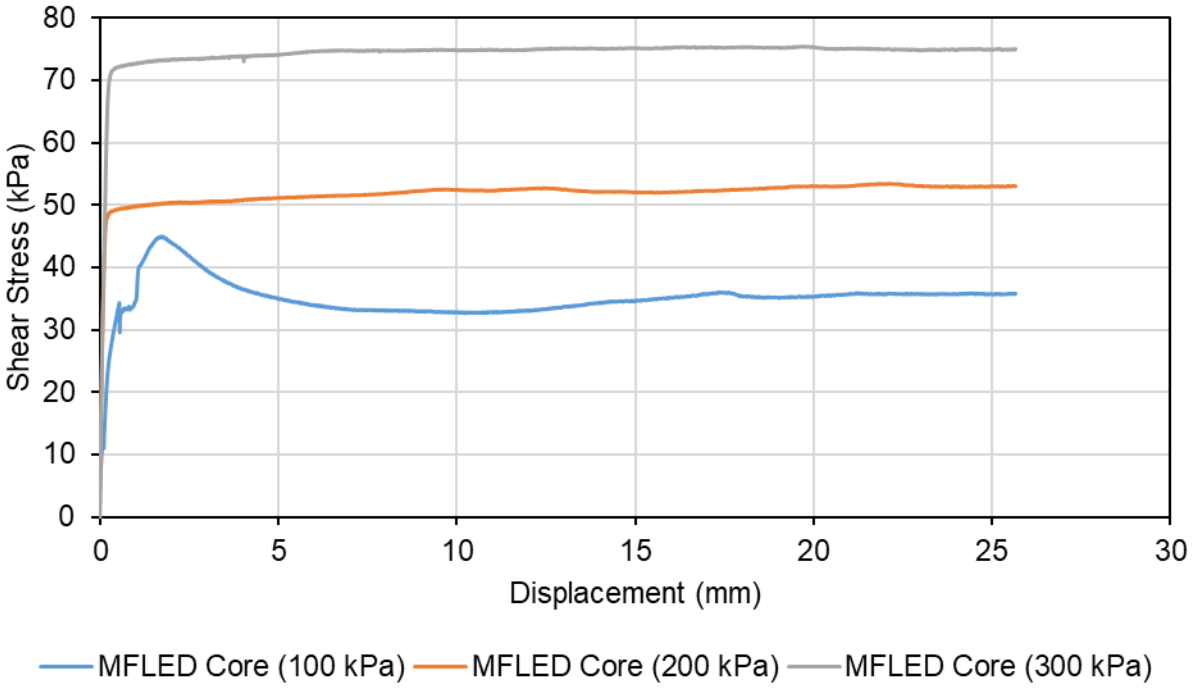

Figure A-C.21 Stress-displacement behaviour of MFLED samples from Torsional Ring Shear Tests

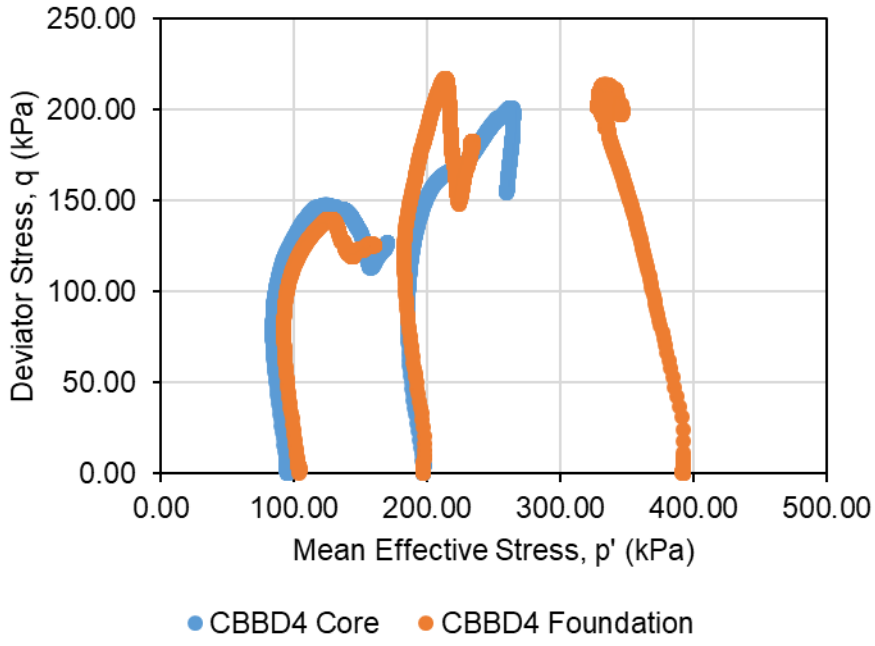

Figure A-C.22 Stress paths in p'-q space of CBBD4 CIU Triaxial Test samples

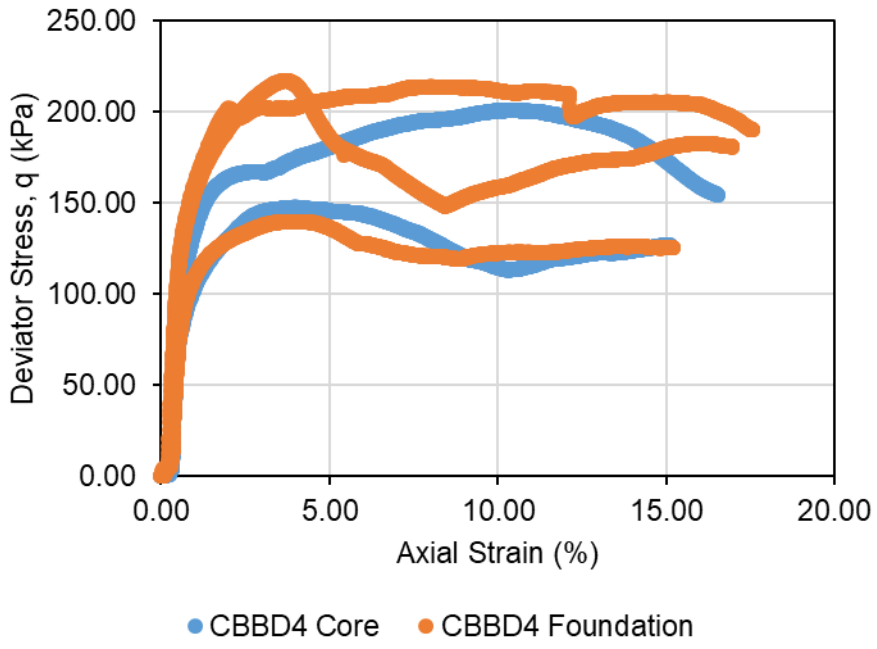

Figure A-C.23 Stress-strain behaviour of CBBD4 CIU Triaxial Test samples

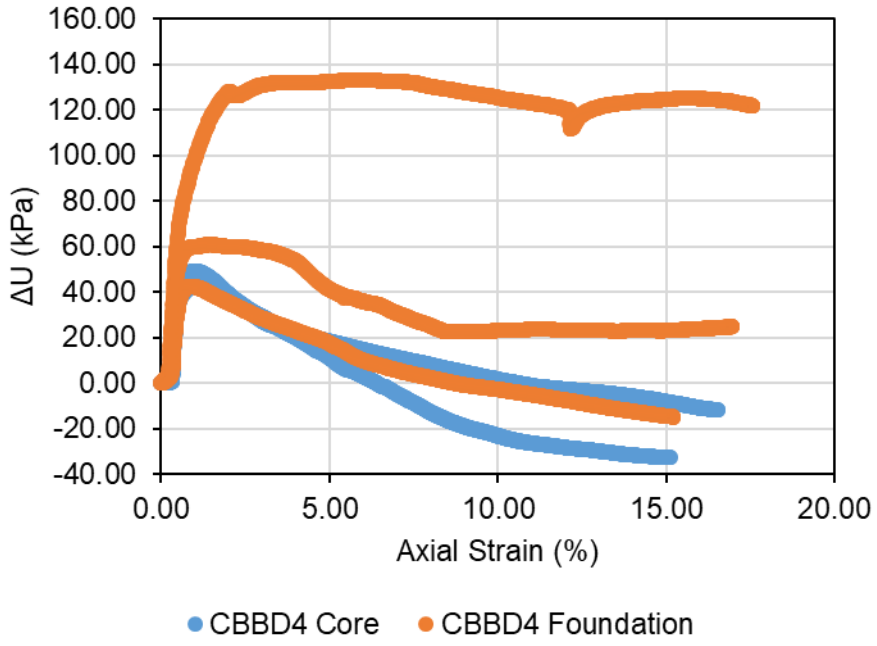

Figure A-C.24 Pore water measurements of CBBD4 CIU Triaxial Test sample

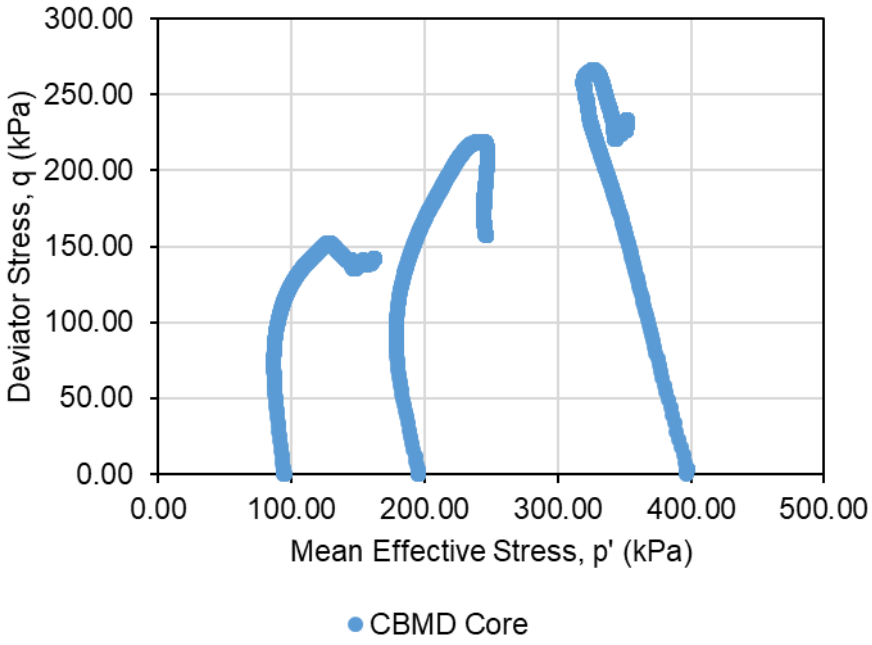

Figure A-C.25 Stress paths in p'-q space of CBMD CIU Triaxial Test samples

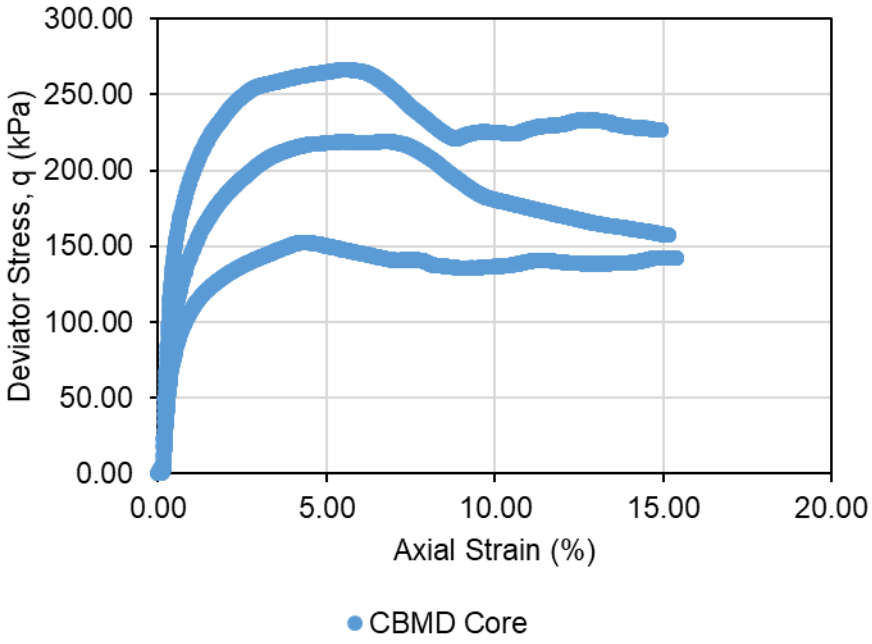

Figure A-C.26 Stress-strain behaviour of CBMD CIU Triaxial Test samples

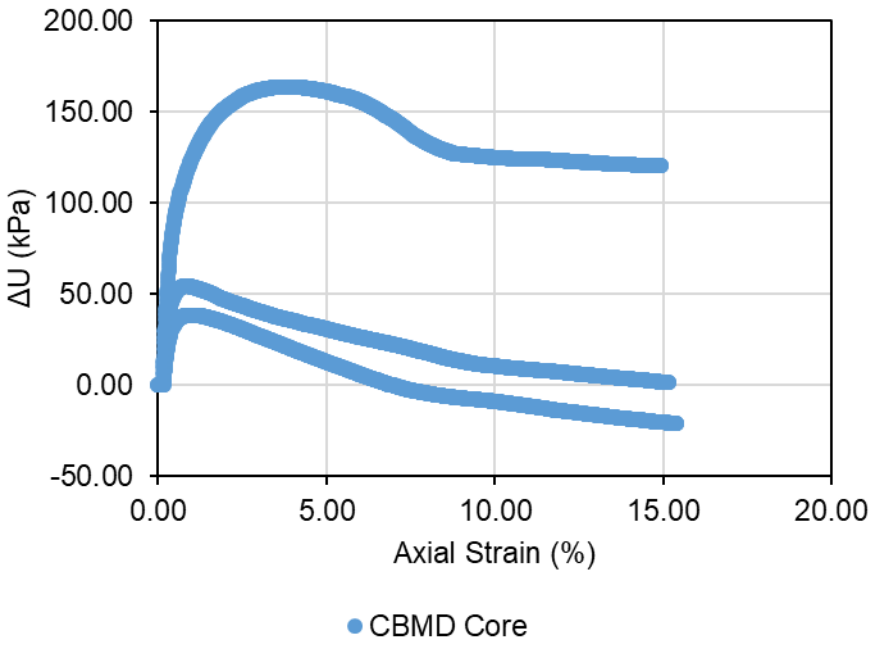

Figure A-C.27 Pore water measurements of CBMD CIU Triaxial Test sample

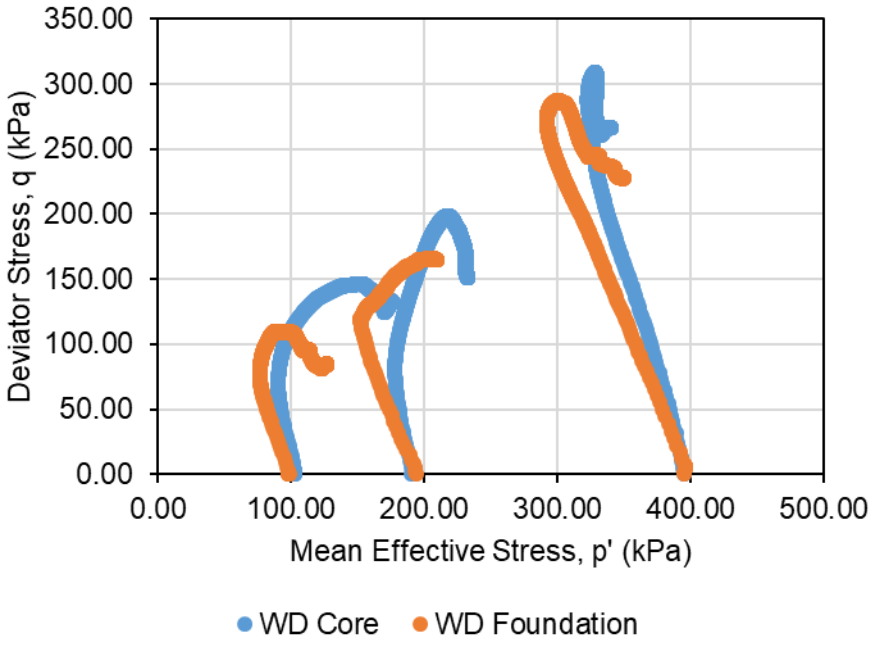

Figure A-C.28 Stress paths in p'-q space of WD CIU Triaxial Test samples

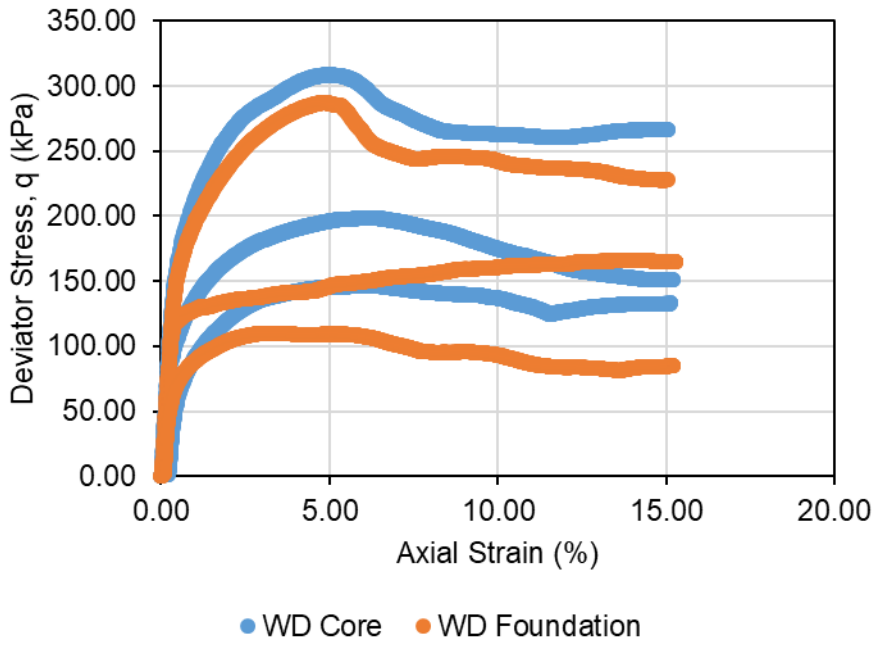

Figure A-C.29 Stress-strain behaviour of WD CIU Triaxial Test samples

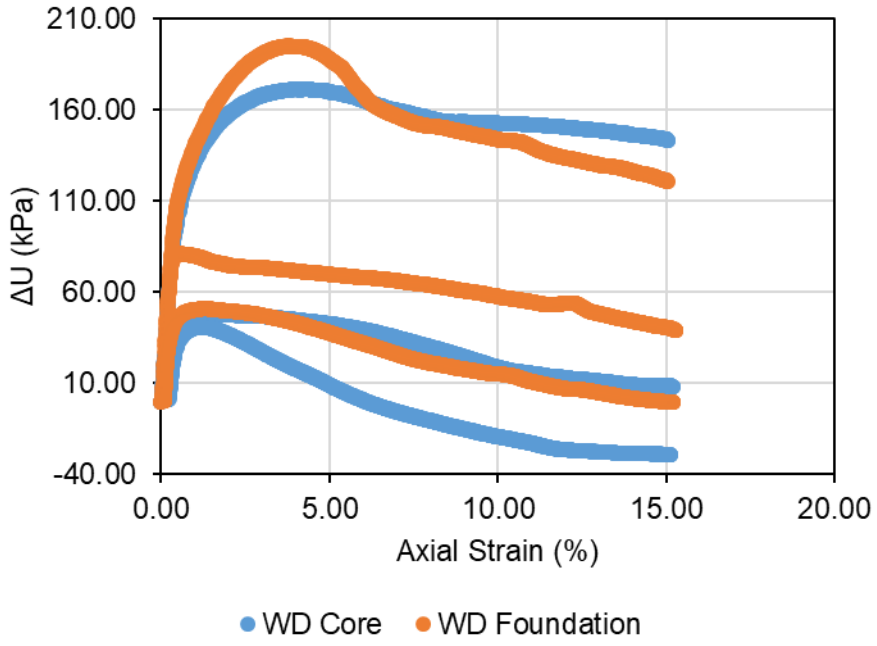

Figure A-C.30 Pore water measurements of WD CIU Triaxial Test sample

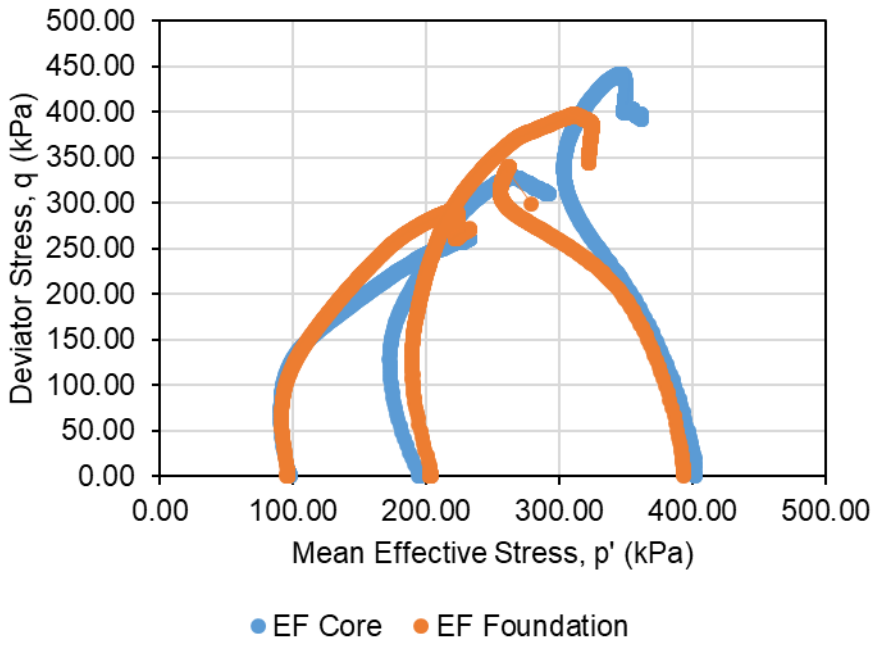

Figure A-C.31 Stress paths in p'-q space of EF CIU Triaxial Test samples

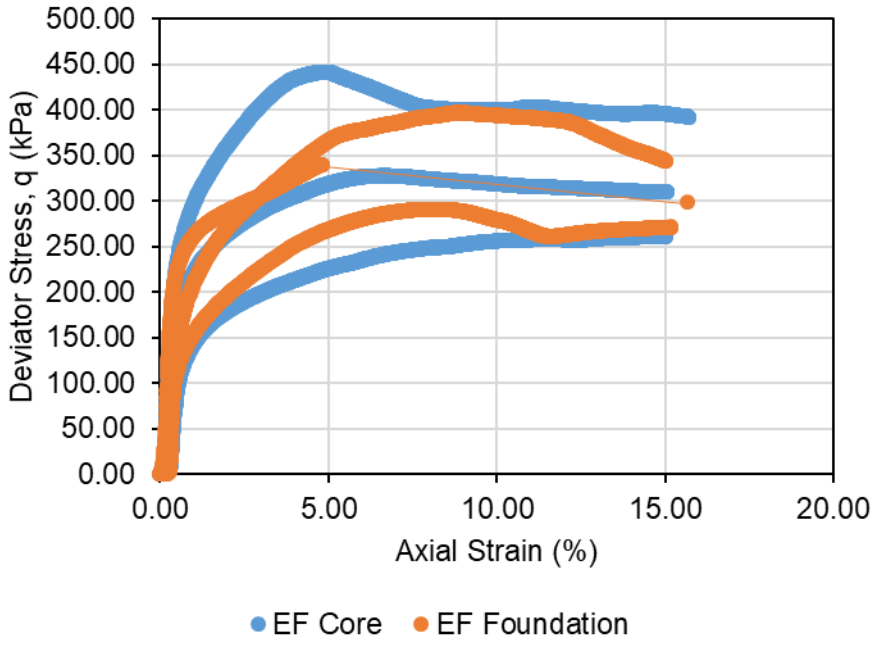

Figure A-C.32 Stress-strain behaviour of EF CIU Triaxial Test samples

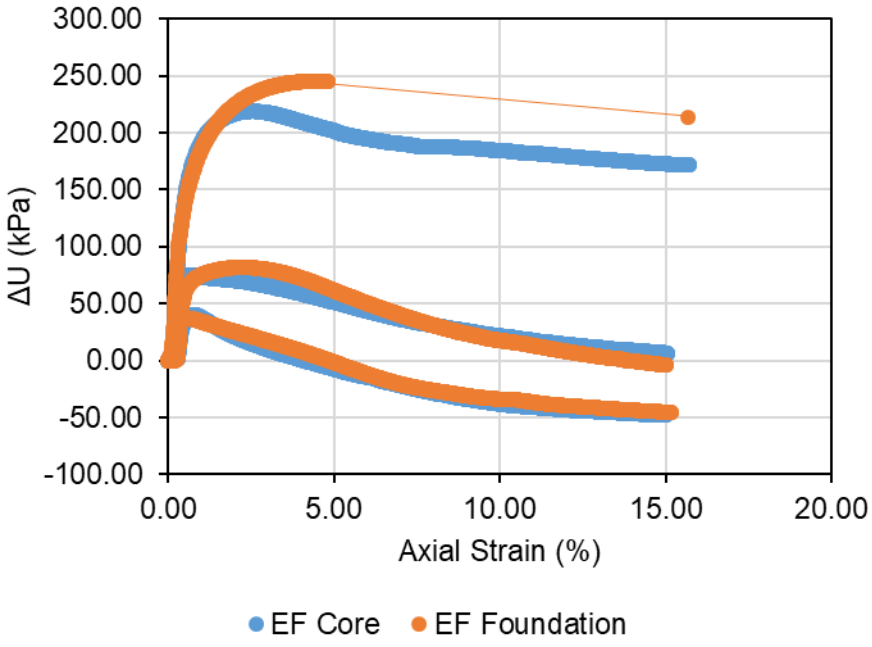

Figure A-C.33 Pore water measurements of EF CIU Triaxial Test sample

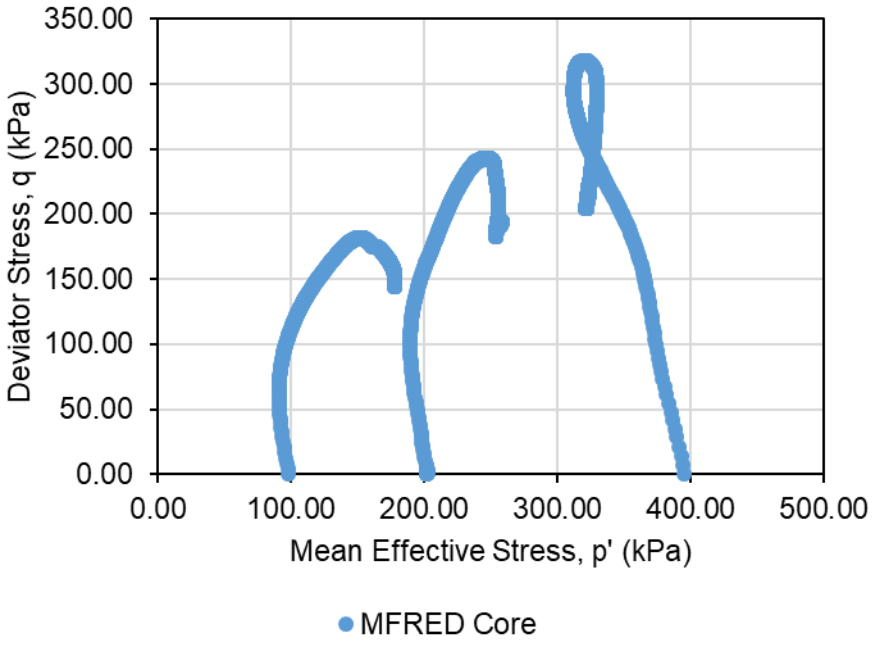

Figure A-C.34 Stress paths in p’-q space of MFRED CIU Triaxial Test samples

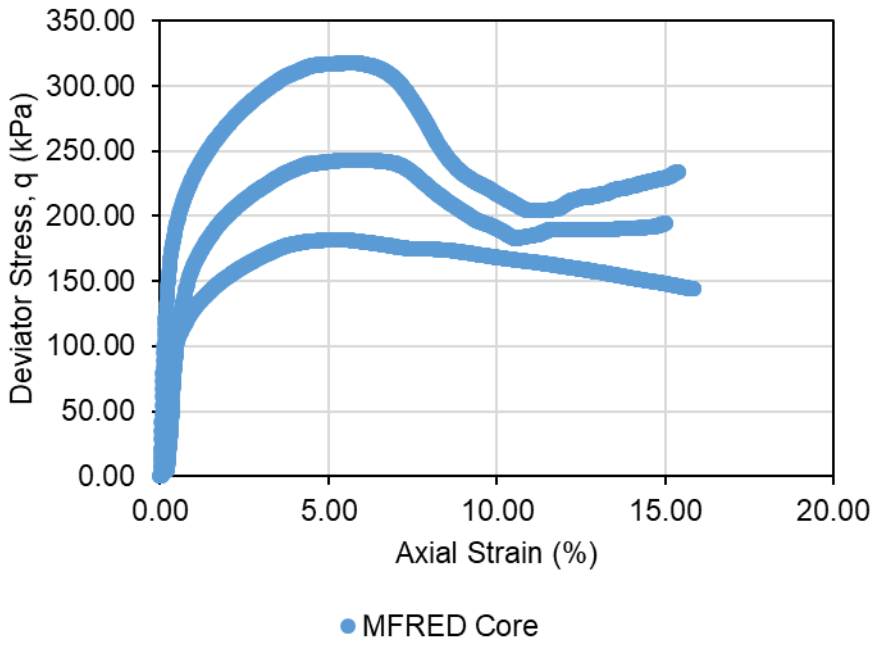

Figure A-C.35 Stress-strain behaviour of MFRED CIU Triaxial Test samples

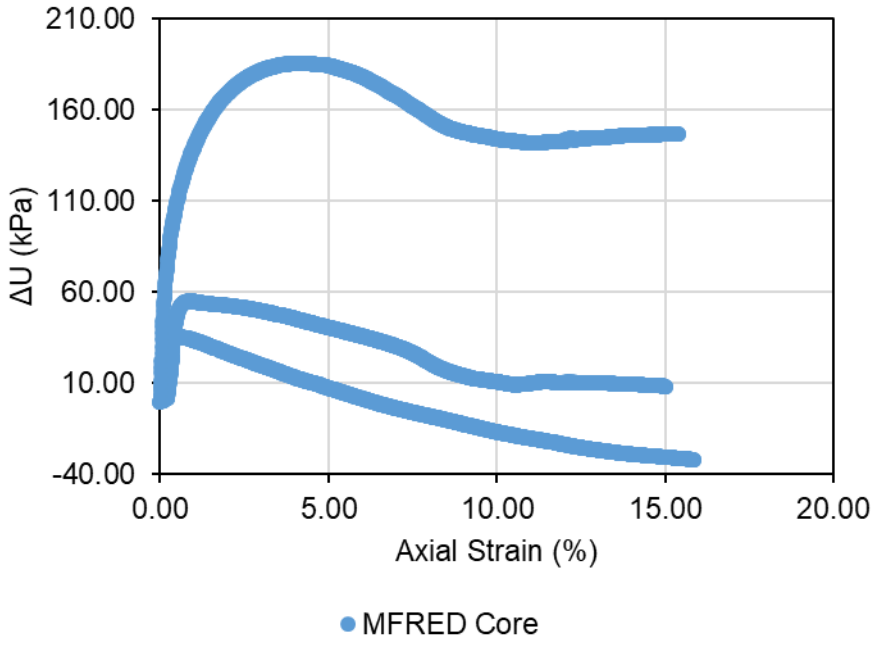

Figure A-C.36 Pore water measurements of MFRED CIU Triaxial Test sample

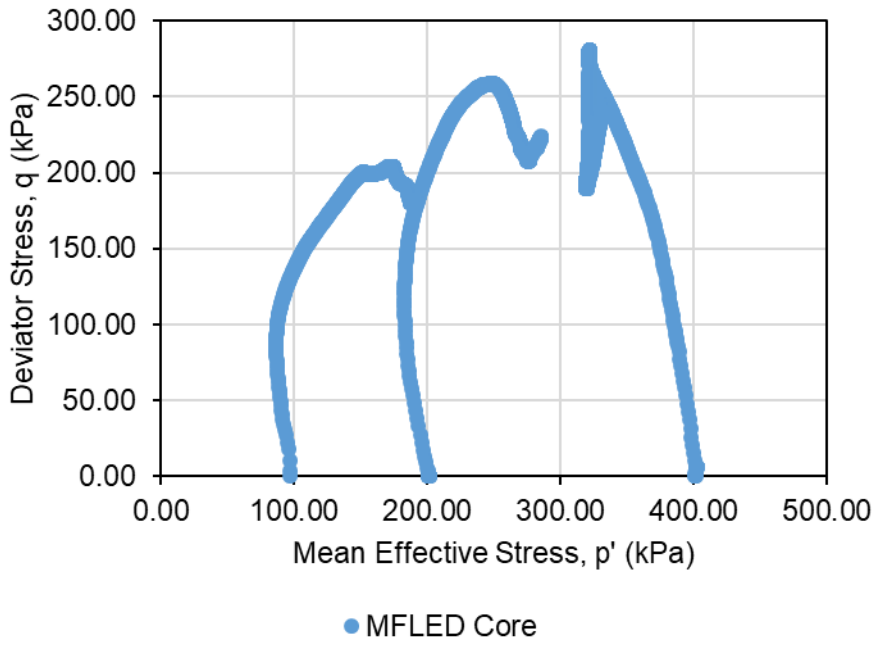

Figure A-C.37 Stress paths in p'-q space of MFLED CIU Triaxial Test samples

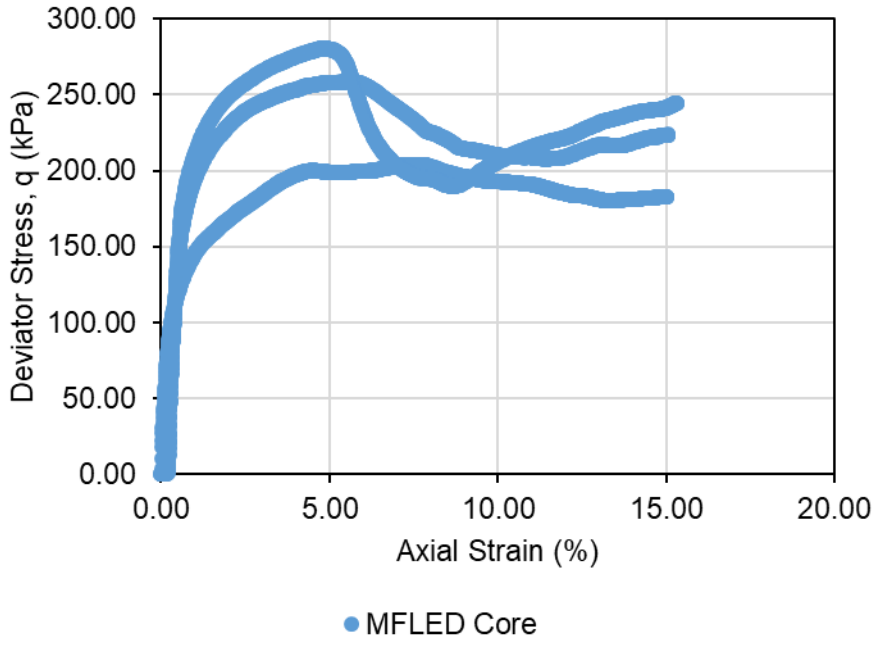

Figure A-C.38 Stress-strain behaviour of MFLED CIU Triaxial Test samples

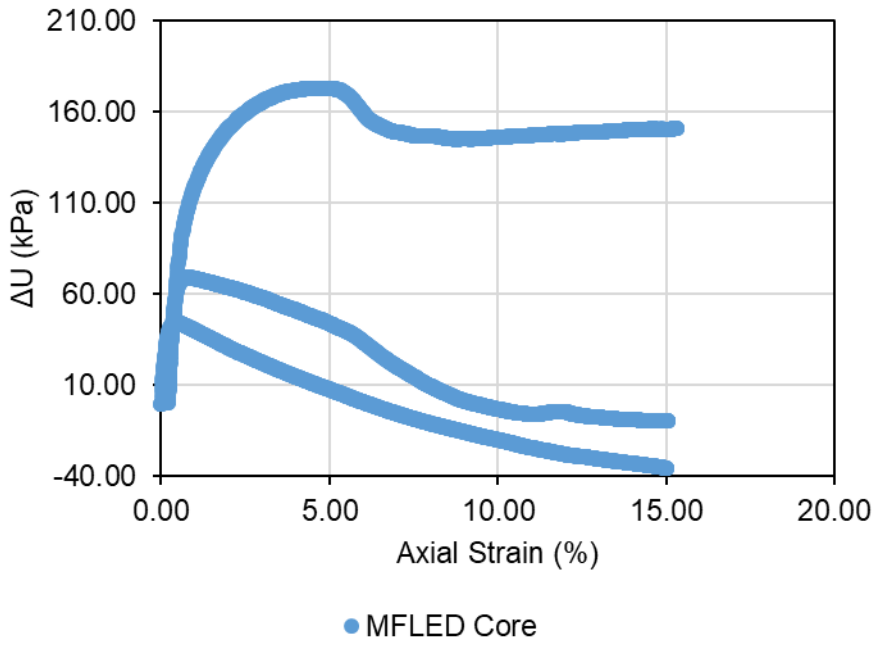

Figure A-C.39 Pore water measurements of MFLED CIU Triaxial Test sample

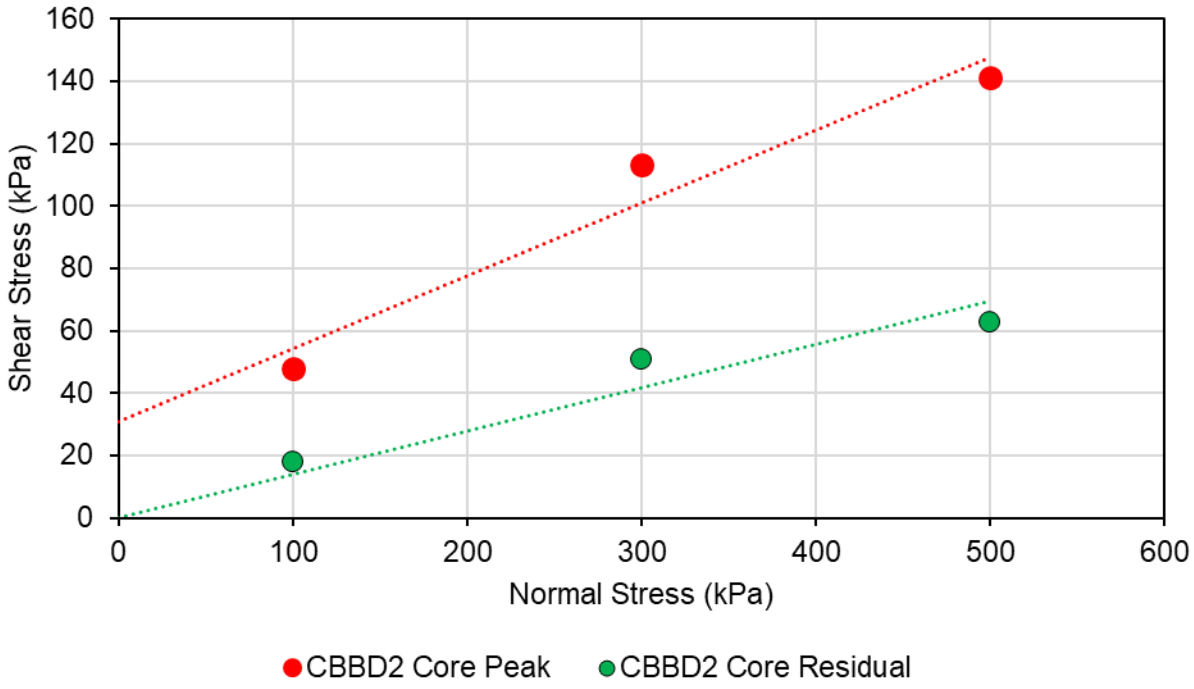

Figure A-C.40 Peak and residual effective shear strengths of CBBD2 core samples from Direct Shear Tests

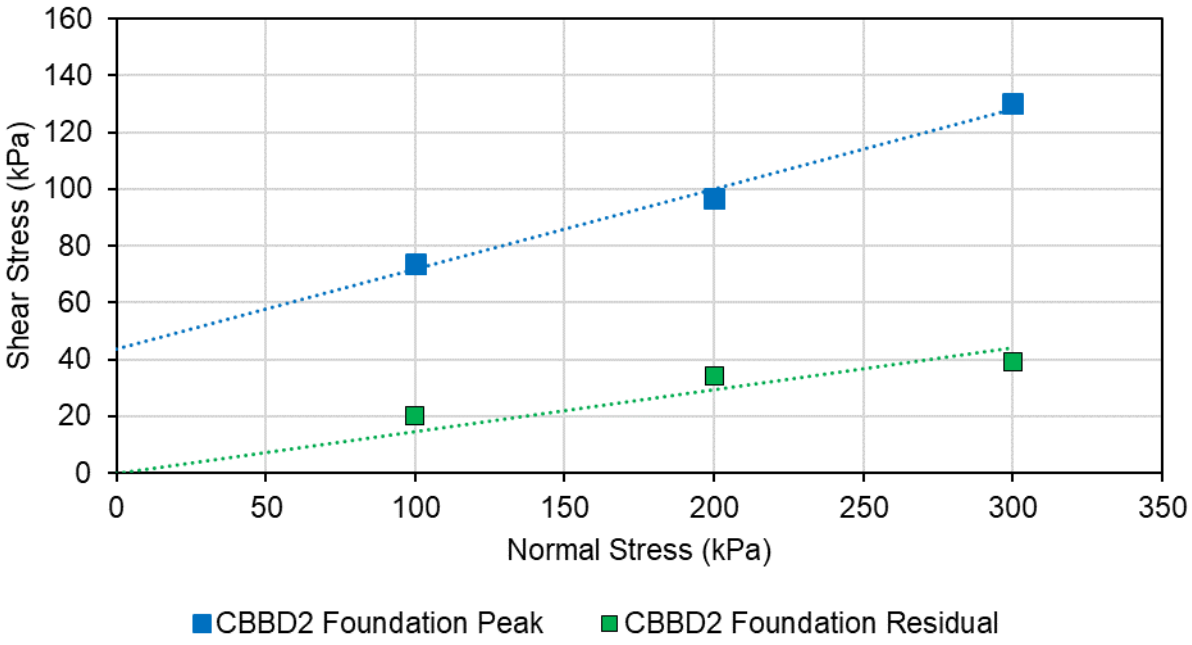

Figure A-C.41 Peak and residual effective shear strengths of CBBD2 foundation samples from Direct Shear Tests

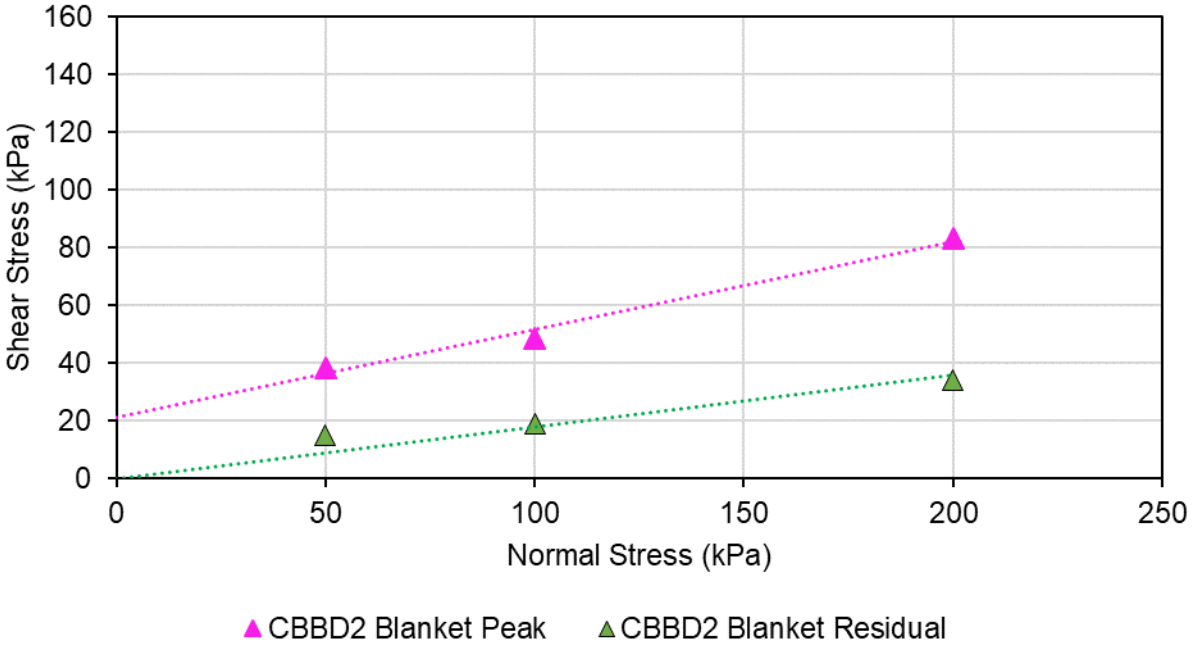

Figure A-C.42 Peak and residual effective shear strengths of CBBD2 blanket samples from Direct Shear Tests

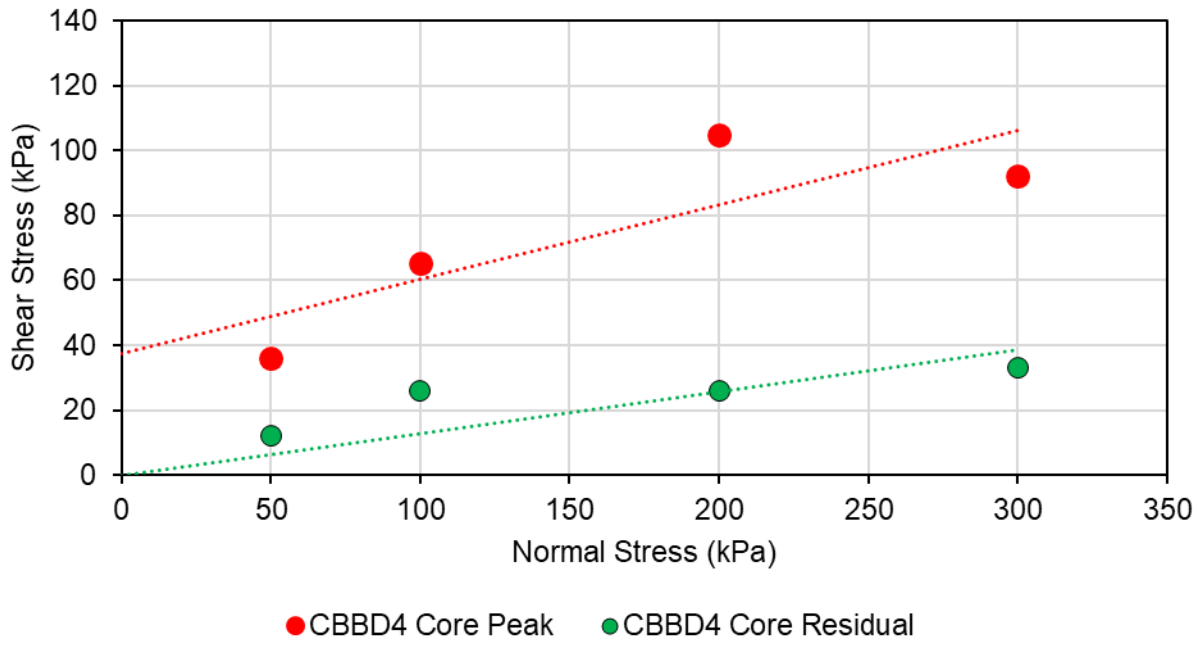

Figure A-C.43 Peak and residual effective shear strengths of CBBD4 core samples from Direct Shear Tests

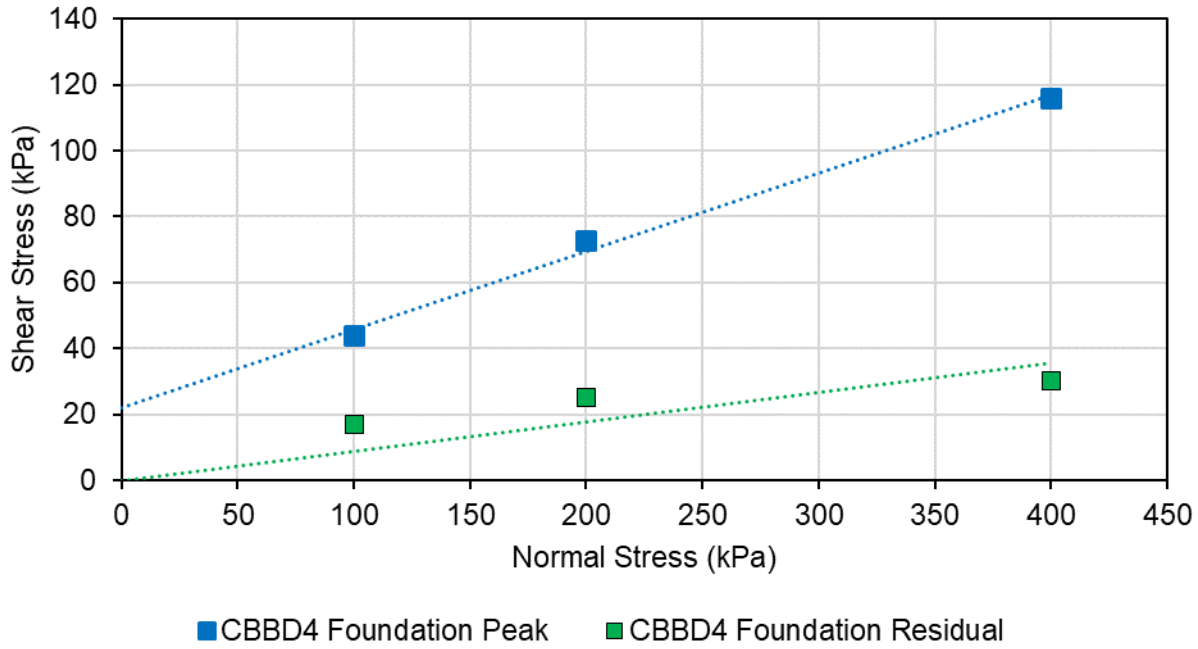

Figure A-C.44 Peak and residual effective shear strengths of CBBD4 foundation samples from Direct Shear Tests

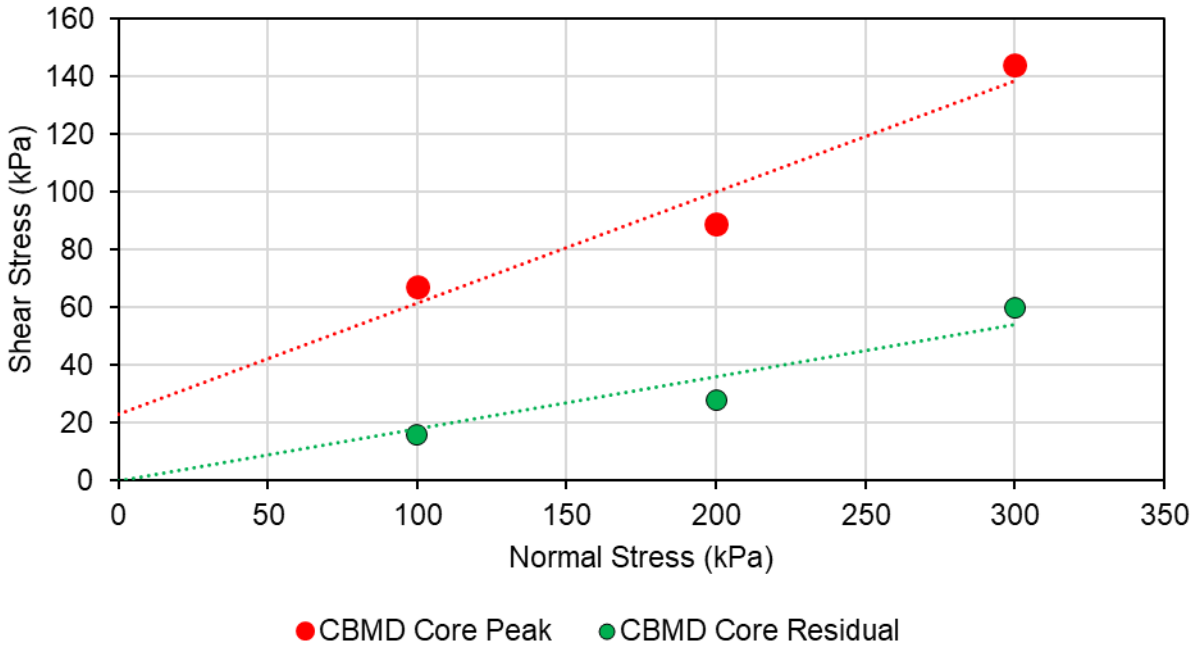

Figure A-C.45 Peak and residual effective shear strengths of CBMD core samples from Direct Shear Tests

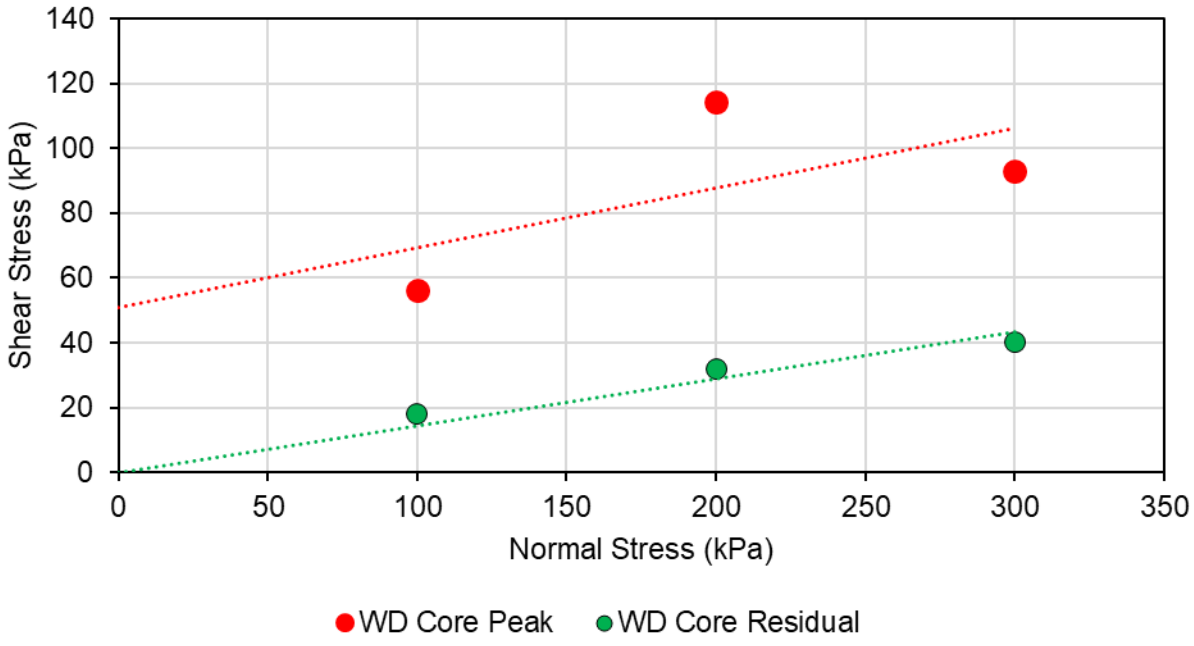

Figure A-C.46 Peak and residual effective shear strengths of WD core samples from Direct Shear Tests

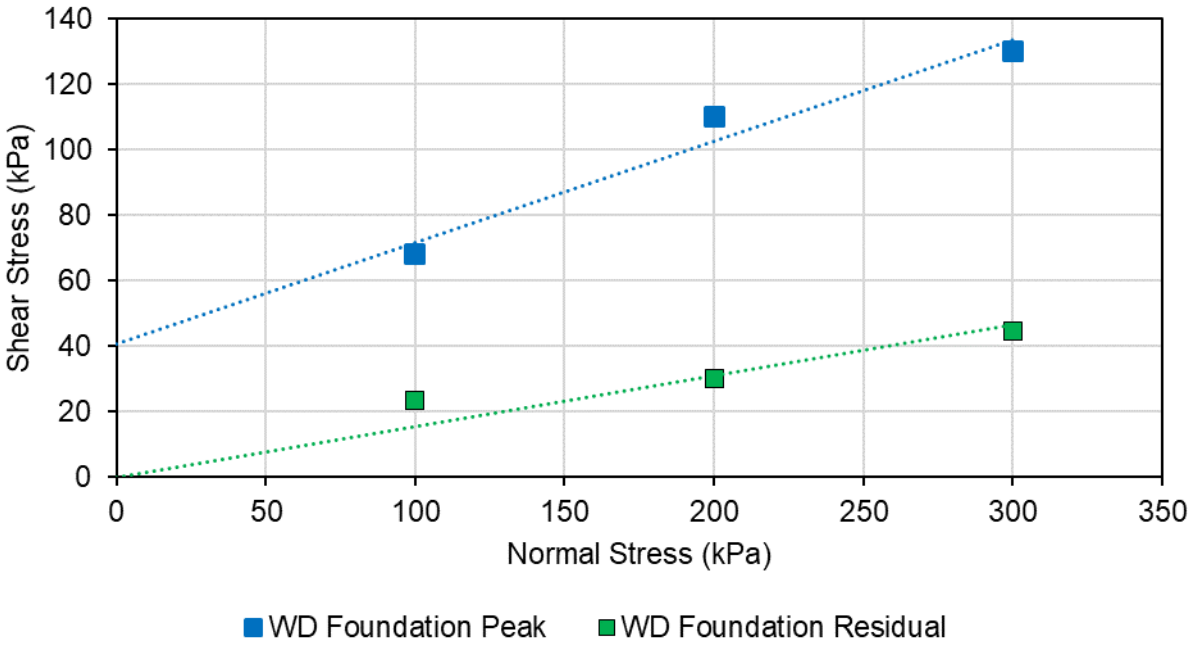

Figure A-C.47 Peak and residual effective shear strengths of WD foundation samples from Direct Shear Tests

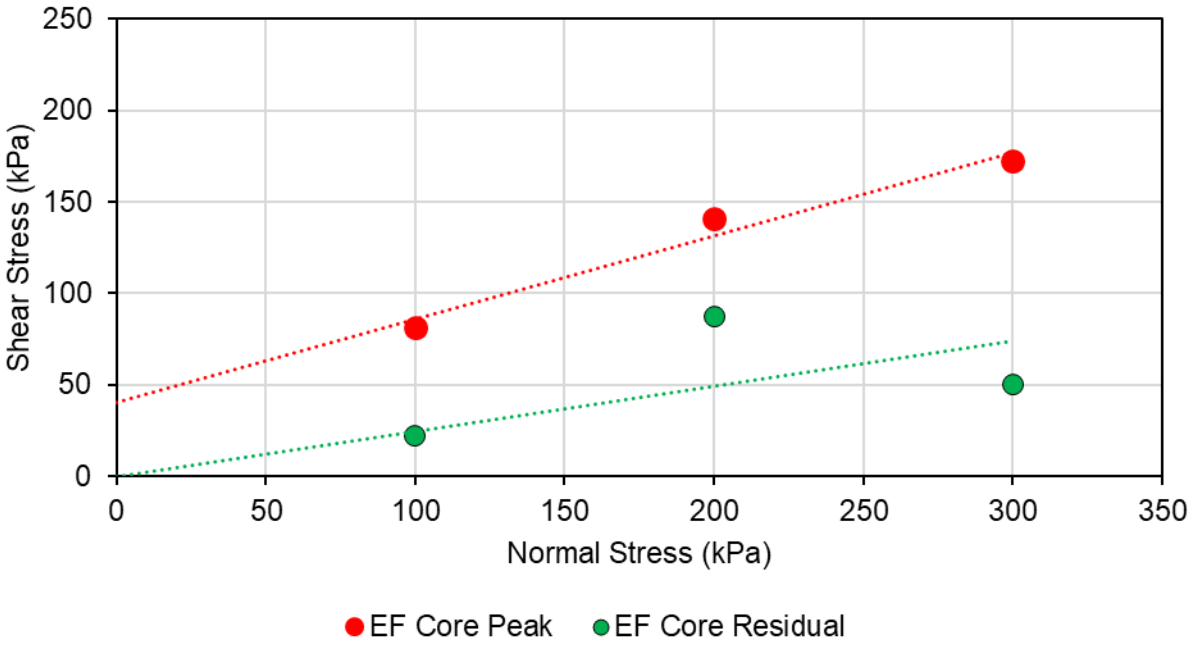

Figure A-C.48 Peak and residual effective shear strengths of EF core samples from Direct Shear Tests

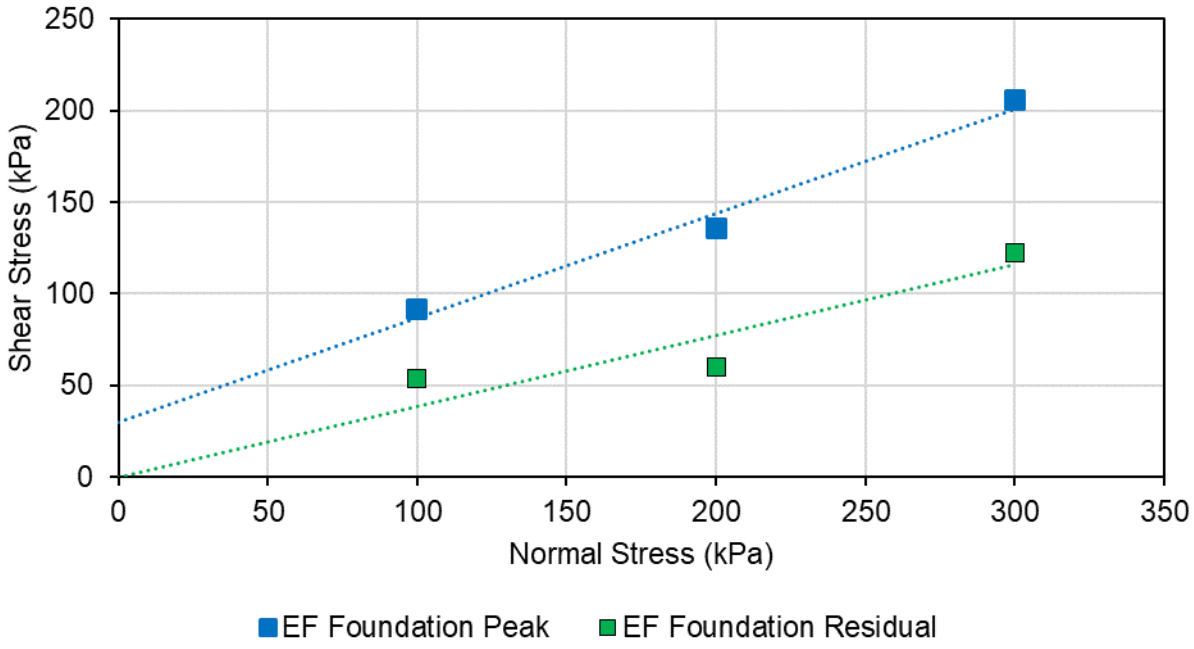

Figure A-C.49 Peak and residual effective shear strengths of EF foundation samples from Direct Shear Tests

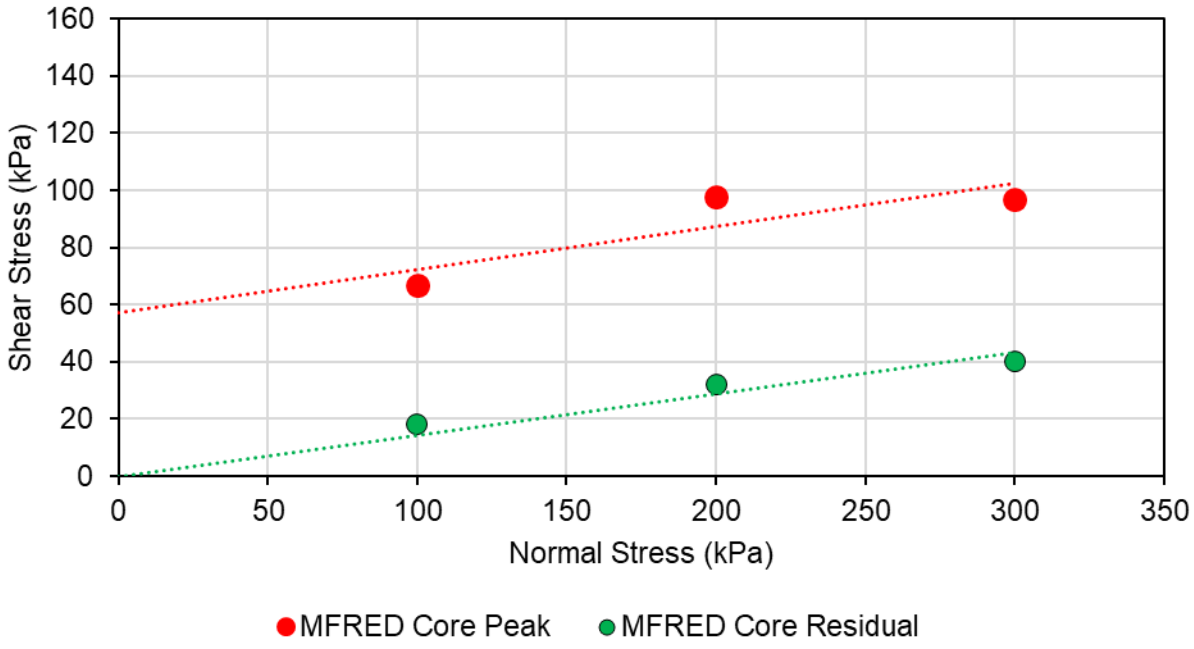

Figure A-C.50 Peak and residual effective shear strengths of MFRED core samples from Direct Shear Tests

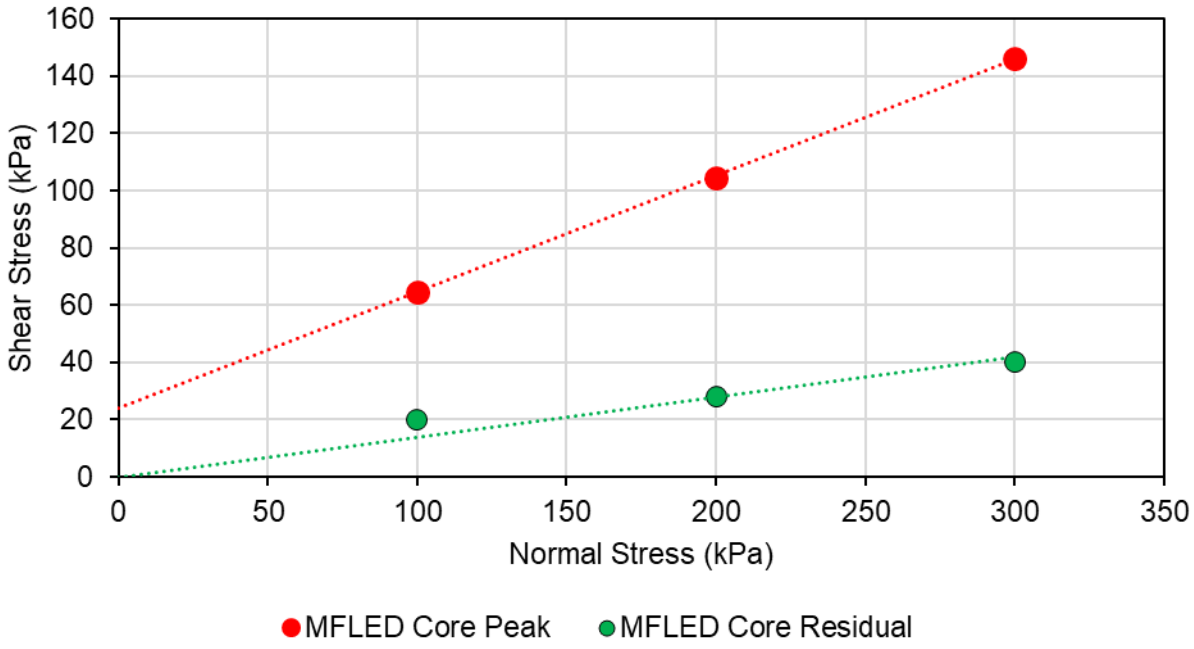

Figure A-C.51 Peak and residual effective shear strengths of MFLED core samples from Direct Shear Tests

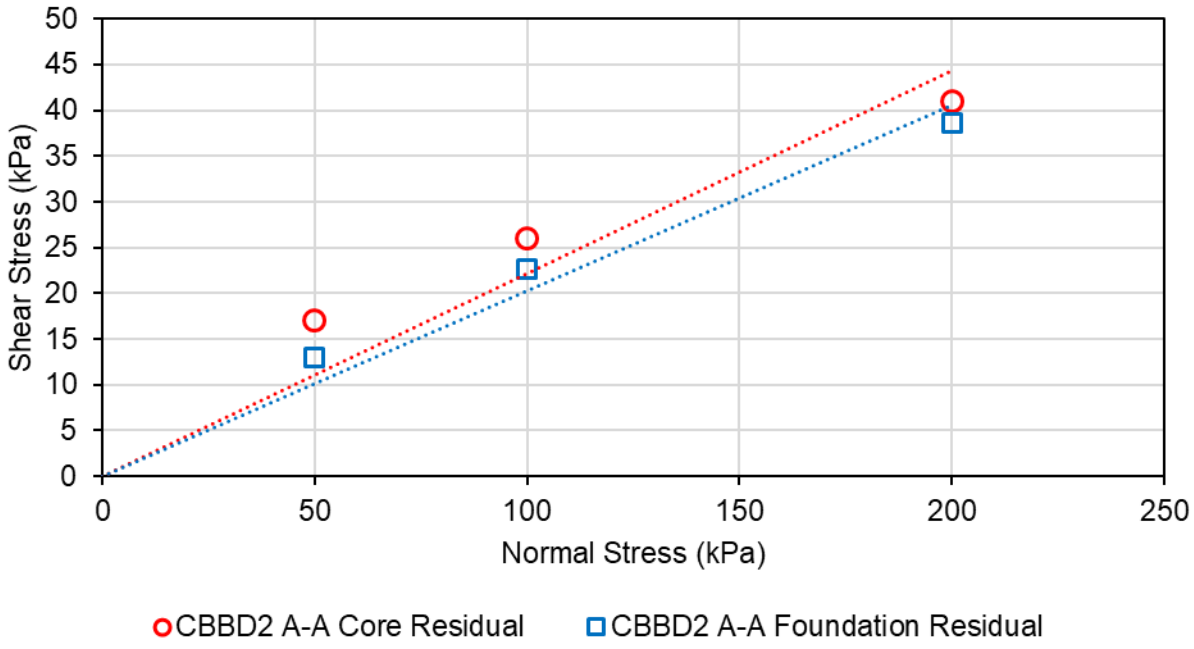

Figure A-C.52 Residual effective shear strengths of CBBD2 Section A-A samples from Torsional Ring Shear Tests

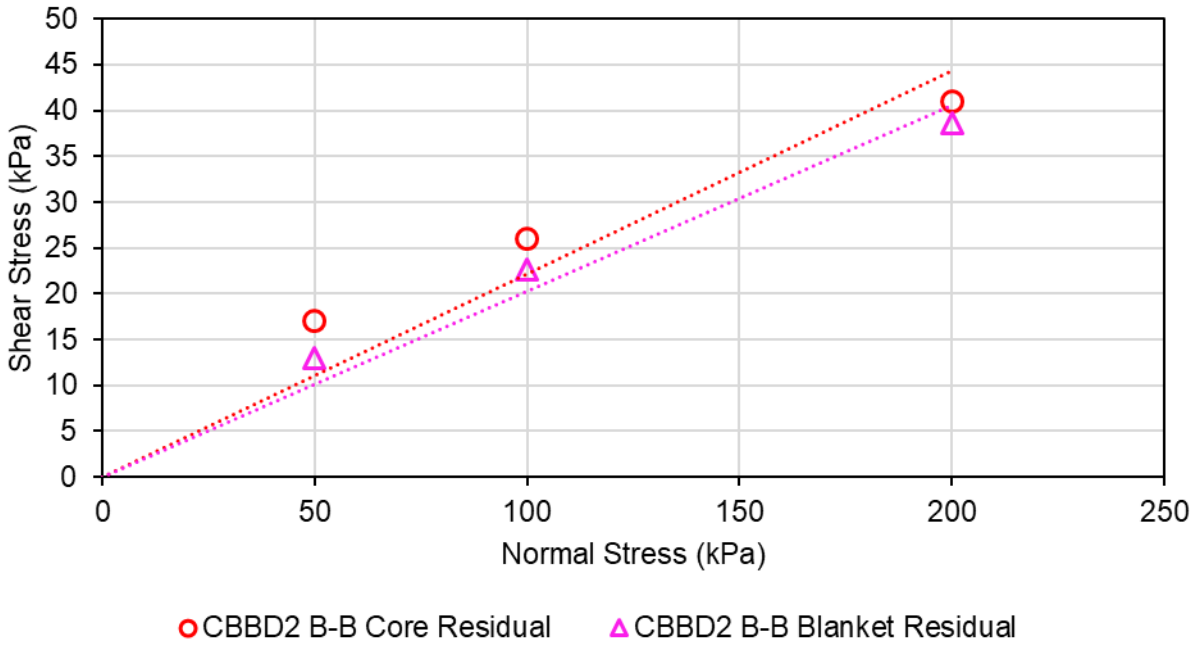

Figure A-C.53 Residual effective shear strengths of CBBD2 Section B-B samples from Torsional Ring Shear Tests

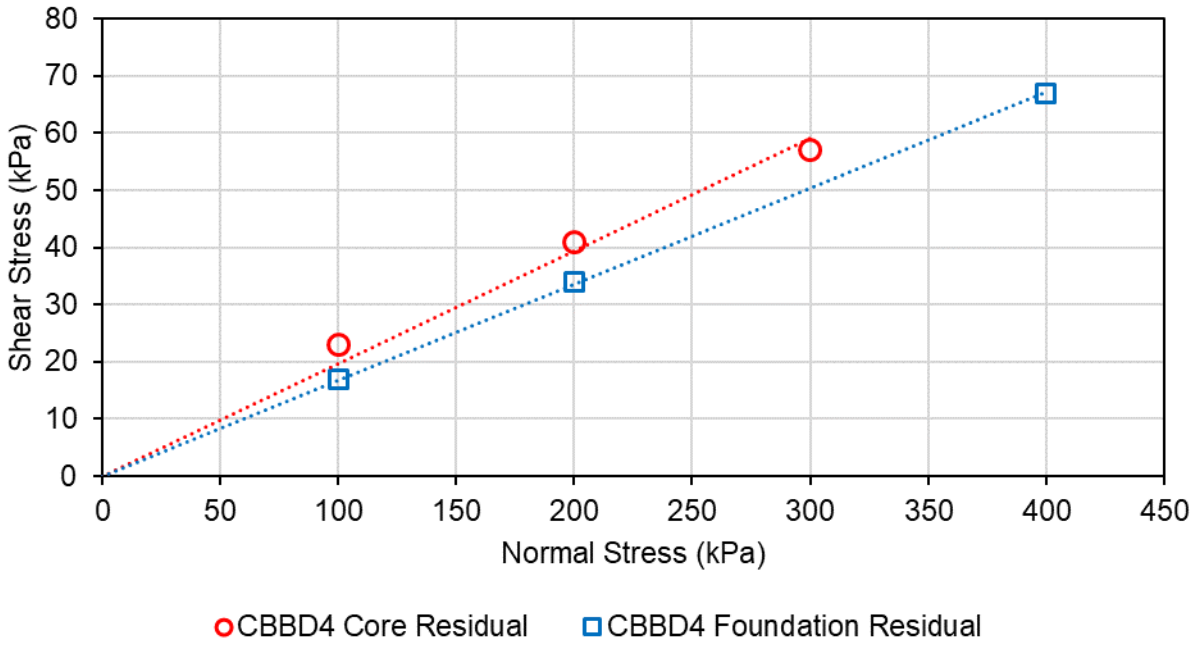

Figure A-C.54 Residual effective shear strengths of CBBD4 samples from Torsional Ring Shear Tests

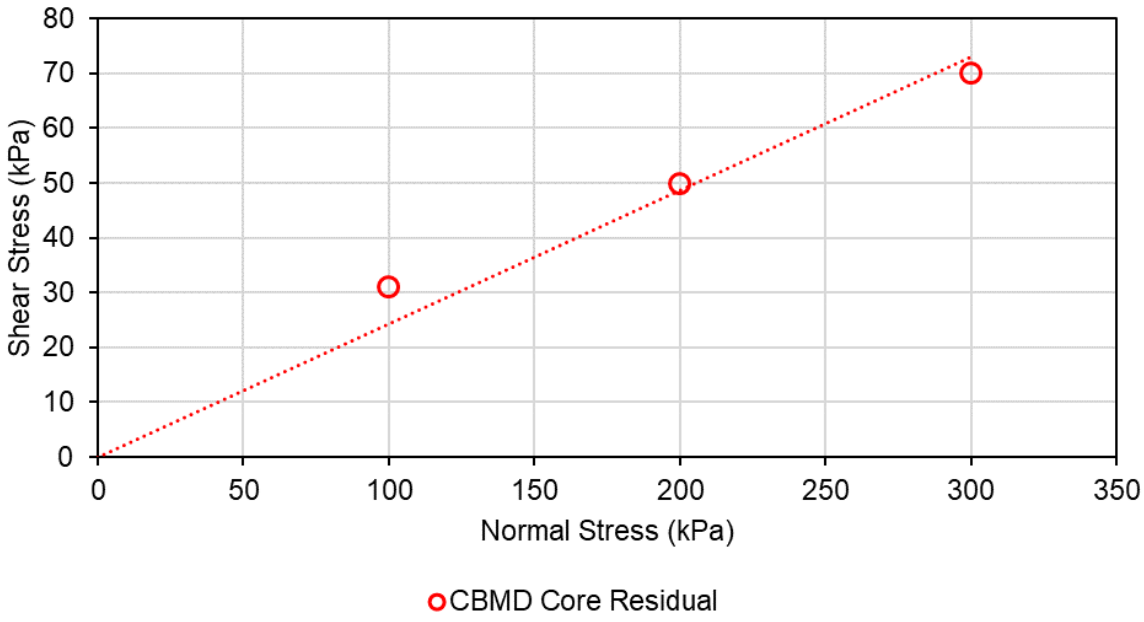

Figure A-C.55 Residual effective shear strengths of CBMD samples from Torsional Ring Shear Tests

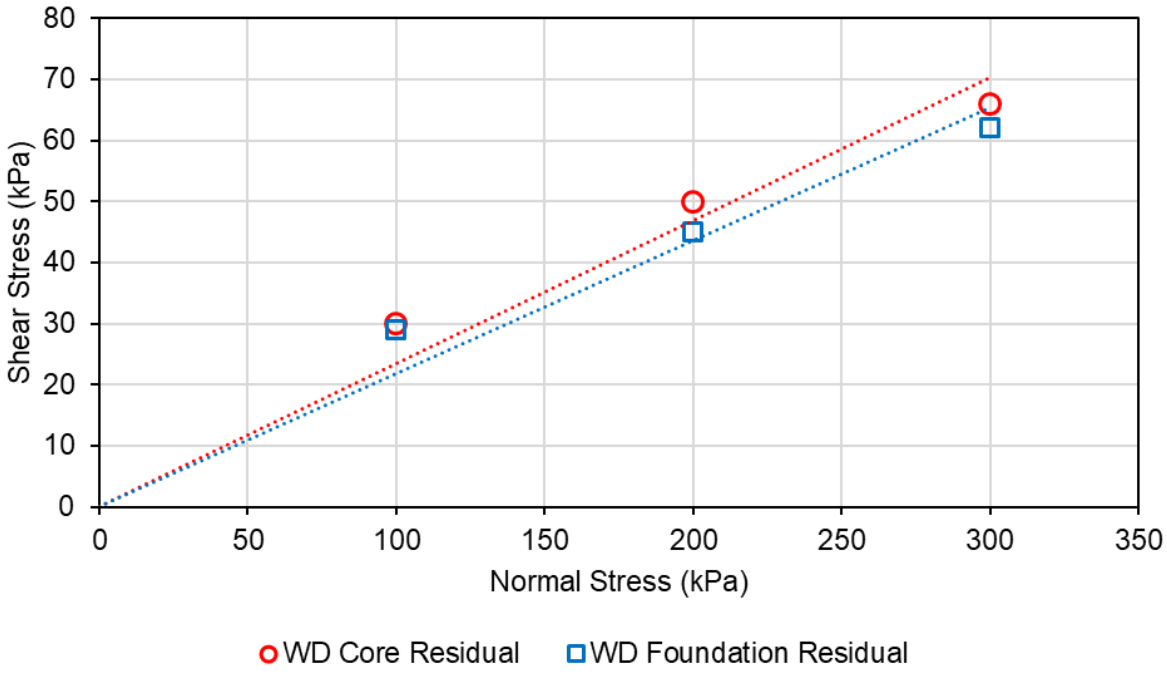

Figure A-C.56 Residual effective shear strengths of WD samples from Torsional Ring Shear Tests

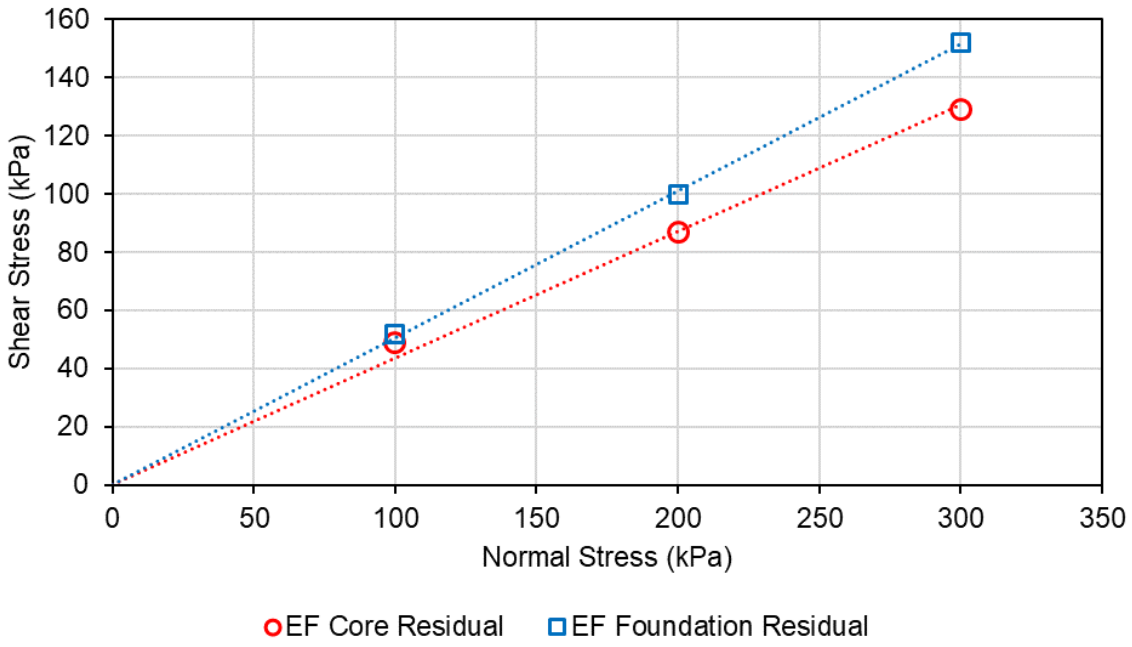

Figure A-C.57 Residual effective shear strengths of EF samples from Torsional Ring Shear Tests

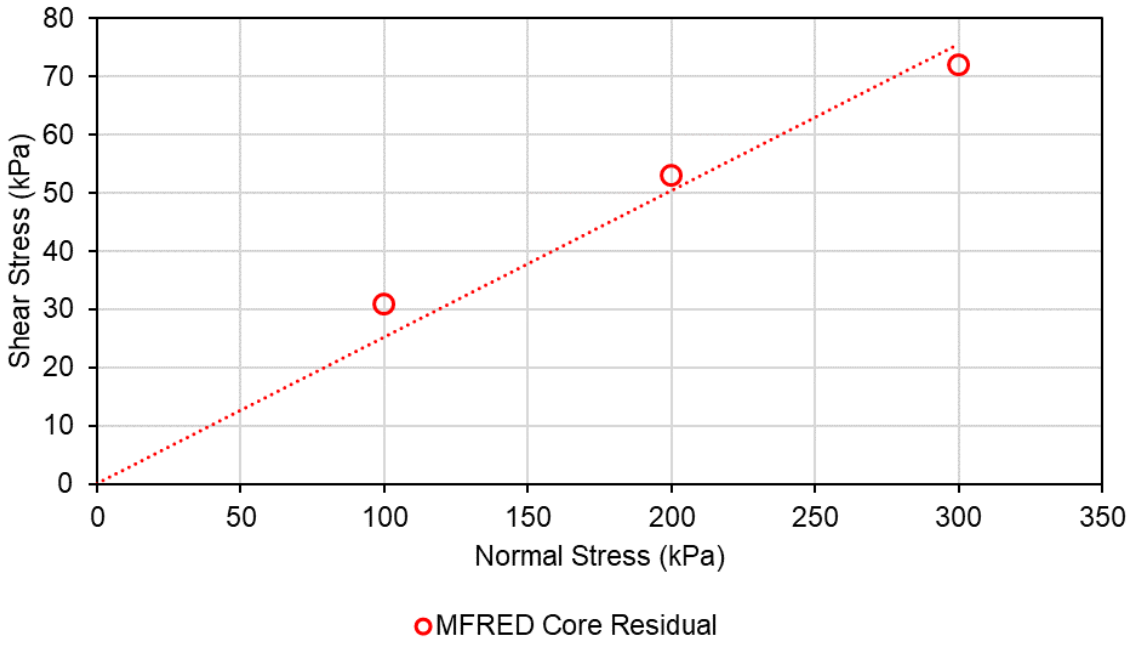

Figure A-C.58 Residual effective shear strengths of MFRED samples from Torsional Ring Shear Tests

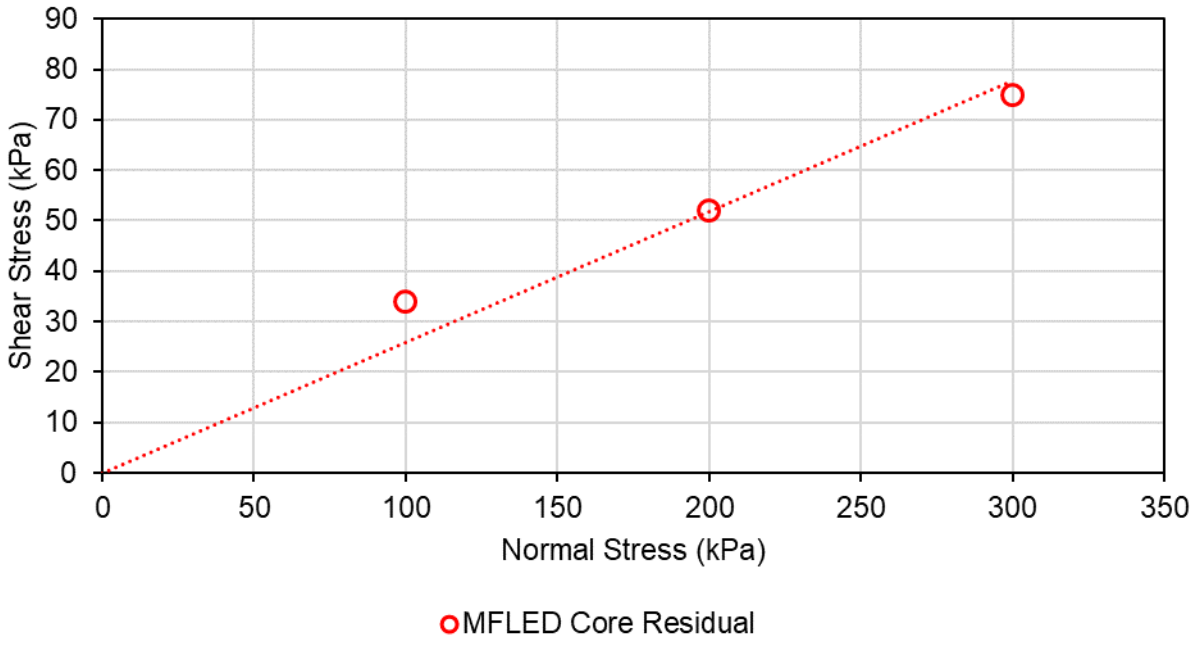

Figure A-C.59 Residual effective shear strengths of MFLED samples from Torsional Ring Shear Tests

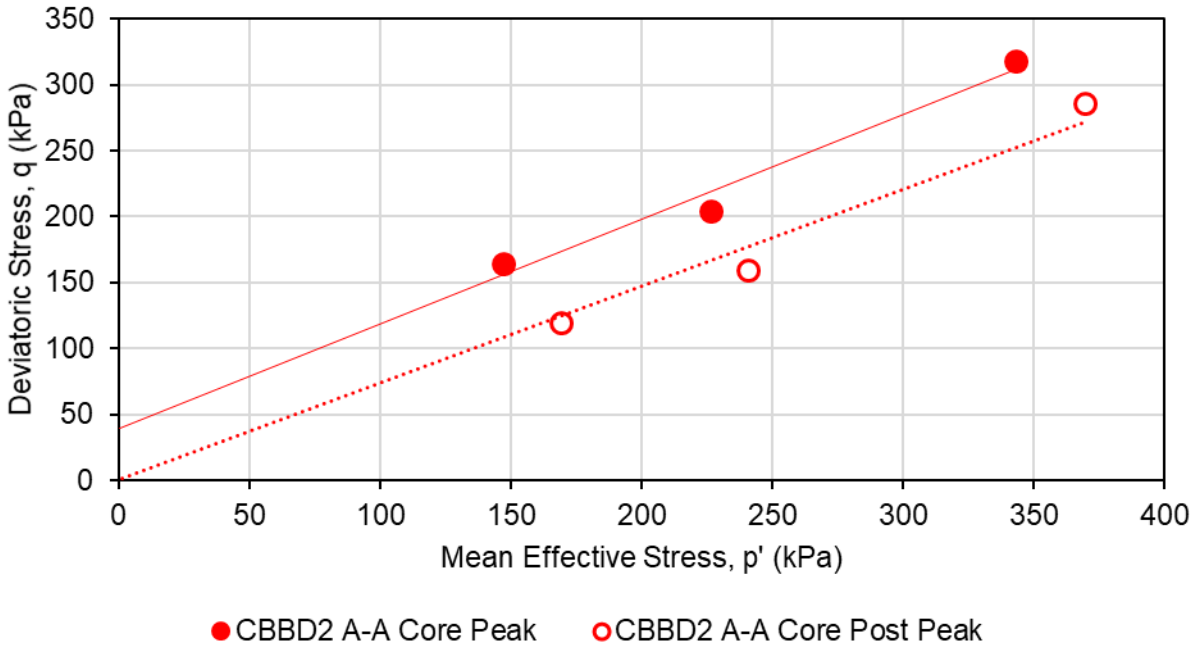

Figure A-C.60 Peak and post peak effective shear strengths of CBBD2 Section A-A core samples from CIU Triaxial Tests

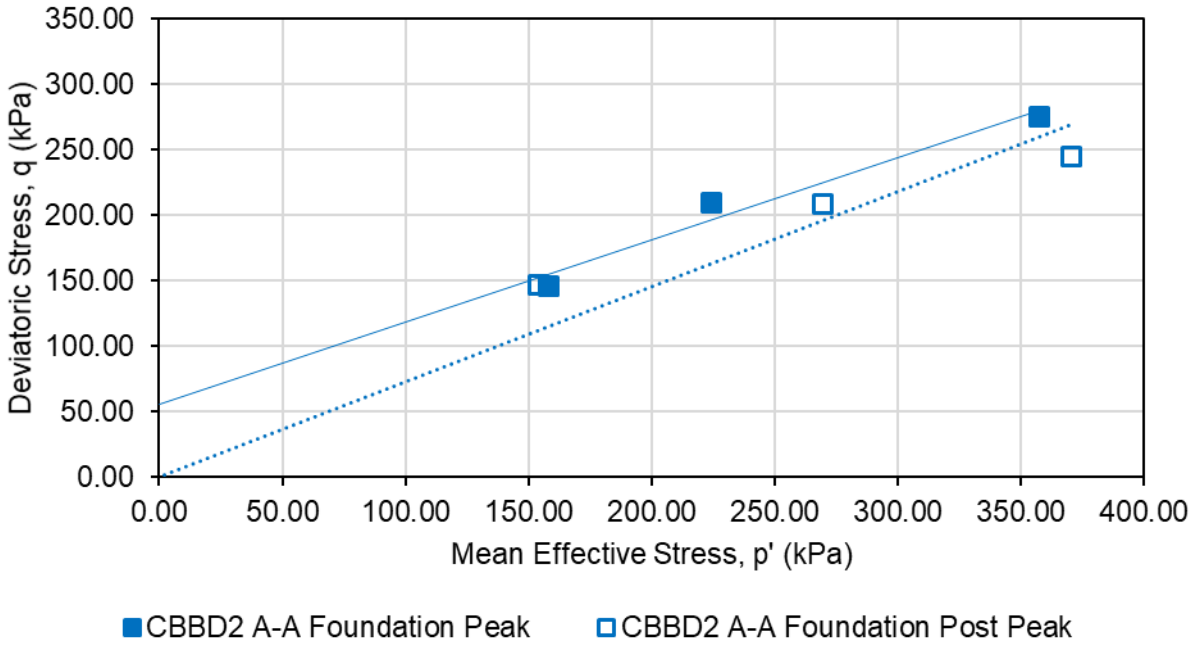

Figure A-C.61 Peak and post peak effective shear strengths of CBBD2 Section A-A foundation samples from CIU Triaxial Tests

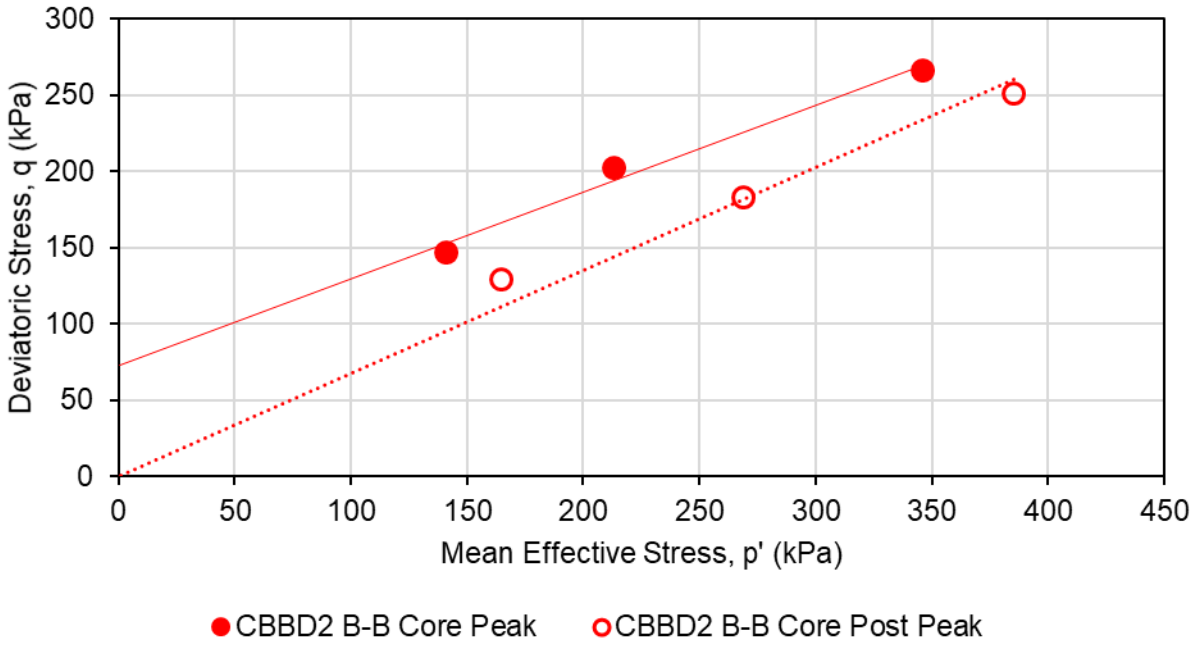

Figure A-C.62 Peak and post peak effective shear strengths of CBBD2 Section B-B core samples from CIU Triaxial Tests

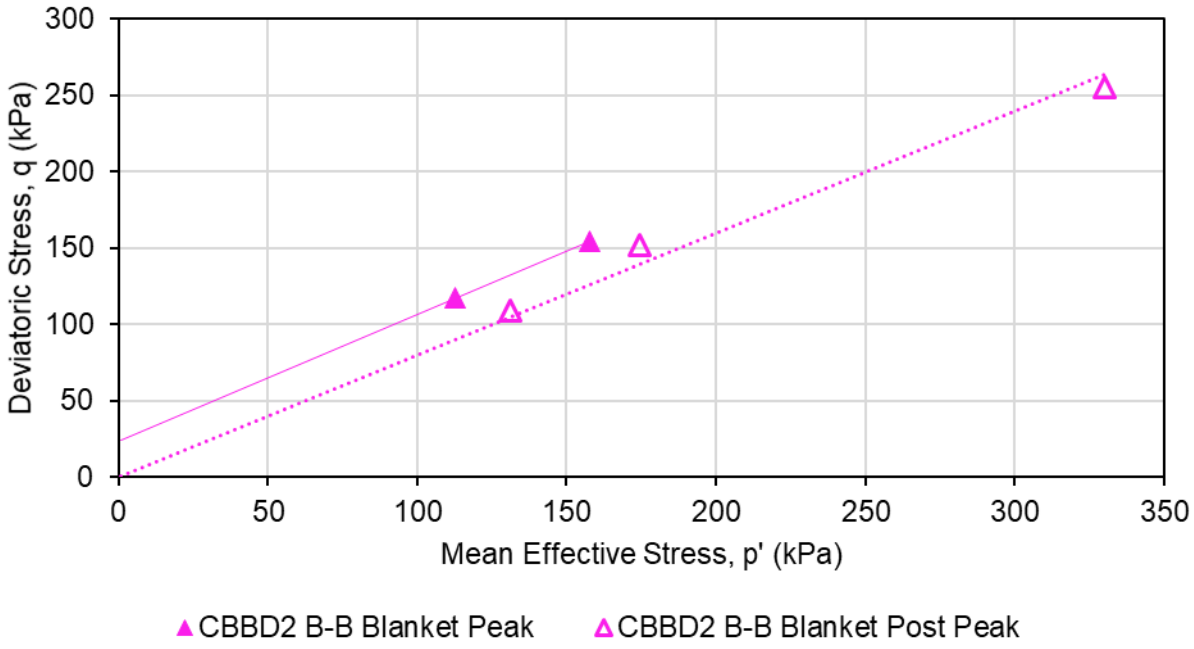

Figure A-C.63 Peak and post peak effective shear strengths of CBBD2 Section B-B clay blanket samples from CIU Triaxial Tests

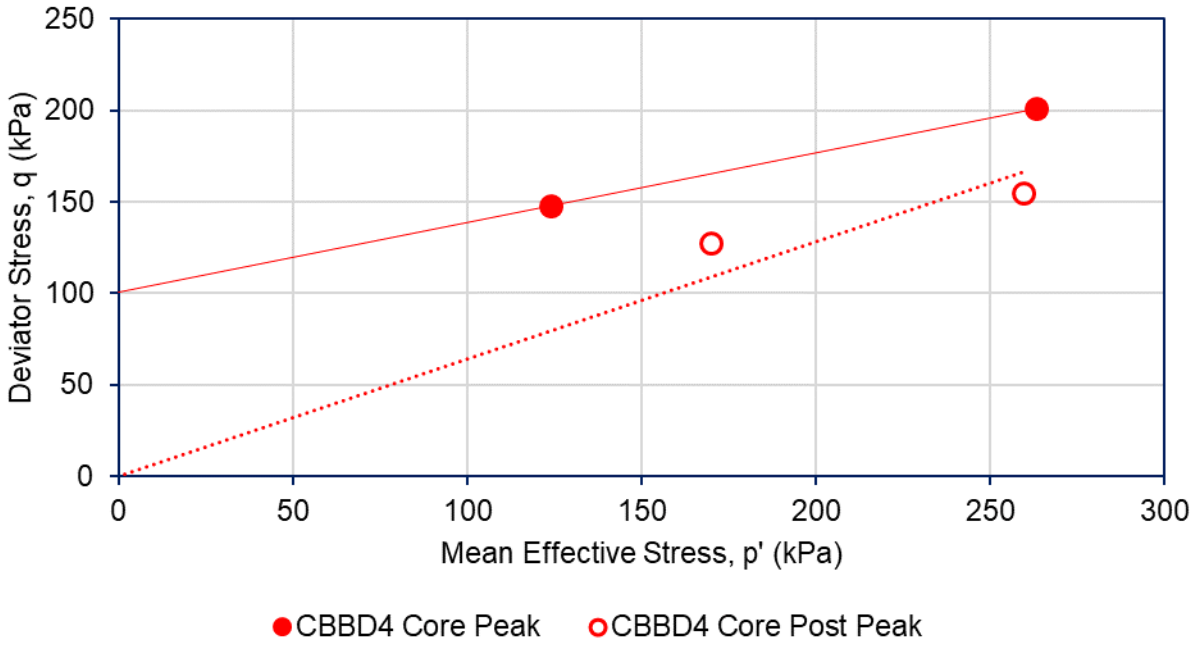

Figure A-C.64 Peak and post peak effective shear strengths of CBBD4 core samples from CIU Triaxial Tests

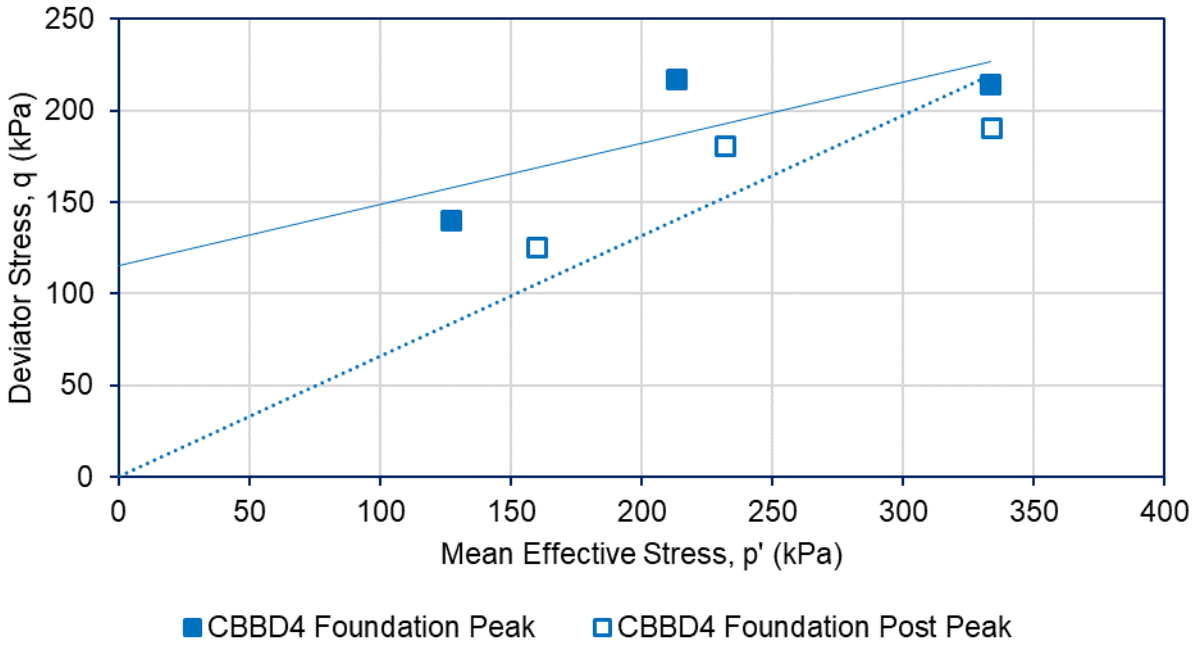

Figure A-C.65 Peak and post peak effective shear strengths of CBBD4 foundation samples from CIU Triaxial Tests

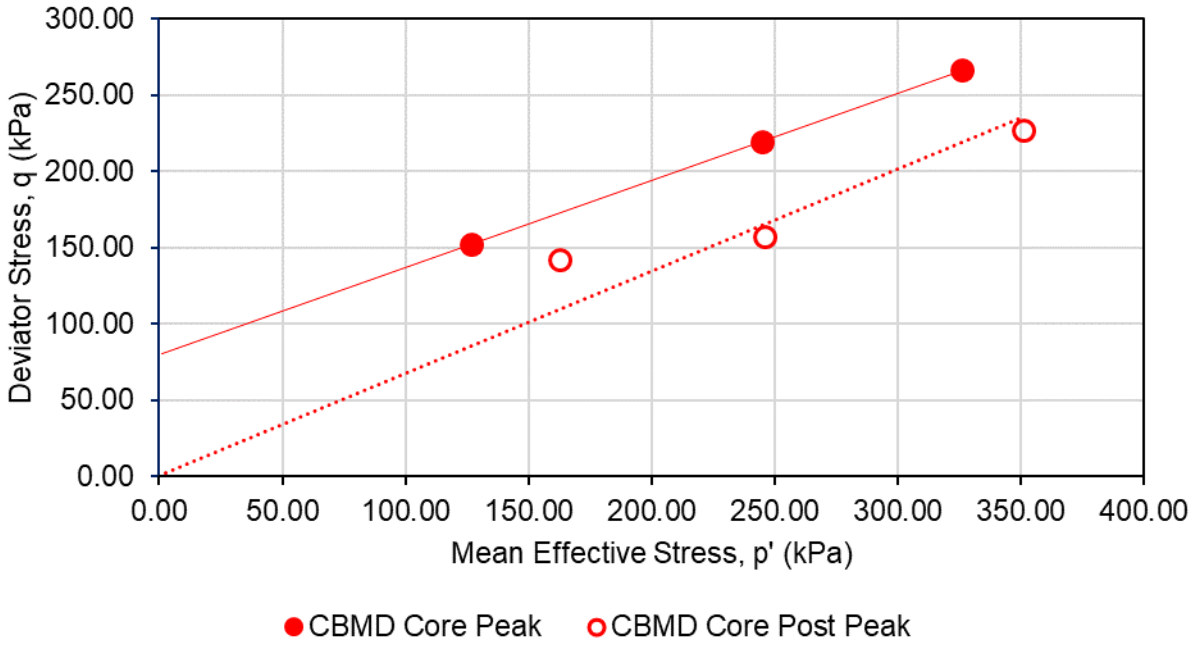

Figure A-C.66 Peak and post peak effective shear strengths of CBMD core samples from CIU Triaxial Tests

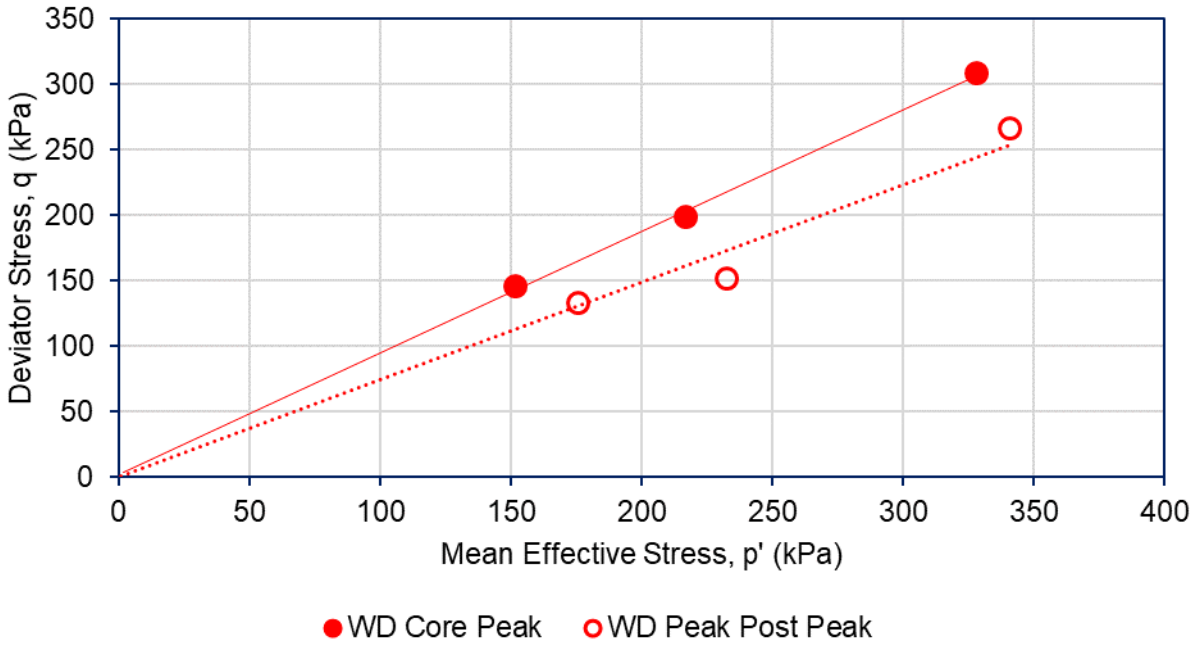

Figure A-C.67 Peak and post peak effective shear strengths of WD core samples from CIU Triaxial Tests

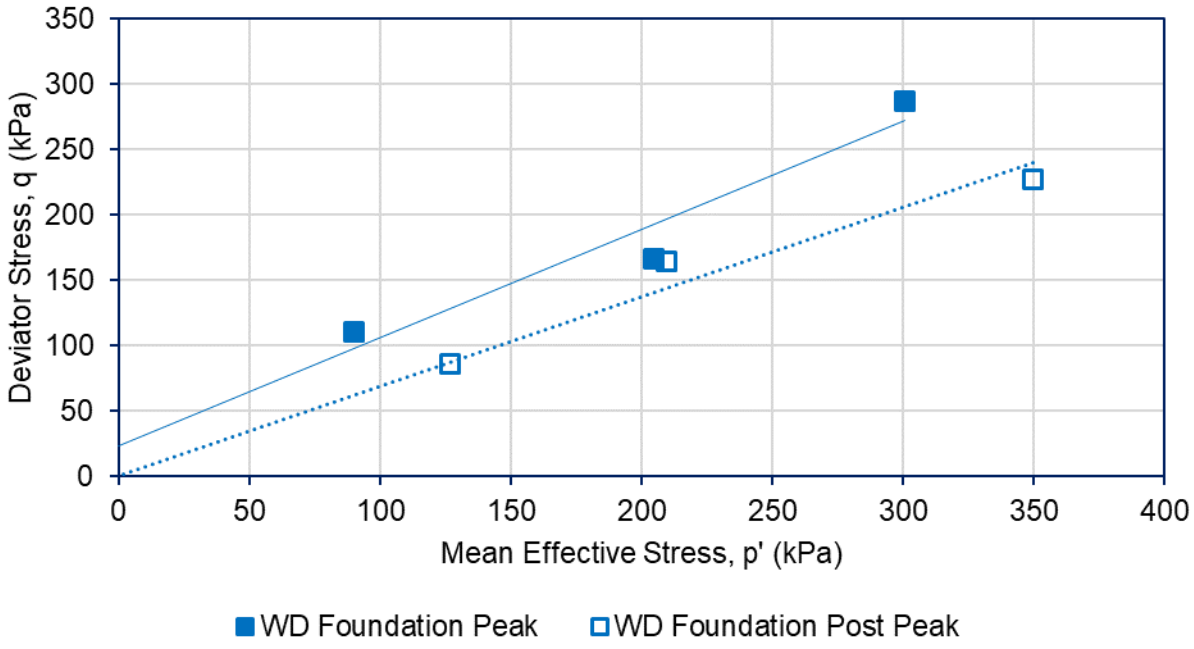

Figure A-C.68 Peak and post peak effective shear strengths of WD foundation samples from CIU Triaxial Tests

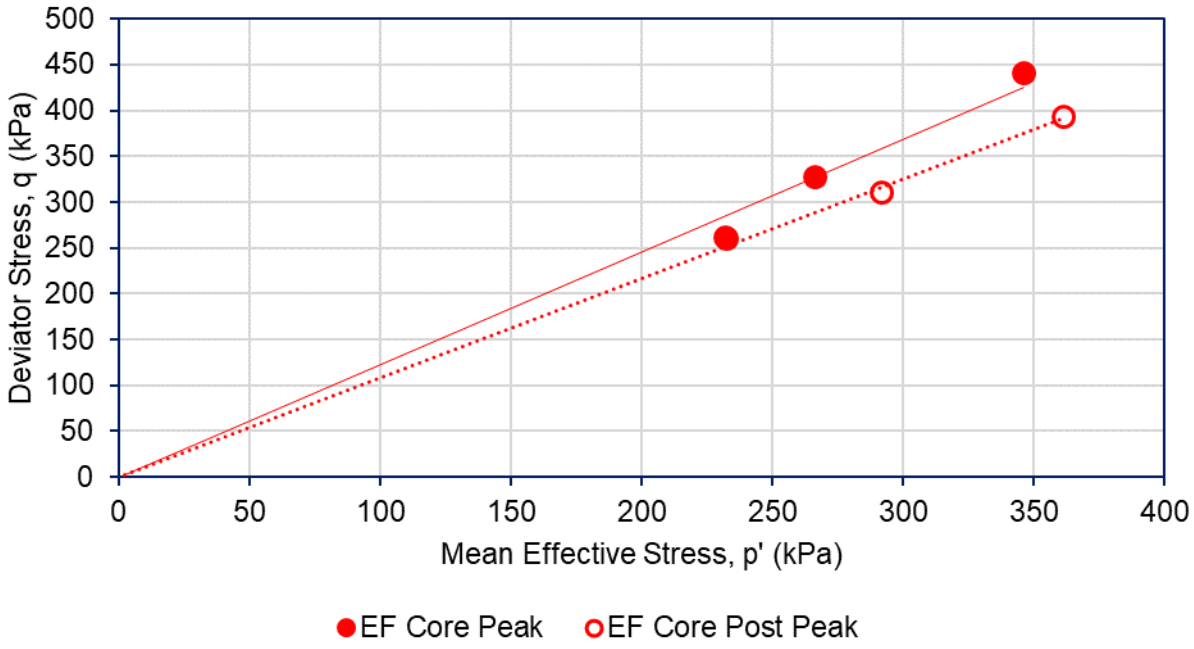

Figure A-C.69 Peak and post peak effective shear strengths of EF core samples from CIU Triaxial Tests

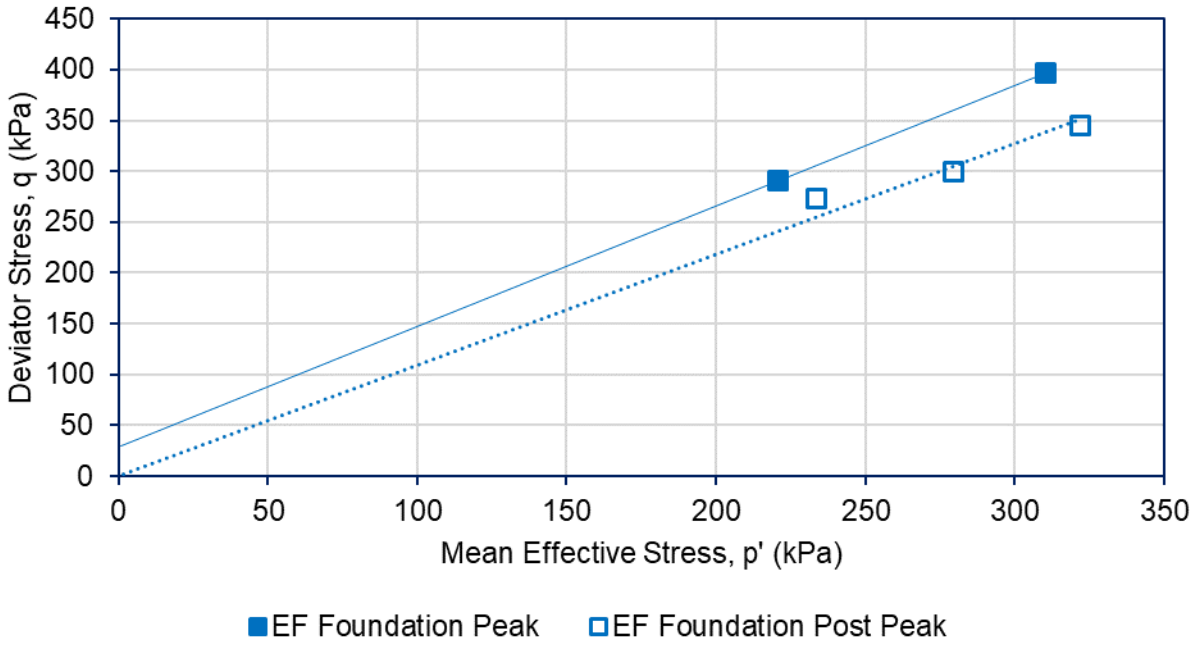

Figure A-C.70 Peak and post peak effective shear strengths of EF foundation samples from CIU Triaxial Tests

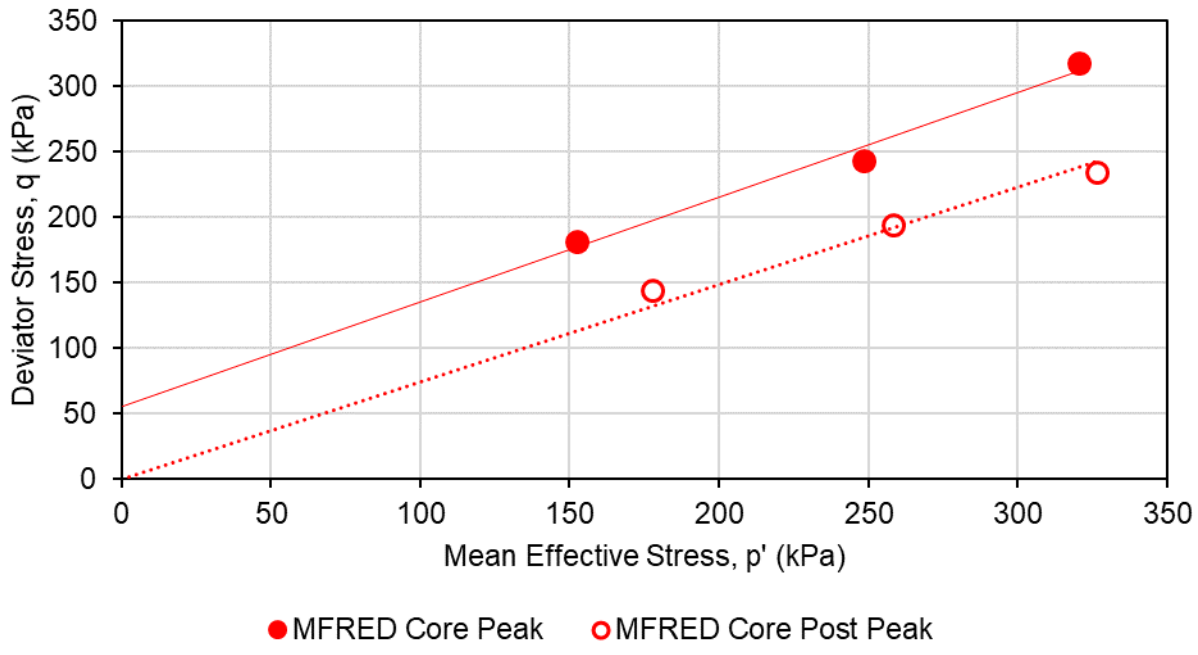

Figure A-C.71 Peak and post peak effective shear strengths of MFRED core samples from CIU Triaxial Tests

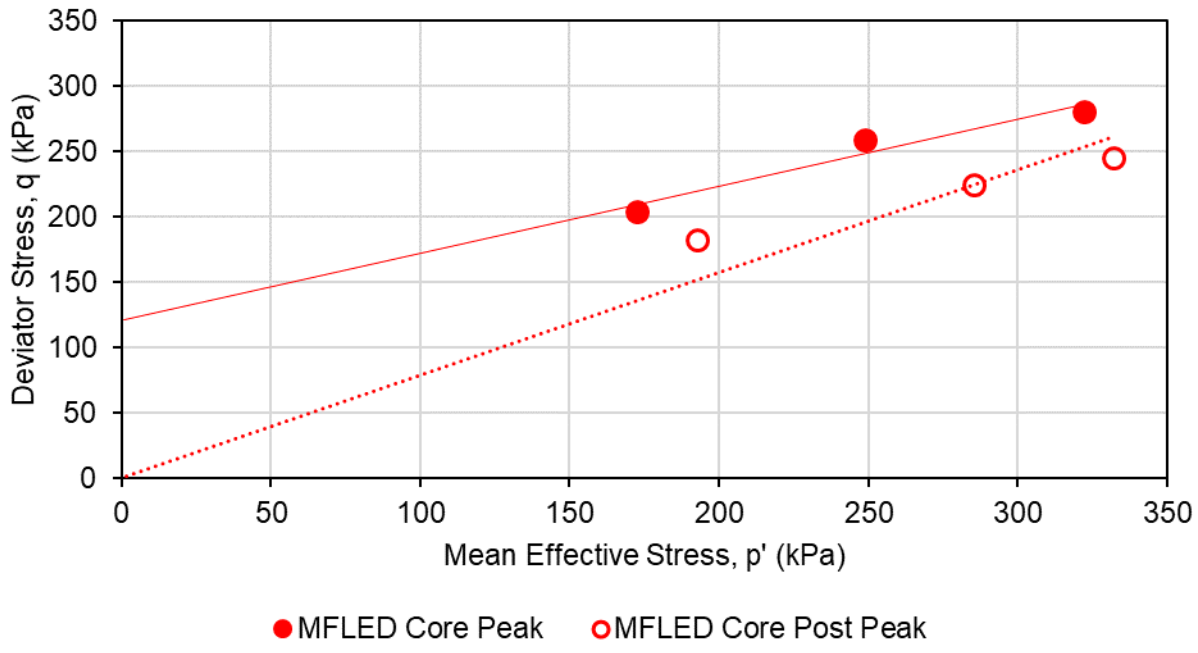

Figure A-C.72 Peak and post peak effective shear strengths of MFLED core samples from CIU Triaxial Tests

APPENDIX D

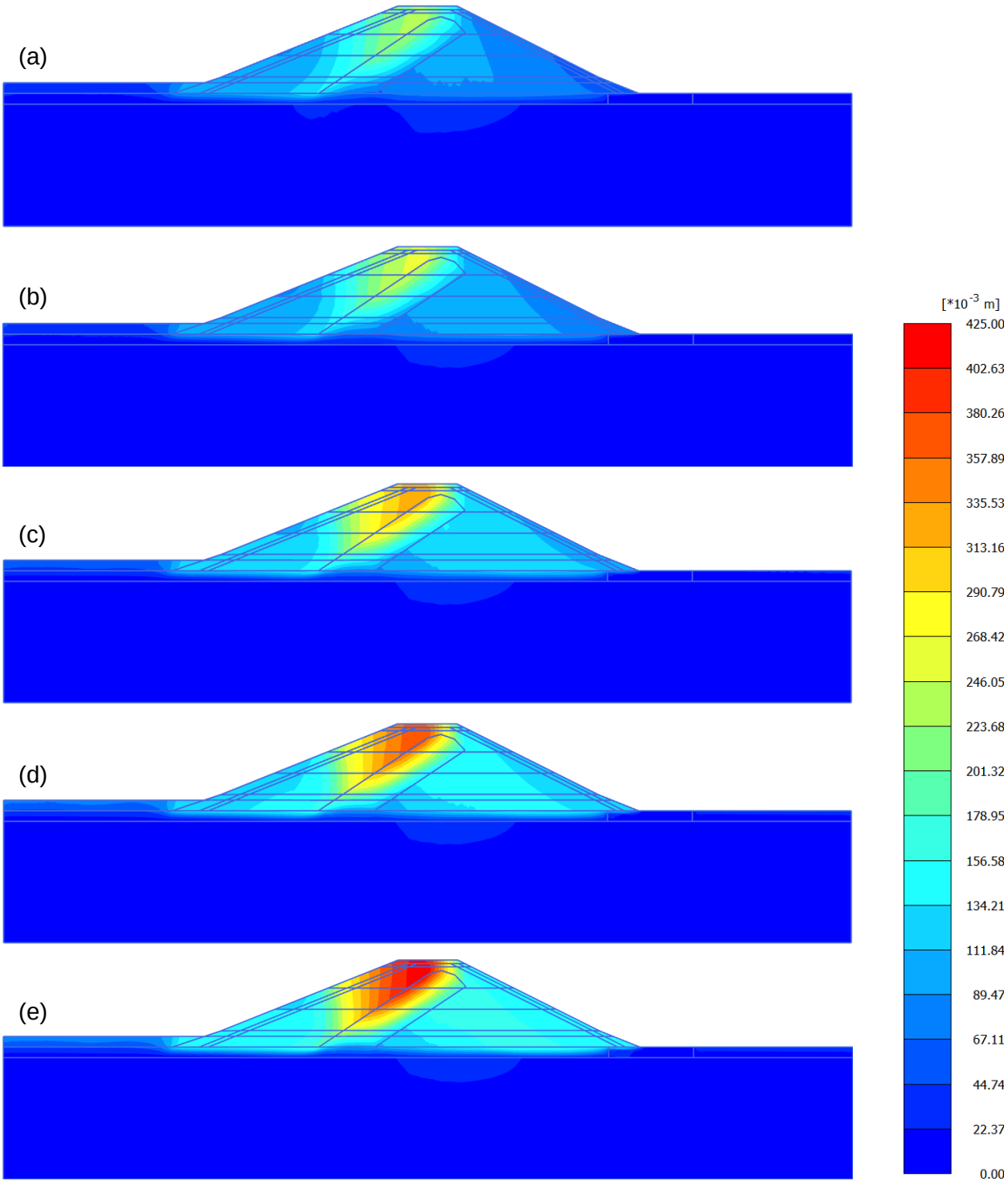

Figure A-D.1 Deformation development in CBB4 without clay blanket at different stages using Case 2: after (a) construction, (b) 1, (c) 10, (d) 30, and (e) 60 years after impounding

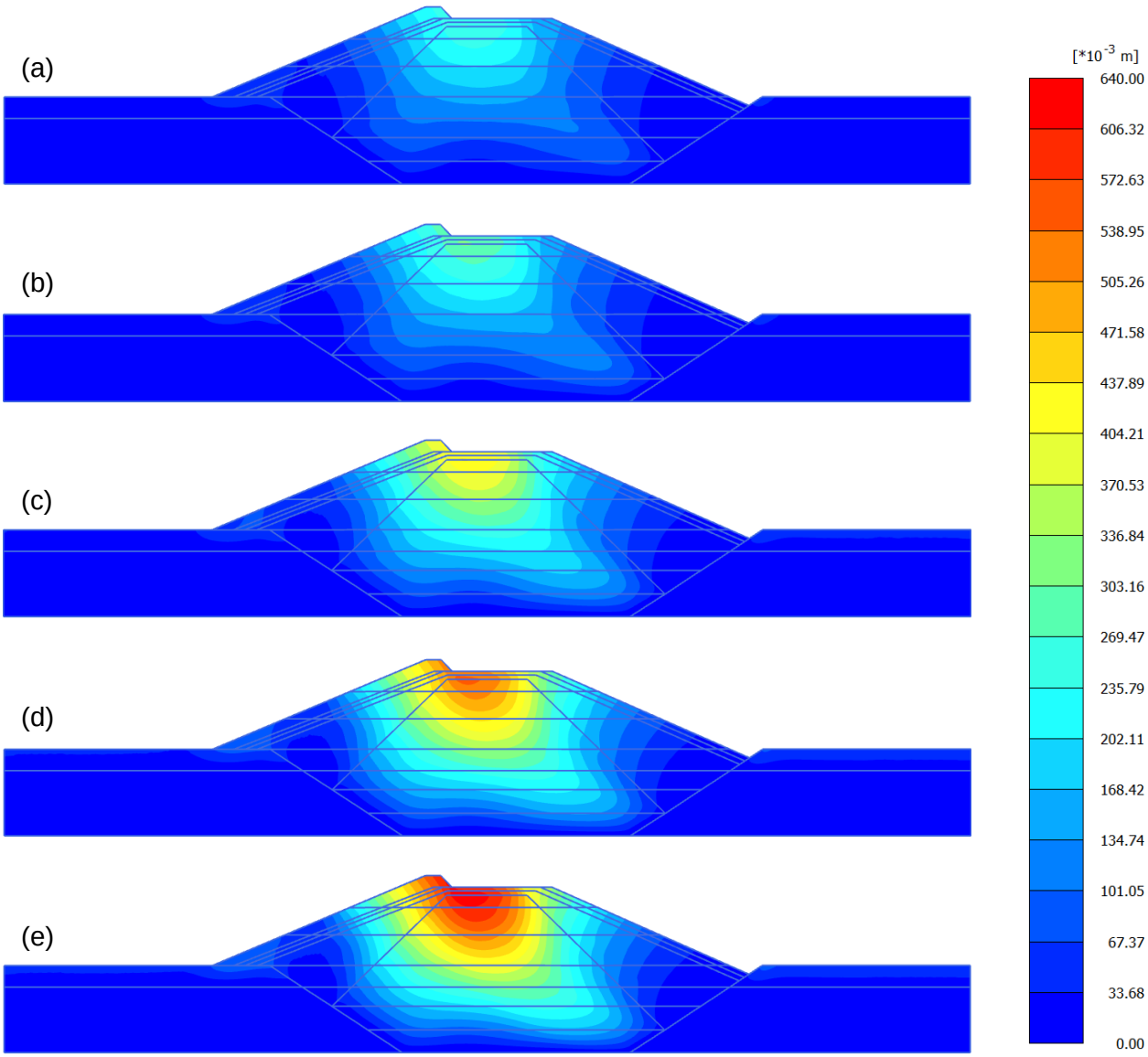

Figure A-D.2 Deformation development in CBMD at different stages using Case 2: after (a) construction, (b) 1, (c) 10, (d) 30, and (e) 60 years after impounding

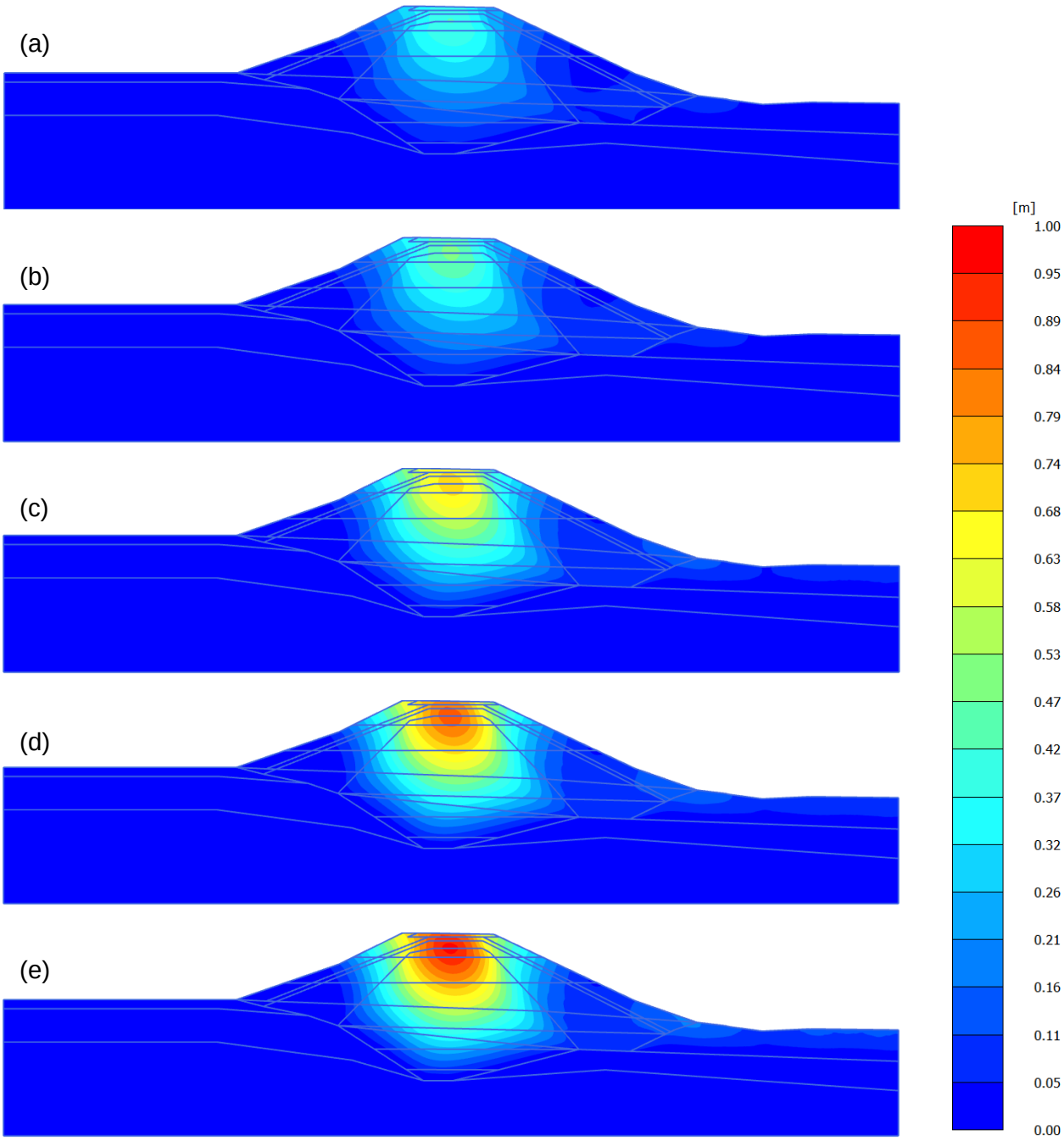

Figure A-D.3 Deformation development in WD at different stages using Case 2: after (a) construction, (b) 1, (c) 10, (d) 30, and (e) 60 years after impounding

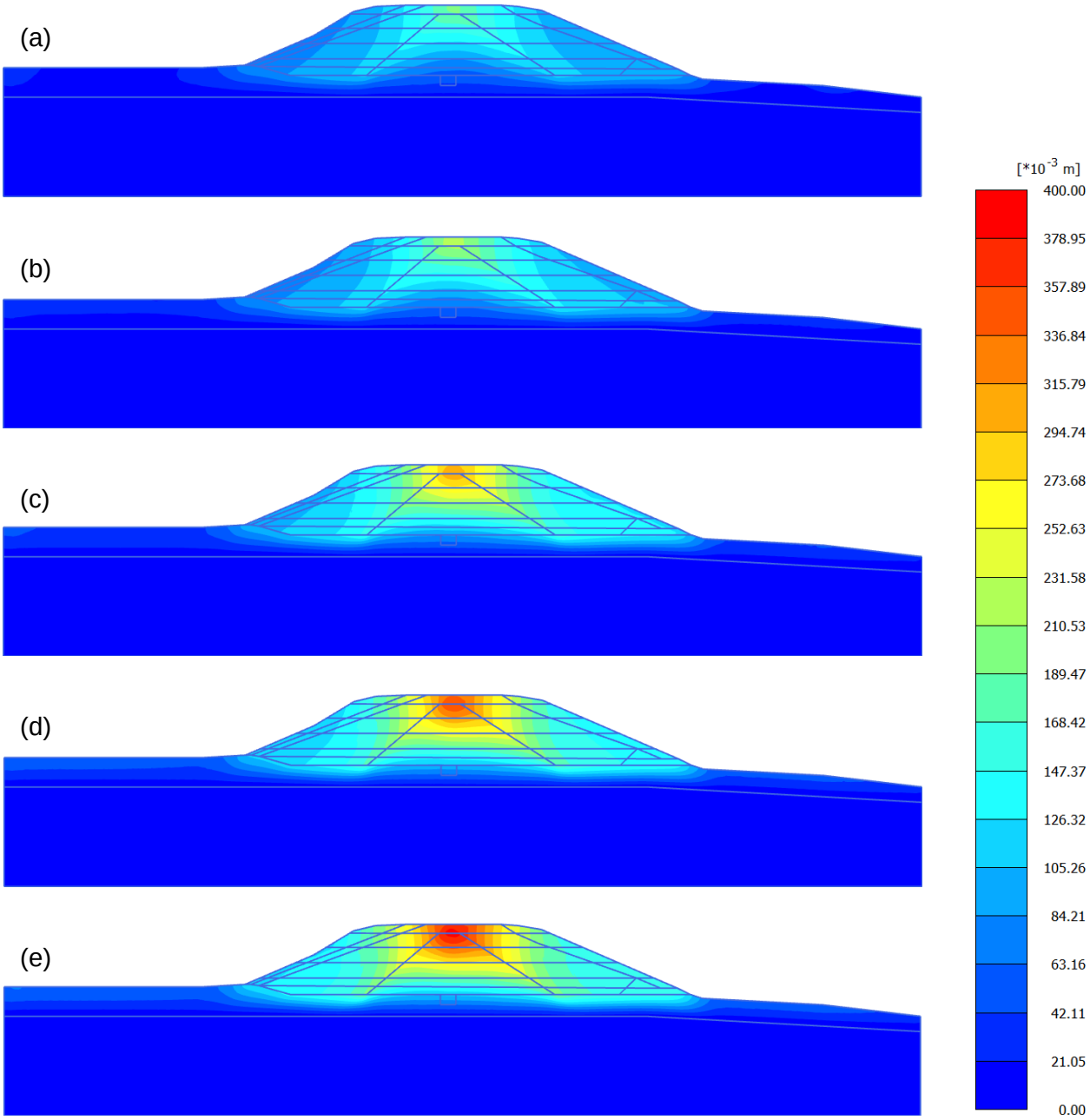

Figure A-D.4 Deformation development in EF at different stages using Case 2: after (a) construction, (b) 1, (c) 10, (d) 30, and (e) 60 years after impounding

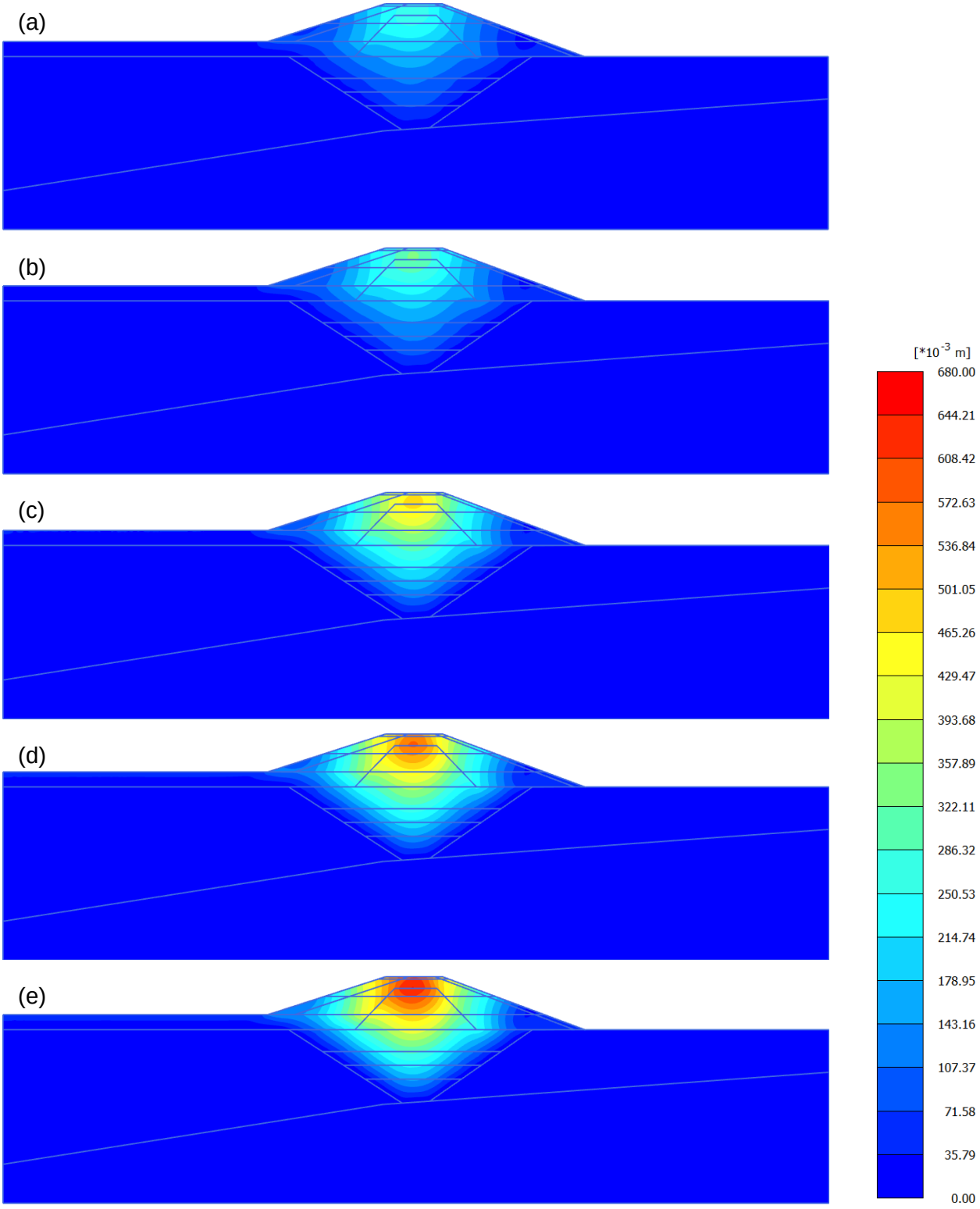

Figure A-D.5 Deformation development in MFRED at different stages using Case 2: after (a) construction, (b) 1, (c) 10, (d) 30, and (e) 60 years after impounding

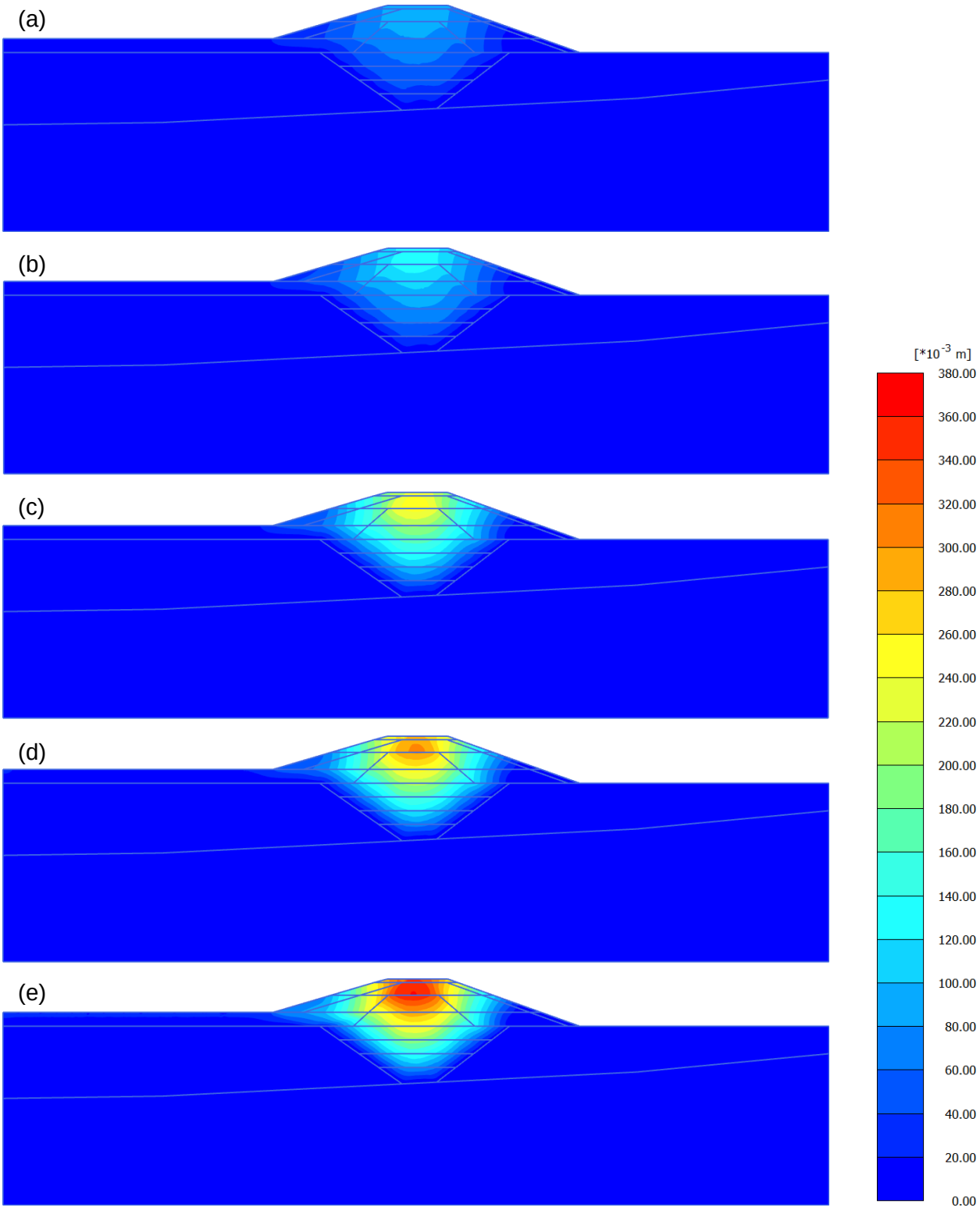

Figure A-D.6 Deformation development in MFLED at different stages using Case 2: after (a) construction, (b) 1, (c) 10, (d) 30, and (e) 60 years after impounding